BEAM-DRIVEN RETURN CURRENT INSTABILITY

IN SOLAR FLARES

by

David Cromwell

Thesis

submitted to the

University of Glasgow

for the degree of

Ph.D.

Department of Physics and Astronomy,
University of Glasgow,
Glasgow, G12 8QW,
U.K.

November, 1987

To Angela

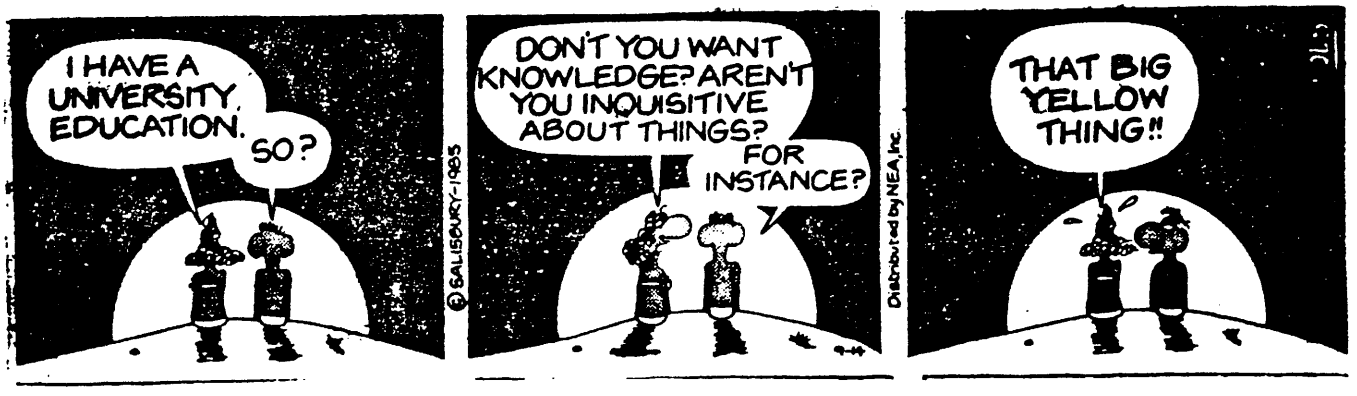

(Cartoon published in the Glasgow Evening Times (14.9.85) and reproduced by permission of Newspaper Enterprise Association Inc.)

ACKNOWLEDGEMENTS

Research for this thesis was carried out while the author was a postgraduate student in the Department of Physics and Astronomy (head - Professor I.S. Hughes) which resulted from the merger of the Departments of Natural Philosophy (former head - Professor E.W. Laing) and Astronomy (former head - Professor A. E.Roy) in August, 1986. Financial support was provided by SERC and computing facilities were made available by the University of Glasgow Computing Service. Grateful thanks are also extended to the University Library, particularly for the photocopying of many papers, and to the University of Leicester, where much of this thesis was actually written.

Very grateful thanks must go to my supervisor, Professor John Brown, for the initial setting up of the problem and for his continual guidance and encouragement throughout, and also outwith, the period of research. Any degree of cohesion and fluency which this thesis may have is, in no small part, attributable to his many constructive comments. The contribution of Dr. Paul McQuillan must also be acknowledged. During our collaboration his direct approach was often crucial in identifying and clarifying difficult problems, as well as in finding solutions to them.

Throughout the course of this research the following people have been helpful in discussing aspects of work contained (and, also, not contained) in this thesis: Bob Bingham (RAL), Gordon Emslie (University of Alabama, Huntsville), Professor Ernest Laing, Ken McClements, Alec McKinnon and Professor Peter Sweet (all at Glasgow).

During September-November, 1986, ten weeks were spent at NASA Goddard Space Flight Center, Maryland. I would like to thank Bill Henze, Jr., for making available to me a room in the UVSP apartment in Greenbelt.

For the provision of financial and administrative assistance I am grateful to Dr. Jeff Childs and Ms. Connie Payne of SASC Technologies, Lanham. I enjoyed many stimulating and, occasionally, provocative discussions with the following: Joe Davila, Francois Goetz, Gordon Holman (who invited me to Goddard), Sig Kutter, Ken Phillips, Greg Slater and Dan Spicer.

Given that thesis-writing should carry with it a mental health warning I would especially like to thank Angela for her patience and support, and for being such a good pal. Encouragement has also come from my mum and dad and, before this research actually took place, from my gran, Ruby Cromwell. The following friends, both recent and long-standing (or should that be "young and old"?) are thanked for their support in many varied ways: Bill Condie, Brian Martin, David Steele, Ian Taft and Stephanie Thornton (all of Drama), Graeme Cornwallis, Paul Davis, Sally Hall, Julia Magan, Stephen Morgan, Malcolm Ramsay, Neil Stewart and Joyce Willigenburg.

This manuscript would not be in front of you now but for the typing abilities of Mrs. Williamson and the graphical skills of Mrs. M. Morris, who assisted in the production of several of the diagrams. Nor must I forget to mention the diverse roles of Miss Daphne Davidson, the astronomy secretary, not least being the ever-reliable provision of tea and biscuits. Finally, I must thank the plasma physics group and, especially, all members of the astronomy group, both past and present, for the fostering of a relaxed and pleasant environment during the seven years of my stay at Glasgow University. To anyone not dutifully acknowledged I can only apologise most profusely and say, consolingly, that your contribution must have been so deep and profound that it exists at the level of my subconscious (okay?).

C O N T E N T S

SUMMARY

It is generally accepted that thick-target electron beams play a major role in the production, by collisional bremsstrahlung, of hard X-ray bursts during the impulsive phase of solar flares. The large electron flux demanded by the observed X-ray photon flux in such an interpretation requires that a beam-neutralising return current be set up. Ohmic dissipation of this return current increases the energy loss of the beam electrons in addition to the energy lost in Coulomb collisions with the ambient plasma. We investigate the effect on the hard X-ray signature when the return current is unstable to the generation of low-frequency electrostatic plasma waves (i.e. waves giving rise to anomalous plasma resistivity). Specifically, we compare the thermal emission, which rises due to enhanced plasma heating, with the non-thermal yield from the beam, which falls when turbulence is excited.

Chapter 1 constitutes a brief summary of the solar flare phenomenon, setting the return current problem in context. A review of beam-plasma systems theory is then presented in Chapter 2 together with a discussion of the two relevant wave modes for return current instability: ion-acoustic and ion-cyclotron.

In Chapter 3 a detailed description of our flare beam-return current model is given. Dimensionless electron and ion heating equations are derived and the fundamental parameters of the problem are discussed. The importance of including the effect of direct collisional heating by the beam, although in an approximate manner, is clearly shown.

Chapter 4 is an investigation of ion-acoustic (IA) instability of the return current in an unmagnetised plasma utilising a marginal stability approach. This method is discussed in some detail before being applied to the model. Our analysis leads to two distinct types of IA unstable heating:

Type (i): a well behaved marginally stable heating for which the electron-ion temperature ratio at onset of instability, i.e. $(T_e/T_i)_{onset}$, exceeds 4.8. Detailed numerical results of two sample cases are given.

Type (ii): a "catastrophic" heating, where $(T_e/T_i)_{onset} < 4.8$, for which the marginal stability hypothesis fails.

We provide an explanation for this failure and suggest an alternative method to describe such cases of catastrophic IA heating. (The work of Chapters 3 and 4, now submitted to Solar Physics, is a collaborative effort by P. McQuillan, D. Cromwell and J.C. Brown).

However, confusion exists in the solar (and, indeed, plasma) literature on the question of whether or not the unstable IA mode can actually be generated when $T_e/T_i \lesssim 5$. To clarify this issue, in Chapter 5 we solve the dispersion relation describing our return current system for various values of T_e/T_i and relative electron-ion drift, v_d. We assume Lorentz distributions for the electrons and ions and show that the IA mode <u>will</u> go unstable at low values of $T_e/T_i \lesssim 5$, provided v_d is sufficiently large.

A wave growth analysis of IA return current instability is developed in Chapter 6. We first apply this method to examples of marginally stable heating and find that the two approaches give

mutually consistent results. Cases of catastrophic heating are then investigated using this wave growth technique. Finally, a unified description, incorporating both approaches, is successfully applied to sample cases of return current heating.

The problem of return current instability in a magnetised plasma, where the ion-cyclotron mode may also be excited, is considerably more complex. An exploratory approach is adopted in Chapter 7 which reveals possible interesting behaviour of a flaring beam-plasma system (e.g. rapid oscillations in the hard X-ray signature).

Chapter 8 provides an overview of the thesis and indicates where improvements and refinements in the original model could be made. In particular, the need for incorporating spatial, as well as temporal, dependence of the plasma parameters in a more advanced treatment is stressed.

The two appendices contain relevant background plasma theory: appendix A, on the Landau initial value problem and dispersion relations, and appendix B, on transport in both classical and weakly turbulent plasmas.

PREFACE

The ancient Greeks regarded the Universe as comprising four basic forms: earth, water, wind and fire. Today, we would more commonly use the terms solid, liquid, gas and ... plasma. The study of this so-called "fourth state of matter" arose in the late nineteenth century from investigations of ionised gases in discharge tubes. It was not until 1928, though, when Langmuir published a paper on oscillations in an ionised gas, that the word "plasma" was introduced. In the subsequent six decades the field has diversified enormously to encompass research ranging from astrophysical plasmas (e.g. the solar corona) to controlled thermonuclear fusion.

One important distinction between the study of laboratory and astrophysical plasmas is that the former are amenable to direct, i.e. in situ, measurements; plasma probes are employed routinely in the laboratory to determine, for example, the plasma density and temperature. On the other hand, astrophysics is an observational, rather than experimental, science: the astrophysicist is constrained to infer information about the object of investigation by analysing data collected by detectors here on Earth, or on board satellites. The "hand of God" is not available for the construction of a plasma with physical characteristics (e.g. magnetic configuration, scale size) agreeable to the astrophysical investigator!

To be fair to the laboratory plasma physicist, though, not everything is within his/her control: plasma impurities, arising from plasma-surface interaction at the walls of the containment device, are a major problem in fusion research as they result in a reduced energy confinement time. Impurity concentrations can be deduced from the

bremsstrahlung radiation, emitted during collisions between electrons and ions, which escapes from the hot plasma. The spectrum can also be analysed to yield the electron temperature. Such plasma diagnostic measurements are common procedure in astrophysics.

In recent years it has been recognised that both communities have many overlapping interests. The development of test fusion reactors has necessitated much research of plasma instabilities and processes such as magnetic reconnection. This knowledge is crucial to our understanding of astrophysical problems, notably solar flares. Today, much time, money and effort is being invested in such plasma containment devices as the Tokamak, which employs a toroidal geometry to confine the plasma. Projects are currently underway at locations throughout the world, including the Kurchatov Institute in Moscow where the Tokamak scheme originated, the Lawrence Livermore Laboratory in California, and JET (Joint European Torus) at the Culham Laboratory near Oxford.

These programmes will, it is hoped, produce self-sustaining controlled thermonuclear fusion by confining the plasma magnetically. An alternative method is by "inertial containment" in laser-produced plasmas, where several beams of laser light are focused onto a small spherical fuel pellet, causing the compression of the inner core to very high densities. The aim of both methods is to heat a sufficiently dense plasma for a given length of time so that the thermonuclear reactions increase the energy output over the energy input. Mathematically, this is expressed by the Lawson criterion which relates the plasma density, n, and energy containment time, τ, at a specific plasma temperature, T. Currently, JET are close to their target parameters of $n\tau = 10^{20} m^{-3} s$ at T = 10-15 keV.

Laboratory plasma physicists have also recognised the possibility

of learning from naturally-occurring plasmas having a wider range of physical characteristics than their own. Measurements of the ionosphere (e.g. EISCAT - European Incoherent Scatter) and the magnetosphere (e.g. AMPTE - Active Magnetospheric Particle Tracer Explorers) have provided evidence of physical mechanisms, including beam-plasma instabilities, parametric decay processes, magnetic reconnection and particle acceleration, which are also observed in test fusion plasmas. Recent solar observations, particularly those from SMM (Solar Maximum Mission), launched in February 1980, have analysed the coronal plasma at an ever-increasing spectral, spatial and temporal resolution and provided an abundance of data indicating previously unknown features. For example, rapid fluctuations in hard X-ray and microwave intensities, with quasi-periodicities of 0.1s or less, have been observed during solar flares, possibly indicating "anomalous" plasma transport.

It is a cliché among astrophysicists, particularly solar physicists, that the only successful fusion reactor we know of resides at the Sun's core (and the centre of every other star)! We do not, however, know the details of its operation. If we did, there would be no solar neutrino flux problem. (Current theories of stellar structure, incorporating modern ideas from nuclear physics, suggest that the neutrino flux should be about three times the observed value). Humour aside, there is much scope for continuing collaboration between physicists with an interest in astrophysical plasmas, the magnetosphere, the ionosphere and controlled fusion.

The work contained in this thesis is an attempt to utilise fundamental plasma physics to derive an understanding of a real astrophysical problem. The interpretation of hard X-ray bursts in solar flares has benefited considerably from a knowledge of particle beams

obtained through laboratory plasma experiments. Initially, the simple collisional effects of electron beam precipitation in the flaring atmosphere attracted much attention. Recently, however, there has been a growing awareness of the importance of collective plasma effects in the electrodynamics of electron and proton beams, and their associated return currents. Much expertise of these issues has already been accumulated in the laboratory plasma community; an insight into beam collective effects and plasma turbulence is of crucial importance in advancing towards successful fusion reactors.

In the presence of a turbulent wave-level, plasma transport is no longer Coulomb collision-dominated and is said to be "anomalous". Simple classical modelling breaks down and must be replaced by a more sophisticated theory which amounts for the vastly modified transport coefficients of the turbulent plasma (e.g. conduction, diffusion, viscosity). In view of this, solar physicists have now recognised the need for a greater understanding of anomalous plasma processes by collaboration with the fusion community. Such developments can only lead to an advance in our knowledge of solar flares. Hopefully, this thesis constitutes some contribution to this progress.

1. A BRIEF REVIEW OF SOLAR FLARES

1.1 INTRODUCTION

The solar flare problem is one of the oldest in astrophysics, flares having been first observed in 1859, independently, by the English astronomers Carrington (1859) and Hodgson (1859). Essentially, a solar flare is a huge magnetic eruption in an active region of the Sun's atmosphere, releasing copious amounts of electromagnetic radiation from radio to γ-rays, as well as high energy electrons and ions. The largest flares are the most energetic events in the solar system.

The increase in solar cosmic-ray flux (energetic protons) at the Earth's magnetic poles can cause intense auroral displays during solar flares. Disturbance of the ionosphere may also occur, leading to disruption of radio communications. An understanding of flares is of great interest and importance, not only in plasma astrophysics, but also in solar-terrestrial relations (especially if flare onset could be predicted), and in plasma physics itself.

This chapter contains a deliberately brief summary of our current knowledge about solar flares which is relevant to the work contained in succeeding chapters of this thesis. There are, by now, many excellent reviews of solar flares and the interested reader is encouraged to refer to the following publications and references contained therein, for more extensive discussion of the topics of this chapter, as well as aspects of flares not discussed here at all: Priest (1984), for a comprehensive monograph on solar magnetohydrodynamics; Kaplan et al. (1974) and Sturrock (1986) on the solar atmosphere; Sturrock (1980), a collection of papers summarising results from Skylab; Priest (1981), containing review articles on various flare issues; Sweet (1969),

Svestka (1976), Brown and Smith (1980), Brown et al. (1981) and Spicer and Brown (1981), each with its own approach to summarising the flare problem; McKinnon (1986), on the theory of the impulsive phase (see below) of flares; and Heyraerts (1981) and de Jager (1986), primarily on the subject of particle acceleration during flares.

1.2 ENERGY RELEASE IN SOLAR FLARES

The total energy content of a large flare is around 10^{32} erg (or 10^{25}J) and is released in a volume having a maximum extent of 10^{28}-10^{29} cm^3. (Note that c.g.s. units will generally be used throughout this thesis). This energy release occurs in a timescale of tens of seconds to tens of minutes. The large energy density of $W \geq 10^3$ erg cm^{-3} can only be provided by the magnetic field; gravitational and thermal energies are not sufficient to power a flare.

Although there is no shortage of suggestions, the details of the pre-flare magnetic configuration and the manner in which the explosive energy release takes place, with magnetic energy being converted into heat, electromagnetic radiation and accelerated particles, are not well understood. The following is an attempt to present a concensus view. (The issue of how the primary energy released is then redistributed in the flaring atmosphere is not addressed here - see reviews above).

Observationally, many, but not all, flares display three characteristic regimes in their time profile: a pre-flare phase, during which some heating takes place and the underlying magnetic fields are changing; a flash, or impulsive, phase lasting for perhaps tens of seconds and marked by particle acceleration, a substantial increase in hard X-ray and microwave emission, mass motions and propagation of

shock waves; and a gradual decay phase lasting possibly for hours, during which the heated flare plasma expands above the flare site and then cools. The impulsive phase is the most energetic and places the greatest constraints on theoretical modelling of flares.

The observation that flare onset is a sudden phenomenon has led theoreticians to develop the following type of model: motions of photospheric footpoints generate currents in the highly-conducting corona giving rise to force-free magnetic fields, i.e. $\nabla \times \underset{\sim}{B} = \alpha \underset{\sim}{B}$, where α is some function of position which is constant along each field line. The more sheared the field, the greater is the magnetic energy. The magnetic topology moves through a series of stable equilibria, adjusting to changing boundary conditions, until the onset of some instability causes the explosive release of magnetic energy into plasma energy.

Broadly speaking, there are two main types of flares: the simple loop flare, in which a single stationary loop is observed to brighten and decay and the magnetic field is relatively static; and the two-ribbon flare, in which a filament erupts and the magnetic field lines are blown open, allowing the ejection of plasma and high energy particles into the interplanetary medium. Two-ribbon flares are more energetic, longer-lasting and occur higher in the solar atmosphere than the smaller, simple loop flares. (See reviews by Craig and Van Hoven on simple loop flares, and by Birn, and Schindler and Pneuman on two-ribbon flares in Priest (1981)).

The earliest flare models were presented by Sweet (1958) and Parker (1963) and developed by Sturrock (1968). Two bipolar fields, associated with sunspot groups, move together so that oppositely directed magnetic field lines approach and annihilate each other. This process is known

as magnetic reconnection. A current sheet passing through the magnetic neutral line is formed, whose thickness is determined by the plasma resistivity and the velocity of the field lines flowing into the sheet. As the field lines diffuse through the plasma they reconnect in the current sheet, converting magnetic energy to kinetic energy. However, the rate of energy dissipation in this simple model is too low to explain even small flares.

Enhancement of the energy dissipation rate is possible by invoking additional mechanisms. In the model devised by Petschek (1964), the current sheet splits into two pairs of magneto-acoustic shock waves, as the two fields being brought together are not strictly anti-parallel. This wave propagation at the Alfven speed increases the rate of field annihilation by orders of magnitude over the Sweet-Parker model, thus resulting in much larger energy dissipation rates. Soward and Priest (1977) have established a well-founded mathematical theory for Petschek's model as a mechanism for fast reconnection in solar flares. This work has been developed by Priest and Forbes (1985), and references therein, though Biskamp (1986) casts doubt, in some cases, on the rapid rates of reconnection they obtain. It is generally accepted, however, that the required energy dissipation rates can be achieved in a Petschek-type process.

A unified theory of solar flares, incorporating these ideas and known as the emerging flux model, has been developed by Heyvaerts et al. (1977). This model is based on the observation that vertical emergence of magnetic flux through the photosphere occurs before many flares (e.g. Rust (1976)). Emergence into a unipolar area near the edge of an active region may produce a simple loop flare; if the new flux appears near the sheared field associated with an active region filament,

then a two-ribbon flare may occur.

The theories described above are, for obvious reasons, known as "current sheet" models. Possibly a more realistic configuration, with observational support from soft X-ray Skylab pictures, is that of an arched magnetic flux tube carrying a current, proposed by Spicer (1977) along the lines of earlier work by Gold and Hoyle (1960) and Alfvén and Carlquist (1967). The idea here is that the sheared magnetic field becomes unstable to perturbations satisfying $\underset{\sim}{k}.\underset{\sim}{B} = 0$ at various locations along the arch, where $\underset{\sim}{k}$ is the wavevector of the perturbation. This is the so-called resistive kink or cylindrical tearing mode whose importance for flares has been considered by Spicer (1976, 1977, 1981). Magnetic reconnection occurs, the current filaments into strands and magnetic island formation takes place. Two, or more, neighbouring tearing modes interacting with each other can produce shorter energy release timescales than the single tearing mode. These effects have been observed in Tokamaks (e.g. Carreras et al. (1980)). Many different unstable modes are possible and different parts of the arch may go unstable at different times.

The perturbing mechanism which leads to an instability of the pre-flare magnetic configuration is likely to be one which increases the resistivity dramatically in a short time. The presence of low frequency waves, for example ion-acoustic, can increase the resistivity by four or five orders of magnitude over the Spitzer (1962) value (Papadopoulos (1975)). The phenomenon of current interruption (another effect also detected in Tokamaks), whereby the current density rises sharply, exciting a micro-instability which rapidly disrupts the current flow, is an alternative mechanism for destabilising the pre-flare magnetic structure. Other possible trigger processes include

rapid heating through thermal nonequilibrium (Hood and Priest (1981)) or the superheating instability (Kadomtsev (1966), Spicer (1976)).

To summarise the preceding few paragraphs: an instability triggers magnetic reconnection in either a Petschek-type or sheared magnetic arch configuration, with magnetic energy being converted into the forms manifest in the impulsive phase of the flare.

1.3 THERMAL AND NON-THERMAL MODELS OF THE X-RAY EMISSION

We now concentrate our attention on the hard X-ray bursts associated with the impulsive phase, as this is of most relevance to subsequent chapters. It is generally accepted that the X-ray emission is bremsstrahlung radiated during collisions between electrons and ions. The inverse Compton and synchrotron mechanisms have also been considered (Korchak (1971), McClements and Brown (1986)) but are not generally as attractive in explaining the observations.

There are both "thermal" and "non-thermal" models of the X-ray bursts. The latter interpretation arose from the power-law nature of the X-ray spectrum. However, it can be shown that the combined emission from many hot thermal sources can reproduce various spectral forms, including a power law (Brown (1974)). Craig and Brown (1976, 1986) have also drawn attention to the fundamental problems inherent in the inversion of spectral data to deduce information about the emitting source, e.g. the temperature structure of the plasma.

On the other hand, the most popular non-thermal interpretation, the thick-target model (Brown (1971)), in which an electron beam propagates down the limb of a coronal loop and loses most of its energy in the chromospheric target, has much observational support. Hard X-ray bursts have been observed in close temporal association with

optical and UV emission from the photosphere and chromosphere respectively, highly suggestive of downward beaming of electrons in the solar atmosphere. X-ray images taken by HXIS (Hard X-ray Imaging Spectrometer on board SMM) indicate simultaneous brightening of footpoints, easily understood in the context of the thick target model (Duijveman et al. (1982)). McKinnon et al. (1985) have, however, pointed out that great care must be taken in interpreting the data in this way, because of the ambiguity arising from statistical effects. Stereo observations of flares, utilising two satellites (e.g. Kane et al. (1979)), are also broadly in agreement with the thick-target model.

The major difficulty with the theory lies in the low bremsstrahlung yield of electrons in the energy range 10-100 keV (i.e. those primarily responsible for the X-ray emission); only about 10^{-5} - 10^{-4} of the electron's energy escapes as radiation, the rest being lost during Coulomb collisions with the ambient plasma. To account for the observed X-ray photon flux requires postulating that a sizable fraction, perhaps as much as one half, of the total flare energy resides in the form of accelerated electrons. This severe restriction on the electron acceleration mechanism has led many to consider a thermal interpretation of X-rays.

The attraction of the thermal hypothesis rests in the fact that in a confined thermal plasma with equal electron and ion temperatures, bremsstrahlung radiation is the only energy loss. There is thus a theoretical energy efficiency improvement of $\sim 10^4$ over non-thermal theories. In the models developed by Brown, Melrose and Spicer (1979) and Smith and Lilliequist (1979), the hot plasma expands behind collisionless conduction fronts at the ion-acoustic speed, $c_s = (T_e/m_i)^{\frac{1}{2}}$. Electrons in the tail of the distribution with speeds, $v \gtrsim 3v_e$

(electron thermal speed) can escape through the conduction front (see Smith (1983) for a brief discussion of this so-called thermal dissipative model). In practice, because of these effects, the efficiency of thermal models may not be significantly better than non-thermal models. In any case, thermal models have difficulty in explaining the observational features discussed above.

Further support for the thick-target interpretation comes from observed photospheric iron Kα emission (Emslie et al. (1985)) and also from spectral line displacements indicating upward convection of hot gas, possibly resulting from footpoint heating by electron beams (Antonucci et al.(1984, 1985)). We also mention here the proposition that the impacting beam is composed of protons (Emslie and Brown (1985); Simnett (1986); Simnett and Benz (1986)). However, while attractive on electrodynamic grounds, it seems inconsistent with observations; in particular, the proton beam energy flux required to produce the hard X-ray bursts would give rise to γ-ray line intensities far higher than those observed.

1.4 PARTICLE ACCELERATION MECHANISMS

Determination of the particle acceleration mechanism is one of the most difficult problems in solar flare theory. Three main suggestions have been put forward: acceleration by shocks (i.e. the Fermi mechanism), D.C. electric fields and stochastic acceleration by resonant interaction with turbulence. (Acceleration by electrostatic double layers has also been considered; see Section 2.2). It is unlikely that the first possibility is responsible for the non-relativistic electrons which form the bulk of the particles; even if shock formation could take

place during the impulsive phase, the acceleration would not proceed sufficiently rapidly. The process, however, may produce the relativistic electrons ($\mathcal{E}$ > 200 keV) and protons ($\mathcal{E}$ > 200 MeV) during second phase acceleration later in the flare (see Brown and Smith (1980); Heyvaerts (1981); Ellison and Ramaty (1985)).

Electron acceleration in the turbulent electric field of various wave modes, particularly Langmuir, has been considered in the past (e.g. Benz (1977); Brown and Loran (1985)). It is difficult to excite Langmuir waves, however, and the radio signature which would apparently be produced by having the required energy density of Langmuir turbulence is not observed (Smith and Spicer (1979); Emslie and Smith (1984); McClements (1987)). This has led Benz and Smith (1986) to consider lower-hybrid waves as the accelerating mode.

During the process of magnetic reconnection (see Section 1.2), D.C. electric fields will be generated inductively (Vasyliunas (1975)). A fraction of the electrons in the initial distribution, with velocities greater than a certain critical velocity, will be accelerated by the electric field as "runaways" out of the thermal plasma (Dreicer (1959), (1960); Papadopoulos (1977)). Holman (1985), taking this assumption, has calculated that, in order to explain the observed X-ray bursts from a non-thermal standpoint, the acceleration region must be divided into $\sim 10^4$ oppositely directed current channels. (The channels must be oppositely directed in order to ensure that the magnetic field associated with the net current in the acceleration region does not exceed the upper limit placed by observations).

Holman's work is in agreement with the earlier result of Spicer (1983) that, in a high inductance flaring loop, any beam current is

limited to the pre-existing drift current, which is at least four orders of magnitude too small to sustain the non-thermal hypothesis. However, the non-thermal interpretation is applicable when a cospatial beam-return current system (see Sections1.5,2.1) is postulated for the propagation region; no return current can exist in the acceleration region, thus the need for oppositely directed current channels there.

In conclusion, we note here that formation of electron beams may arise as a consequence of loss-cone anisotropy whereby some mechanism scatters electrons into the loss-cone region of pitch-angle space, thus resulting in precipitation. One candidate is the electron-cyclotron maser instability (e.g. Holman et al. (1980); Melrose and Dulk (1982)) which is driven by electron distributions having a positive $\partial f/\partial v_\perp$. Such distributions result naturally from the conservation of magnetic moment of electrons traversing a region of converging magnetic field in a flux tube. The perpendicular kinetic energy of the electrons is reduced on emission of the cyclotron radiation, leading to the formation of a low pitch-angle distribution, i.e. beam precipitation occurs. Maser emission at the electron-cyclotron frequency Ω_e is likely to be reabsorbed in the corona and produce heating; higher harmonic emission can escape to produce observed solar microwave spike bursts (Winglee and Dulk (1986), and references therein).

1.5 RETURN CURRENTS

It has been recognised for about a decade now that the large electron fluxes inferred from the thick-target model of hard X-ray bursts are so large that a cospatial neutralising return current must exist (Hoyng et al. (1976); Brown and Melrose (1977)). The reasoning is as follows. The inferred electron fluxes are $\sim 10^{36}$ electrons s^{-1}

(for a large flare). This is a current flow of 5.10^{26} statamp, which exceeds the Alfvén-Lawson current limit (see Section 2.1) by around thirteen orders of magnitude, i.e. the current at which the pinching effect of the self-magnetic field prevents propagation of the beam (Alfvén (1939); Lawson (1957)). The consequence of this is that a current-neutralising flow of plasma electrons is set up such that $j_{net} = j_{beam} + j_{plasma} \simeq 0$. In other words, the return current drift velocity, v_d, must satisfy:

$$n_p v_d = n_b v_b = \frac{F}{A} \qquad (1.1)$$

where the subscripts p and b refer to plasma and beam respectively, F is the thick-target electron flux (electrons s^{-1}) and A is the beam cross-sectional area. Such beam-plasma systems are commonly produced in the laboratory (see Section 2.1). The return current is also capable of replenishing the acceleration region to provide the large number ($\sim 10^{38}$ - 10^{39}) of electrons required throughout the flare, thus solving the "electron number problem" (Brown and Melrose (1977)).

Electron beam injection gives rise to a decelerating electric field which sustains the return current flow against the finite resistivity of the flare plasma. Ohmic dissipation of the return current, i.e. joule heating, represents an additional energy loss to the beam, over and above the Coulomb collisional losses in the standard thick-target model. This leads to an aggravation of the problem of low bremsstrahlung efficiency (or, equivalently, the high acceleration efficiency demanded) of this model.

Knight and Sturrock (1977) analysed the case of an electron beam driving a stable return current and calculated the beam energy deposited in the form of joule heating (beam collisional losses were ignored).

They concluded that return current heating probably has an important effect on X-ray bursts, particularly in the initial stages of the flare, in the low temperature plasma (ohmic heating $\sim T_e^{-3/2} j^2$).

The justification for using a steady-state treatment (in which $j_{beam} = - j_{plasma}$), as in Knight and Sturrock (1977), has been called into question by Spicer and Sudan (1984), hereafter referred to as SS. They claim that such an approach is invalid since the "return current is primarily maintained by inductive effects" and since their calculated beam propagation times are less than 1s. However, the issue of inductive/electrostatic effects, indeed whether such a question is meaningful, and the validity of a steady-state treatment was examined by Brown and Bingham (1984) (BB). They found that, using generally accepted solar flare parameters, the resistive timescale for decay of the return current (which, in turn, determines the beam propagation time) is so large that a steady-state analysis is perfectly legitimate.

We might mention here that SS claim that flare acceleration mechanisms cannot produce electron beams with radii larger than $\sim 10^6$cm (cf. 10^9 - 10^{10} cm adopted in the standard thick-target model), thus leading to their small values of resistive decay and propagation times. However, this requires that n_b/n_p is impossibly large ($>> 1$) if the X-ray emission is to be understood in the context of the thick-target model. On the other hand, if <u>many</u> beams are formed, each with an acceptable density, then their formation and interaction must be explained. We discuss the opposing views of BB and SS in more detail in Section 2.1.

If the return current drift velocity, v_d, exceeds some threshold velocity, v_{crit}, for the generation of a plasma microinstability

(Kindel and Kennel (1971)), then turbulence is generated and collective effects can become very important. The type of instability (e.g. ion-acoustic, ion-cyclotron: see Sections 2.2, 2.3) depends on the physical properties of the plasma (e.g. n_b/n_p, T_e/T_i). Thick target fluxes, F/A, for acceleration sites at reasonable coronal densities, lie close to the criterion for stability of the return current to ion-acoustic wave production. This led Brown and Melrose (1977) to raise the possibility that instability of the return current acts as a feedback mechanism on the electron beam, thus limiting the thick-target flux.

There are, therefore, three hypothetical regimes for the dynamics and heating of a thick-target beam and its accompanying return current (Hoyng et al. (1978)):

1. Domination by Coulomb collisions of the electron beam with the ambient plasma as in the standard thick-target model;

2. Domination by ohmic dissipation, via Spitzer resistivity, of a stable (i.e. $v_d < v_{crit}$) return current;

3. Instability of the return current ($v_d \gtrsim v_{crit}$) leading to enhanced ohmic dissipation arising from the anomalous transport coefficients, specifically the resistivity, associated with wave-particle scattering.

Emslie (1980, 1981) considered the effect of a stable return current on the plasma heating (using the Spitzer resistivity) and X-ray spectrum during a flare, i.e. regime 2. In particular he calculated the ratio, β, of return current losses to collisional losses for a beam electron of energy, $\mathcal{E}$:

$$\beta \sim \frac{F\mathcal{E}}{n_p T_e^{3/2}} \qquad (1.2)$$

For a given flux, F, return current losses will be important near injection in the corona (small n_p) at the start of the flare (low T_e). The variation of β with depth, z, in the atmosphere obviously depends on $\mathscr{E}$ (z) and an assumed model atmosphere for $n_p(z)$, $T_e(z)$.

In his 1981 paper, Emslie concluded that, apart from the initial transient state of the flare, return current heating may not play as important a role as had been previously thought. We note, however, that his analysis assumed that the electron beam gave rise to a return current having a drift velocity just below the threshold for plasma turbulence.

Brown and Hayward (1982) derived analytic expressions for the stopping length, s, of the beam in the cases of (Spitzer) ohmic losses only, and combined collisional and ohmic losses. In a time-dependent treatment, incorporating a mean conductive cooling, $\underset{\sim}{\nabla}.\underset{\sim}{F}_{cond}$, over the length s, they find that it is impossible for return current losses to dominate collisional losses unless the ratio F/n_p is so high that the return current is unstable. In other words, regime 2 can never occur.

Recently, Emslie (1985) has claimed that the conductive cooling calculated by Brown and Hayward (1982) assumed unreasonably large values for s (exceeding coronal loop half-lengths), and was therefore underestimated. The effect of this is to overestimate values of T_e and hence underestimate the ratio of ohmic to collisional heating for a given flux, as this scales as $T_e^{-3/2}$ (from Equation 1.2)). He concludes that regime 2 <u>is</u> possible and that, in any case, the heating effects of even stable return currents should not be neglected.

Emslie (1985) has also derived scaling laws relating the peak loop temperature and electron flux for the two extreme cases of beam collisional heating only and return current heating only. To discriminate

between these two models of flare coronal heating, a comparison was made with coordinated hard and soft X-ray observations from HXRBS (Hard X-Ray Burst Spectrometer) and XRP (X-ray Polychromator), respectively, on board SMM (Emslie (1986)). The results, though, are inconclusive, apparently related to the difficulties involved in deducing temperatures unambiguously from soft X-ray line ratios (cf. Craig and Brown (1976)).

1.6 BEAM-RETURN CURRENT INTERACTION

The interplay between the primary precipitating electron beam and its associated return current has barely been touched upon in the solar flare literature. Wave generation by the beam itself has attracted some attention, though. Collisional depletion of low-energy electrons in the beam distribution, as the beam propagates through the atmosphere, results in the formation of a positive slope in velocity space. This bump in the distribution is unstable to the generation of Langmuir waves and is rapidly removed; this process is termed quasi-linear relaxation and has been investigated by Emslie and Smith (1984) and McClements (1987). It is found that taking account of quasi-linear relaxation in the thick-target model leads to unobservably small differences in the X-ray bremsstrahlung yield; its effect is merely to broaden the beam spectrum. The wave level i.e. energy density, of Langmuir waves in the calculations of Emslie and Smith leads to a predicted microwave flux very much larger than that observed. McClements (1987), however, claims that this anomaly arises because Emslie and Smith (1984) wrongly assume an isotropic Langmuir wave distribution.

Vlahos and Rowland (1984) and Rowland and Vlahos (1985) have investigated the interaction between the beam and the return current. Using a system of rate equations to describe the time evolution of the

energies of waves generated by the beam and the return current they conclude the following:

1. The beam is modulated, i.e. consists of many short-lived pulses.

2. The beam loses only a few percent of its energy to maintain plasma oscillations.

3. The formation of non-thermal electron tails can stabilise the beam against the anomalous Doppler resonance instability driven by the velocity anisotropy $v_{11} >> v_{\perp}$ (e.g. Parail and Pogutse (1976); Liu and Mok (1977); Haber et al. (1978)).

In addition, they find that strong Langmuir turbulence can substantially alter the way in which the return current is carried by the ambient plasma."Collisionless" effects, where the return current comprises a small number of very energetic electrons, may be important. If the plasma is strongly magnetised (i.e. $\Omega_e/\omega_{pe} \gtrsim 1$, where Ω_e is the electron gyrofrequency and ω_{pe} is the electron plasma frequency), which is actually highly uncertain in the case of the solar corona, then current-driven instabilities may lead to anomalous resistivities only slightly higher than the classical (i.e. Spitzer) values.

Certainly, the beam-return current forms a unified system, and ideally should be studied as such, but for the purposes of simplicity and a step-by-step understanding of the many processes involved, it is often convenient and, indeed, necessary to decouple the beam and the return current. This is the approach adopted in the following chapters; we investigate the instability of the return current electrons drifting with respect to the ambient protons (a fully ionised hydrogen plasma is assumed). Chapter 2 presents a brief review of the relevant physics of beam-return current systems, including a discussion of the ion-acoustic/ cyclotron instabilities.

2. BEAM-PLASMA SYSTEMS

2.1 INTRODUCTION

Interest in particle beams stems from fusion plasmas, astrophysical environments and, ominously, from a preoccupation with beam weapon technology. In particular, much attention has recently been focused on the SDI (Strategic Defence Initiative) project, popularly termed "Star Wars", which has been implemented by the current U.S. administration. On the other hand, the peaceful development of intense beams of relativistic electrons and ions has taken place in the attempt to create thermonuclear temperatures in magnetised plasmas. The additional heating provided by ohmic dissipation of the return current, particularly if there is anomalous (i.e. non-Spitzer) resistivity, has also been investigated. Beam-plasma systems are of importance in solar physics, stellar atmospheres, binary systems (for example, an understanding of proton beam bombardment during white dwarf accretion may resolve the so-called "soft X-ray puzzle"; see Thompson et al. (1986)) and galactic and extra-galactic radio jets. For an overview of the wide-ranging interest in beam-plasma systems in astrophysics see Kundu and Holman (1985).

The physics of the interaction of a beam of particles with a plasma is complicated; there are many different modes of oscillation which may be excited and a variety of nonlinear processes which can exchange energy between them. Extensive discussions of collective beam-plasma interaction can be found in the following reviews: Benford and Book (1971); Brejzman and Ryutov (1974); Miller (1982); Sudan (1984). In Section 2.2 we concentrate on the electrodynamics of the beam and its attendant return current. Two particular instabilities which may be excited by the return current are the ion-acoustic and ion-cyclotron

modes; their properties are discussed in Sections 2.3 and 2.4. We will be drawing heavily on these sections in later chapters when analysing the problem of instability of return currents in solar flares.

2.2 BEAM-RETURN CURRENT ELECTRODYNAMICS

The phenomenon of pinching of an electron beam by its self-magnetic field has been well known for over fifty years now (Bennett (1934)). Taking a cylindrically symmetric, monoenergetic, uniform current density model of identical particles, Alfvén (1939) calculated the maximum possible fully electrostatically neutralised current flow, I_A. (Alfvén's work dealt with cosmic rays and assumed that ionised particles in interstellar space would provide charge neutralisation). By assuming propagation to be disrupted when the beam electron Larmor radius becomes of the order of the beam radius he obtained

$$I_A = \frac{m_e c^3}{e} \beta\gamma \qquad (\simeq 5.10^{13} \beta\gamma \text{ stat A}) \qquad (2.1)$$

where $\beta = v_b/c$, $\gamma = (1-\beta^2)^{-\frac{1}{2}}$ and v_b is the beam velocity.

Lawson (1957) confirmed this result and also evaluated the current limit for a fractional electrostatic beam neutralisation, f_e:

$$I_A = \frac{m_e c^3}{e} \cdot \frac{\beta^3 \gamma}{(\beta^2 + f_e - 1)} \qquad (2.2)$$

Therefore, I_A could be made as large as one wishes by arranging f_e to be close to $1-\beta^2$. In practice this is extremely difficult to do. It is known, however, that injection of a beam into a plasma generates a return current which is equal, or nearly equal, to the injected current (Roberts and Bennett (1968); Cox and Bennett (1970)). This results in a net current and, therefore, magnetic field which is

very nearly zero. In other words, another method of propagating currents $I > I_A$ is by magnetic neutralisation of the beam by a return current. For a fractional magnetic/current neutralisation, f_m, we have (Hammer and Rostoker (1970)):

$$I_A = \frac{m_e c^3}{e} \cdot \frac{\beta^3 \gamma}{[\beta^2(1-f_m)+f_e-1]} \qquad (2.3)$$

Hammer and Rostoker (1970) also consider a third way of beating the self-magnetic pinch in their analysis of self-consistent equilibrium solutions to the Vlasov-Maxwell equations for given beam current density profiles $j_b(\underset{\sim}{r})$. Essentially, they find that if the current density is concentrated close to the edge of the beam, pinching removes electrons from high-field regions before beam propagation is disrupted. Currents exceeding the Alfven-Lawson limit can therefore be obtained. We do not discuss this effect further.

The limiting currents, I_A, above (2.1, 2.2, 2.3) all assume propagation in magnetic field-free regions. However, the presence of a strong axial guide field, B_o, will prevent beam electrons from being carried across the beam radius and will thereby stabilise the beam if,

$$B_o >> \frac{B_{max}}{\beta^2} \left| 1 - \beta^2 - f_e \right| \qquad (2.4)$$

where B_{max} is the maximum value of the self-magnetic field of the partially current-neutralised beam. Condition (2.4) is derived by specifying that $v_\perp << v_{||}$. For solar atmosphere conditions, $f_e \simeq 1$, and (2.4) reduces to $B_o >> B_{max}$. We mention here that if B_o is too large, such that $\Omega_e >> \omega_{pe}$, then the formation of the return current is very difficult (Lee and Sudan (1971)). However, it is very unlikely that this condition holds true in the solar atmosphere.

The setting up of a return current flow of electrons upon injection of an electron beam can be considered to be a consequence of Lenz's law: the return current is produced in order to keep the net current of the system zero, just as it was before beam injection. There has, however, been some confusion in the literature over electrostatic/inductive aspects of return currents (Spicer and Sudan (1984) hereafter (SS); Brown and Bingham (1984) hereafter (BB)). We therefore discuss the relevant electrodynamics below.

Assume a beam current is switched on at t=0 in the form of a rigid uniformly charged rod of radius, a, and extending from $z = 0$ to $z = -\infty$ with current profile $\underset{\sim}{j}_b = \hat{\underset{\sim}{z}}\, j_o(r)\, U(z - v_b t)$ where U is the unit Heaviside step function. We would like to calculate the response of the plasma to this beam injection. The analysis below assumes that the beam electrons are not affected by the plasma, either through collisions or the setting-up of an electric field. In other words, deceleration of the beam is neglected. We discuss this point later.

Following Lovelace and Sudan (1971) we write down the wave equation for the electric field from Maxwell's curl equations:

$$c^2 \underset{\sim}{\nabla} \times \underset{\sim}{\nabla} \times \underset{\sim}{E} + \frac{\partial^2 \underset{\sim}{E}}{\partial t^2} = - 4\pi \frac{\partial \underset{\sim}{j}}{\partial t} \qquad (2.5)$$

where $\underset{\sim}{j} = \underset{\sim}{j}_b + \underset{\sim}{j}_p$ and the plasma current, $\underset{\sim}{j}_p$, is obtained from the generalised Ohm's law (e.g. Miyamoto (1980))

$$\left(\frac{\partial}{\partial t} + \nu_{ei}\right) \underset{\sim}{j}_p = \frac{\omega_{pe}^2}{4\pi} \underset{\sim}{E} - \frac{e}{m_e c} \underset{\sim}{j}_p \times (\underset{\sim}{B}_o + \underset{\sim}{B}) \qquad (2.6)$$

where ν_{ei} is the electron-ion collision frequency and $\underset{\sim}{B}_o$ is the external (i.e. guide) field. Neglecting the Hall term in (2.6) (see Lovelace and Sudan (1971); SS) and then substituting for $\underset{\sim}{E}$ in (2.5) gives

$$\frac{c^2}{\omega_{pe}^2}\left(\frac{\partial}{\partial t}+\nu_{ei}\right)\left[\underset{\sim}{\nabla}(\underset{\sim}{\nabla}.\underset{\sim}{j}_p)-\underset{\sim}{\nabla}^2\underset{\sim}{j}_p+\frac{1}{c^2}\frac{\partial^2\underset{\sim}{j}_p}{\partial t^2}\right]$$

$$=-\frac{\partial}{\partial t}(\underset{\sim}{j}_b+\underset{\sim}{j}_p) \qquad (2.7)$$

For times $t < \tau_{prop}$, the beam propagation time, i.e. near the beam head, we may assume $j_{pr} << j_{pz}$. Taking $\underset{\sim}{\nabla}_r \sim a^{-1}$, (where a is the beam radius) $\underset{\sim}{\nabla}.\underset{\sim}{j}_p = 0$ and $\frac{\partial}{\partial t} >> \nu_{ei}$ gives:

$$\omega_{pe}^{-2}\frac{\partial^2 j_{pz}}{\partial t^2}-\left(1+\frac{\lambda_E^2}{a^2}\right)j_{pz}=j_b \qquad (2.8)$$

where $\lambda_E = c/\omega_{pe}$ is the electromagnetic skin depth (e.g. Sudan (1984)). The solution of (2.8) is

$$j_{pz} = -\frac{j_b}{(1+\lambda_E^2/a^2)}(1-\cos\omega_{pe}t) \qquad (2.9)$$

Including the effect of collisions introduces a damping factor $e^{-\nu_{ei}t/2}$ multiplying the cosine term. Note that $\lambda_E/a << 1$ is required for neutralisation in the case $B_o = 0$ or, if $B_o \neq 0$, $a^2/\lambda_E^2(1+\zeta^2) >> 1$, where $\zeta \equiv \Omega_e/\omega_{pe}$ (Lee and Sudan (1971)). The oscillatory term in (2.9) arises as a consequence of the displacement current in Maxwell's $\underset{\sim}{\nabla}\times\underset{\sim}{B}$ equation. Recognising that these rapid oscillations average to zero on timescales much longer than a plasma period, ω_{pe}^{-1}, gives the solution

$$j_{pz} \simeq -j_b \qquad (\text{for times } \omega_{pe}^{-1} << t << \nu_{ei}^{-1}) \quad (2.10)$$

The return current flows cospatially with the beam resulting in current, and magnetic, neutralisation.

For long timescales, $t >> \nu_{ei}^{-1}$, the effect of the plasma resistivity,

η , is that the return current decays on the characteristic time constant for magnetic diffusion. To see this, we take $\nu_{ei}\, t >> 1$ and $\frac{a}{c}\,\frac{\partial}{\partial t} << 1$ so that (2.7) is approximated by

$$(\frac{\partial}{\partial t} - \frac{\eta c^2}{4\pi}\nabla^2_{\sim})j_{pz} = -\frac{\partial j_b}{\partial t} \qquad (2.11)$$

where $\eta \simeq 2\pi\nu_{ei}/\omega_{pe}^2$ (see Appendix B). If we assume a "sharp" beam head we can take $\frac{\partial j_b}{\partial t} \simeq 0$ everywhere else. In other words, j_{pz} satisfies a diffusion equation with a characteristic decay time

$$\tau_D = \frac{4\pi a^2}{\eta c^2} = (\frac{a}{\lambda_E})^2 \nu_{ei}^{-1} \qquad (2.12)$$

Note that a large beam radius, a, and a small resistivity, η , result in a very large τ_D. In fact, assuming the usual Spitzer resistivity, BB show that

$$\tau_D \simeq 10^{14}\, R_9^2\, T_6^{3/2} \text{ seconds} \qquad (2.13)$$

where $R_9 \equiv R(\text{cm})/10^9$, $T_6 \equiv T(K)/10^6$, scaled to solar parameters. Therefore, on timescales $\gtrsim \tau_D$, the return current decays away and the beam current is no longer completely magnetically neutralised. Beam propagation will cease when the field, B, associated with the net current becomes comparable to B_o, the guide field (see Equation (2.4)).

Again scaling to solar flare parameters, BB calculated the maximum beam propagation time to be

$$\tau_{max} \simeq 2\times 10^8\, B_2\, R_9^3\, T_6^{3/2} / \mathcal{J}_{36} \text{ seconds} \qquad (2.14)$$

where $B_2 \equiv B_o(\text{gauss})/10^2$ and $\mathcal{J}_{36}$ is the beam electron injection rate in units of $10^{36}\,s^{-1}$. Note that this assumes that guide field

limitation, not Alfven-Lawson current limitation, is applicable, which seems likely to be the case in the solar atmosphere.

We therefore have the following model of the net current system in which beam deceleration is ignored (Lee and Sudan (1971)). At the head of the beam (see Figure 2.1) there is a region of oscillations which decay away on a length scale $\sim v_b \tau_E$, where τ_E is a phenomenological momentum relaxation time for the plasma electrons (Hammer and Rostoker (1970)). For a beam having a rise time, t_r, the amplitude of the oscillations will be $\sim (\omega_{pe} t_r)^{-1}$. The length of the region where the beam is almost completely current-neutralised is $\sim v_b \tau_E a^2/\lambda_E^2$. Beyond this region the return current decays away and there is a net current.

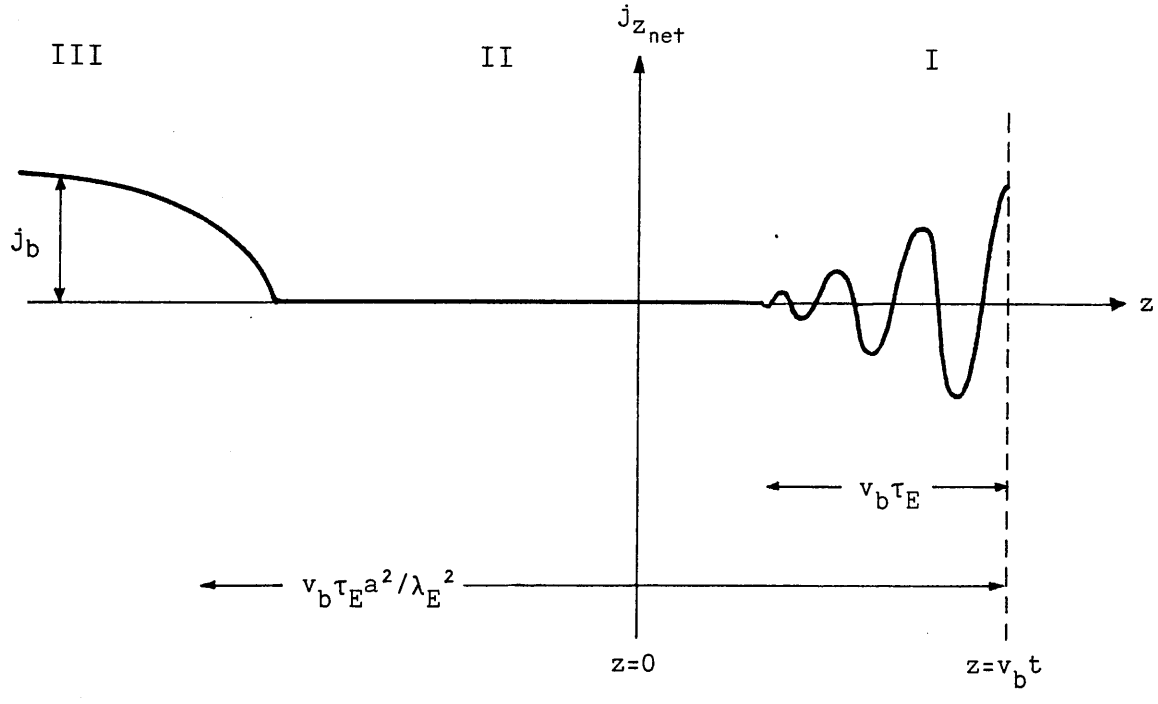

Figure 2.1 The net current in a beam-plasma system in which beam deceleration is ignored (after Lee and Sudan (1971))

In reality, the beam is decelerated by the electric field driving the return current (Lovelace and Sudan (1971)) and also by collisions with plasma electrons, and is therefore stopped in some distance s (see Brown and Hayward (1982); Chapter 3 of this thesis). For solar parameters the diffusive decay length $\ell_d = v_b \tau_D$ is huge in comparison to s; e.g. with $v_b \sim c$ and τ_D given by (2.13), $\ell_d \sim 3.10^{24}$ cm which is $\sim 5.10^{13}\ R_\odot$, where $R_\odot \simeq 7.10^{10}$ cm is the solar radius. In other words, in solar beam-plasma systems, diffusive decay of the return current is totally negligible and region III of Figure 2.1 does not exist.

For all practical purposes then, the steady-state model of Knight and Sturrock (1977) (see Section 1.5) is correct: beam electrons injected at z = 0 are decelerated and brought to rest at a distance z = s, while a slow reverse current-neutralising drift of plasma electrons, maintained by an electric field, replenishes electrons at the beam injection site. This is the physical picture of the flare beam-plasma system implicit in subsequent chapters. As far as the two can meaningfully be distinguished, we make no attempt to present a unified treatment of the acceleration and propagation regions; this is beyond the scope of this thesis.

As shown by Sudan (1984), to allow charge neutralisation of the injected beam to take place, a process which occurs on a timescale $\simeq \tau_E$, the beam propagation time must satisfy

$$\tau_{prop} >> \left(\frac{L}{a}\right)^2 \frac{\eta}{4\pi} \simeq 8.10^{-16} \left(\frac{L_{10}}{a_9}\right)^2 T_6^{-3/2} \text{ seconds} \quad (2.15)$$

where L is the length of the plasma system into which the beam is injected (e.g. scale size of plasma containment vessel, coronal

loop half-length). Appropriately scaled solar parameters have again been taken. Combining Equations (2.14) and (2.15), the beam propagation time must satisfy

$$8.10^{-16}\left(\frac{L_{10}}{a_9}\right)^2 T_6^{-3/2} \ll \tau_{prop} \ll 2.10^8 B_2 R_9^3 T_6^{3/2} \mathcal{Y}_{36}^{-1} \qquad (2.16)$$

The stopping length, s, and beam propagation time, τ_{prop}, are related simply by

$$s = \int_0^{\tau_{prop}} v_b(t)\, dt \qquad (2.17)$$

As already noted (see Section 1.5), the injected beam loses energy in driving the return current against the plasma resistivity. Energy conservation in the beam-plasma system can be expressed by

$$\int_0^t RI_p^2\, dt_* + \frac{1}{2}\ell I_n^2 = \int_0^t I_b \frac{d}{dt_*}(\ell I_n) dt_* \qquad (2.18)$$

where $R = \eta/\pi a^2$ is the resistance of the plasma column per unit length, ℓ is the inductance per unit length and $I_n = I_p + I_b$ is the net current (Lovelace and Sudan (1971)). The first term on the LHS of Equation (2.18) represents ohmic dissipation of the return current and the second term is the stored magnetic energy in the net current system. The RHS represents work done by the beam in establishing the return current.

Let an injected beam current, I_b, have the time profile shown in Figure 2.2; the associated return current, I_p, decays away such that $I = \alpha I_b$, where $0 < \alpha \lesssim 1$, at the end of the beam pulse ($t = \tau_{prop}$).

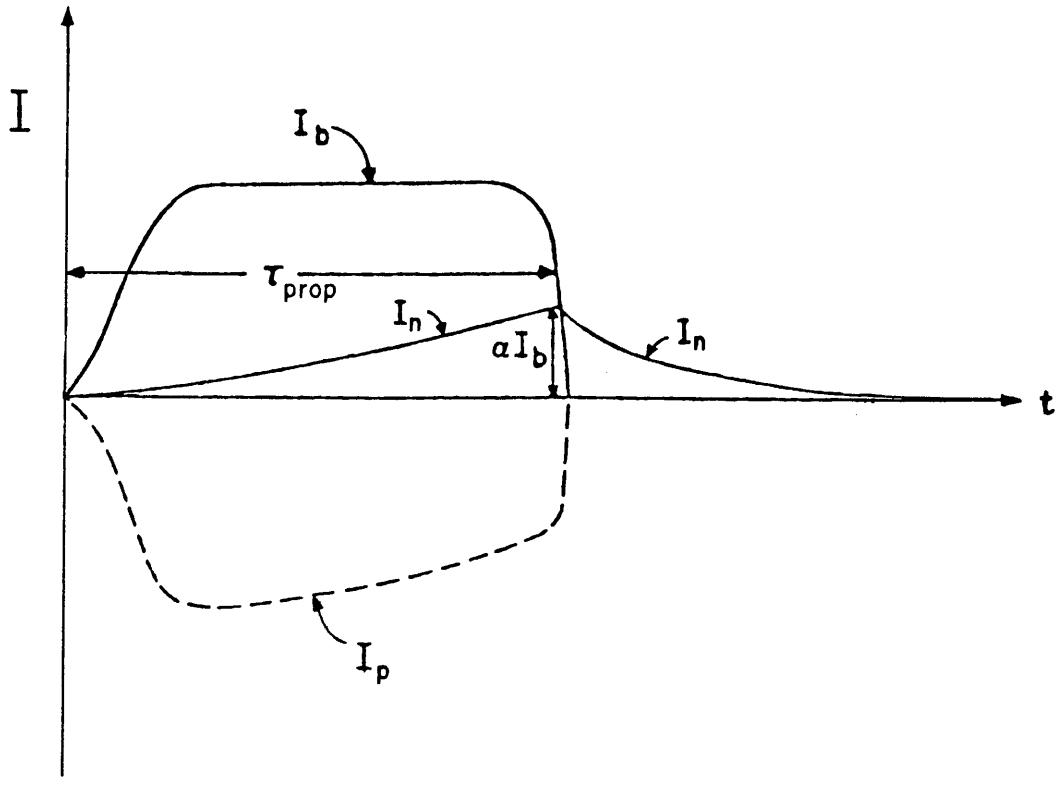

Figure 2.2: Beam current profile, I_b, with decay of return current, I_p, leaving a net current, $I_n = I_b$, at $t = \tau_{prop}$.

Assuming that the beam transit time, $L/v_b \ll \tau_{prop}$, and that beam energy and particle losses are negligible, the resistive energy loss is, from Equation (2.18),

$$W_R(\tau_{prop}) = \int_0^{\tau_{prop}} RI_p^2 \, dt = \frac{1}{2} \ell I_b^2 (2\alpha - \alpha^2) \qquad (2.19)$$

After the beam is switched off, a plasma current $I_p = \alpha I_b$ is induced in an attempt to maintain the net field (Lenz's law). This current decays, dissipating its energy $\frac{1}{2} \ell (\alpha I_b)^2$, so that the total resistive loss per unit length of the plasma channel is

$$W_R = \alpha \ell I_b^2 \qquad (2.20)$$

As shown by SS,

$$\alpha \simeq \frac{\tau_{prop}}{\tau_D} = \frac{\eta c^2 \tau_{prop}}{4\pi a^2} \qquad (2.21)$$

An enhanced resistivity, arising from anomalously large values of the effective electron-ion collision frequency in the presence of turbulence (e.g. ion-acoustic; see Appendix B), will obviously increase the energy taken from the beam and deposited in the plasma through ohmic dissipation. Such return current heating has been numerically simulated by Thode and Sudan (1975b). They find that, for return current drift velocities $v_d \gtrsim (T_e/m_e)^{\frac{1}{2}}$, the effective collision frequency $\nu_{eff} \simeq (0.2 - 0.4)\omega_{pi}$. The return current heats the ions and also the bulk of the electron distribution. Thode and Sudan (1975a,b) have also investigated the two-stream instability between the beam and plasma, and the interaction of this with the return current instability. However, we do not deal with these topics in this thesis (cf. Section 1.6).

We now return to the controversy over electrostatic/inductive effects as encapsulated in SS v BB (see Section 1.5). SS claim that an induction electric field is generated at the beam head due to the large value of $\frac{\partial \tilde{B}}{\partial t}$ as the beam head passes any given location in the plasma. Spicer (personal communication, 1986) has, in fact, claimed that electrostatic effects are unimportant because there is no net space charge at the head of the beam. He refers to solution (2.9) for the plasma current density which has a rapidly oscillating component and concludes that the mean charge density is zero at the beam head. One must be careful here. Solution (2.9) does not incorporate the damping term $e^{-\nu_{ei}t/2}$ due to collisions; also the existence of a net space

charge depends upon both the plasma and beam components. In fact, there is a net charge, sustained by beam electrons at the head and confined to a layer of thickness $\Delta z \simeq v_b \tau_E$ (region I in Figure 2.1) as shown by BB.

We can consider this net charge to give rise to an electric field, E, in accordance with $\nabla . \underset{\sim}{E} = 4\pi\rho$ (Poisson's equation). The curl of this $\underset{\sim}{E}$ describes the time rate of change in $\underset{\sim}{B}$, through $\nabla \times \underset{\sim}{E} = -\frac{1}{c}\frac{\partial \underset{\sim}{B}}{\partial t}$. Inductive effects may be non-negligible at large times, t, after beam head passage: $\tau_E << t \sim \tau_D$, when ohmic decay of the return current becomes important. In this regime there exist large values of $(\nabla \times \underset{\sim}{B})_z$. However, as explained earlier, the effect of $\underset{\sim}{E}$ and collisions is to stop the beam on a timescale $<< \tau_D$, in the solar case at least, so that inductive effects are never important. SS claim that flare beam radii are somewhat smaller than generally believed, which would lead to smaller values of τ_D (see Equation (2.12)). However, as explained in Section 1.5, there are several major difficulties with this supposition. In any case, it is not central to the understanding of the physics of electrostatic/inductive aspects of return current generation.

In this section we have discussed the phenomenon of beam injection into a plasma and the resultant setting-up of a return current. There are many aspects of beam-plasma processes not touched upon here and the reader is again referred to the reviews mentioned earlier. As this thesis deals with the effects of the return current instability, we next look at the two important wave modes which can be excited: the ion-acoustic and ion-cyclotron instabilities.

2.3 ION-ACOUSTIC INSTABILITY

One of the objectives of plasma kinetic theory is, given the

distribution functions of the particles present (e.g. electrons, ions), to determine the possible collective modes of plasma oscillation. The initial value problem of Landau (1946), in which a small perturbation is applied to a plasma equilibrium, yields a dispersion relation of the form $D[k,\omega(k)] = 0$ (see Appendix A). For each plasma mode this relates the angular frequency, ω, to the wave number k. (See Chapter 5 for an analysis of the dispersion relation describing a population of electrons drifting through a charge-neutralising ion background: the return current problem).

If one of the solutions (i.e. modes) of the dispersion relation has a positive growth rate, $\gamma \equiv I_m(\omega(k)) > 0$, then it is said to be unstable. Electrostatic modes become unstable when the relative drift, v_d, between two species of plasma particles becomes sufficiently large (Penrose (1960)). The wave energy density (i.e. wave level) associated with the unstable mode grows exponentially, in the linear theory, and the plasma becomes turbulent. The particle distributions may deviate considerably from Maxwellians, with the formation of high energy tails, and non-linear mechanisms may occur, such as trapping of particles in the potential wells associated with the waves. Saturation of wave-growth will then take place.

The effect of turbulence on the transport properties of the plasma is probably the most important aspect of kinetic theory. If the wave level is not too high: $W/nT \ll 1$, i.e. wave energy density $\ll$ thermal energy density, then anomalous transport coefficients are frequently derived analogously to classical coefficients by use of an enhanced effective collision frequency (see Appendix B). A general theory of anomalous transport is not easily obtainable, but the ion-acoustic instability is one of the most well-researched and we review its

relevant features in this section.

Ion-acoustic waves are longitudinal electrostatic plasma oscillations in which the ions participate, and have the following properties:

1. $\omega \propto k$ for small k: $\omega/k \simeq c_s = (T_e/m_i)^{\frac{1}{2}}$, the ion sound speed.
2. small phase velocity, $\omega/kv_e << 1$
3. short wavelength, $\lambda << v_e/\Omega_e$ (i.e. distance travelled by thermal electron in one gyro period).
4. low fluctuation levels, $W/nT << 1$.

In the case of an electrostatic instability, the threshold drift speed, v_{crit}, for generation of the fastest growing mode, given the value of T_e/T_i (we assume a simple electron-ion plasma here), is found by setting $\gamma = \frac{d\gamma}{dk} = 0$ (Fried and Gould (1961); Stringer (1964); Kindel and Kennel (1970)). Therefore, if $v_d > v_{crit}$, unstable wavegrowth takes place and transport properties are modified. It is of particular interest to calculate the ratio of electron and ion heating rates in the presence of anomalous resistivity arising from wave-particle "collisions". Kovrizhnykh (1967a) has derived heating equations for the electrons and ions in the case of the ion-acoustic instability driven by an applied electric field, and we discuss his work below.

Assume a spatially homogeneous, non-magnetised fully ionised plasma with $T_e >> T_i$ in an external electric field $\underset{\sim}{E}$. The electron and ion distribution functions are <u>not</u> assumed to be Maxwellians; however, $f_i(\underset{\sim}{v},t)$ is taken to be isotropic. The equations representing the evolution in time of $f_e(\underset{\sim}{v},t)$ and $W(\underset{\sim}{k},t)$, the spectral density of the ion-acoustic wave energy, are

$$\frac{\partial f_e}{\partial t} - \frac{e\underset{\sim}{E}}{m_e} \cdot \frac{\partial f_e}{\partial \underset{\sim}{v}} = \frac{\partial}{\partial v_i} D_{ij} \frac{\partial f_e}{\partial v_j} + St(f_e); \quad ij=1,2,3 \qquad (2.22)$$

$$\frac{\partial W}{\partial t} = (\gamma_s - \gamma)W \quad ; \quad \gamma = \gamma_i + \gamma_{coll} \tag{2.23}$$

The first term on the RHS of (2.22), which is proportional to the diffusion coefficient

$$D_{ij} = \frac{\pi m_i}{m_e^2 n_e} \int d\underset{\sim}{k}\, s^2 W(\underset{\sim}{k}) k_i k_j \delta(\omega_{\underset{\sim}{k}} - \underset{\sim}{k}.\underset{\sim}{v}) \tag{2.24}$$

describes electron scattering by ion-acoustic waves, and the second takes into account electron-ion and electron-electron collisions. In (2.24), $s = s(k) = \omega(k)/k$, the phase velocity of the waves.

In (2.23), γ_s describes the excitation of ion-acoustic waves by the electrons drifting through the ions, γ_i represents ion Landau damping, and γ_{coll} represents damping due to ion-ion collisions. Note that, since we assume $T_e >> T_i$, $\frac{\partial f_e}{\partial v} \simeq 0$ in the phase velocity region of the sound waves and so electron Landau damping/growth is negligible.

The evolution of the ion-acoustic instability can be broken up into two stages:

1. The applied electric field causes v_d to grow until v_{crit} is reached and ion-acoustic waves are generated, initially at an exponential rate. Scattering of electrons by sound waves becomes significant, $\gamma_s(k)$ decreases and its maximum value shifts to larger k. Waves with small k begin to attenuate. The anistropic part of $f_e(\underset{\sim}{v},t)$ changes quite rapidly.

2. W and v_d change slowly, increasing only with increasing T_e and T_i.

The first stage is not amenable to analytic solution and can be investigated in detail only by means of numerical computation. Kovrizhnykh (1967a) therefore limits his study to the second, quasi-

stationary stage. It is this stage of the instability which we attempt to model by means of a marginal stability approach (see Chapter 4) in later parts of this thesis. It is assumed that the first stage, which lasts on a very short timescale $\sim \omega_{pe}^{-1}$, is unimportant energetically (plasma heating takes place on a timescale of order $\nu_{ei}^{-1} >> \omega_{pe}^{-1}$).

The most rapid process for the bulk of the particles (i.e. with $v \sim v_e$, the electron thermal speed) is momentum relaxation. It is therefore assumed that the isotropic part, $f_e^{(o)}$, of the electron distribution is large compared to the anisotropic part, $f_e^{(1)}$. In the equation describing the time evolution of $f_e^{(1)}$, obtained from (2.22), the derivative $\frac{\partial f_e^{(1)}}{\partial t}$ is taken to be negligible compared to the diffusion terms. Finally, assuming that W varies on a timescale $<<\gamma_s^{-1}$, so that $\frac{\partial W}{\partial t} << \gamma_s W$, it is possible to solve the system of nonlinear equations (2.22) and (2.23). This yields the quasistationary electron distribution function and spectrum of ion-acoustic turbulence.

The electron heating equation is obtained from the second velocity moment of (2.22):

$$\frac{dT_e}{dt} = \frac{2}{3}\left[eEv_d - \gamma(k_o)\frac{\mathcal{E}}{n}\right] - \frac{2\sqrt{2}m_e}{3\sqrt{\pi}m_i}\nu_{ei}(T_e - T_i) - \left(\frac{dT_e}{dt}\right)_{inel} \qquad (2.25)$$

(1) (2) (3) (4)

where $\mathcal{E} = \int W(\underset{\sim}{k})d\underset{\sim}{k}$ is the total energy content of the ion-acoustic waves and k_o is the wave number corresponding to the phase velocity,

$$s_o \simeq \left(\frac{T_e}{m_i}\right)^{\frac{1}{2}}\left[\frac{\nu_{ei}}{\omega_{pe}}\left(\frac{m_i}{m_e}\frac{T_e}{T_i}\right)^{\frac{1}{2}}\right]^{1/5} \qquad (2.26)$$

(Note that the phase velocity increases slowly with increasing electron-ion collision frequency, ν_{ei}).

The physical meaning of the terms on the RHS of (2.25) are as follows:

(1): ohmic heating of the electrons,

(2): cooling due to excitation of ion-acoustic waves,

(3): collisional energy exchange between electrons and ions,

(4): losses due to inelastic processes (e.g. bremsstrahlung).

Note that the ion heating equation can be obtained simply from energy conservation:

$$\frac{dT_i}{dt} = \frac{2}{3}\gamma(k_o)\frac{\mathcal{E}}{n_e} + \frac{2\sqrt{2}\, m_e}{3\sqrt{\pi} m_i}\nu_{ei}(T_e - T_i) - \left(\frac{dT_i}{dt}\right)_{inel} \qquad (2.27)$$

As shown by Kovrizhnykh, the term $\gamma(k_o)\mathcal{E}/n_e$ can be transformed to a simpler form, not containing $\gamma(k_o)$:

$$\frac{\gamma(k_o)\mathcal{E}}{n_e} \simeq e\, Es_o \qquad (2.28)$$

The cooling of the electrons, represented by term (2), in equation (2.25), proceeds at a rate proportional to the external electric field E. This represents an energy gain to the ions (see Equation (2.27)). Terms (1) and (2) in (2.25) can be combined as follows:

$$n_e E v_d - \gamma(k_o)\mathcal{E} = n_e e\, v_d\, E\left(1 - \frac{s_o}{v_d}\right), \quad \text{by (2.28)}$$

$$= \chi_{IA}\, \eta_{IA}\, j^2$$

using $E = \eta_{IA} j$ (Kovrizhnykh implicitly neglects the Spitzer resistivity, η_{cl}), $j = n_e e\, v_d$ and setting

$$\chi_{IA} = 1 - \frac{s_o}{v_d} \qquad (2.29)$$

The electron and ion heating equations, (2.25) and (2.27), can therefore be rewritten as

$$\frac{3}{2} n_e \frac{dT_e}{dt} = \chi_{IA} \eta_{IA} j^2 + \frac{3}{2} n_e \nu_{eq}(T_i - T_e) - \frac{3}{2} n_e \left(\frac{dT_e}{dt}\right)_{inel} \quad (2.30)$$

$$\frac{3}{2} n_e \frac{dT_i}{dt} = (1 - \chi_{IA})\eta_{IA} j^2 + \frac{3}{2} n_e \nu_{eq} (T_e - T_i) - \frac{3}{2} n_e \left(\frac{dT_i}{dt}\right)_{inel} \quad (2.31)$$

where $\nu_{eq} = \left(\frac{2}{\pi}\right)^{\frac{1}{2}} \frac{m_e}{m_i} \nu_{ei}$. Classical ohmic dissipation can be included by adding $\eta_{cl} j^2$ to the RHS of (2.30)

We can regard the ion-acoustic waves as acting as an intermediary for energy exchange between electrons and ions. The function χ_{IA} therefore incorporates the anomalous transport effects and gives the fraction of ohmic dissipation $\eta_{IA} j^2$ absorbed by the electrons as a result of ion-acoustic turbulence being present. Consequently, $(1-\chi_{IA})$ is the fraction absorbed by the ions. A turbulent wave level requires a current density to sustain it; with $j = 0$, the wave energy density is that of the random electrostatic fluctuations in thermal equilibrium and the electrons and ions exchange energy by Coulomb collisions only, i.e. via the terms in $(T_e - T_i)$ in (2.30) and (2.31).

Kovrizhnykh (1967a) assumed that the ion distribution function is isotropic and that quasi-linear effects reduce the wave spectrum to a single wave number, k_o, with constant growth rate $\gamma > 0$ in a cone with opening angle $|\theta| < \frac{\pi}{2}$ about the drift direction. Particle simulations and experiments, however, show a broad spectrum in k and the formation of strongly anisotropic ion tails (Dum (1978a)). In addition to the collisional damping due to ion-ion pair collisions (see (2.23)), Cerenkov absorption of the waves by the ions can then take place. This may result in rapid heating of resonant ions, whose effective temperature may considerably exceed the bulk electron temperature (Kovrizhnykh (1967b)).

Although the assumptions were made of having a driving external electric field, an isotropic $f_i(\underset{\sim}{v}.t)$ and $T_e >> T_i$, the result (2.29) has been confirmed in a more general treatment by Tange and Ichimaru (1974). In developing their theory of anomalous resistivity and turbulent heating in plasmas, they derived the following expression for the ratio of electron and ion heating rates due to some scattering process, ℓ:

$$\frac{\chi_\ell}{1 - \chi_\ell} = \frac{\langle\omega\rangle_\ell - \langle \underset{\sim}{k} \rangle_\ell \cdot \underset{\sim}{v}_d}{\langle \omega \rangle_\ell} \qquad (2.32)$$

where $\langle\ \rangle_\ell$ indicates averaging over the spectrum of turbulent fluctuations. Rearranging (2.32):

$$\chi_\ell = 1 - \frac{\langle \omega \rangle_\ell}{\langle \underset{\sim}{k} \rangle_\ell \cdot \underset{\sim}{v}_d} \qquad (2.33)$$

Using the fact that the typical phase velocity $\langle\omega\rangle / |\langle \underset{\sim}{k} \rangle|$ of ion-acoustic waves is around c_s, we obtain

$$\chi_{IA} \simeq 1 - \frac{c_s}{v_d} \qquad (2.34)$$

in agreement with (2.29). We may conclude that the method by which the instability is excited leads to the same result: either an applied $\underset{\sim}{E}$ - field or given drift speed profile, $v_d(t)$, prescribed by beam injection, may be employed. Equation (2.34) will be utilised in Chapters 4, 6 and 7 when we consider anomalous ohmic dissipation due to ion-acoustic waves generated by the return current for a specified injected beam current profile $j_b(t)$. The more general expression, (2.33), can be applied to other types of turbulence, e.g. ion-cyclotron (see Section (2.4)).

As mentioned previously, the growth in wave level, which is initiated by the drift speed exceeding the threshold speed for instability, proceeds until saturation occurs. The growth rate is determined by the combined effects of the destabilising electron resonance and the stabilising ion resonance in the velocity region of the sound waves. As the wave level grows, the resonance widths are broadened with the delta function, $\delta(\omega_{\underset{\sim}{k}} - \underset{\sim}{k}.\underset{\sim}{v})$ of (2.24) being replaced by a function of the form,

$$R_{\underset{\sim}{k}} = \frac{1}{(2\pi)^{\frac{1}{2}}\, \underset{\sim}{k}\, \Delta W_{\underset{\sim}{k}}} \exp\left[- \frac{(\omega_{\underset{\sim}{k}} - \underset{\sim}{k}.\underset{\sim}{v})^2}{2k^2 \Delta W^2_{\underset{\sim}{k}}} \right] \qquad (2.35)$$

where $\Delta W_{\underset{\sim}{k}}$ measures the width of the resonance (Wesson and Sykes (1973)). The effect of the resonance broadening is to stabilise the turbulent wavegrowth; saturation occurs when the resulting nonlinear growth rate becomes zero.

Which saturation mechanism actually occurs depends on the physical conditions of the plasma. Smith and Priest (1972) and Hasegawa (1974) discuss several candidates, the non-linear three-wave interaction investigated by Tsytovich (1971) having the lowest threshold. Tsytovich's mechanism is the decay of an ion-acoustic wave into two ion-acoustic waves with wave vectors $\underset{\sim}{k}'$ and $\underset{\sim}{k}''$, and frequencies ω' and ω'' satisfying the conservation laws

$$\omega = \omega' + \omega'' \qquad (2.36)$$

$$\underset{\sim}{k} = \underset{\sim}{k}' + \underset{\sim}{k}'' \qquad (2.37)$$

Saturation occurs at an effective electron collision frequency given by,

$$\nu_{eff} \simeq 10^{-2} \left(\frac{v_d}{c_s}\right) \omega_{pi} \qquad (2.38)$$

The saturation wave level can then be found from

$$\left(\frac{W}{n_e T_e}\right)_{sat} \simeq \frac{\nu_{eff}}{\omega_{pe}} \qquad (2.39)$$

(Note that both W itself and W normalised to the electron thermal energy density are frequently referred to as the "wave level" ; see Appendix B).

In our wavegrowth analysis of return current instability in Chapter 6, because of the difficulties in properly describing the complicated evolution of ion-acoustic turbulence, we make the following simplifying assumption: at the threshold of wave generation, i.e. at $v_d = v_{crit}$, ion-acoustic waves are allowed to grow from the thermal level (see Appendix B) with an assumed linear growth rate, until the saturation wave level, given by (2.38) and (2.39) is reached. The subsequent behaviour of the plasma then depends on whether or not v_d ever drops below v_{crit} again (see Chapter 6).

For completeness, we mention briefly the phenomenon of ion-acoustic double layers. As the name implies, a double layer consists of two equal, oppositely charged, laminar space-charge layers and can sustain a large potential difference over a local region (see Carlquist (1979a); Michelsen and Rasmussen (1982); Sehrittwieser and Eder (1984)). This potential difference is capable of accelerating electrons and ions; such an acceleration mechanism has been proposed for solar flares by Carlquist (1969, 1979b). Numerical simulations suggest that the ion-acoustic instability leads to the formation of double layers in a sufficiently long system (Sato and Okuda (1980, 1981)). Since the collisional mean free path greatly exceeds the double layer thickness, double layers are essentially collisionless. Mathematically, the equations describing them are nonlinear and yield shocklike solutions

(Raadu (1986)). However, the role of double layers in anomalous transport is not well established and, in any case, they are not generally considered relevant to flares (Heyvaerts (1981)). We do not discuss the issue further, referring the reader to the cited references instead.

2.4 ION-CYCLOTRON INSTABILITY

In a magnetised plasma, there arises the possibility of the ion-cyclotron mode being excited. For $0.1 \lesssim T_e/T_i \lesssim 8$, the threshold drift speed for this instability is less than that for the ion-acoustic mode. (Kindel and Kennel (1971)). Ion-cyclotron waves are electrostatic ion oscillations which propagate almost perpendicular to the external field, $\underset{\sim}{B}_o$. (If the oscillations have wave vector $\underset{\sim}{k} \perp \underset{\sim}{B}_o$ they are known as lower hybrid waves and have different properties; see Chen (1984)). Their general characteristics are:

1. $k^2\rho_i^2 \sim 1$
2. $k^2\rho_e^2 << 1$
3. $k \simeq k_\perp >> k_{\parallel}$

where $\rho_\alpha \equiv v_\alpha/\Omega_\alpha$, $v_\alpha^2 \equiv T_\alpha/m_\alpha$, $\Omega_\alpha \equiv q_\alpha B_o/m_\alpha c$ (α is the species type).

Drummond and Rosenbluth (1962) derived the dispersion relation for ion-cyclotron waves, assuming Maxwellian distributions for the electrons and ions, with a relative drift v_d:

$$1 + \zeta Z(\zeta) - \frac{T_e}{T_i} \sum_{n=-\infty}^{\infty} \frac{\Gamma_n n\Omega_i}{\omega - n\Omega_i} = 0 \qquad (2.40)$$

where $\zeta = \dfrac{\omega - kv_d}{\sqrt{2}\, k_{\parallel} v_e}$, Z is the plasma dispersion function (see Appendix A) and $\Gamma_n(s_i) = \exp(-s_i) I_n(s_i)$, where $s_i = k_\perp^2 \rho_i^2$ and I_n is the modified Bessel function. The theory was confirmed by the first observations of ion-cyclotron waves by D'Angelo and Motley (1962).

The work of Drummond and Rosenbluth (1962) was later extended by others, including Kindel and Kennel (1971), Lee (1972), Dakin et al. (1976) and Benford (1976). We may obtain a simple analytic form, with T_e/T_i as the independent variable, for the critical ion-cyclotron drift speed, v_{IC}, as follows. By solving the dispersion relation (2.40) for the fastest growing mode, Dakin et al. (1976) find

$$\frac{v_{IC}}{v_e} = \frac{\omega}{k_{\parallel} v_e} + \frac{T_e}{T_i} \cdot \frac{\omega \Gamma_1}{k_{\parallel} v_i} \exp(-\zeta_i^2) \qquad (2.41)$$

where $\Gamma_1 \simeq 0.22$, $\zeta_i^2 \simeq \ell n\,[2(m_i/m_e)^{\frac{1}{2}} \Gamma_1]$. Algebraic manipulation yields the result,

$$\frac{v_{IC}}{v_e} \simeq \frac{\omega}{k_{\parallel} v_e} \left[1 + 0.5 \left(\frac{T_e}{T_i}\right)^{3/2} \right] \qquad (2.42)$$

If we substitute the following approximations into (2.42):

$$\omega \simeq \Omega_i \qquad (2.43)$$

$$k_{\parallel} \rho_i \simeq \delta[\ell n\,(m_i/m_e)]^{-\frac{1}{2}}, \quad \delta \equiv \Gamma_1 \frac{T_e}{T_i} \qquad (2.44)$$

(Drummond and Rosenbluth (1962)) we find that,

$$\frac{v_{IC}}{v_e} \simeq 0.29 \left(\frac{T_i}{T_e}\right)^{3/2} \left[1 + 0.5 \left(\frac{T_e}{T_i}\right)^{3/2} \right] \qquad (2.45)$$

The term $0.5\,(T_e/T_i)^{3/2}$ has frequently been neglected by authors on the ill-founded supposition that $T_i >> T_e$ in ion-cyclotron turbulence, e.g. Hinata (1980) ; Pritchett et al. (1981); Benford (1981).

The expression (2.45) is a reasonable fit to the numerically derived curve of Kindel and Kennel (1971). Taking the more accurate term $\omega \simeq \Omega_i(1+\delta)$ in (2.42) (Dakin et al., 1976), rather than using

(2.43), actually leads to a poorer fit; i.e. the other approximations used in the derivation of (2.45) must also be taken concurrently to higher order. We therefore take the following direct analytic fit to the function $v_{IC}(T_e/T_i)$ as depicted in Kindel and Kennel (1971):

$$\frac{v_{IC}}{v_e} \simeq 0.6 \left(\frac{T_e}{T_i}\right)^{-0.78} \tag{2.46}$$

As in the case of ion-acoustic turbulence, we would like to derive an expression for the ratio of heating rates for electrons and ions. Dakin et al., (1976) find,

$$\chi_{IC} \simeq 1 - \frac{\Omega_i}{k_{11} v_d} \tag{2.47}$$

in agreement with the result of Tange and Tchimaree (1974) - Equation (2.33) - where $<\omega> \simeq \Omega_i$ and $<\underset{\sim}{k}>.\underset{\sim}{v_d} \simeq k_{11} v_d$. In principle, we should be able to obtain an expression for χ_{IC} in <u>marginal stability</u> (see Chapter 4) by setting $v_d = v_{IC}$. Substituting (2.44) into (2.47) using $\rho_i = v_i/\Omega_i$, gives

$$\chi_{IC} \simeq 1 - 0.29 \left(\frac{T_e}{T_i}\right)^{3/2} \frac{v_e}{v_{IC}} \tag{2.48}$$

Taking representative values of $\frac{T_e}{T_i}$ and calculating the corresponding values of $\frac{v_{IC}}{v_e}$ from (2.46), we find the following results for χ_{IC} in marginal stability:

$\frac{T_e}{T_i}$	$\frac{v_{IC}}{v_e}$	χ_{IC}
0.5	1.0	0.20
0.6	0.89	0.30
1.0	0.60	0.52
2.0	0.35	0.71
3.0	0.26	0.79
4.0	0.20	0.82
5.0	0.17	0.85

<u>Table 2.1</u>: Values of χ_{IC}, $\frac{v_{IC}}{v_e}$ for Representative Values of $\frac{T_e}{T_i}$.

From Table 2.1 we might conclude that χ_{IC} is a monotonically increasing function of T_e/T_i and that for $T_e/T_i > 1$, electrons are preferentially heated ($\chi_{IC} > 0.5$). These two ostensible properties of ion-cyclotron waves are in direct contradiction with the work of Dakin et al. (1976), in which ions are preferentially heated, and Duijveman et al., (1981) who show that not only is $\chi_{IC} < 0.5$, but that $\chi_{IC}(T_e/T_i)$ is a monotonically decreasing function. Our conclusion must be that the above analysis, based on the linear characteristics of ion-cyclotron waves, is too simplistic and does not properly describe the heating of the electrons and ions by the unstable mode.

It would appear that Duijveman et al., (1981) have performed the most rigorous calculations of χ_{IC} in marginal stability, based on the work of Tange and Tchimaru (1974). They do not, however, give an explicit form for the function $\chi_{IC}(T_e/T_i)$; we therefore take the following approximate analytic fit to their curve:

$$\chi_{IC} \simeq 0.14 \left(\frac{T_e}{T_i}\right)^{-0.5} \qquad (2.49)$$

When saturation occurs (see below) and the plasma is no longer in a state of ion-cyclotron marginal stability, χ_{IC}^{sat} can be derived by utilising continuity of χ_{IC} in T_e/T_i. Assuming that the wave spectrum is still peaked about the wave vector where the growth rate is a maximum, Duijveman et al. (1981) show that the quantity $\omega/k_{ll}v_e$ is a constant for a given T_e/T_i. Hence

$$\chi_{IC}^{sat} = 1 - \frac{\omega}{k_{ll}\, v_e} \cdot \frac{v_e}{v_d}$$

$$= 1 - \text{constant} \cdot \frac{v_e}{v_d}$$

The constant is found by noting that when $v_d = v_{IC}$, $\chi_{IC}^{sat} = \chi_{IC}$

(assuming continuity of χ_{IC}).

$$\therefore \text{ constant } = (1 - \chi_{IC}) \frac{v_{IC}}{v_e}$$

$$\therefore \chi_{IC}^{sat} = 1 - (1 - \chi_{IC}) \frac{v_{IC}}{v_d}$$

$$\therefore \chi_{IC}^{sat} = 1 - 0.6 \left(\frac{T_e}{T_i}\right)^{-0.78} \left[1 - 0.14 \left(\frac{T_e}{T_i}\right)^{-0.5}\right] \frac{v_e}{v_d} \qquad (2.50)$$

from (2.46) and (2.49).

In early models of ion-cyclotron turbulence, saturation was assumed to occur at low levels by quasi-linear formation of a plateau in the electron distribution function (Drummond and Rosenbluth (1962)) at an effective collision frequency

$$\nu_{eff} \simeq \nu_{ei} \left(1 + \frac{v_d}{v_e}\right) \qquad (2.51)$$

(Petviashvili (1974)). However, studies of ionospheric ion heating (Palmadesso et al. (1974)) indicate that this process is inhibited by collisions and spatial effects, and that saturation takes place by ion resonance broadening (Dum and Dupree (1970)). This mechanism is described by a modified quasi-linear theory which takes account of the random particle motion on the linear wave-particle resonance. The phase relation between the wave and a resonant particle is destroyed over a collision time. This limitation in time is equivalent to a broadening of frequencies for resonance, allowing more particles to exchange energy with the wave mode. Saturation will result if the ion resonance is broadened adequately such that a sufficient number of particles (ions) can extract energy from the wave.

Adopting this model of saturation, Ionson (1976) obtained the effective collision frequency at saturation:

$$\nu_{eff} \simeq 0.2\ \Omega_i \left(1 - \frac{12\ v_i}{v_d}\right) \qquad (2.52)$$

The anomalous resistivity (and therefore the wave level) derived by Ionson is found to be in agreement with numerical simulations of the ion-cyclotron instability (Pritchett et al (1981)). In these particle simulations, saturation actually occurs due to the flattening of the parallel electron distribution; the saturation levels are higher than those attained in the quasi-linear theory of Drummond and Rosenbluth (1962) which breaks down when the wave level becomes too high. (A point of interest is that the ion-acoustic instability is also excited in these simulations; it is found that, typically $\eta_{IA} \gtrsim 10\eta_{IC}$). These levels of saturation have been confirmed by satellite observations of auroral regions (Hudson et al. (1978)). In other words, there is good agreement between theory, observation and particle simulations in predicting turbulent wave levels for the ion-cyclotron instability; the levels attained are not very sensitive to the details of the saturation mechanism.

The result of Ionson (1976), i.e. Equation (2.52), is strictly only valid in an isothermal (i.e. $T_e/T_i \simeq 1.0$), Maxwellian plasma in which $v_d \lesssim 13\, v_i$. A more general form can be derived for the saturation amplitude which is given by (Dum and Dupree (1970); Palmadesso et al. (1974)).

$$W_{IC}^{sat} = \frac{k_l^2 T_i^2}{2\pi e^2 n_e T_e} \left(\frac{\omega - \Omega_i}{\Omega_i} \right)^2 \qquad (2.53)$$

Using $s_i \equiv k_l^2 \rho_i^2 \simeq 1.2^2$ and $\omega \simeq \Omega_i(1+\delta)$ (Drummond and Rosenbluth (1962)) in Equation (2.53) we arrive at the result

$$W_{IC}^{sat} \simeq 0.14 \frac{\Omega_i^2}{\omega_{pi}^2} \cdot \frac{T_e}{T_i} \qquad (2.54)$$

or, normalising to solar flare parameters,

$$W_{IC}^{sat} \simeq 7.4 \ 10^{-7} \ \frac{B_2^2}{n_{e_{ll}}} \cdot \frac{T_e}{T_i} \qquad (2.55)$$

in the usual notation; e.g. with $B_2 = 5$, $n_{e_{ll}} = 1$, $\frac{T_e}{T_i} = 1$, we find that $W_{IC}^{sat} \simeq 1.8 \ 10^{-5}$. We make use of the result (2.55) in Chapter 7 when considering the excitation of the ion-cyclotron instability by return currents in solar flares. This concludes our survey of beam-plasma electrodynamics and of the two relevant wave modes for return current instability.

3. THE RETURN CURRENT MODEL

3.1 INTRODUCTION

In this chapter we set out explicitly our model of the flare beam-return current system. Dimensionless heating equations for the electrons and ions are derived and the important parameters of the problem are discussed. The ways in which the classical heating phase depend on these parameters are examined. In addition, we calculate the stopping length of the beam under the action of the decelerating electric field and collisions with the ambient plasma. A comparison is made between return current models with and without the effect of direct collisional heating by the beam. The work of this chapter forms the basis for later chapters when we consider the effects of the ion-acoustic (Chapters 4 and 6) and/or ion-cyclotron instabilities (Chapter 7).

As we saw in Section 1.3, the evidence is very strong that thick-target electron beams play a major role in the production of hard X-rays, via collisional bremsstrahlung, during the impulsive phase of solar flares. Such electron beams will also give rise to a considerable amount of flare atmospheric heating. It has been noted by several authors (e.g. Hoyng et al (1976)) that the large electron flux inferred from the observed X-ray emission in the thick-target model can only exist if a beam-neutralising return current is set up (see Section 1.5). Ohmic dissipation of this return current increases the energy loss of the beam electrons, which also lose energy in Coulomb collisions with the ambient plasma; because of this, the non-thermal bremsstrahlung efficiency is reduced. The effect of stable return current losses on the flare X-ray emission has already been analysed by Emslie (1980, 1981). In Chapters 4 and 7 we will investigate cases of a return

current unstable to the ion-acoustic and/or ion-cyclotron instabilities, and the resultant hard X-ray emission.

3.2 THEORETICAL MODEL

We consider a warm, initially isothermal ($T_e = T_i = T_o$) fully ionised, homogeneous hydrogen plasma with number density $n_p (= n_e = n_i)$. Into this coronal plasma we inject a downward-moving electron beam with density $n_b(t)$ comprising electrons of a single constant energy, $\mathcal{E}_o$. The value $\mathcal{E}_o$ is intended, for simplicity, to represent a mean beam energy and not a delta function distribution which would be smeared out by quasi-linear relaxation of the beam (Emslie and Smith (1984); McClements (1987).

We assume a steady state for the beam-return current system (Knight and Sturrock (1977); Brown and Bingham (1984)): beam electrons are injected at a coronal site $z = 0$ and are brought to rest in a distance s (see below). The beam acceleration mechanism is not specified (see Section 1.4). Since, for coronal parameters, the beam stopping length $s \ll \ell_d$, the diffusive decay length, inductive effects are unimportant (see Section 2.2). A beam-neutralising backward drift of plasma electrons is maintained electrostatically and can replenish electrons at the beam injection site. In summary, current neutralisation demands that a return current is set up in the plasma such that the net current, i.e. plasma current $j_p(t)$ plus beam current $j_b(t)$, is zero.

We therefore have $j_p(t) = - j_b(t)$ which implies that

$$v_d(t) = - \frac{n_b(t)}{n_p(t)} v_b \qquad (3.1)$$

where $v_b = (2\mathcal{E}_o/m_e)^{\frac{1}{2}}$ is the constant injected beam velocity and $v_d(t)$ is the drift velocity of the plasma electrons with respect to the plasma ions.

We concentrate purely on electrostatic instability (ion-acoustic and/or ion-cyclotron) of the return current itself, assuming the beam to have been quasi-linearly relaxed with mean energy $\mathcal{E}_o$ (this process extracts little energy from the beam - McClements (1987)) and neglecting any interaction between the beam and the return current (cf. Section 1.6 and references therein). The anomalous resistivity η_{an} associated with a particular low-frequency wave mode (see Appendix B) has the property that $\eta_{an} = 0$ if the plasma drift speed $v_d < v_{crit}(T_e, T_i)$, the critical drift speed for that mode. When $v_d \geq v_{crit}$, electrostatic waves are generated and the total resistivity $\eta = \sum_{\ell} \eta_{\ell}$ increases due to wave-particle collisions (where the sum is taken over all scattering processes ℓ). As a result, the ohmic dissipation term ηj_p^2 rises, leading to enhanced plasma heating.

At this point we should state that, physically, there are two distinct models of plasma heating:

1. Cases where a specified beam current profile $j_b(t)$ $(= - j_p(t))$ is assumed, prescribed by beam injection from an "electron gun" at $z = 0$.
2. Cases where the electric field $E(t)$ is prescribed.

Model 2 was taken by Duijveman et al.(1981) in an attempt to simulate rapid plasma heating by anomalous effects in the solar atmosphere. However, in this model, the ohmic dissipation term E^2/η is reduced by any turbulent increase in the resistivity, a fact they appear to have overlooked. In other words, with a prescribed electric

field, anomalous resistivity leads to reduced rather, than increased, plasma heating. For this reason and because prescribing $j_b(t)$ corresponds more closely to the usually envisaged thick-target beam injection process, we have discarded model 2 and adopted model 1. Whether or not it is possible to set up such a beam injection process in the solar atmosphere in an electrodynamically self-consistent fashion is beyond the scope of this thesis.

We assume that a typical large solar flare value for the electron injection rate $F_o(s^{-1})$ is obtained after a linear increase from zero over t_r seconds, the rise time of the electron beam. However, we choose the beam area A to be well below the upper limit set by hard X-ray images. This is to ensure that unstable return current drift velocity thresholds are exceeded (since the purpose of this thesis is to investigate the effect of such instability):

$$F_o = 10^{36}\ s^{-1} \quad ; \quad A = 10^{16}\ cm^2 \qquad (3.2)$$

(see Hoyng et al.(1976) and Duijveman et al.(1982)). Our prescribed plasma current density as a function of time is, therefore,

$$j_p(t) = 5.10^{10}\ \frac{t}{t_r} \quad \text{statamps cm}^{-2} \qquad (3.3)$$

Although, in a magnetised plasma, ion-cyclotron waves have a lower threshold drift speed v_{crit} for $T_e/T_i \lesssim 8$ than ion-acoustic waves (Kindel and Kennel (1971)) they do not necessarily contribute greatly to the anomalous resistivity, depending on their saturation level (Papadopoulos (1977); Pritchett et al.(1981)). For this reason, and to gain insight, we first consider the problem of an unmagnetised plasma with only ion-acoustic waves generated. We do, however, return to the magnetised plasma problem and the effects of ion-cyclotron waves

later in this thesis (Chapter 7). By following this approach we hope to obtain a good understanding of the physics associated with the beam-driven return current instability.

The heating equations for the plasma electrons and ions, neglecting thermal conduction, convective and radiation losses (cf. Duijveman et al.(1981) and Section 4.4) are:

$$\frac{3}{2} n_p \frac{dT_e}{dt} = \frac{3}{2} n_p \frac{(T_i - T_e)}{\tau_{eq}} + \frac{2\pi e^3 \ell n \Lambda n_p j_p}{\epsilon_o} + \eta_{cl} j_p^2 + \chi_{IA} \eta_{IA} j_p^2 \quad (3.4a)$$

$$\frac{3}{2} n_p \frac{dT_i}{dt} = \frac{3}{2} n_p \frac{(T_e - T_i)}{\tau_{eq}} + (1 - \chi_{IA}) \eta_{IA} j_p^2 \quad (3.4b)$$

Note that the electron and ion temperatures T_e, T_i are expressed in energy units, unless stated explicitly otherwise.

The first quantity on the RHS of (3.4b) is the heat exchange term Q_i (cf. Appendix B, Equation (B.11)) where the electron-ion equilibration time $\tau_{eq} = \frac{m_i}{2m_e} \tau_e$.

$$\text{i.e. } \tau_{eq} = \left(\frac{9}{128\pi}\right)^{\frac{1}{2}} \frac{m_e m_i}{\ell n \Lambda n_p e^4} \left(\frac{T_e}{m_e}\right)^{3/2} \quad (3.5)$$

The classical, i.e. Spitzer (1962), resistivity is

$$\eta_{cl} \simeq \left(\frac{8\pi}{9}\right)^{\frac{1}{2}} m_e^{\frac{1}{2}} e^2 \ell n \Lambda T_e^{-3/2} \quad (3.6)$$

(see Appendix B).

As explained in Section 2.3, $\chi_{IA} = \chi_{IA} (T_e/T_i)$ represents the anomalous heating effects of scattering by ion-acoustic waves: χ_{IA} and $(1 - \chi_{IA})$ are the fractions of the anomalous ohmic power dissipation $\eta_{IA} j_p^2$ absorbed by the electrons and ions respectively; η_{IA} is the component of the total resistivity due to electrons scattering off ion-acoustic waves.

The second term on the RHS of (3.4a) denotes direct Coulomb collisional heating of the plasma electrons by the beam. Collisional heating by the beam electrons is, in fact, an inhomogeneous process; it varies with the energy and, therefore, depth of penetration into the plasma of the beam electrons. In order to avoid this complication and keep our equations homogeneous in space over the beam stopping length, we use a fixed collisional heating rate corresponding to the initial injection energy of $\mathcal{E}_o$.

The electron beam is decelerated by the effect of Coulomb collisions with the ambient plasma and also by the electric field that drives the return current (see Section 2.2). If we assume that the electron time of flight is short compared to the other timescales of the problem (e.g. rise time, heating time), then the beam has a "stopping length", s, due to collisional and ohmic losses (Brown and Hayward (1982)). We may calculate s as follows.

The energy loss equation for a beam electron of energy $\mathcal{E}$ is

$$\frac{d\mathcal{E}}{dt} = - e \eta j_p v_b - \frac{K v_b}{\mathcal{E}} \qquad (3.7)$$

where $K = 2\pi e^4 \ell n \Lambda n_p$ (Emslie (1978)). Making the change of variable $dz = v_b dt$, Equation (3.7) can be rewritten as

$$\frac{d\mathcal{E}}{dz} = -e \eta j_p - \frac{K}{\mathcal{E}} \qquad (3.8)$$

By integrating and using the boundary condition $\mathcal{E} = 0$ at $z = s$, we derive the correct energy-dependent solution for the stopping length:

$$s = s_o \left[1 - \frac{1}{\beta} \ell n(1 + \beta) \right] \qquad (3.9)$$

where $s_o = \frac{\mathcal{E}_o}{e\eta j_p}$ is the stopping length for injected electrons of energy $\mathcal{E}_o$ when ohmic losses only are considered, and $\beta = e\eta j_p \mathcal{E}_o/K$.

In our simplified model we take the collisional loss term in (3.7) to be $-Kv_b/\mathcal{E}_o$, independent of z. The beam stopping length in this case is

$$s = \frac{\mathcal{E}_o}{e\eta j_p + (\frac{K}{\mathcal{E}_o})} \qquad (3.10)$$

Since j_p is increasing with time (Equation (3.3)), and since the resistivity will change as the plasma evolves, we anticipate, from Equation (3.10), that the stopping length of the beam will also be varying considerably with time. It is important to realise, therefore, that the heating equations (3.4a) and (3.4b) apply, for all time, only to the plasma layer of thickness s_{min}, the smallest depth of beam penetration into the atmosphere. Only this region is heated continuously throughout the simulation.

The solution of Equations (3.4a) and (3.4b) for $T_e(t)$, $T_i(t)$ and $\eta(t)$ can be found numerically in a straightforward manner as long as v_d remains less than v_{crit}, but as soon as $v_d \geq v_{crit}$ we require an additional equation in order to determine η_{IA}. In the next section we will investigate in some detail the classical heating regime throughout which $v_d < v_{crit}$, and in Chapter 4 we will use the hypothesis of marginal stability to determine η_{IA} when $v_d \geq v_{crit}$.

3.3 CLASSICAL HEATING PHASE

We introduce for convenience the following dimensionless variables:

$$x \equiv \frac{T_e}{T_o} \quad , \quad y \equiv \frac{T_i}{T_o} \quad , \tau \equiv \frac{t}{\tau_{eq}(o)} \quad , \quad z_{IA} \equiv \frac{\eta_{IA}}{\eta_{cl}(o)} \qquad (3.11)$$

where T_o, $\tau_{eq}(o)$ and $\eta_{cl}(o)$ are the initial values of temperature, electron-ion equilibration time and classical resistivity respectively. With respect to these new variables, and using Equation (3.3) to substitute for $j_p(t)$, the heating Equations (3.4a) and (3.4b) become

$$\frac{dx}{d\tau} = \frac{(y-x)}{x^{3/2}} + B\tau + C\tau^2 \left(\frac{1}{x^{3/2}} + \chi_{IA} z_{IA}\right) \qquad (3.12a)$$

$$\frac{dy}{d\tau} = \frac{(x-y)}{x^{3/2}} + C\tau^2 (1 - \chi_{IA}) z_{IA} \qquad (3.12b)$$

where $$B = \frac{2.82\ 10^{34} T_o}{n_p^2 t_r \mathcal{E}_o} \quad \text{and} \quad C = 1.84\ 10^{65} \left(\frac{T_o}{n_p^2 t_r}\right)^2 \qquad (3.13)$$

We have assumed that the Coulomb logarithm $\ell n \Lambda = 20.0$ (see Appendix B). Note the initial conditions $x = 1$ and $y = 1$ at $\tau = 0$.

For the remainder of this section we will restrict our attention to classical heating for which $v_d < v_{crit}(T_e, T_I)$, the critical drift speed for ion-acoustic waves. The function $v_{crit}(T_e, T_i)$ was first calculated by Fried and Gould (1961) and we will take the following approximate analytic form for it:

$$v_{crit} = \frac{1.2\ T_i}{T_e} \left(\frac{T_e}{m_e}\right)^{\frac{1}{2}} \qquad (3.14)$$

i.e. in dimensionless variables,

$$v_{crit} = 1.2 \left(\frac{T_o}{m_e}\right)^{\frac{1}{2}} \frac{y}{x^{\frac{3}{2}}} \qquad (3.15)$$

In the classical heating regime $z_{IA} = 0$, and from Equations (3.12a), (3.12b) and (3.13) it is clear that the classical heating is completely specified as a function of dimensionless time τ by the two parameters $(T_o/n_p^2 t_r)$ and $T_o/\mathcal{E}_o$. Further, it is also clear, using

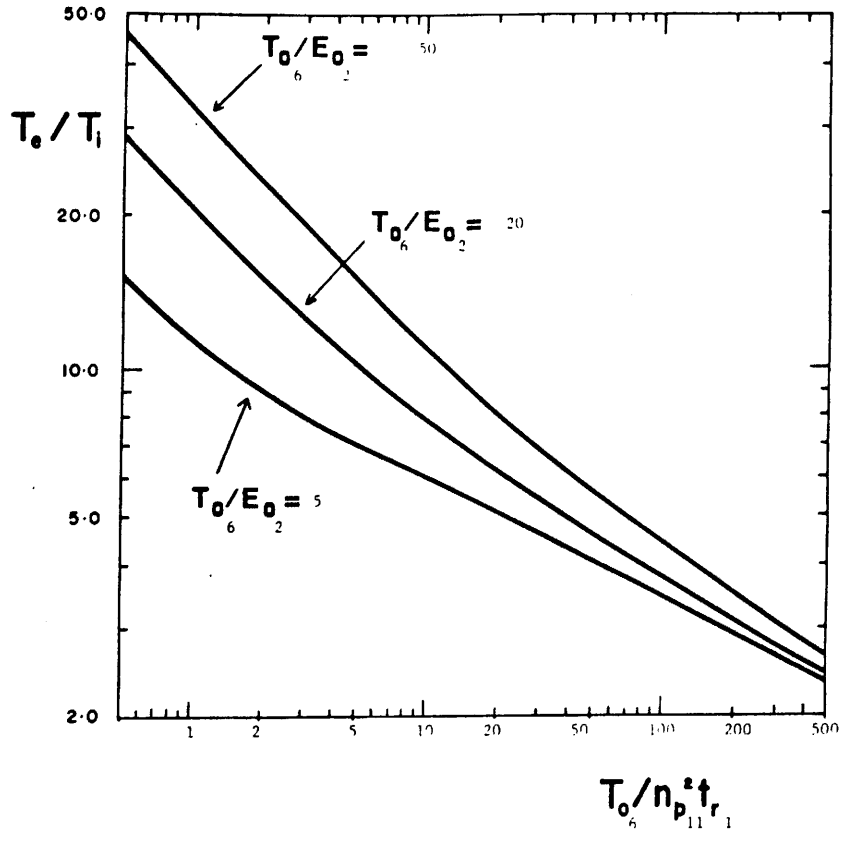

Figure 3.1: The electron-ion temperature ratio at onset of IA instability for the prescribed beam current profile (see text).

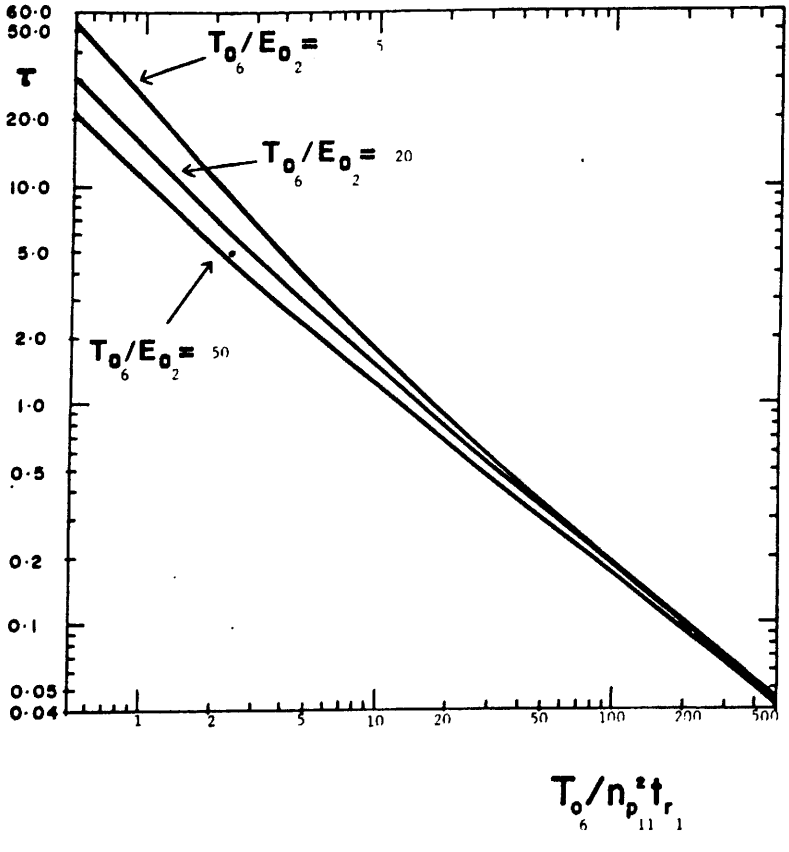

Figure 3.2: The dimensionless time τ taken to reach IA instability for the prescribed beam current profile.

Equation (3.5), that the classical heating is completely specified as a function of time t(= $\tau_{eq}(o)\,\tau$) by three parameters: $T_o/n_p^2\,t_r$, $T_o/\mathcal{E}_o$ and $T_o^{3/2}/n_p$.

As we shall see in Chapter 4, the value of T_e/T_i at the onset of the ion-acoustic instability turns out to be crucial for the subsequent anomalous evolution of the plasma. We have therefore solved Equations (3.4a) and (3.4b) numerically for various values of the parameters $T_o/n_p^2\,t_r$ and $T_o/\mathcal{E}_o$ relevant to the flaring corona, starting at $\tau = 0$ and stopping when $v_d = v_{crit}$, i.e. halting the simulation when the ion-acoustic instability is reached.

In Figure 3.1 we have graphed the value of T_e/T_i at onset of instability for $T_o/n_p^2\,t_r$ in the range $0.5 \lesssim T_{o_6}/(n_{p_{11}}^2\,t_r) \lesssim 500$ for $T_{o_6}/\mathcal{E}_{o_2} = 5, 20, 50$ where scaling appropriate to solar flare parameters has been taken: $T_{o_6} \equiv T_o(K)/10^6$, $n_{p_{11}} \equiv n_p(cm^{-3})/10^{11}$, $t_{r_1} \equiv t_r(secs)/10$ and $\mathcal{E}_{o_2} \equiv \mathcal{E}_o(keV)/10^2$.

In Figure 3.2 we have plotted the dimensionless time τ taken to arrive at the onset of ion-acoustic instability for the same range of $T_{o_6}/n_{p_{11}}^2\,t_r$ and values of $T_{o_6}/\mathcal{E}_{o_2}$.

Figures 3.1 and 3.2, in conjunction with Equation (3.5) can be used to give the T_e/T_i value at the onset of ion-acoustic instability and the time t (in seconds) taken to reach instability for any classical heating phase within the parameter range which we have explored; e.g. with $T_o = 5.10^6$ K, $n_p = 10^{11}$ cm^{-3}, $t_r = 10$ secs and $\mathcal{E}_o = 100$ keV, we have $T_{o_6}/(n_{p_{11}}^2\,t_{r_1}) = 5$ and $T_{o_6}/\mathcal{E}_{o_2} = 5$. Using Figure 3.1 tells us that the value of T_e/T_i at onset of turbulence will be $\simeq 7.0$. From Figure 3.2, this will occur at dimensionless time $\tau \simeq 3.9$ which, using Equation (3.5), is at time $t \simeq 5.5$ secs.

To demonstrate the importance of including the effects of beam collisional heating, albeit in an approximate manner, we consider, as an example, the case where $T_{o_6} = 5$, $n_{p_{11}} = 1$, and $\mathcal{E}_{o_2} = 1$ (as above). The values of T_e/T_i and t at onset of ion-acoustic instability, are plotted as functions of rise time t_r for the cases where beam heating is included (Figures 3.3 and 3.4) and neglected (Figures 3.5 and 3.6).

Comparison of Figures 3.3 and 3.5 indicate that, while in both cases T_e/T_i is a monotonically increasing function of t_r, beam heating results in a rapid rise in T_e/T_i with increasing t_r whereas T_e/T_i levels off if beam heating is ignored. The reason for this is a consequence of the behaviour exhibited in Figures 3.4 and 3.6: the larger the rise time of the beam, the longer it takes before instability sets in. There is therefore more time for the beam to collisionally heat the plasma electrons and thereby increase the value of T_e/T_i at which instability arises. For larger values of t_r it is noticeable that beam heating models take less time to go unstable than models in which beam heating is not taken account of.

We have taken t_r in the range 0.1 secs $\lesssim t_r \lesssim$ 100 secs, as this encompasses likely durations for the impulsive phase of the flare (see Section 1.2). It is possible that, in models where beam heating is neglected, the value of T_e/T_i at onset of instability may reach a maximum at large t_r and thereafter fall off. However, this would require a time scale possibly exceeding that of the flare itself and is therefore of no practical importance. In addition, for such large times, the neglect of convection and, particularly, thermal conduction in our model will become invalid. In any case, the effects of direct collisional heating by the beam are likely to be of comparable magnitude

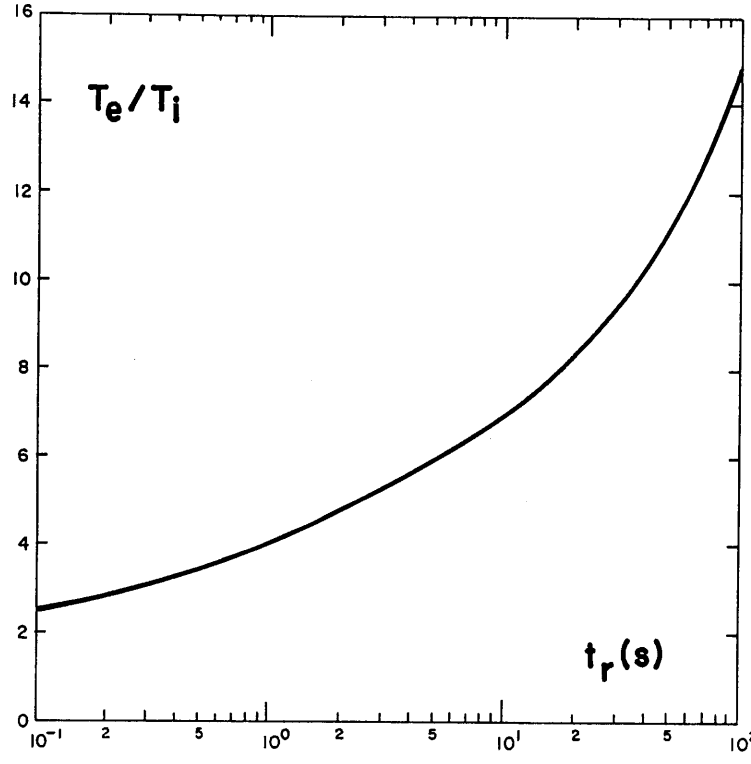

Figure 3.3: Value of T_e/T_i at onset of instability as a function of rise time, t_r, when beam heating is included.

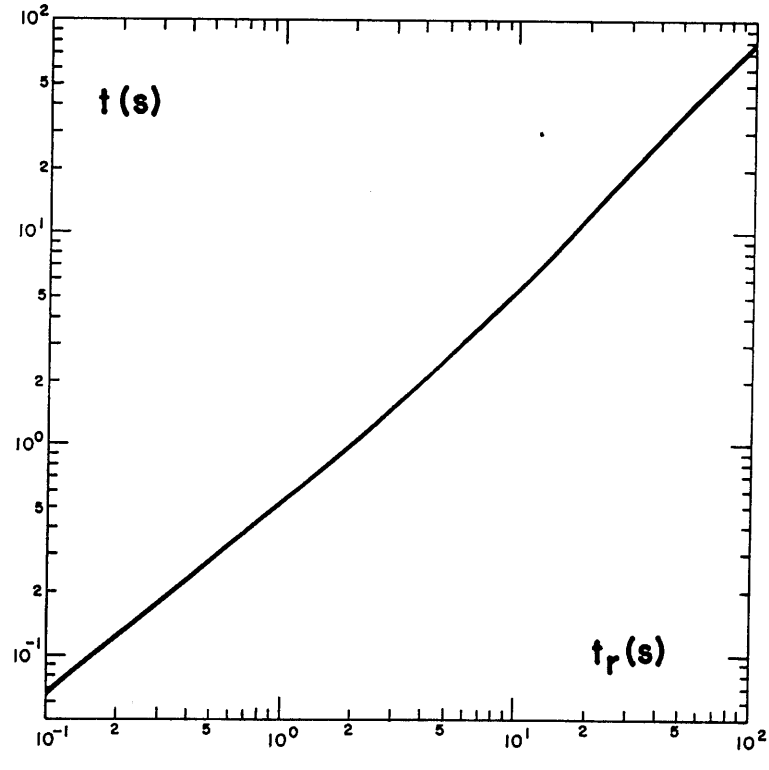

Figure 3.4: Time, t, taken to reach instability as a function of rise time, t_r, when beam heating is included.

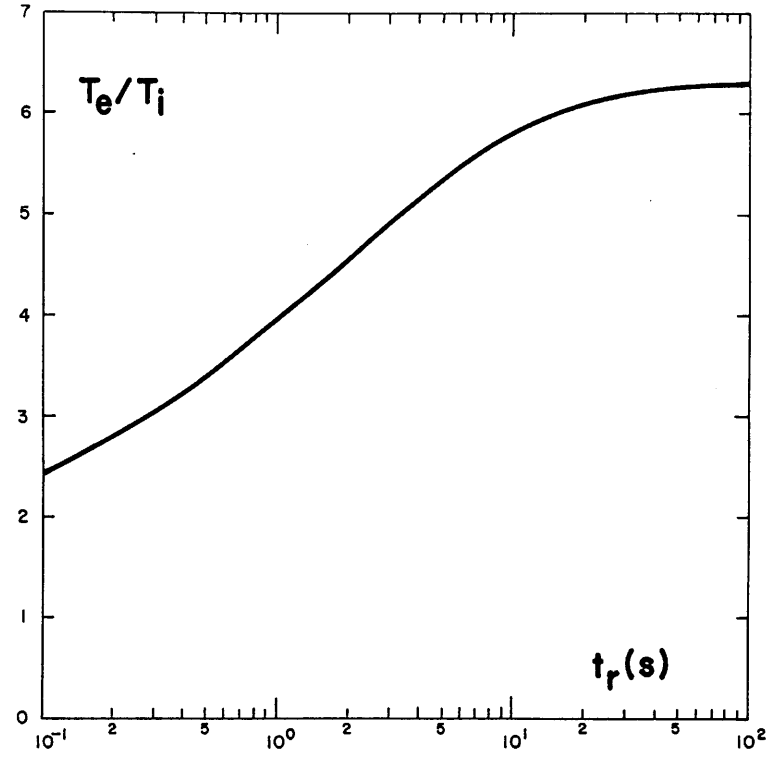

Figure 3.5: Value of T_e/T_i at onset of instability as a function of rise time, t_r, when beam heating is neglected

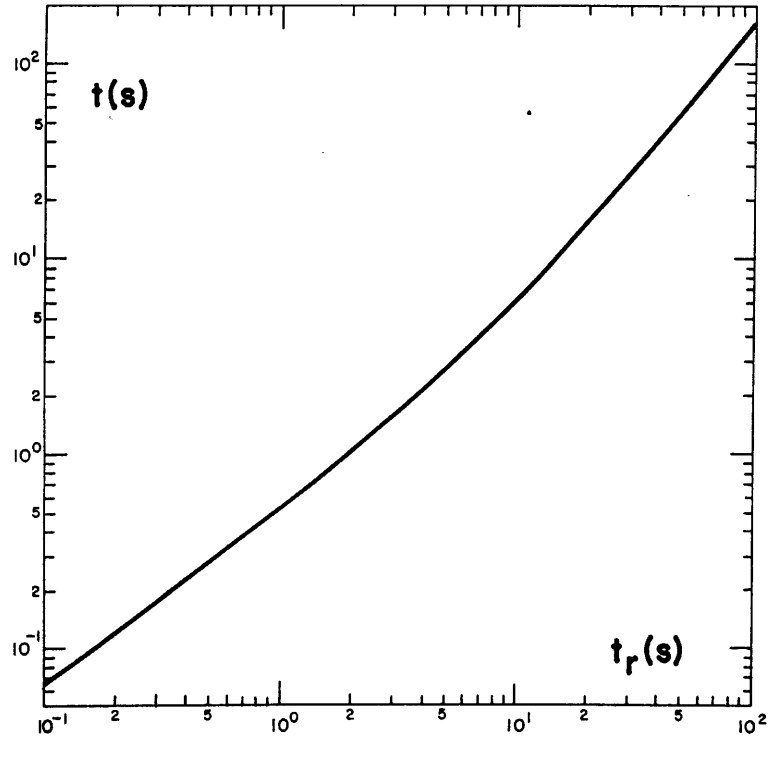

Figure 3.6: Time, t, taken to reach instability as a function of rise time, t_r, when beam heating is neglected.

to those produced by ohmic dissipation of the return current (see Chapter 4), and so should certainly not be disregarded.

Having given the classical heating phase of our return current model much detailed attention, we now turn to the unstable regime. We attempt to model this by means of a marginal stability technique as explained in the following chapter.

4. ION-ACOUSTIC INSTABILITY OF THE RETURN CURRENT: A MARGINAL STABILITY ANALYSIS

4.1 INTRODUCTION

In the previous chapter we considered the classical heating phase of the flare plasma during which the return current drift velocity $v_d < v_{crit}$, the threshold speed for the onset of (ion-acoustic) instability. Since $z_{IA} = 0$ (i.e. zero anomalous resistivity) in this regime, we were able to solve the heating equations (3.12) to find $T_e(t)$ and $T_i(t)$. The plasma resistivity is simply $\eta = \eta_{cl}(o)T_e^{-3/2}$.

We would now like to be able to describe the evolution of the plasma for $v_d \gtrsim v_{crit}$, i.e. the unstable heating regime. Specifically, as in Chapter 3, we wish to determine $T_e(t)$, $T_i(t)$ and $\eta(t)$ (Section 4.3). In addition, it is of some importance to calculate the resultant emission measure $\int n_p^2 \, dV$ and the hard X-ray signature; in particular, we investigate the effect on the ratio of thermal to non-thermal bremsstrahlung emission (Section 4.4).

We apply a marginal stability approach (Section 4.2) to the problem of tracking the plasma evolution when $v_d \gtrsim v_{crit}$. Examples of the success of this method are given. It is found that, although it is a powerful tool, the concept of marginal stability in the present problem completely fails if $(T_e/T_i)_{onset} \lesssim 4.8$, where $(T_e/T_i)_{onset}$ is the electron-to-ion temperature ratio at onset of IA (ion-acoustic) instability. This breakdown of the marginal stability method is discussed in some detail in Section 4.5. Finally, the results of this chapter are summarised in Section 4.6.

4.2 THE MARGINAL STABILITY METHOD

A rigorous treatment of the unstable heating regime would require

the self-consistent determination of the wave spectrum W(k) together with the electron and ion distribution functions. To circumvent the complexities of this procedure, however, we make the hypothesis of marginal stability. This approach has been successfully applied to many problems in anomalous plasma transport, such as shock structures and Tokamak temperature profiles, as described by Manheimer and Boris (1977). Put simply, the marginal stability hypothesis is that under the influences of two opposing tendencies, a plasma will oscillate rapidly about the boundary between stability and instability (Figure 4.1).

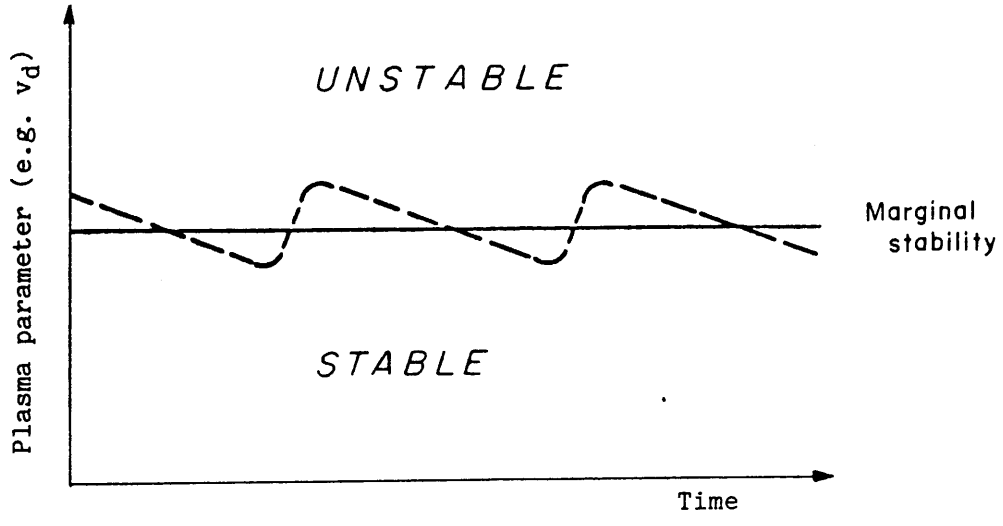

Figure 4.1: Possible Loci of the System (After Manheimer and Boris (1977)).

The validity of the marginal stability hypothesis depends on the following three conditions being satisfied:

1. Macroscopically, mechanisms operate which tend to drive the system towards microscopic instability e.g. "free" energy source provided by the return current (which itself is driven by the precipitating electron beam).

2. The time scales associated with the plasma instabilities (e.g. growth time) must be much less than the time scales on which the plasma can respond by cooling or changing its configuration in some other way. This assumption means that the plasma is always close to a state of marginal stability (see Figure 4.1).

3. The plasma instability is assumed to saturate at an average mode amplitude and heating rate which is much higher than that needed to provide the observed turbulent transport. Thus, the instability can be off most of the time (see Chapter 6) and yet provide the necessary transport to ensure that the stabilising and de-stabilising factors are balanced in the macroscopic system.

In the marginal stability approach, the anomalous transport coefficient is not the fundamental quantity to be found first (as in conventional non-linear theory). In fact, we first determine the plasma profile, e.g. spatial structure of T_e, η . Once this is known, the anomalous transport coefficients needed to produce that profile can be found. Quasi-linear theory can then be used (if desired) to calculate the turbulent fluctuation amplitudes needed to give that required value of transport coefficient (see Appendix B for approximate treatment). Thus, a marginal stability anomalous transport calculation proceeds in a direction opposite to that of conventional theory, as depicted in Figure 4.2.

The marginal stability concept has previously been applied to problems relating to the solar atmosphere. For example, Karpen and Boris (1986) use this approach to describe the response of an emerging magnetic flux tube to a current-driven instability, and Duijveman et al. (1983) invoke marginal stability in their model of rapid plasma heating in unstable current systems (see, however, the comments on this latter paper in Section 3.2).

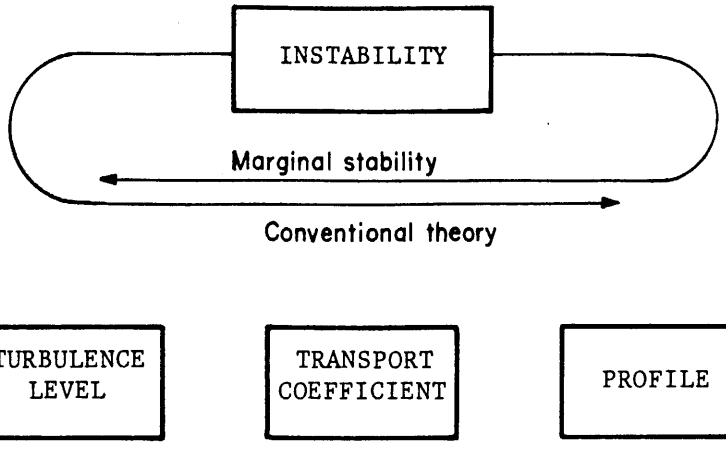

Figure 4.2: The Logical Paths for Marginal Stability and Conventional Non-linear Theory (Manheimer and Boris 1977)).

4.3 SOLUTION OF THE HEATING EQUATIONS IN MARGINAL STABILITY

In our model of return current instability, marginal stability is represented by the v_{crit} curve in the $(\frac{v_d}{v_e}, \frac{T_e}{T_i})$ plane, where $v_e = (T_e/m_e)^{\frac{1}{2}}$ is the electron thermal speed (e.g. Figure 4.5a). Essentially, the marginal stability hypothesis is the assumption that as soon as v_d reaches v_{crit}, where the fastest growing mode has zero growth rate (see Chapter 5; Appendix A), we can set $v_d = v_{crit}$. Thereafter, the system is constrained to evolve along the marginal stability curve. Physically, this means that the rapid anomalous heating raises v_{crit} in step with $v_d(t)$ such as to just keep the system at wave growth onset. Using Equation (3.14), we therefore set

$$v_d = 1.2 \left(\frac{T_o}{m_e}\right)^{\frac{1}{2}} \frac{y}{x^{\frac{1}{2}}} \qquad (4.1)$$

and rearranging this we have

$$y = \frac{v_d}{1.2} \left(\frac{m_e}{T_o}\right)^{\frac{1}{2}} x^{\frac{1}{2}} \qquad (4.2)$$

Now, since v_d (= $j_p(t)/n_p e$) is a prescribed function of time (see Section 3.2), Equation (4.2) gives us an extra relationship between x and y in marginal stability, in addition to the heating Equations (3.12). This relationship, together with the functional form of χ_{IA} (Section 2.3) is, in principle, enough information to continue the solution of Equations (3.12) into the anomalous regime. However, there is a fundamental problem which can arise in this marginal stability approach. Its origin is most easily demonstrated by retaining only the anomalous IA terms in Equations (3.12), as pointed out by P.A. Sweet (personal communication, 1985). We then have

$$\frac{dx}{d\tau} = c\,\tau^2 \chi_{IA}\, Z_{IA} \qquad (4.3a)$$

$$\frac{dy}{d\tau} = c\,\tau^2 (1 - \chi_{IA}) Z_{IA} \qquad (4.3b)$$

We also take the following analytic form for χ_{IA} (Tange and Ichimaru (1974); Section 2.3):

$$\chi_{IA} = 1 - \frac{c_s}{v_{crit}} \qquad (4.4)$$

where c_s is the ion-sound speed. Using (3.14) to substitute for v_{crit}, we obtain

$$\chi_{IA} = 1 - \frac{1}{1.2} \left(\frac{m_e}{m_i}\right)^{\frac{1}{2}} \frac{x}{y} \qquad (4.5)$$

i.e. $$\chi_{IA} \simeq 1 - \frac{x}{51.4y}$$

Using $v_d = j_p(t)/n_p e$, the marginal stability relationship (4.2) can be written in the form

$$y = D\,\tau\, x^{\frac{1}{2}} \qquad (4.6)$$

where $D = (4.17\ 10^{10}\ \tau_{eq}(o)/n_p e t_r)(m_e/T_o)^{\frac{1}{2}}$ is a constant. Differentiating expression (4.6) w.r.t. τ and using Equations (4.3) to eliminate $\frac{dx}{d\tau}$ and $\frac{dy}{d\tau}$, the normalised anomalous resistivity Z_{IA} can be expressed explicitly as

$$Z_{IA} = \frac{Dx^{\frac{1}{2}}}{c\ \tau^2} \cdot \frac{1}{1 - \chi_{IA}(1 + \frac{y}{2x})} \qquad (4.7)$$

Looking at this expression we see that Z_{IA} is positive or negative according to the sign of the denominator. Substituting for χ_{IA} from (4.5) it is easy to show that Z_{IA} is positive for $\frac{x}{y} > 4.8$ and negative for $\frac{x}{y} < 4.8$. In other words, the marginal stability hypothesis leads to negative values of anomalous resistivity if T_e/T_i ($\equiv x/y$) < 4.8 at onset of IA instability. A more detailed discussion of this result is given in Section 4.5.

If we add Equations (4.3a) and (4.3b) we find that $d(x+y)/d\tau = c\,\tau^2 Z_{IA}$, so that negative resistivity implies a net cooling of the plasma. This is obviously unphysical. We note that we have implicitly assumed the electrostatic wave energy to be negligible. A more rigorous analysis should explicitly include the wave energy which may become rather large in these cases.

We therefore conclude that the IA instability, driven by a prescribed plasma current, may lead to two quite distinct types of anomalous plasma heating:

Type (i): if $T_e/T_i > 4.8$ at onset of instability, then we have a rather well-behaved heating throughout which the plasma is in a state of marginal stability.

Type (ii): if $T_e/T_i < 4.8$ at onset of instability, a marginal stable evolution is impossible, and we anticipate that the plasma

drift speed will exceed the marginal stability condition (4.1) and, as a result, the plasma will enter a "catastrophic" heating regime in which the IA wave levels and the resulting ohmic heating will reach very much larger values than the marginally stable values.

This bifurcation of the plasma behaviour may have interesting observational ramifications and so it is important to relate its occurrence to the parameters of the problem. Specifically, looking at Figure 3.1, we see that from within the range of parameters $0.5 \lesssim T_{06}/n_{p_{11}}^2 t_{r_1} \lesssim 500$, a marginally stable heating is only possible for

$$T_{06}/\mathcal{E}_{02} = 5 \quad \text{if} \quad T_{06}/n_{p_{11}}^2 t_{r_1} \lesssim 23 \tag{4.8a}$$

$$T_{06}/\mathcal{E}_{02} = 20 \quad \text{if} \quad T_{06}/n_{p_{11}}^2 t_{r_1} \lesssim 41 \tag{4.8b}$$

$$T_{06}/\mathcal{E}_{02} = 50 \quad \text{if} \quad T_{06}/n_{p_{11}}^2 t_{r_1} \lesssim 78 \tag{4.8c}$$

More generally, Figure 3.1 also reveals that, with a fixed $T_{06}/\mathcal{E}_{02}$, a marginally stable heating is more likely for small values of $T_{06}/n_{p_{11}}^2 t_{r_1}$ and, with a fixed $T_{06}/n_{p_{11}}^2 t_{r_1}$, a marginally stable heating is more likely for large values of $T_{06}/\mathcal{E}_{02}$. Therefore, with a fixed initial plasma temperature T_o, for example, we conclude that catastrophic heating will be more likely for large electron injection energies ($\mathcal{E}_o$), small plasma densities (n_p) and small rise times of the beam (t_r).

If we choose typical flaring coronal values for temperature and density, viz. $T_o = 5.10^6$ K and $n_p = 10^{11}$ cm^3 (e.g. Smith and Lilliequist (1979); Brown, Melrose and Spicer (1979)), and we take $\mathcal{E}_o = 100$ keV, then (4.8a) tells us that for a marginally stable IA heating phase to be possible we require $t_r \gtrsim 2$ secs. Conversely, if $t_r \lesssim 2$ secs we may expect catastrophic heating to take place (see also Figure 4.3).

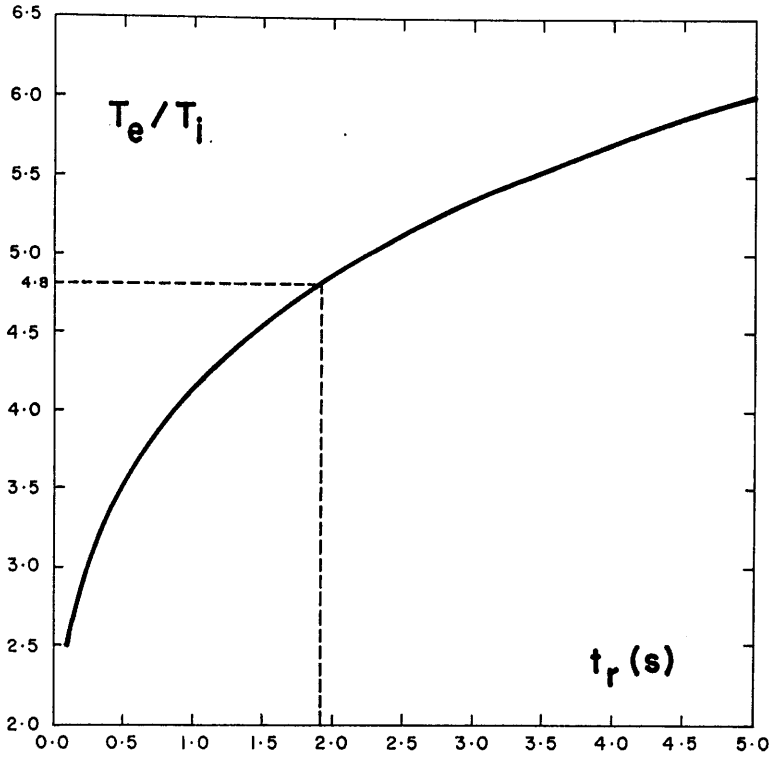

Figure 4.3: Value of T_e/T_i at onset of instability versus rise time, t_r (seconds), for the prescribed beam current evolution and $\mathcal{E}_o$ = 100 keV (see text). Marginally stable heating occurs if, and only if, $t_r \gtrsim 2$s.

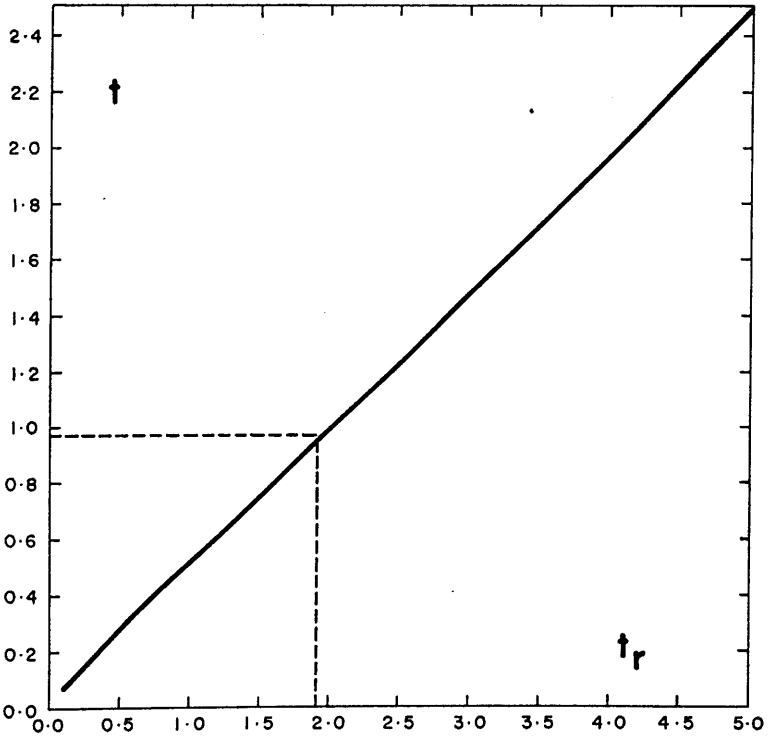

Figure 4.4: Time, t (seconds), taken to reach instability against rise time, t_r (seconds), for the prescribed beam current evolution and $\mathcal{E}_o$ = 100 keV (see text).

Equivalently, from Figure 4.4, it can be seen that if instability onset occurs at a time $t \gtrsim 1$ sec after beam switch-on, then marginally stable heating results. Otherwise, the plasma undergoes catastrophic heating.

Having described qualitatively the two types of heating which are possible, we will now give some detailed numerical results for two cases of marginally stable heating:

case (a): $T_o = 5.10^6$ K, $n_p = 10^{11}\text{cm}^{-3}$, $\mathcal{E}_o = 100$ keV and $t_r = 10$ secs, which is comfortably within the marginally stable regime.

case (b): $T_o = 5.10^6$ K, $n_p = 10^{11}\text{cm}^{-3}$, $\mathcal{E}_o = 100$ keV and $t_r = 4$ secs, which is rather closer to the catastrophic regime.

We solve Equations (3.4) starting from x=y=1.0 at τ=0, and using the marginal stability condition (4.2) when the ion-acoustic threshold is reached.

Case (a)

Figure (4.5a) shows the evolution of the plasma in the $(\frac{v_d}{v_e}, \frac{T_e}{T_i})$ plane. Initially, classical ohmic heating and beam collisional heating cause an increase in T_e/T_i from its starting value of 1.0, while the drift velocity rises until the IA marginal stability curve is reached. The system is then constrained by condition (4.1) to evolve along the marginal stability curve. Figure (4.6a) shows the variation of the normalised resistivity with time, IA turbulence switching on after about 5.5 secs. Figure (4.7a) depicts the variation of T_e and T_i throughout the simulation. The increase in the heating rate at about 5.5 secs, due to the generation of IA waves, is clearly displayed. The stopping length of the beam is shown in Figure (4.8a) from which we see that s_{min}, the smallest depth of beam penetration into the plasma, is $\simeq 8.5\ 10^9$ cm.

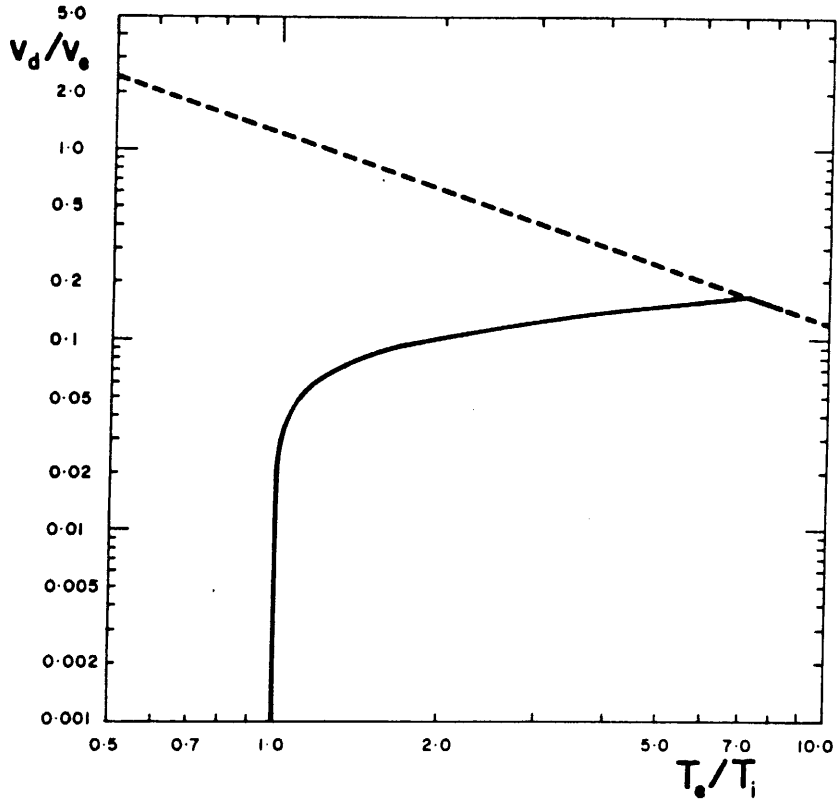

Figure 4.5a: Evolution of the plasma in the $(v_d/v_e, T_e/T_i)$ plane for case (a) (see text). The dashed line is the IA marginal stability curve.

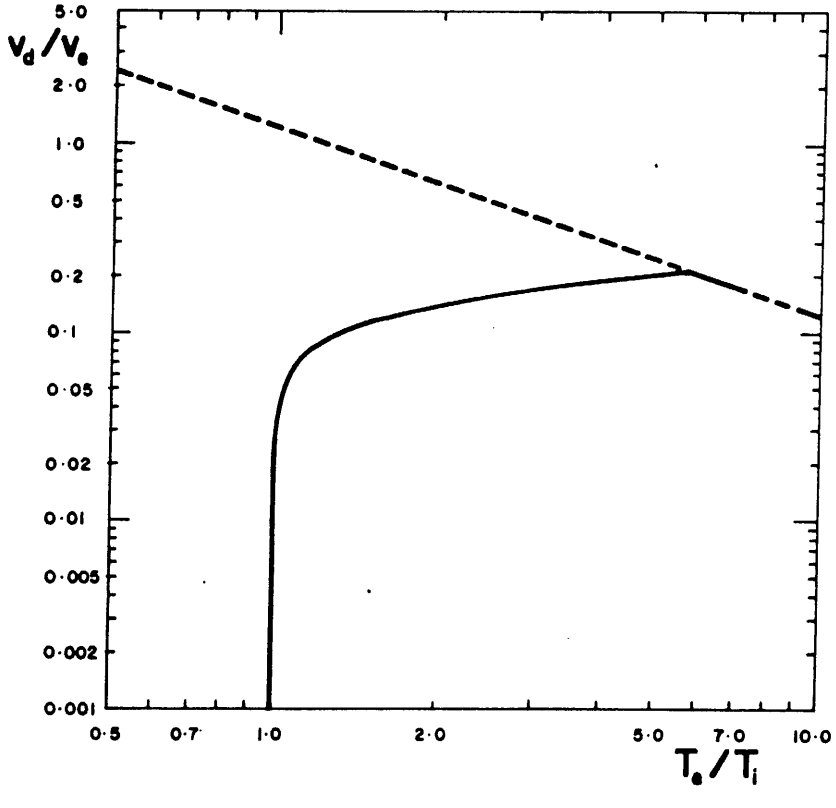

Figure 4.5b: Evolution of the plasma for case (b).

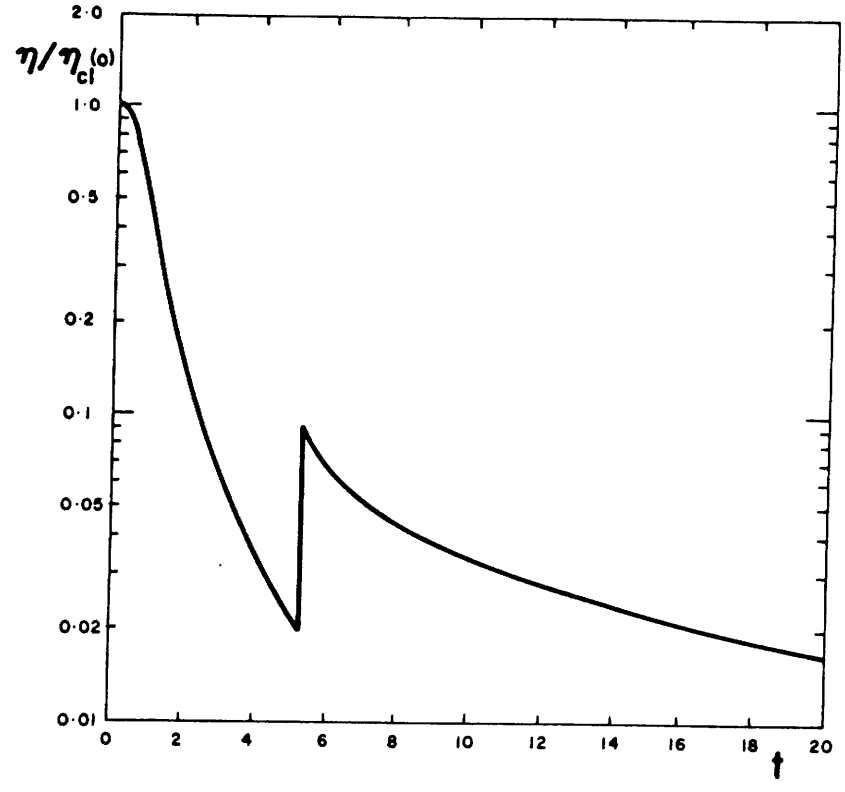

Figure 4.6a: Variation of the total resistivity, η, normalised to the initial classical resistivity, with time t(secs) for case (a). IA waves are generated at about 5.5 secs.

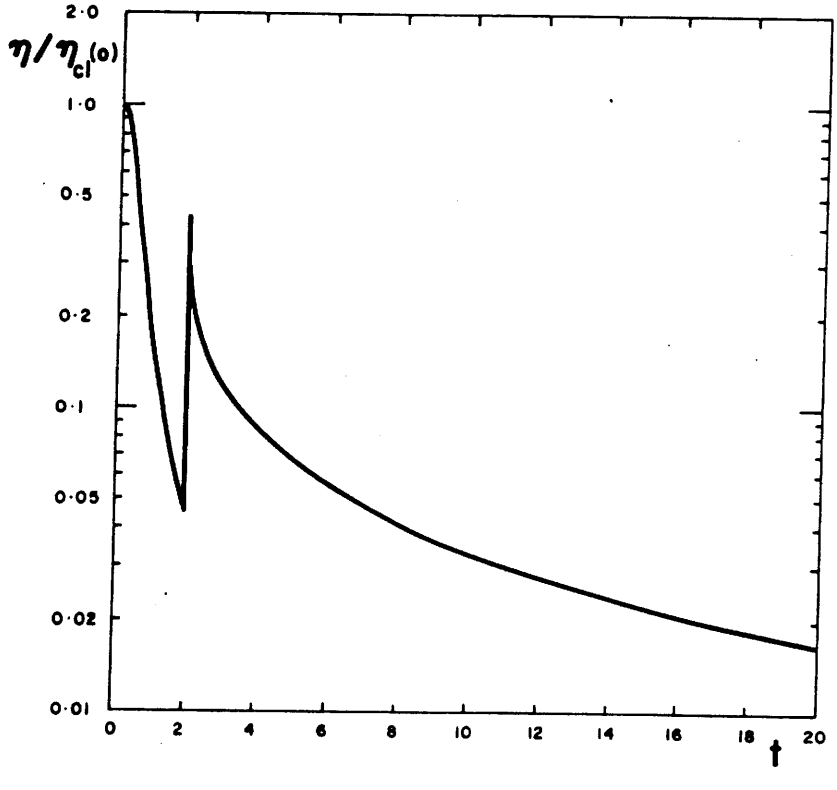

Figure 4.6b: Variation of the normalised resistivity with time for case (b). IA waves are generated at about 2.0 secs.

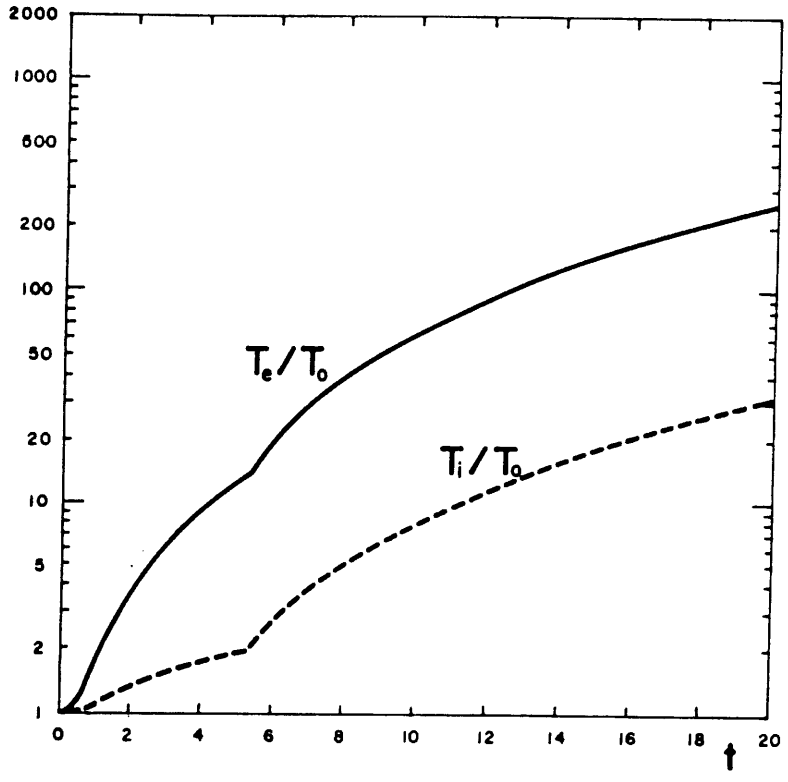

Figure 4.7a: The electron (T_e) and ion (T_i) temperature profiles, normalised to the initial temperature (T_o) for case (a).

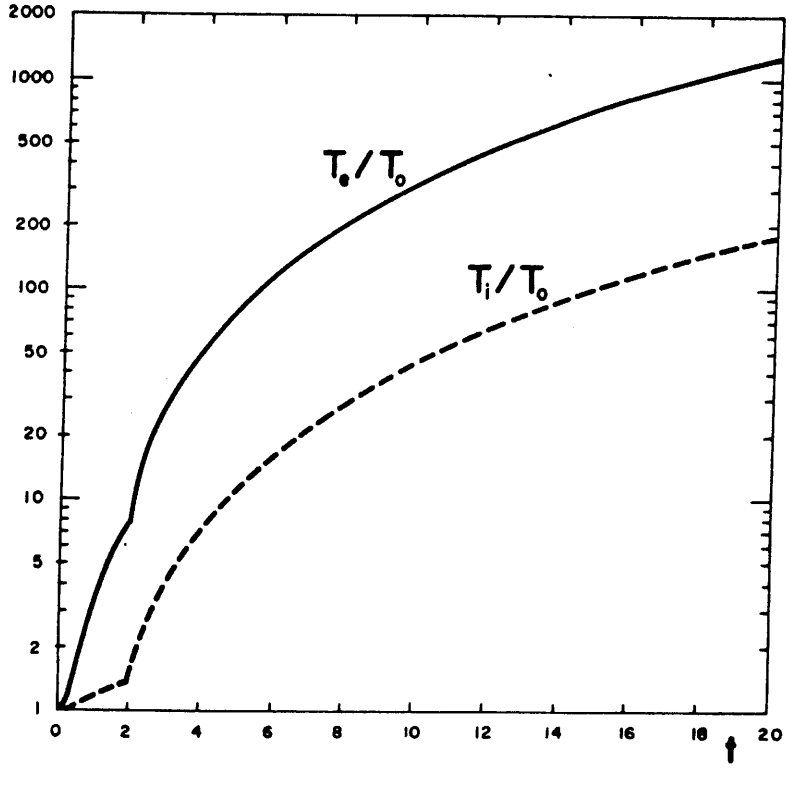

Figure 4.7b: The temperature profiles for case (b).

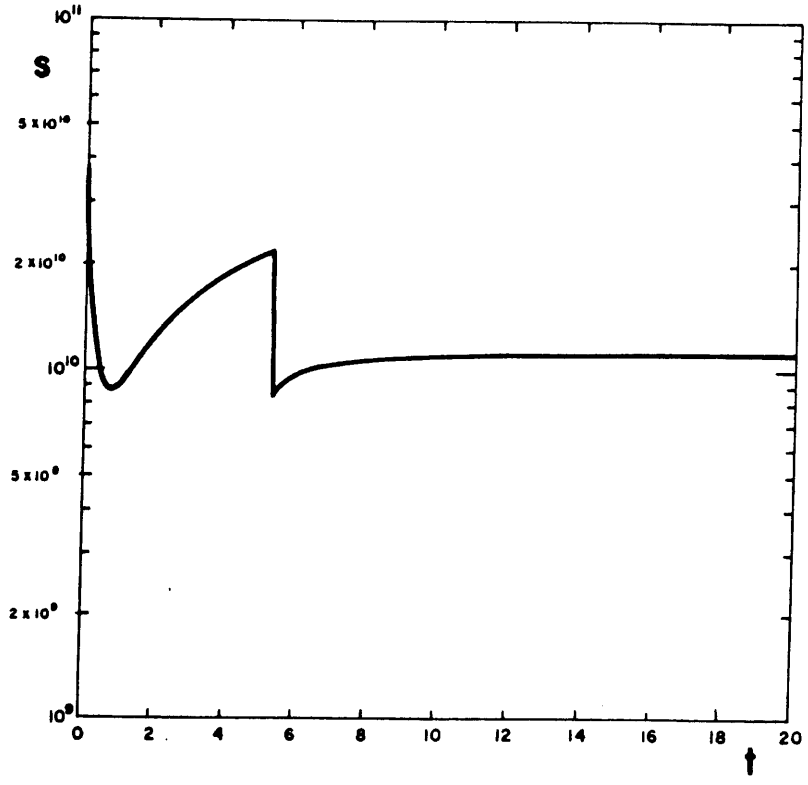

Figure 4.8a: Electron beam stopping length s(cm) v. time t(secs) for case (a).

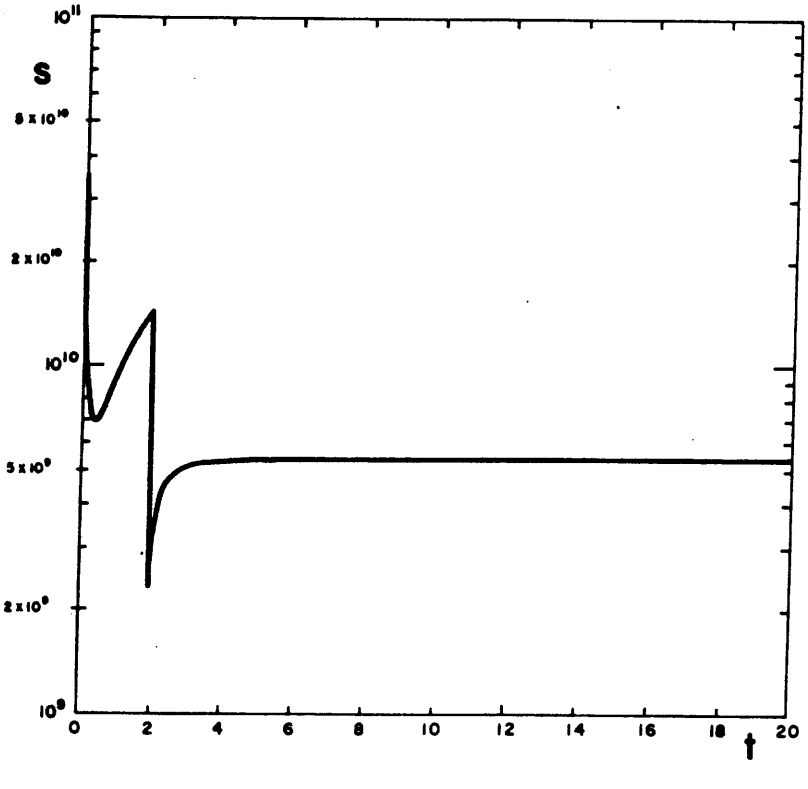

Figure 4.8b: Electron beam stopping length s(cm) v. time t(secs) for case (b).

The final temperatures obtained after 20 secs, $T_e \simeq 250\ T_o$ and $T_i \simeq 30\ T_o$ (see Figure 4.7a)) therefore only relate to the plasma layer of thickness s_{min} because, as we pointed out earlier, it is only this region which is heated continuously during the simulation.

Therefore, the attained emission measure is $n_p^2\ V \equiv n_p^2\ A\, s_{min}$ $\simeq 8.5\ 10^{47}\ cm^{-3}$ and the final electron temperature is $T_e \simeq 10^9$ K although, admittedly, losses have been neglected (however, cf. Section 4.6). We must emphasize, though, that this emission measure is only that of the very hottest part of the plasma (for which $s \lesssim s_{min}$); the total emission measure will be even larger. If the observed hard X-rays from the solar flare plasma are interpreted as thermal bremsstrahlung, then we require

$$\int n_p^2\ dV = 10^{45} cm^{-3} \quad \text{and} \quad T_e \simeq 5.10^8\ K \quad \text{(e.g. Batchelor } \underline{\text{et al.}} \text{ (1985))}$$

Consequently, heating through ohmic dissipation of a beam-driven return current may thermally provide the observed flare X-ray emission. The possibility that a narrow channel electron beam might produce more thermal bremsstrahlung through return current plasma heating than direct non-thermal bremsstrahlung has already been suggested by Brown and Hayward (1982), and by Spicer and Sudan (1984). However, the former paper considered only Spitzer resistivity, while the latter evaluated only the temperature of the anomalously heated plasma and not its emission measure. We return to this topic in more detail in Section 4.4.

In Figure (4.9a) we have graphed the ratio of beam collisional heating/ohmic electron heating against time, i.e. $B\tau\ /c\tau^2(1/n^{3/2} + \chi_{IA} Z_{IA})$ against time (see Equation (3.12a)). This graph clearly shows that the beam collisional heating is $\gtrsim \frac{1}{2}\ \times$ ohmic heating rate throughout the

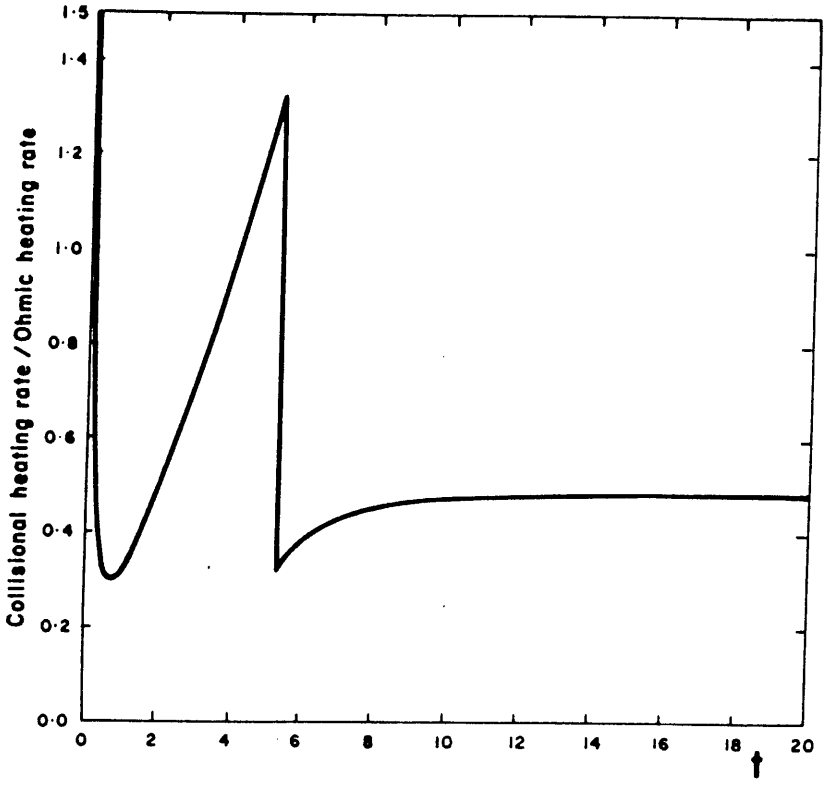

Figure 4.9a: The ratio of collisional to ohmic electron heating as a function of time t(secs) for case (a).

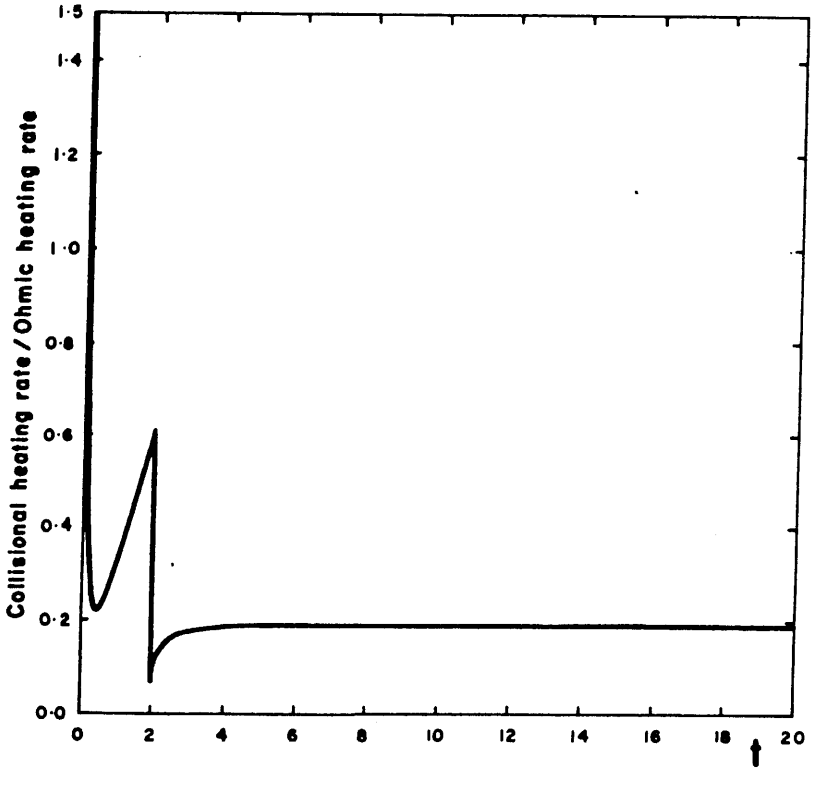

Figure 4.9b: The ratio of collisional to ohmic electron heating as a function of time t(secs) for case (b).

20 secs of the simulation. We therefore conclude that even in this anomalous regime, for the parameter set of case (a), collisional and ohmic heating are equally important (cf. Emslie (1980, 1981)).

Case (b)

Figures (4.5b) to (4.9b) comprise the graphs corresponding to Figures (4.5a) to (4.9a), for the parameter set (b) representing heating which is closer to the catastrophic regime. Figures (4.5b) and (4.6b), when compared to (4.5a) and (4.6a), confirm the results of Figures (3.1) and (3.2), i.e. they demonstrate that, with increasing values of $T_o/n_p^2\, t_r$, the T_e/T_i value at onset of instability and also the dimensionless time τ taken to arrive at instability are reduced. Figures (4.6a) and (4.6b) also reveal that the closer the heating is to being catastrophic the larger is the anomalous jump in resistivity at onset of instability. Looking at Figure (4.7b), we see that the large values of anomalous resistivity obtained for this case lead to even greater electron and ion heating than case (a): after 20 secs we find that $T_e \simeq 1300\ T_o$ and $T_i \simeq 180\ T_o$. However, Figure (4.8b) reveals that $s_{min} \simeq 2.3\ 10^9$ cm for this case, and so a smaller volume of plasma is heated to these temperatures (emission measure $n_p^2\ V \simeq 2.3\ 10^{47}\ cm^3$). Finally, Figure (4.9b) shows that beam collisional heating is much less important than the ohmic heating for the parameter set of case (b).

In comparing cases (a) and (b), an interesting parameter to look at is the fraction of the beam kinetic energy which has been converted into plasma heating inside the volume bounded by s_{min}. In other words, a measure of the efficiency of heating after a time interval t, for a given parameter set, is the quantity

$$\Delta(t) = \frac{\text{INCREASE IN THERMAL ENERGY IN REGION BOUNDED BY } s_{min}}{\text{ENERGY INPUT PROVIDED BY THE BEAM}}$$

$$\text{i.e.} \quad \Delta(t) \simeq \frac{\frac{3}{2} n_p (T_e(t) + T_i(t)) A s_{min}}{\frac{1}{2} F_b(t) \, t. \, \mathcal{E}_o}$$

where $F_b(t) = 10^{36} t/t_r \ \text{sec}^{-1}$ (see Section 3.2) is the number flux of beam electrons. It can be easily shown that:

$$\Delta(t) \simeq 4.31 \, 10^{11} \frac{(x(t) + y(t)) \, s_{min} \, t_r}{t^2} \qquad (4.9)$$

At t = 20 secs we find that $\Delta \simeq 0.80$ for case (a) and $\Delta \simeq 0.44$ for case (b). In other words, 80% of the beam's kinetic energy has been converted into plasma heating inside the region bounded by s_{min} in case (a), while in case (b) this quantity is only 44%. Obviously, about 20% (case (a)) and 56% (case (b)) of the beam kinetic energy has gone into plasma heating outside the volume bounded by s_{min}. We therefore conclude that our simple treatment of the plasma heating, with no spatial dependence, is adequate for cases which are well within the marginally stable regime, but the closer we go to the catastrophic regime the more energy will be lost outside s_{min} and the poorer our approximate treatment will become. A more accurate approach, incorporating a spatial dependence for the temperature and resistivity of the plasma, is outlined in Chapter 8.

4.4 THERMAL AND NON-THERMAL RADIATION SIGNATURES

In this section, we take the two preceding sets of results for the marginally stable heating and calculate the thermal bremsstrahlung from the resulting rapidly heated plasmas. For comparison, we also calculate

the conventional collisional thick-target non-thermal bremsstrahlung from the beam which incorporates Coulomb collisional losses only (i.e. the regime relevant to large beam areas $A \simeq 10^{18}$- 10^{19} cm^2). We examine the ratio of these emissivities as a function of time throughout the 20 secs of the simulations.

The thermal emissivity from the volume $V = As_{min}$ is

$$\left(\frac{dJ}{d\varepsilon}\right)_T = Vn_p \int_{\varepsilon}^{\infty} v(\mathcal{E}) \frac{dn}{d\mathcal{E}} \frac{dQ}{d\varepsilon}(\varepsilon,\mathcal{E}) d\mathcal{E} \qquad (4.10)$$

where $\frac{dn}{d\mathcal{E}}$, the number density of plasma electrons per unit energy range, is assumed to be Maxwellian, $v(\mathcal{E})$ is the velocity of an electron with energy $\mathcal{E}$, and $\frac{dQ}{d\varepsilon}(\varepsilon,\mathcal{E})$ is the bremsstrahlung cross section differential in photon energy. Here, as an approximation, we assume Kramer's cross section

$$\frac{dQ}{d\varepsilon}(\varepsilon,\mathcal{E}) = \frac{Q_o m_e c^2}{\varepsilon \mathcal{E}} \qquad (4.11)$$

where $Q_o = \frac{8}{3} \alpha r_e^2$ in the usual notation, neglecting any heavy element correction.

The non-thermal emissivity (Brown (1971)) from a beam is

$$\left(\frac{dJ}{d\varepsilon}\right)_{NT} = \int_{\varepsilon}^{\infty} F(\mathcal{E}) \nu(\varepsilon,\mathcal{E}) d\mathcal{E} \qquad (4.12)$$

where $F(\mathcal{E}) = F_b \delta(\mathcal{E} - \mathcal{E}_o)$, F_b is the number of electrons, of a single constant energy $\mathcal{E}_o$ (see Section 3.2), injected per second, and $\nu(\varepsilon, \mathcal{E})$, the number of photons of energy ε emitted by an electron with initial energy $\mathcal{E}$, is given by

$$\nu(\varepsilon,\mathcal{E}) = n_p \int_{\mathcal{E}_*=\mathcal{E}}^{\mathcal{E}_*=\varepsilon} \frac{dQ}{d\varepsilon}(\varepsilon,\mathcal{E}_*) \frac{v(\mathcal{E}_*)}{\left(\frac{d\mathcal{E}_*}{dt}\right)} d\mathcal{E}_* \qquad (4.13)$$

The energy loss equation for beam losses due to Coulomb collisions alone is

$$\frac{d\mathcal{E}_*}{dt} = - \frac{K n_p v(\mathcal{E}_*)}{\mathcal{E}_*} \qquad (4.14)$$

where $K = 2\pi e^4 \ell n \Lambda$.

We find that the (anomalous) thermal emissivity is

$$\left(\frac{dJ}{d\varepsilon}\right)_T = \left(\frac{8}{\pi m_e T_e}\right)^{\frac{1}{2}} \frac{Q_o m_e c^2 n_p^2 A s_{min}}{\varepsilon} \exp\left(-\frac{\varepsilon}{T_e}\right) \qquad (4.15)$$

and the (maximum) non-thermal thick-target emissivity for a beam undergoing collisional losses only (i.e. a large area beam) is, from (4.12) to (4.14)

$$\left(\frac{dJ}{d\varepsilon}\right)_{NT} = \frac{Q_o m_e c^2 F_b}{\varepsilon K} (\mathcal{E}_* - \varepsilon) \qquad (4.16)$$

We are specifically interested in the ratio of these two quantities:

$$\frac{\left(\frac{dJ}{d\varepsilon}\right)_T}{\left(\frac{dJ}{d\varepsilon}\right)_{NT}} = \left(\frac{8}{\pi m_e T_e}\right)^{\frac{1}{2}} \frac{n_p^2 A s_{min}}{F_b(\mathcal{E}_o - \varepsilon)} \exp\left(-\frac{\varepsilon}{T_e}\right) \qquad (4.17)$$

Using the marginally stable results of the last section, together with our specified beam injection rate $F_b = 10^{36}\ t/t_r\ sec^{-1}$ (see Section 3.2), Figures (4.10a) and (4.10b) show the variation of the thermal to non-thermal emissivity ratio (Equation (4.17)) throughout the 20 secs of our simulations for a representative hard X-ray photon energy of ε = 20 keV, for cases (a) and (b) respectively.

Looking at these graphs, we see that the thermal to non-thermal emissivity ratio actually instantaneously drops by a small amount at the onset of IA instability ($t \simeq 5.5$ secs for Figure (4.10a) and $t \simeq 2.0$ secs

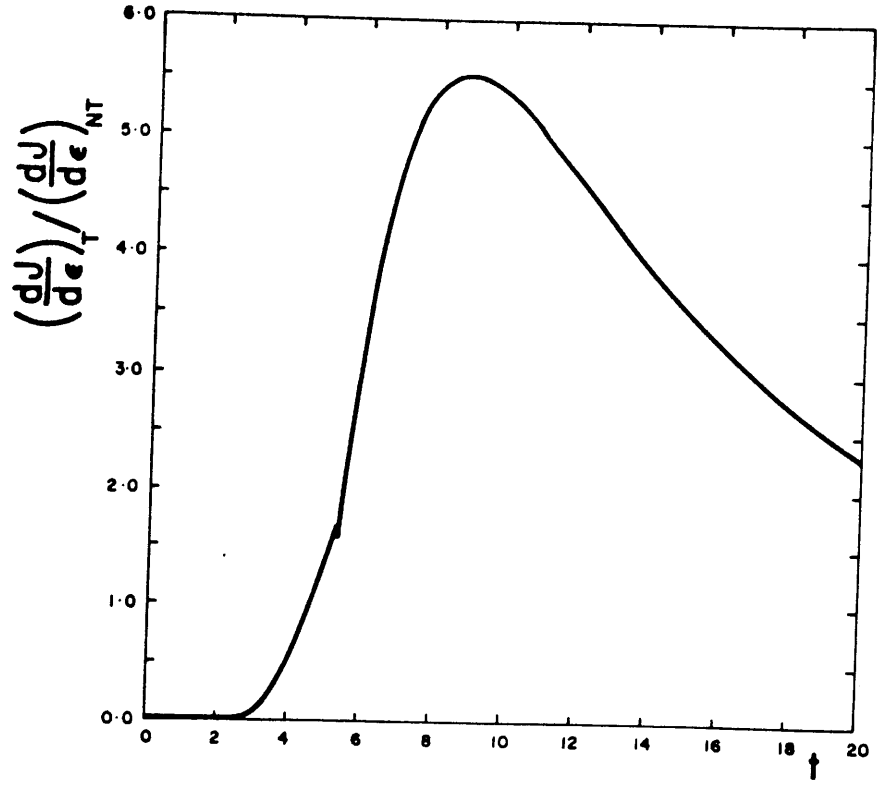

Figure 4.10a: The ratio of thermal to collisional non-thermal thick-target emissivity as a function of time t(secs) for an emitted photon energy of ε=20 keV (case (a)).

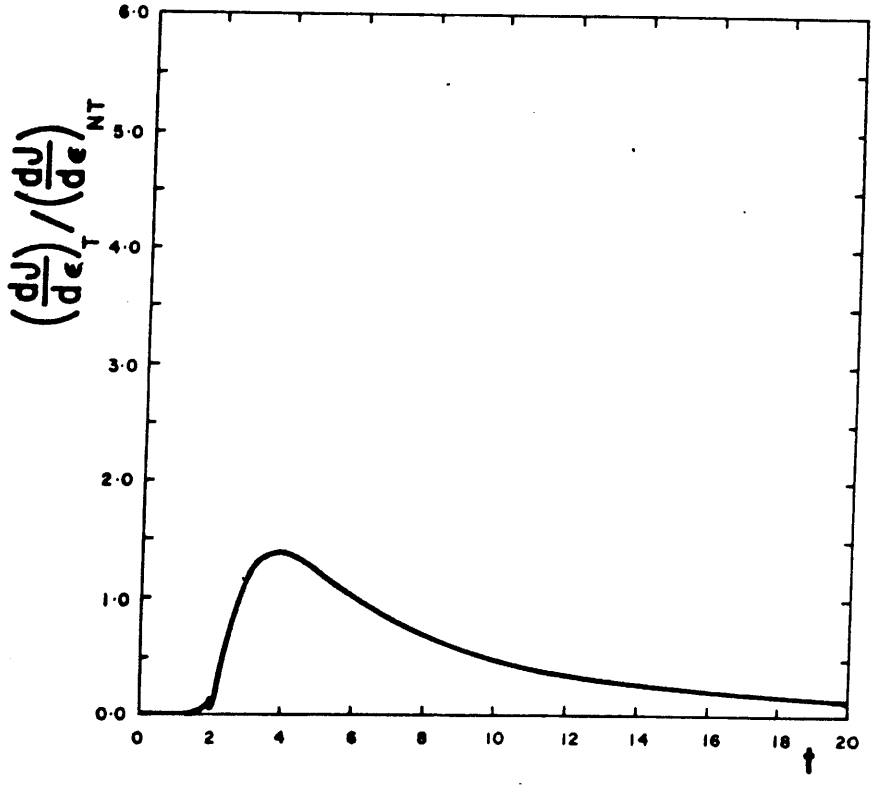

Figure 4.10b: The ratio of thermal to collisional non-thermal thick-target emissivity as a function of time t(secs) for an emitted photon energy of ε = 20 keV (case (b)).

for Figure (4.10b)). This drop is due to the instantaneous decrease in s_{min} which occurs at the onset of IA instability (see Figures (4.8a) and (4.8b)). In fact, this change in the emissivity ratio is rather artificial; clearly, by using s_{min} in Equation (4.17), we are ignoring the plasma heating which has already taken place outside s_{min}, and we are therefore underestimating the thermal emissivity. Even neglecting the emission from outwith the minimum volume, however, Figures (4.10a) and (4.10b) also reveal that after 3 to 4 seconds of anomalous resistive heating, the thermal emissivity has risen to approximately 5.0 times (case (a)) and 1.5 times (case (b)) the non-thermal and thick-target emissivity.

Thus, when one considers a beam injection rate, F_b, and reduces the beam area, A, until the return current goes IA unstable, the beam length and non-thermal bremsstrahlung are greatly reduced as is usually assumed (e.g. Hoyng et al (1978)), but enhanced thermal bremsstrahlung from the rapidly heated plasma exceeds the collisional thick-target emission which could be directly produced by the same beam (over a larger area $A \simeq 10^{18}$- $10^{19} cm^2$) in the standard model. In practice, this means that a substantially lower beam current is required to produce hard X-rays thermally by anomalous return current heating of the plasma, than by non-thermal emission direct from a collisional beam.

4.5 FAILURE OF MARGINAL STABILITY

We return to the topic of failure of marginal stability and consider the reasons for this in more detail. From Equation (4.7) we deduced that if $(T_e/T_i)_{onset} \lesssim 4.8$, then application of marginal stability leads to negative values of Z_{IA}, and so its use is invalid in this regime. An equivalent way of analysing the problem is to proceed as follows.

As before, we retain only the anomalous terms in the heating Equations (3.12), to obtain Equations (4.3). Dividing (4.3a) by (4.3b) gives

$$\frac{dx}{dy} = \frac{\chi_{IA}}{1 - \chi_{IA}} \tag{4.18}$$

Now, introduce the variable $R \equiv x/y$, the electron-to-ion temperature ratio. Noting that $y = x/R$, we find that

$$dy = \frac{dx}{R} - \frac{x}{R^2}\, dR \tag{4.19}$$

Substituting $\chi_{IA}(R)$ from (4.5), and eliminating dy from (4.18) using (4.19), we obtain, after a little algebraic manipulation,

$$\frac{dx}{x} = \frac{R - 51.4}{R\,(R-R_1)(R+R_2)}\, dR \tag{4.20}$$

where $R_1 \simeq 6.69$, $R_2 \simeq 7.69$ (i.e. $R_2 = R_1 + 1$). Integrating (4.20) leads to the solution

$$x = \frac{R}{R_o} \left| \frac{R_1 - R_o}{R_1 - R} \right|^a \left(\frac{R_o + R_2}{R + R_2} \right)^{1-a} \tag{4.21}$$

where $a \simeq 0.53$ and R_o is the value of R at $t = 0$. (In all our simulations, $R_o = 1.0$).

We also have the constraint imposed by the marginal stability condition, Equation (3.15), which can be rewritten as

$$x = \left(\frac{v_{crit}}{1.2\, v_{e_o}} R \right)^2 \tag{4.22}$$

where $v_{e_o} = (T_o/m_e)^{\frac{1}{2}}$ is the electron thermal speed at $t = 0$. Eliminating x between (4.21) and (4.22) and inserting $R_o = 1.0$, $R_2 = R_1 + 1$, we arrive at the following result

$$\frac{v_{crit}}{1.2\, v_{e_o}} = G(R) \qquad (4.23)$$

where

$$G(R) = \left[\frac{1}{R} \left| \frac{R_1 - 1}{R_1 - R} \right|^{0.53} \left| \frac{R_1 + 2}{R_1 + R + 1} \right|^{0.47} \right]^{\frac{1}{2}} \qquad (4.14)$$

By evaluating $G'(R)$ it can be easily shown that $G(R)$ has a minimum at $R \simeq 4.8$. The function $G(R)$ is plotted in Figure (4.11). Note the singularity at $R = R_1 \simeq 6.7$. This corresponds to a limiting value of T_e/T_i for IA heating, as explained below.

Consider the rate of change of R w.r.t. time:

$$\frac{dR}{dt} = \frac{d}{dt}\left(\frac{T_e}{T_i}\right)$$

$$= \frac{\dot{T}_e T_i - \dot{T}_i T_e}{T_i}$$

$$= \frac{\dot{T}_i T_e}{T_i} \left(\frac{\dot{T}_e}{\dot{T}_i} \cdot \frac{T_i}{T_e} - 1 \right)$$

$$\text{i.e.} \quad \frac{dR}{dt} = \frac{T_e}{T_i} \cdot \dot{T}_i \left(\frac{\chi_{IA}}{1 - \chi_{IA}} \cdot \frac{T_i}{T_e} - 1 \right), \text{ using (4.18)} \qquad (4.25)$$

We note that if $\dot{T}_i > 0$ (i.e. $\frac{dy}{d\tau} > 0$), which follows from (4.36), provided $Z_{IA} > 0$, and if the following condition is satisfied

$$\frac{T_e}{T_i} < \frac{\chi_{IA}}{1 - \chi_{IA}} \qquad (4.26)$$

then $\frac{dR}{dt} > 0$. It is easily shown that the (physical) solution of (4.26) is $R < R_1$. In other words, when $\frac{T_e}{T_i} \lesssim 6.7$, the value of $\frac{T_e}{T_i}$ must rise

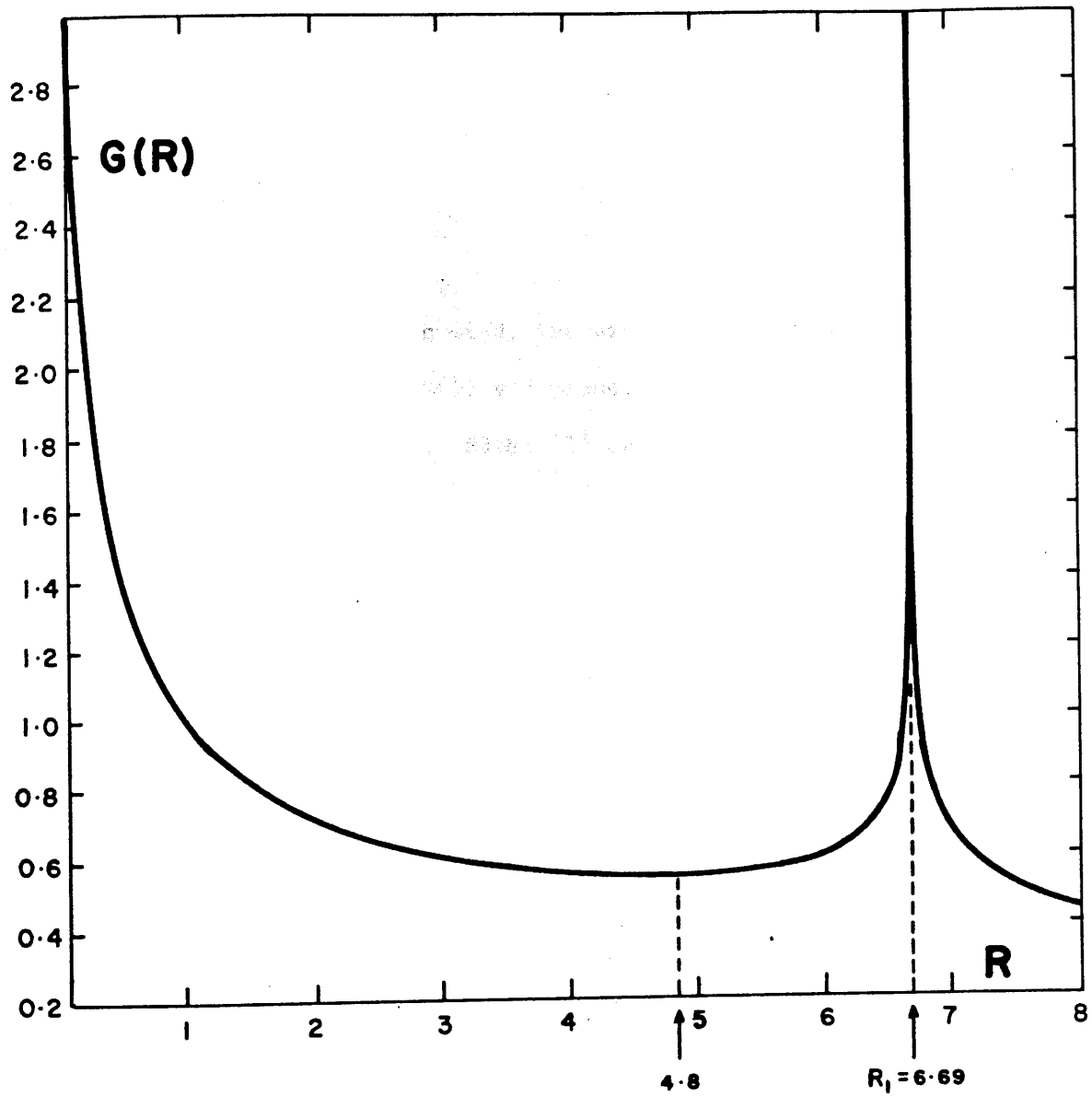

Figure 4.11: Plot of the function G(R) v. R, where R is the electron-ion temperature ratio, showing the minimum at R = 4.8 and singularity at R = 6.69.

as a consequence of IA wave heating. Conversely, if $\frac{T_e}{T_i} \gtrsim 6.7$, then, from Equation (4.25), $\frac{dR}{dt} < 0$: the ratio $\frac{T_e}{T_i}$ must decrease with time. Hence $R_1 \simeq 6.7$ is the limiting value for IA heating. Using a more accurate functional form for $\chi_{IA}(\frac{T_e}{T_i})$, Duijveman et al (1981) obtain the more exact value of $\frac{T_e}{T_i} \simeq 6.37$ as the limiting value.

Bearing the above in mind, let us consider the possible loci of plasma evolution in the G(R) v R plane. Figure (4.12) shows examples of all the possibilities. Paths (1) and (2) both have turbulence onset at $\frac{T_e}{T_i} > 4.8$ followed by a period of marginally stable heating; in the case of (1), onset occurs below $\frac{T_e}{T_i} = 6.7$ so that $\frac{T_e}{T_i}$ increases with time to the limiting value R_1 and, in the case of (2), the opposite occurs. In Figure 4.12 we have enlarged a segment of path (1) to demonstrate the behaviour of the plasma in marginal stability. When v_d exceeds v_{crit}, rapid (anomalous) heating occurs and the electron-ion temperature ratio R increases swiftly, driving the plasma back onto the marginal stability curve G(R). This behaviour is repeated at very short intervals so that $|v_d - v_{crit}|$ is kept very small, i.e. $v_d \simeq v_{crit}$ throughout marginal stability.

By contrast, path (3) shows what happens when the plasma is constrained to be in marginal stability for $\frac{T_e}{T_i} < 4.8$. The form of the curve dictates that $\frac{T_e}{T_i}$ decreases with time, i.e. $\frac{dR}{dt} < 0$, since v_d increases with time. Mathematically, this is only possible if $T_i < 0$ (from Equation (4.25)), i.e. if $\eta < 0$ (from Equation (4.3b))which is unphysical. Marginal stability is therefore inapplicable in this regime and, in fact, we expect that catastrophic heating will take place along paths of the form (4a) or (4b). In the case of (4a), a state of marginal stability is reached at a subsequent time, but, in the case of

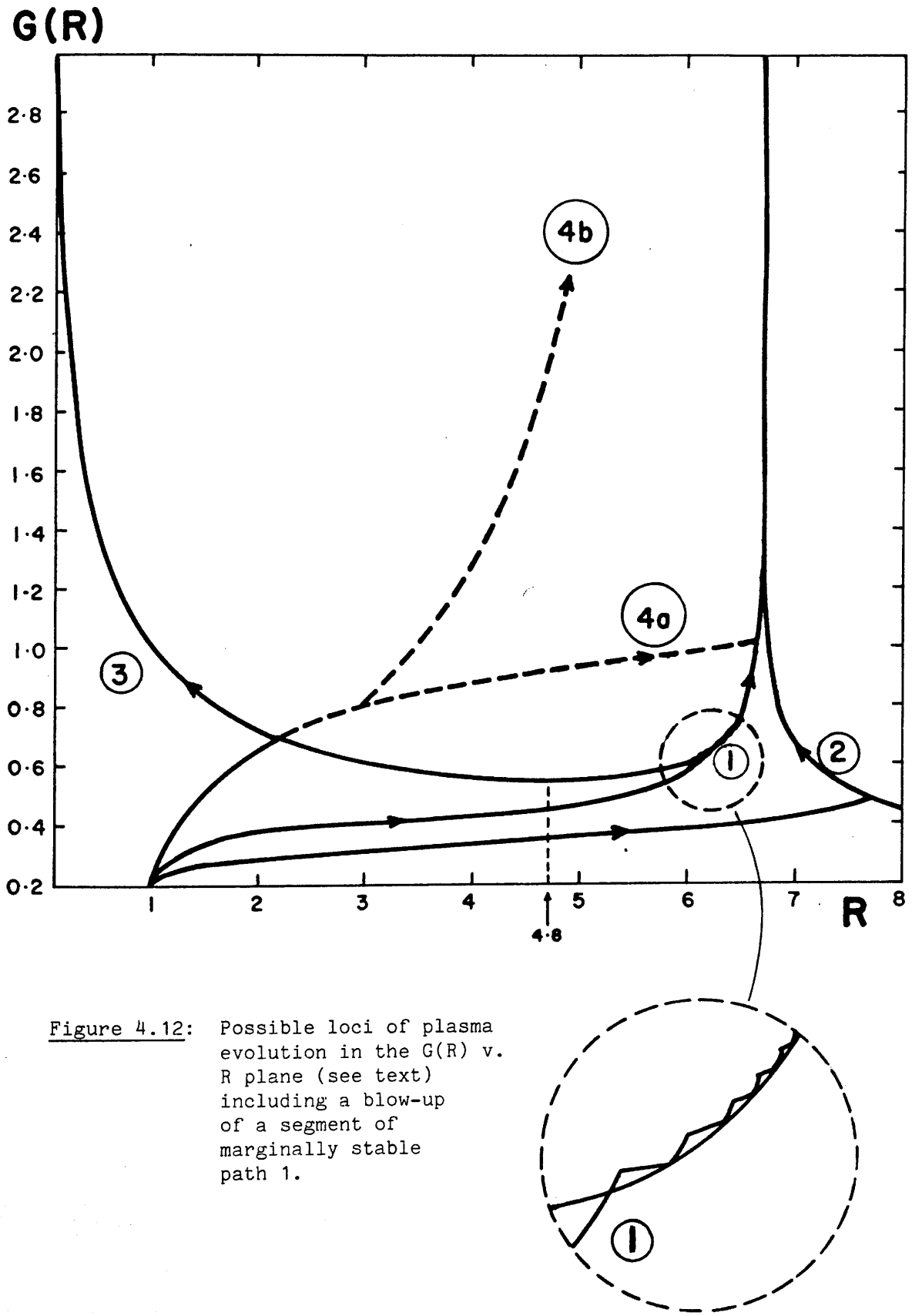

Figure 4.12: Possible loci of plasma evolution in the G(R) v. R plane (see text) including a blow-up of a segment of marginally stable path 1.

(4b), marginal stability is never attained. In Chapter 6 we attempt to model cases of catastrophic heating. By catastrophic we mean that a small excess of v_d over v_{crit} leads to larger values of $|v_d - v_{crit}|$ and the plasma moves further from a state of marginal stability (initially, at least; in the case of path (4a), v_{crit}, i.e. G(R), rises sufficiently rapidly that $v_d \simeq v_{crit}$ at a later time).

Briefly, the failure of the marginal stability hypothesis occurs for $\frac{T_e}{T_i} \lesssim 4.8$ because of the incompatible requirements of tracking the marginal stability curve and specifying $v_d(t)$ as a monotonically increasing function of time. In terms of the original assumptions behind the marginal stability concept (Section 4.2), the hypothesis breaks down because of the extremely large (anomalous) ohmic dissipation rates in the catastrophic regime: the plasma instability time scale is no longer negligible in comparison to the (very short) heating time scale.

4.6 DISCUSSION

We have presented, in this chapter, a simple analysis of the problem of IA wave generation by a prescribed, beam-driven, return current. In addition, it has been demonstrated that there exist two distinct types of IA unstable heating. The first is a marginally stable heating where the onset of instability occurs at $T_e/T_i \gtrsim 4.8$, and the second is a "catastrophic" heating where the onset of instability occurs at $T_e/T_i \lesssim 4.8$ and a marginal stability treatment is impossible.

Further, using typical flaring corona parameters: $T_o = 5\ 10^6$ K, $n_p = 10^{11}\ cm^{-3}$, $\mathcal{E}_o = 100$ keV, together with $t_r = 10$ secs (case (a)) and $t_r = 4$ secs (case (b)), we have shown that the resultant marginally stable plasma evolution leads to rapid heating, by both anomalous ohmic

dissipation of the return current and direct beam collisions, of substantial plasma volume, viz.

$$T_e \simeq 250T_o, T_i \simeq 30\ T_o \quad \text{and } V \simeq 8.5\ 10^{25}\ \text{cm}^3 \quad \text{(case (a))}$$

$$T_e \simeq 1300T_o, T_i \simeq 180\ T_o \quad \text{and } V \simeq 2.3\ 10^{25}\ \text{cm}^3 \quad \text{(case (b))}$$

These hot plasmas emit so much thermal bremsstrahlung that, contrary to previous expectations, the unstable beam-plasma systems may actually emit more hard X-rays than the beam does in the purely collisional thick-target regime relevant to larger injection areas (see Figures (4.10)).

The results we have presented are representative of many cases which may be obtained using different values of the parameters $T_o/n_p^2\ t_r$ and $T_o/\mathcal{E}_o$. In summary, we find that the closer the heating is to being catastrophic then

(i) the larger are the subsequent values of anomalous resistivity, therefore

(ii) the larger are the values of T_e and T_i attained,

(iii) the smaller is the plasma volume heated to these temperatures,

(iv) the less important is the beam collisional term compared to the ohmic term (see Equations (3.4a), (3.12a))

(v) the smaller is the peak thermal to thick-target non-thermal emissivity ratio and, finally,

(vi) the smaller is the percentage of the beam kinetic energy which is converted into plasma heating inside the volume bounded by s_{min} (i.e. the smaller is the "heating efficiency" Δ - see Equation (4.9)).

For simplicity, we have neglected the effect of a magnetic field and the possibility of ion-cyclotron (IC) waves being generated. It is

known that for $T_e/T_i \lesssim 8$, the threshold drift speed for IC waves is lower than that for IA waves (Kindel and Kennel (1971)). Since IC waves preferentially heat ions (i.e. $\chi_{IC} < 0.5$: see Section 2.4), the net effect of these waves is a reduction in the T_e/T_i value at onset of IA instability (if it occurs). The inclusion of IC waves will, therefore, make the possibility of catastrophic heating more likely (see Chapter 7). In Chapter 6 we investigate the time evolution of the plasma in this catastrophic regime by incorporating a wave energy equation of the form

$$\frac{dW}{dt} = \gamma W \qquad (4.27)$$

where γ is the linear growth rate for IA waves, together with a saturation level $W_{sat}(T_e,T_i)$ at which the linear growth of the wave energy W is switched off.

As shown in Figures (4.8), the stopping length of the beam varies considerably throughout the simulations but, as emphasized previously, the model presented here only allows us to calculate the uniform plasma heating in the volume bounded by s_{min}. In order to describe the heating outside s_{min}, a treatment of the combined spatial and temporal dependence is required (see Chapter 8). As explained in Section 3.2, a constant beam collisional heating term, independent of depth z, was assumed. One may wonder if the results we have obtained and the conclusions reached in this chapter are sensitive to the form of the beam collisional heating term we have used. However, it should be noted that we have run our numerical simulations using a collisional term which is twice as large as the term in Equation (3.4a) and we have found that, although the detailed numerical values change somewhat, the conclusions remain valid.

Our neglect of thermal conduction is not as serious an omission as one may initially suspect because, in the anomalous regime, the thermal

conduction is reduced by the same factor as the electrical resistivity is increased. The shortest conductive cooling time attainable by classical conduction is $\simeq s_{min}/(T_e/m_e)^{\frac{1}{2}}$ or about 1.5 secs for the parameters of Figures (4.7a) and (4.8a) at t = 10 secs. However, IA waves typically increase the conductive cooling time to around $s_{min}/(T_e/m_i)^{\frac{1}{2}} \simeq 43$ times longer (Brown, Melrose and Spicer (1979)) $\simeq$ 65 secs. Convective time scales are longer still, being $\simeq s_{min}/(T_i/m_i)^{\frac{1}{2}} \simeq 180$ secs for the parameters of Figures (4.7a) and (4.8a) at t = 10 secs. Consequently, for heating which is well within the marginally stable regime, we do not expect any radical change in our conclusions when convective and anomalous conductive losses are included. We also anticipate that radiation losses will be insignificant at the temperatures achieved here (Summers and McWhirter (1979)).

In conclusion, we believe that the essential result presented here of enhanced ohmic return current dissipation leading to rapid plasma heating to hard X-ray temperatures will remain unaltered. The simple model we have described has yielded useful information and clearly demonstrated the importance of return current instability on the hard X-ray signature of solar flares.

5. A DISPERSION RELATION ANALYSIS OF RETURN CURRENT INSTABILITY

5.1 Introduction

In the previous chapter it was found that the marginal stability approach fails for onset of ion-acoustic instability at electron-ion temperature ratios $T_e/T_i \lesssim 4.8$. We saw that the reason for the failure in this regime derives from the contradictory constraints of specifying $v_d = v_{crit}$, together with the associated function $X(T_e/T_i)$.

However, there is confusion in the solar physics and, indeed, plasma physics literature on the issue of whether or not there is a lower limit of T_e/T_i below which the ion-acoustic instability cannot be excited. For example, Kaplan, Pikelner and Tsytovich (1974) state quite explicitly (p.53) that "...it is necessary that $T_e \gtrsim 5T_i$" (for the growth of ion-acoustic waves). If this were correct, then it would be invalid to apply our v_{crit} and X curves for ion-acoustic waves below $T_e/T_i \simeq 5$, and so it would not be surprising that unphysical results arise in this region. Similar statements are to be found elsewhere, e.g. Melrose (1985) and also Stix (1962), p.214, where a precise lower limit of $T_e/T_i \simeq 3.5$ is set. However, all of these statements are based on the assumption that the relative electron-ion drift speed is much less than the electron thermal speed, i.e. $v_d \ll v_e$. In contrast, Fried and Gould (1961) and Kadomtsev (1965) state that the ion-acoustic instability will arise in an isothermal (i.e. $T_e/T_i \simeq 1.0$) plasma if the drift velocity is large enough: $v_d \gtrsim v_e$

In this chapter we confirm the latter view by solving the linearised dispersion relation describing longitudinal plasma oscillations (see Appendix A) in a field-free hydrogen plasma with a relative electron-ion drift. By doing this we justify using our curves for ion-acoustic

waves below $T_e/T_i \simeq 5$. The drifting electrons constitute the return current and the ions represent the ambient coronal plasma.

We assume Lorentz profiles for the particle distribution functions as they give rise to dispersion relations in the form of polynomial equations in $\omega(k)$ whose roots can be found easily. The behaviour of these modes, both stable and unstable, is explicitly shown for various values of v_d and T_e/T_i. We find that, for sufficiently large v_d, one of the plasma modes (and only this one) goes unstable, i.e. has a positive imaginary angular frequency, ω_i (or growthrate, γ) over a certain range of wavenumber, k. For small k ($<< 1/\lambda_{De}$) this mode exhibits acoustic-type behaviour (i.e. $\omega_r \propto k$) and, for larger k, we find that $\omega_r \sim \omega_{pi}$: hence the terminology "ion-acoustic".

5.2 SINGLE LORENTZ PARTICLE DISTRIBUTIONS

In this section we take the simplest form of the Lorentz profile to describe both the electron and ion velocity distributions:

$$f_\alpha(v) = \frac{1}{\pi} \frac{n_\alpha v_\alpha}{(v-V_\alpha)^2 + v_\alpha^2} \qquad (5.1)$$

where α represents the species type, v_α is a measure of the width of the velocity profile (i.e. the thermal speed) and V_α is the mean drift of the particles with respect to some reference frame. Note that $\int_{-\infty}^{\infty} f_\alpha(v)dv = n_\alpha$ as required by our definition of distribution function (see Appendix A). In our calculations we assume, without loss of generality, that the electrons are drifting with speed v_d through a stationary background of ions, i.e. $V_e \equiv v_d$, $V_i \equiv 0$. Galilean transformations to other frames can easily be made. We assume that the electric and magnetic fields associated with the net current in a given reference frame are sufficiently small that the field-free plasma

equilibrium of the Landau initial value problem is a valid approximation (see Appendix A).

Noting that, in our return current model, the electron and ion streams have the same particle density, n_p, the electron and ion velocity distributions are, respectively,

$$f_e(v) = \frac{1}{\pi} \frac{n_p v_e}{(v-v_d)^2 + V_e^2} \tag{5.2a}$$

$$f_i(v) = \frac{1}{\pi} \frac{n_p v_i}{v^2 + v_i^2} \tag{5.2b}$$

From Appendix A, the linearised dispersion relation describing longitudinal oscillations which arise from a small-amplitude perturbation to the initial plasma equilibrium is:

$$k^2 = \sum_\alpha \frac{\omega_{p\alpha}^2}{n_\alpha} \int_{-\infty}^{\infty} \frac{\partial f_\alpha / \partial v}{v - \omega/k} \, dv \tag{5.3}$$

Equivalently, using integration by parts

$$k^2 = \sum_\alpha \frac{\omega_{p\alpha}^2}{n_\alpha} \int_{-\infty}^{\infty} \frac{f_\alpha \, dv}{(v - \omega/k)^2} \tag{5.4}$$

Substituting from (5.1) we obtain

$$k^2 = \sum_\alpha \frac{\omega_{p\alpha}^2}{\pi} \int_{-\infty}^{\infty} \frac{dv}{[(v-V_\alpha)^2 + v_\alpha^2](v-\omega/k)^2} \tag{5.5}$$

The integral can be evaluated using the Residue Theorem of complex analysis to give the dispersion relation in the form

$$k^2 = \sum_\alpha \frac{\omega_{p\alpha}^2}{(V_\alpha - iv_\alpha - \omega/k)^2} \tag{5.6}$$

For our return current model described above we therefore arrive at the following result:

$$\frac{1}{\omega_{pe}^2} - \frac{\mu}{(\omega+ikv_i)^2} - \frac{1}{(\omega-kv_d + ikv_e)^2} = 0 \qquad (5.7)$$

where $\mu \equiv m_e/m_i$. It is convenient at this stage to introduce the following dimensionless variables

$$W \equiv \frac{\omega}{\omega_{pe}} \quad , \quad K \equiv \frac{kv_e}{\omega_{pe}} \quad , \quad V_d \equiv \frac{v_d}{v_e} \quad , \quad T \equiv \frac{T_i}{T_e} \qquad (5.8)$$

Note that $v_i = T^{\frac{1}{2}} \mu^{\frac{1}{2}} v_e$. The dispersion relation (5.7) can then be re-written as

$$1 - \frac{\mu}{(W+i\,KT^{\frac{1}{2}}\mu^{\frac{1}{2}})^2} - \frac{1}{(W-KV_d + iK)^2} = 0 \qquad (5.9)$$

In order to solve Equation (5.9) in terms of W(K) for each possible mode, it is convenient to re-express the dispersion relation in the following way:

$$\sum_{n=0}^{4} (R_n + i\,I_n)W^n = 0 \qquad (5.10)$$

i.e. as a polynomial equation in W of order 4 where R_n, I_n are the real, imaginary parts of the complex coefficient of W^n. These coefficients are tabulated for ease of reference in Table 5.1.

In practice, especially for higher order Lorentz profiles (e.g. square/double, see Section 5.3), it is advisable to use an algebraic computing language such as FORMAC to obtain these coefficients. Note that the single Lorentz profile has given rise to a dispersion relation in the form of a fourth order polynomial equation in W. We shall find

n	R_n	I_n
0	$K^4T\mu(1-V_d^2)+ K^2\mu(1+T-V_d^2)$	$2K^2V_d\mu(1+K^2T)$
1	$2K(K^2TV_d\mu+2K^2V_dT^{\frac{1}{2}}\mu^{\frac{1}{2}}+V_d\mu)$	$2K^3T^{\frac{1}{2}}\mu^{\frac{1}{2}}(V_d^2-1-T^{\frac{1}{2}}\mu^{\frac{1}{2}})$ $-2K\mu^{\frac{1}{2}}(T+\mu^{\frac{1}{2}})$
2	$K^2(V_d^2 -1-T\mu-4T^{\frac{1}{2}}\mu^{\frac{1}{2}})-(\mu+1)$	$-2K^2V_d(1+2T^{\frac{1}{2}}\mu^{\frac{1}{2}})$
3	$-2KV_d$	$2K(1+T^{\frac{1}{2}}\mu^{\frac{1}{2}})$
4	1	0

Table 5.1: The real and imaginary parts of the complex coefficients of dispersion relation (5.10).

in the next section that the double Lorentz particle distribution for electrons and ions leads to a polynomial of order six.

For the single Lorentz case there are four plasma modes. Mathematically, we may derive these by use of a NAG subroutine which finds the roots of a polynomial equation of a given order with complex coefficients. These roots, which physically represent the sought-after plasma oscillations, can then be depicted graphically by plotting the real and imaginary parts of W against K. Before proceeding to give examples of such solutions it is instructive to derive the asymptotic behaviour of all four modes (i.e. for $K \to 0$ and $K \to \infty$).

We first consider the behaviour of the solutions of the dispersion relation for $K \to 0$. Two of the modes may be obtained approximately ($\forall K$, in fact) by taking the limiting case of infinitely massive ions, i.e. $\mu \to 0$. From Equation (5.9) we then have:

$$W = \pm 1 + KV_d - iK \qquad (5.11)$$

or, in terms of the real and imaginary parts of the angular frequency:

$$W_r = \pm 1 + KV_d \qquad (5.12a)$$

$$W_i = - K \qquad (5.12b)$$

Note that for $K \to 0$, or alternatively $\forall K$ if $V_d = 0$, we have the result that $W_r = \pm 1$. Recalling our normalisation convention, i.e. (5.8), we see that $\omega_r = \pm \omega_{pe}$. For this reason we may refer to these two modes as electron plasma oscillations. They are analogous to the well-known Langmuir mode associated with the Maxwellian velocity distribution. These oscillations are <u>always</u> damped in our system, at a rate proportional to the wavenumber. The opposite signs in W_r simply indicate that the plasma modes have phase velocities in opposite directions: one moves to the right (i.e. positive direction) in our frame of reference (i.e. w.r.t. the stationary ion background) and the other moves to the left.

The other two solutions of the dispersion relation can be found for $K \to 0$ by assuming them to represent low-frequency modes so that we may drop the term in ω_{pe}^2 in Equation (5.7). The dimensionless dispersion relation (5.9) then becomes:

$$\frac{\mu}{(W + iKT^{\frac{1}{2}}\mu^{\frac{1}{2}})^2} + \frac{1}{(W-KV_d + iK)^2} = 0 \qquad (5.13)$$

After some algebraic manipulation we find that

$$W_r = \frac{K}{1+\mu}\left[\pm \mu^{\frac{1}{2}} (T^{\frac{1}{2}}\mu^{\frac{1}{2}} - 1) + \mu V_d\right] \qquad (5.14a)$$

$$W_i = \frac{K}{1+\mu}\left[\pm \mu^{\frac{1}{2}} V_d - \mu - T^{\frac{1}{2}}\mu^{\frac{1}{2}}\right] \qquad (5.14b)$$

Strictly, Equations (5.14) hold for $K \ll 1$. Note that, for a given T and V_d, $W_r \propto K$, i.e. these two solutions represent acoustic plasma oscillations. This justifies *a posteriori* our initial assumption of low-frequency modes since $W_r \ll 1$ for $K \ll 1$. As shown explicitly below for these two modes, as $K \to \infty$ the real part of the angular frequency $W_r \to \pm\mu^{\frac{1}{2}}$, i.e. $\omega_r \to \pm\omega_{pi}$. We may refer to solutions (5.14) then, as "ion-acoustic" modes.

The upper sign in (5.14b) gives the condition for instability, since $W_i > 0$ corresponds to exponentially growing solutions of the dispersion relation (see Appendix A):

$$V_d > V_{crit} \equiv T^{\frac{1}{2}} + \mu^{\frac{1}{2}} \qquad (5.15)$$

For example, in an isothermal plasma (T = 1), instability occurs if, and only if, the drift speed $v_d \gtrsim 1.02\ v_e$. The unstable mode is the "upper" ion-acoustic oscillation, i.e. the plasma wave with phase velocity to the right, in the same direction as the drifting electrons. It is important to realise that only one mode may go unstable in a two-component plasma. This follows from the Penrose (1960) criterion which states in a precise mathematical way that a minimum in the combined particle distribution function must exist, and be of sufficient depth, for instability to arise. Each such minimum in the distribution function corresponds to an unstable mode. It can be shown that a two-component velocity distribution can have only one minimum at most. There can therefore be only one unstable mode.

We now derive the behaviour of the modes for $K \to \infty$ with some rigour, along lines suggested by P.A. Sweet (personal communication, 1985). Let us introduce a new dimensionless variable W*, such that W=KW*. The

dispersion relation (5.9) then becomes

$$K^2 = \frac{1}{(W^* + i - V_d)^2} + \frac{\mu}{(W^* + i\,\mu^{\frac{1}{2}}\,T^{\frac{1}{2}})^2} \qquad (5.16)$$

As $K \to \infty$ we have two possibilities to consider

Case (i): $W^* \to V_d - i$

Introduce another new dimensionless variable, W_1, such that $W^* + i - V_d = W_1/K$. Then

$$K^2 = \frac{K^2}{W_1^2} + \frac{\mu}{(W_1/K - i + V_d + i\mu^{\frac{1}{2}}T^{\frac{1}{2}})^2}$$

$$\text{i.e.} \qquad 1 = \frac{1}{W_1^2} + \frac{1}{K^2}\,\frac{\mu}{(W_1/K + V_d - i + i\mu^{\frac{1}{2}}T^{\frac{1}{2}})^2} \qquad (5.17)$$

We may rewrite (5.17) as

$$1 = \frac{1}{W_1} + \frac{a}{K} \qquad (5.18)$$

where we assume that a is a well-behaved function of K such that $a/K^2 \to 0$ as $K \to \infty$ (i.e. assume that W_1 is well-behaved as $K \to \infty$). Therefore, we have that

$$W_1 = (1 - \frac{a}{K^2})^{-\frac{1}{2}}$$

$$\text{i.e.} \qquad W_1 = \pm(1 + \frac{a}{2K^2})$$

$$\text{i.e.} \qquad W_1 = \pm 1 + 0\,(\frac{1}{K^2})$$

$$\text{i.e.} \qquad W^* + i - V_d = \pm\frac{1}{K} + 0(\frac{1}{K^3})$$

$$\text{i.e.} \qquad W^* = -i + V_d \pm \frac{1}{K} + 0\,(\frac{1}{K^3})$$

$$\text{i.e.} \qquad W = -iK + (KV_d \pm 1) + 0\,(\frac{1}{K^2})$$

Therefore, the behaviour of two of the modes for $K \to \infty$ is

$$W_r = \pm 1 + KV_d \qquad (5.19a)$$

$$W_i = -K \qquad (5.19b)$$

Compare with (5.12): these are the same modes found previously $\forall K$, assuming infinitely massive ions.

Case (ii) $W^* \to -i\mu^{\frac{1}{2}} T^{\frac{1}{2}}$

Introduce W_2 such that $W_2/K = W^* + i\mu^{\frac{1}{2}} T^{\frac{1}{2}}$. Then (5.16) becomes

$$K^2 = \frac{1}{(W_2/K - i\mu^{\frac{1}{2}} T^{\frac{1}{2}} + i - V_d)^2} + \frac{\mu K^2}{W_2^2}$$

i.e. $$1 = \frac{1}{K^2} \frac{1}{(W_2/K - i\mu^{\frac{1}{2}} T^{\frac{1}{2}} + i - V_d)^2} + \frac{\mu}{W_2^2} \qquad (5.20)$$

We may rewrite this in the form

$$1 = \frac{b}{K^2} + \frac{\mu}{W_2^2} \qquad (5.21)$$

Assuming that $b/K^2 \to 0$ as $K \to \infty$ (for well-behaved W_2) then:

$$W_2 = \mu^{\frac{1}{2}} \left(1 - \frac{b}{K^2}\right)^{-\frac{1}{2}}$$

i.e. $$W_2 = \pm \mu^{\frac{1}{2}} + O\left(\frac{1}{K^2}\right)$$

i.e. $$W^* + i\mu^{\frac{1}{2}} T^{\frac{1}{2}} = \pm \frac{\mu^{\frac{1}{2}}}{K} + O\left(\frac{1}{K^3}\right)$$

i.e. $$W^* = \pm \frac{\mu^{\frac{1}{2}}}{K} - i\mu^{\frac{1}{2}} T^{\frac{1}{2}} + O\left(\frac{1}{K^3}\right)$$

i.e. $$W = \pm\mu^{\frac{1}{2}} - i\mu^{\frac{1}{2}} T^{\frac{1}{2}} K + O\left(\frac{1}{K^2}\right)$$

Therefore, we have obtained the other two modes for $K \to \infty$.

$$W_r = \pm\mu^{\frac{1}{2}} \qquad (5.22a)$$

$$W_i = -\mu^{\frac{1}{2}} T^{\frac{1}{2}} K \qquad (5.22b)$$

These are the two "ion-acoustic" modes found earlier (Equations (5.14)). Note that the real part of the frequency approaches a constant ($\omega_r \to \pm\omega_{pi}$) and that the modes are always damped at large K. We also see that the damping is smaller for larger values of $T_e/T_i (\equiv 1/T)$.

Having shown analytically the asymptotic behaviour of the four plasma modes associated with the single Lorentz dispersion relation, we will now present specific numerical solutions of Equation (5.9) for various pairs of the parameters V_d, T.

Figures 5.1 depict plots of W_r, W_i v. K for the simplest possible case of an isothermal plasma with no relative electron-ion drift, i.e. T = 1, V_d = 0. Modes 1 and 2 are the Langmuir-type oscillations and have a constant real frequency, $W_r = \pm 1$, in agreement with Equation (5.12a). Figure 5.1b shows that the imaginary part of the frequency of these modes is -K, as predicted by Equation (5.21b). Modes 3 and 4 are the acoustic modes. In Figure 5.1 we see that $W_r \alpha$ K (Equation (5.14a)) while, at larger K, $W_r \to \pm\mu^{\frac{1}{2}} \simeq \pm 0.023$ (Equation (5.22a)). The behaviour of the imaginary part of the frequency, W_i, confirms (5.14b), (5.22b).

Figures 5.2 indicate the behaviour of the modes on the introduction of a drift speed. Here $T_e/T_i = 1$ and $V_d = 2$ ($> V_{crit}$: see Equation (5.15)). Figures (5.2c,d) are blow-ups of Figures (5.2a,b) respectively. The drift speed, V_d, determines the gradient of the real parts of modes 1 and 2 (see Equation (5.12a)) and we note that the acoustic mode 3 is unstable (see Figures 5.2 b,d) over the range K = 0,0.5 with a maximum growth rate of $\gamma \simeq 6.10^{-3}$ at K = 0.5. As expected from Equation (5.12b),

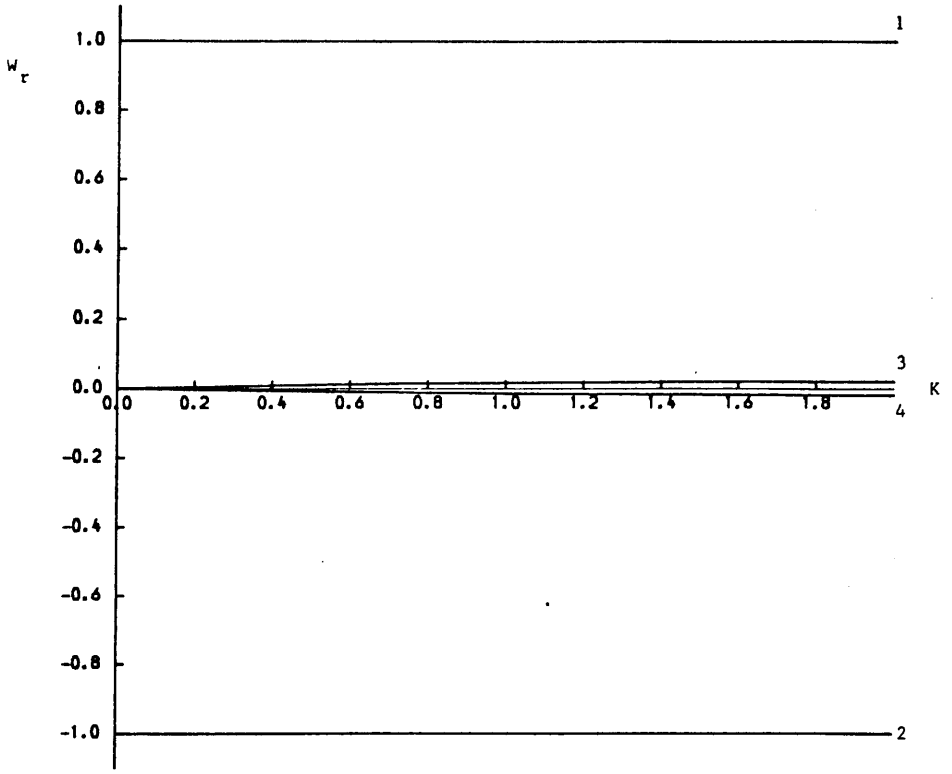

Figure 5.1a: Single Lorentz: W_r v. K for $V_d = 0$, $T_e/T_i = 1$

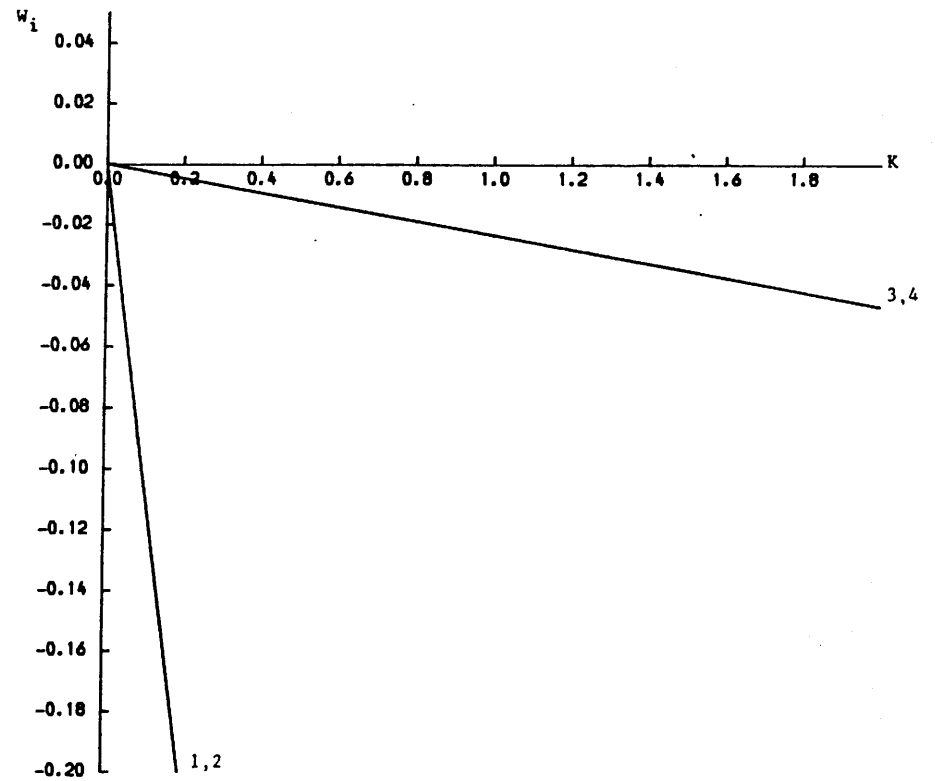

Figure 5.1b: Single Lorentz: W_i v. K for $V_d = 0$, $T_e/T_i = 1$

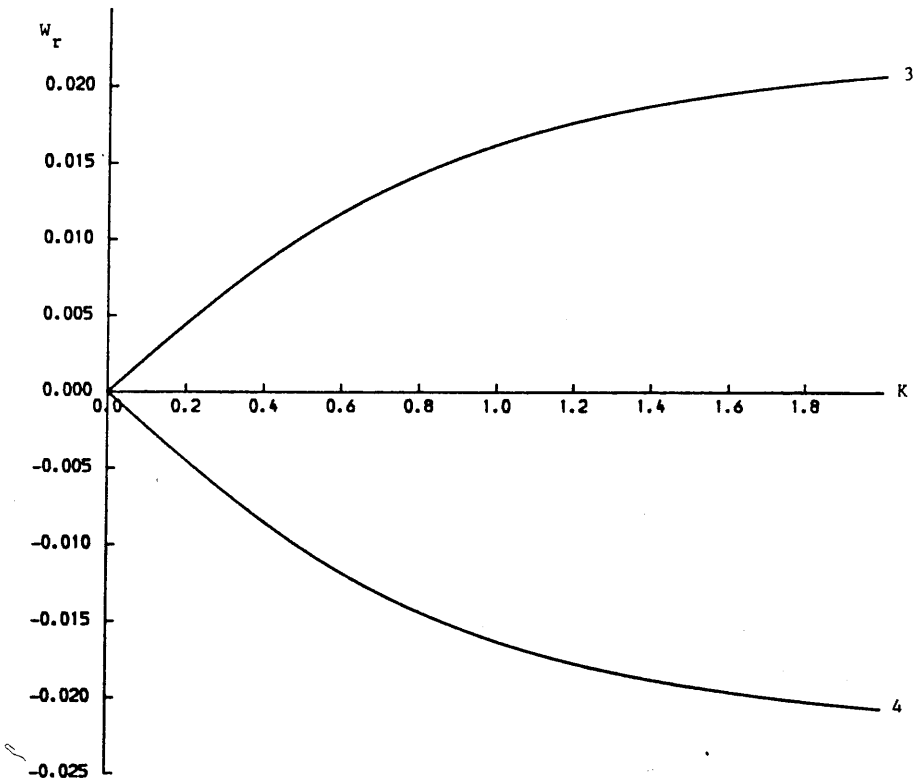

Figure 5.1c: Blow-up of Figure 5.1a.

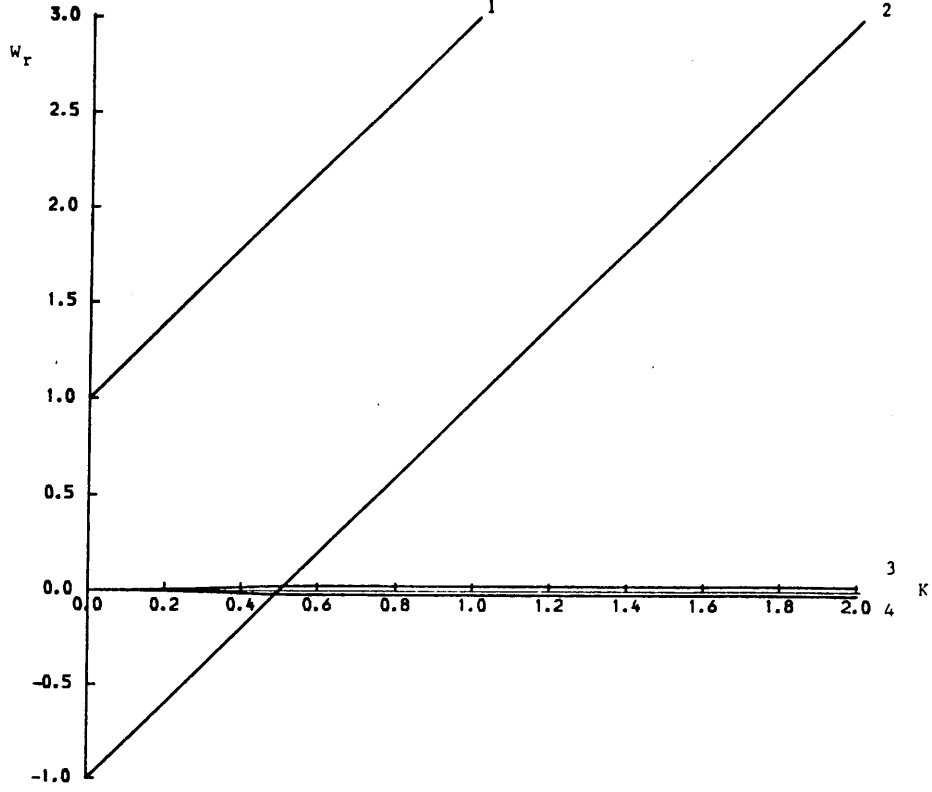

Figure 5.2a: Single Lorentz: W_r v. K for $V_d = 2$, $T_e/T_i = 1$

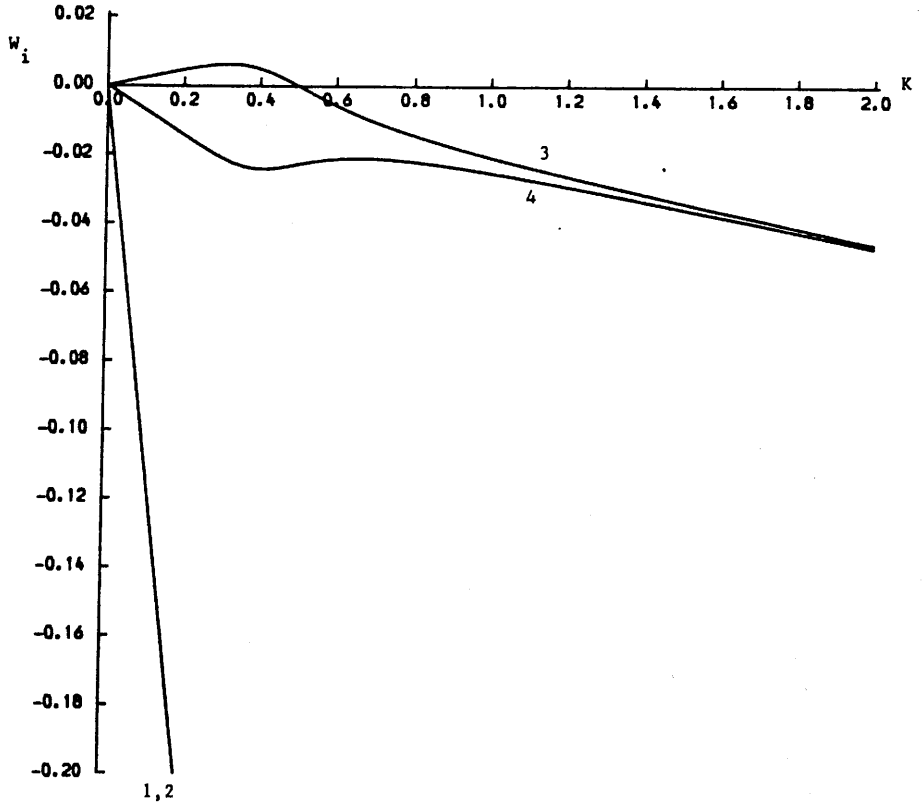

Figure 5.2b: Single Lorentz: W_i v. K for $V_d = 2$, $T_e/T_i = 1$

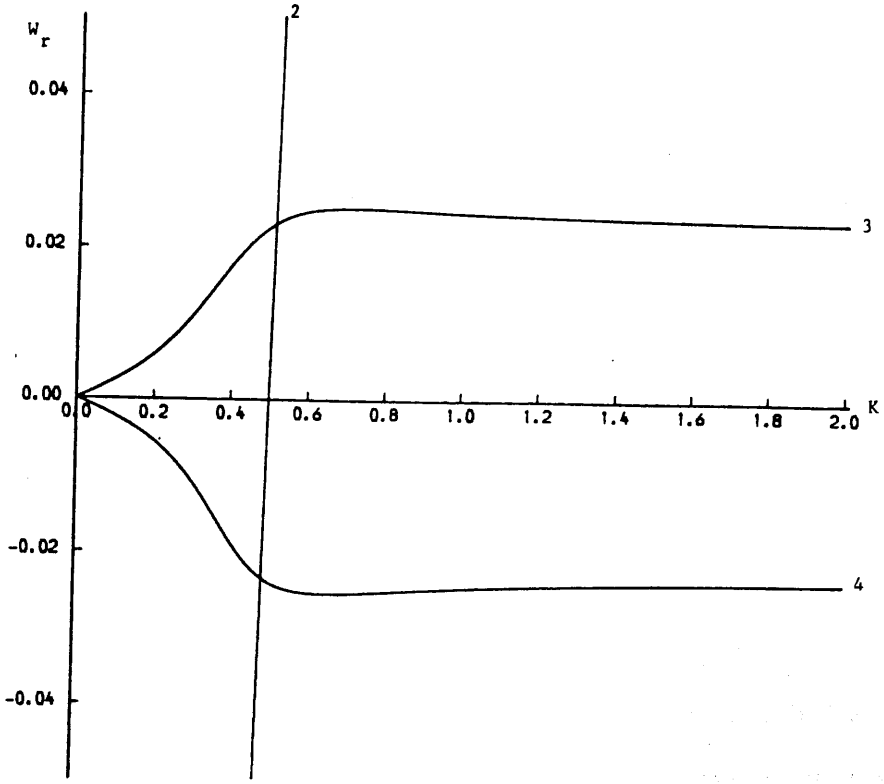

Figure 5.2c: Blow-up of Figure 5.2a

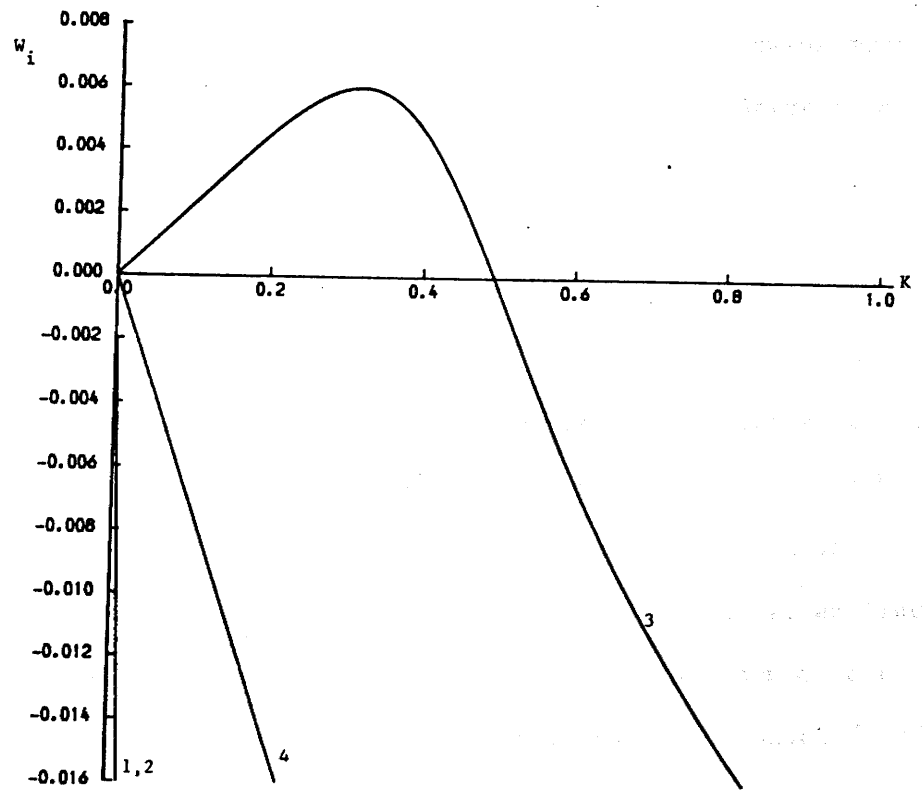

Figure 5.2d: Blow-up of Figure 5.2b.

the "electron Langmuir" modes 1, 2 have the same damping rate. Figures (5.2 c,d) depict clearly the properties of the unstable mode. Note that over the range of unstable wavenumber, K, the real part of the frequency displays acoustic-type behaviour, i.e. $W_r \alpha K$. Outside this range of unstable wavenumber, i.e. for $K > 0.5$, W_r tends to a constant value, $\mu^{\frac{1}{2}}$.

As a further example, we now turn our attention to an electron-ion plasma with $T_e/T_i = 5$ (i.e. $T = 0.2$). Equation (5.15) yields the critical drift speed for onset of instability as $V_{crit} \simeq 0.47$. Figures 5.3 show the behaviour of the modes for a drift speed just below V_{crit}, i.e. $V_d = 0.4$, while figures 5.4 are for the case $V_d = 0.6$. As expected, we again find that mode 3 is unstable. Here, the acoustic oscillations having positive phase velocities with wavenumbers in the range $K = 0,\ 0.44$ are unstable, with maximum growth rate $\gamma \simeq 5.10^{-4}$ at $K \simeq 0.24$. Figure 5.3c is a blow-up of Figure 5.3a showing more clearly the frequencies of the acoustic modes in the stable drift speed case. Figures 5.4c,d are blow-ups of Figures 5.4a,b respectively, for the unstable case. Again we note the property $W_r \alpha K$ of mode 3 in the range of unstable wavenumber.

In summary, we have demonstrated that assuming single Lorentz distributions for an electron-ion plasma leads to a dispersion relation which generates four modes. One of these modes becomes unstable for a sufficiently large drift speed, V_d. This unstable oscillation, with positive phase velocity, may be termed "ion-acoustic" as we find that $W_r \alpha K$, for small K, while $W_r \to \mu^{\frac{1}{2}}$ as $K \to \infty$. (The counterpart of this mode, with negative phase velocity, is also an "ion-acoustic" mode). Instability arises in a single Lorentz isothermal plasma if, and only if, $V_d \gtrsim 1.02$, i.e. $v_d \gtrsim v_e$.

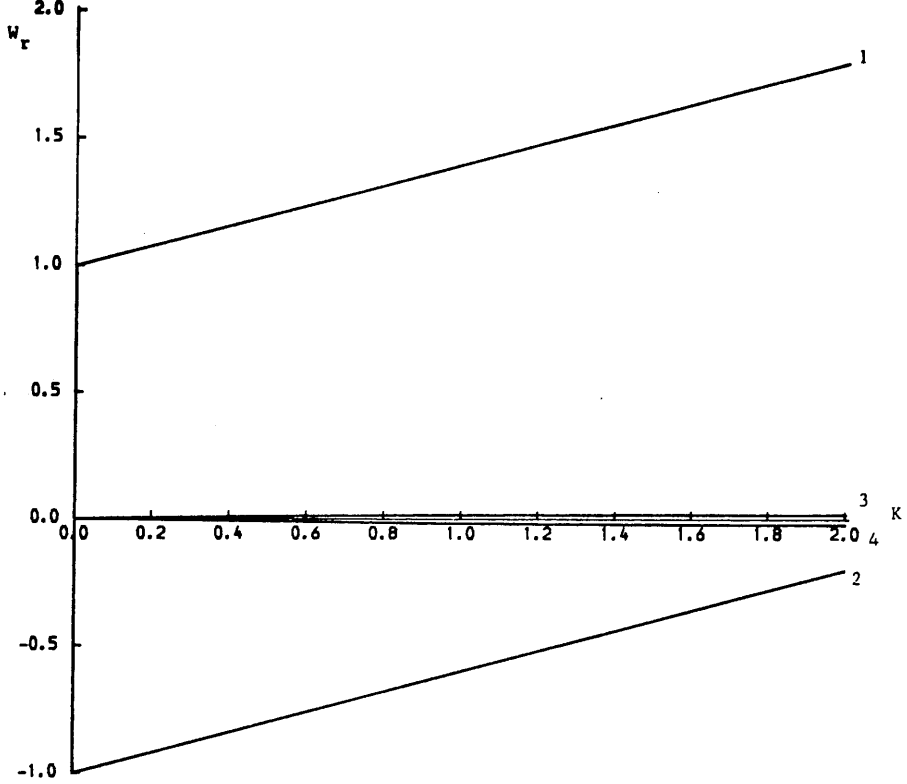

Figure 5.3a: Single Lorentz: W_r v. K for $V_d = 0.4$, $T_e/T_i = 5$

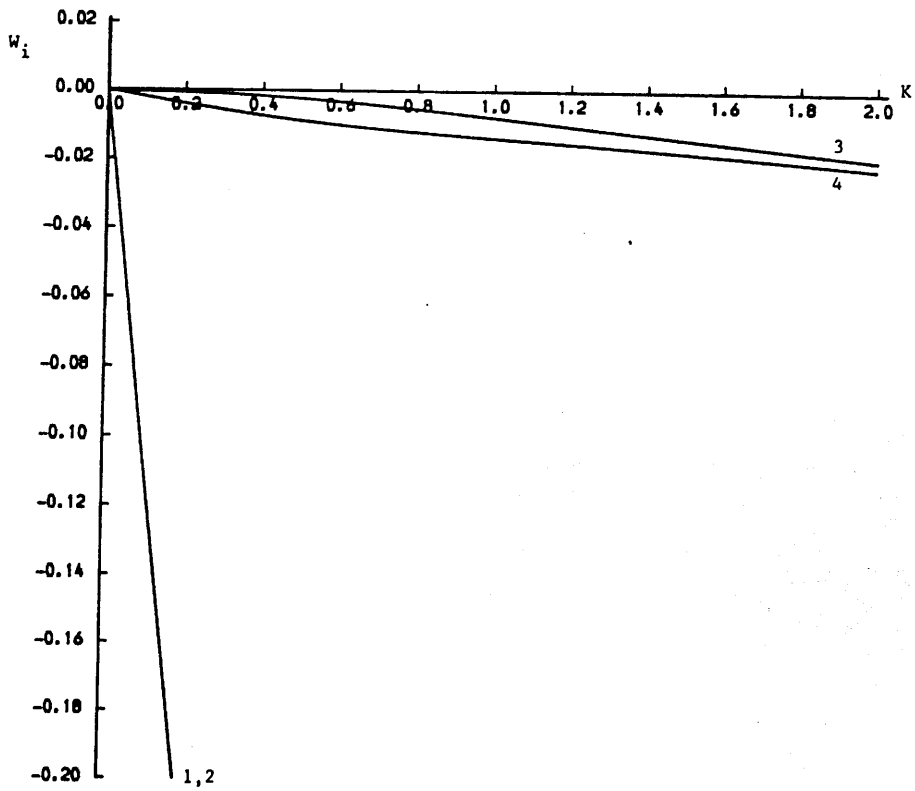

Figure 5.3b: Single Lorentz: W_i v. K for $V_d = 0.4$, $T_e/T_i = 5$

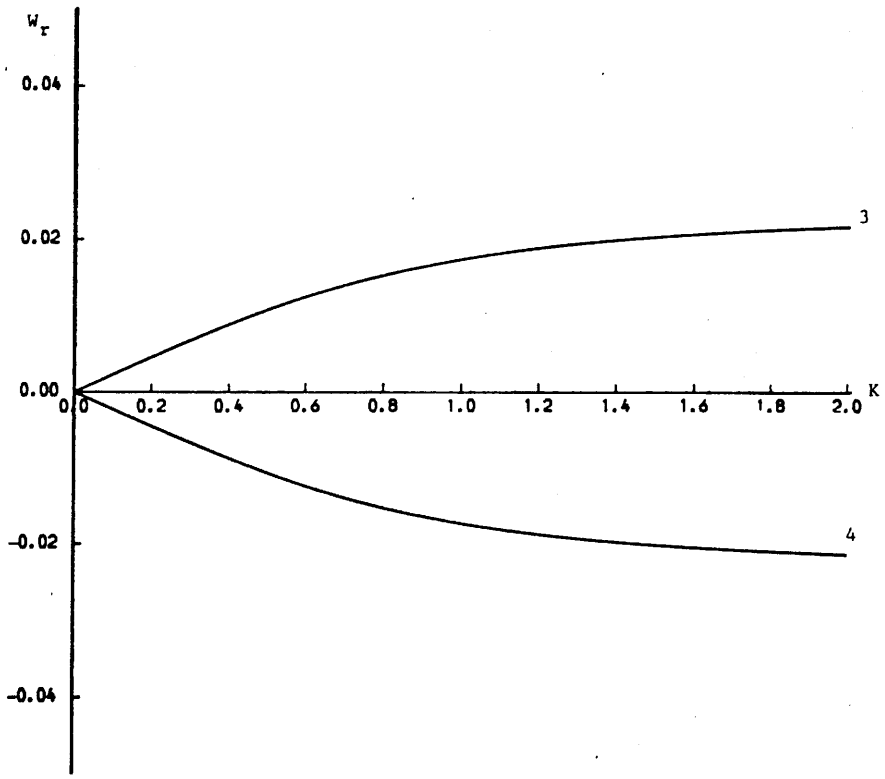

Figure 5.3c: Blow-up of Figure 5.3a.

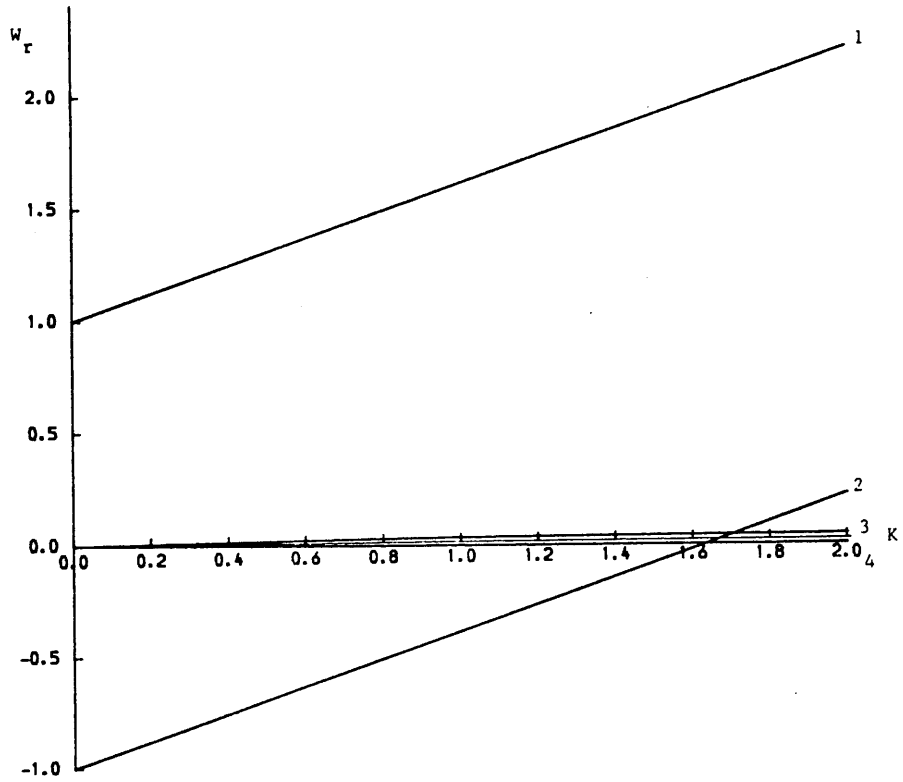

Figure 5.4a: Single Lorentz: W_r v K for $V_d = 0.6$, $T_e/T_i = 5$

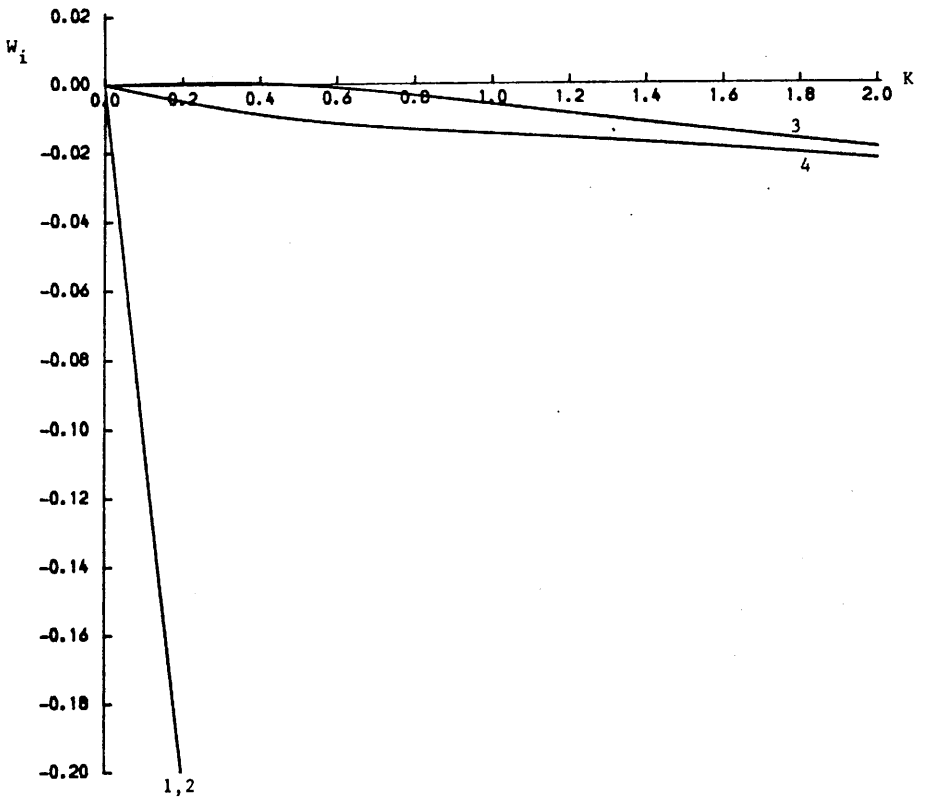

Figure 5.4b: Single Lorentz: W_i v. K for $V_d = 0.6$, $T_e/T_i = 5$

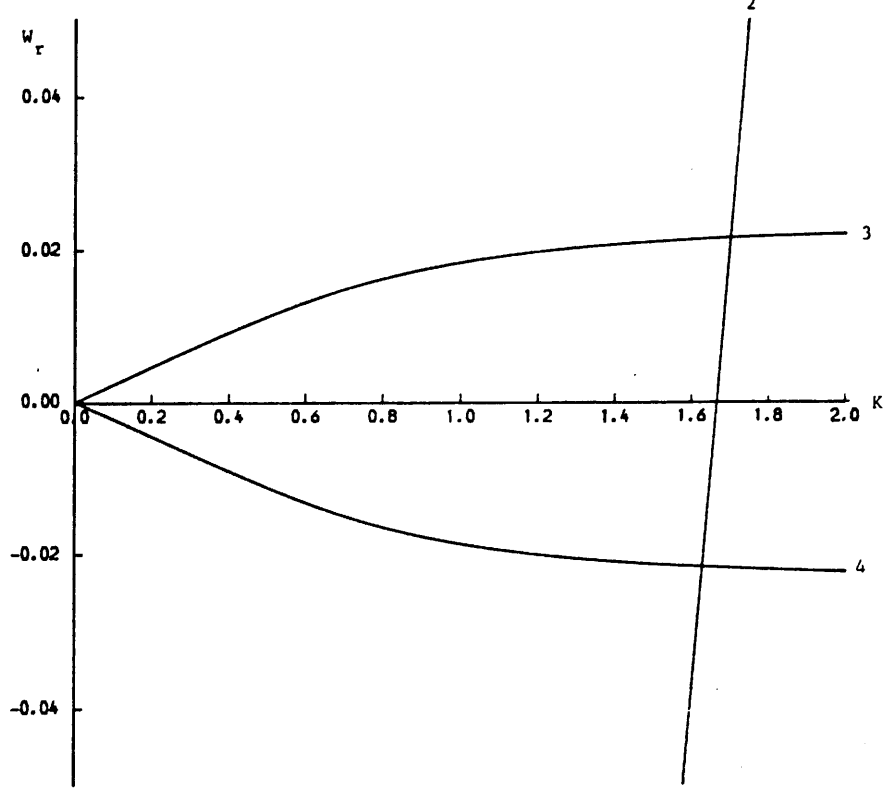

Figure 5.4c: Blow-up of Figure 5.4a.

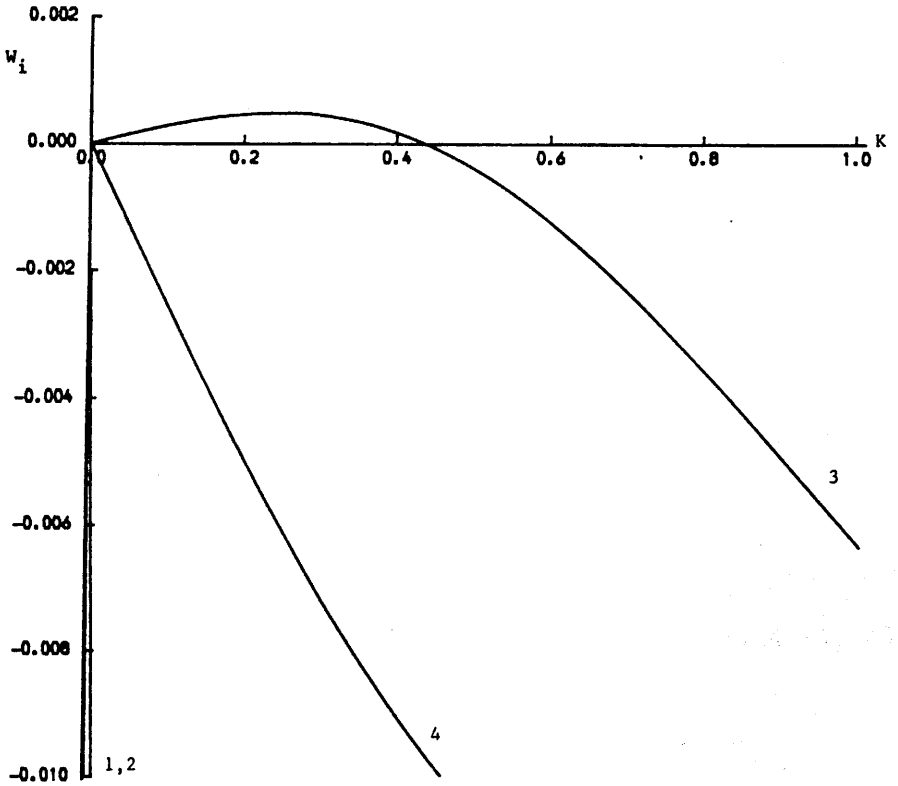

Figure 5.4d: Blow-up of Figure 5.4b.

5.3 Double Lorentz Particle Distributions

In the previous section we assumed that the velocity distributions of the electrons and ions were described by the single Lorentz profile of (5.1). This enabled us to derive a simple dispersion relation describing the behaviour of the plasma modes. Although this gave us some very useful information, it must be noted that the single Lorentz distribution has unphysical characteristics. One of these is the infinite energy content of such a distribution: the integral $\int_{-\infty}^{\infty} v^2 f_\alpha(v)dv$, where $f_\alpha(v)$ is as given in (5.1), does not converge. In addition, although our simple dispersion relation yielded the well-known Langmuir mode, this mode did not display a "thermal correction" associated with a realistic velocity distribution such as the Maxwellian (see Equation (A.43)).

We can, however, utilise a higher order Lorentz profile which more closely matches the properties of a Maxwellian and yet still generates a dispersion relation whose roots can be fairly readily found. The distribution function we now take is the so-called square, or double, Lorentz:

$$f_\alpha(v) = \frac{2}{\pi} \frac{n_\alpha v_\alpha^3}{[(v-V_\alpha)^2 + v_\alpha^2]^2} \qquad (5.23)$$

where v_α is some measure of the thermal spread of the profile and V_α is the mean drift speed. Again, the distribution function satisfies the normalisation convention $\int_{-\infty}^{\infty} f_\alpha(v)dv = n_\alpha$.

We now show that the energy content associated with (5.23) is the same as for the one-dimensional Maxwellian:

$$f_M(v) = \frac{n_\alpha}{\sqrt{2\pi}\, v_M} \text{Exp}\left(-\frac{(v-V_M)^2}{2v_M^2}\right) \qquad (5.24)$$

where $v_M = \sqrt{T_\alpha/m_\alpha}$ is the thermal speed associated with the Maxwellian distribution and V_M is the mean drift speed. For ease of the present calculation, and without loss of generality, let the mean drift speeds of both distributions be zero . Now, the total energy content of the double Lorentz distribution is:

$$\mathcal{E}_L = \int_{-\infty}^{\infty} v^2 \, f_\alpha(v) dv$$

$$= \frac{2n_\alpha v_\alpha^3}{\pi} \underbrace{\int_{-\infty}^{\infty} \frac{v^2 \, dv}{(v^2+v_\alpha^2)^2}}_{I}$$

The integral I can be evaluated by introducing a new variable x such that $v = v_\alpha \tan x$. We find that $I = \pi/2v_\alpha$,

$$\mathcal{E}_L = n_\alpha v_\alpha^2 \qquad (5.25)$$

The total energy content of the Maxwellian distribution is

$$\mathcal{E}_M = \int_{-\infty}^{\infty} v^2 \, f_M(v) dv$$

$$= \frac{n_\alpha}{\sqrt{2\pi} \, v_M} \int_{-\infty}^{\infty} v^2 \exp(-v^2/2v_M^2) dv$$

The integral can be expressed in terms of the gamma function $\Gamma(u)$ and we then obtain:

$$\mathcal{E}_M = n_\alpha v_M^2 \qquad (5.26)$$

Comparing (5.25) and (5.26) we see that the energy contents of both distributions are the same <u>if</u> we identify the double Lorentz half-width, v_α, with the thermal speed $v_M = \sqrt{T_\alpha/m_\alpha}$.

We now derive the thermal correction of the Langmuir mode as shown by P. McQuillan (personal communication, 1985). Consider the double

Lorentz dispersion relation for a single electron component plasma (with a charge-neutralising substrate of infinitely massive ions):

$$\frac{1}{\omega_{pe}^2} - \frac{1}{(\omega + i k v_e)^2} - \frac{2i k v_e}{(\omega + i k v_e)^3} = 0 \qquad (5.27)$$

Introducing the same dimensionless variables as before (see (5.8)), the dispersion relation takes the form:

$$1 - \frac{1}{(W + iK)^2} - \frac{2i K}{(W + i K)^3} = 0 \qquad (5.28)$$

To solve this for W(K) set $Q = W + iK$. Then (5.28) becomes

$$Q^3 - Q - 2iK = 0 \qquad (5.29)$$

Now let $Q = iX$ so that

$$X^3 + X + 2K = 0 \qquad (5.30)$$

We have thus obtained a polynomial of order 3 which has real coefficients. There must exist at least one real root, a, of this polynomial. The polynomial can then be rewritten:

$$X^3 + X + 2K = (X-a)(X^2 + bX + c), \text{ where } b,c \text{ are real} \qquad (5.31)$$

By equating coefficients of the powers of X, we find that $b=a$, $c= a^2 + 1$. The roots of Equation (5.30) are then found to be

$$X = a, \; -\frac{a}{2} \pm \frac{i}{2}(3a^2 + 4)^{\frac{1}{2}} \qquad (5.32)$$

When $X = a$, $W = i(a-K)$. This mode is purely imaginary and therefore has zero group and phase velocity. For the other two modes we have

$$W = -i\left(\frac{a}{2} + K\right) \pm \frac{1}{2}(3a^2 + 4)^{\frac{1}{2}} \qquad (5.33)$$

Now, from Equation (5.30) we note that $X \simeq -2K$ for $K \ll 1$, since $X^3 \ll X$ for small K. By equating the RHS of (5.31) to zero we also obtain $X = a(a^2+ 1)$. As we know that $X \simeq -2K \ll 1$ for $K \ll 1$, we

conclude that $X \simeq a$ and hence $a \simeq -2K$. Substituting $a = -2K$ in (5.33) gives us $W_i = 0$ and:

$$W_r = \pm(1 + 3K^2)^{\frac{1}{2}}$$

$$\text{i.e.} \quad W_r \simeq \pm (1 + \frac{3}{2} K^2) \quad , \quad K \ll 1 \qquad (5.34)$$

or, in the usual terms,

$$\omega_r \simeq \pm \omega_{pe} (1 + \frac{3}{2} k^2 \lambda_{De}^2) \quad , \quad k \ll \frac{1}{\lambda_{De}} \qquad (5.35)$$

In other words, the double Lorentz distribution gives the same thermal correction to the Langmuir mode, for small k, as the Maxwellian (see Equation (A.43)).

As before, we wish the dispersion relation describing equal density electron and ion streams with a relative drift speed, v_d, in order to examine return current instability. Evaluated in the rest frame of the ions we have:

$$\frac{1}{\omega_{pe}^2} - \frac{\mu}{(\omega + i k v_i)^2} - \frac{2i\ k v_i}{(\omega + i k v_i)^3} - \frac{1}{(\omega - kv_d + ikv_e)^2} - \frac{2i k v_e}{(\omega - kv_d + ikv_e)^3} = 0 \qquad (5.36)$$

and, in dimensionless form:

$$1 - \frac{\mu}{(W + iKT^{\frac{1}{2}}\mu^{\frac{1}{2}})^2} - \frac{2i\ KT^{\frac{1}{2}}\mu^{3/2}}{(W + i\ KT^{\frac{1}{2}}\mu^{\frac{1}{2}})^3} - \frac{1}{(W - KV_d + i\,K)^2} - \frac{2i\,K}{(W - KV_d + i\,K)^3} = 0 \qquad (5.37)$$

This can be re-expressed in the following way (cf. Equation (5.10)):

$$\sum_{n=0}^{6} (R_n + i\ I_n) W^n = 0 \qquad (5.38)$$

i.e. a polynomial equation in W of order 6, where R_n, I_n are the real, imaginary parts, respectively, of the complex coefficient of W^n. These are tabulated in Table 5.2.

n	R_n	I_n
0	$K^6T^{3/2}\mu^{3/2}(3V_d^2-1)+3K^4T^{1/2}\mu^{3/2}(3V_d^2-T-1)$	$K^6V_dT^{3/2}\mu^{3/2}(V_d^2-3)$ $+K^4V_dT^{1/2}\mu^{3/2}(3V_d^2-T-9)$
1	$3K^5V_dT\mu(V_d^2-2T^{1/2}\mu^{1/2}-3)$ $+K^3V_d\mu(V_d^2-18T^{1/2}\mu^{1/2}-3T-3)$	$-3K^5T\mu(V_d^2T^{1/2}\mu^{1/2}+3V_d^2$ $-T^{1/2}\mu^{1/2}-1)-K^3\mu(9V_d^2T^{1/2}\mu^{1/2}$ $+3V_d^2-T^{3/2}\mu^{1/2}-9T^{1/2}\mu^{1/2}-9T-1)$
2	$-3K^4T^{1/2}\mu^{1/2}(3V_d^2T^{1/2}\mu^{1/2}+3V_d^2-T\mu$ $-3T^{1/2}\mu^{1/2}+1)-3K^2\mu(V_d^2\mu^{1/2}-3T^{1/2}\mu$ $-T\mu^{1/2}-\mu^{1/2}-3T^{1/2})$	$-3K^4V_dT^{1/2}\mu^{1/2}(V_d^2-T\mu-9T^{1/2}\mu^{1/2}-3)$ $+3K^2V_d\mu^{1/2}(T^{1/2}\mu+2\mu^{1/2}+T^{1/2})$
3	$-K^3V_d(V_d^2-9T\mu-18T^{1/2}\mu^{1/2}-3)$ $+KV_d(3\mu+1)$	$K^3(9V_d^2T^{1/2}\mu^{1/2}+3V_d^2-T^{3/2}\mu^{3/2}$ $-9T\mu-9T^{1/2}\mu^{1/2}-1)$ $-3K(T^{1/2}\mu^{3/2}+\mu+T^{1/2}\mu^{1/2}+1)$
4	$3K^2(V_d^2-T\mu-3T^{1/2}\mu^{1/2}-1)-\mu-1$	$-3K^2V_d(3V_dT^{1/2}\mu^{1/2}+2)$
5	$-3KV_d$	$3K(T^{1/2}\mu^{1/2}+1)$
6	1	0

Table 5.2: The real and imaginary parts of the complex coefficients of dispersion relation (5.38)

Although it is still possible to employ the same NAG routine to find the roots of Equation (5.38), the dispersion relation is considerably more complex than before and we do not offer an analytic analysis of the asymptotic behaviour of the modes. Such a treatment has been performed, however, by P. McQuillan and P. A. Sweet (personal communication, 1985) and confirms the numerical work presented below.

We again take the simplest case of an isothermal plasma with no relative electron-ion drift: $V_d = 0$, $T = 1$. Figures 5.5 show the variation of W_r and W_i with K. Essentially, we find the same four modes as before (numbers 1-4; see Figures 5.1) plus an additional two modes, making six in total, as expected. Mode 5 can be regarded as another electron mode, more heavily damped than modes 1 and 2, while mode 6 is a new ion mode, also more heavily damped than its counterparts, modes 3 and 4.

With the introduction of a drift speed, $V_d = 1$, some of the degeneracy of the modes is removed (Figures 5.6). It is seen that the electron modes (1,2,5) have a gradient in their W_r v K variation equal to the drift speed, just as in the single Lorentz case. In contrast, however, instability has already set in at $V_d = 1$, with mode 3 being unstable over the range of wave numbers K = 0, 1.0. The maximum growth rate is $\gamma \simeq 3.5\ 10^{-3}$ at K = 0.65, and occurs for the same mode, obviously, as before (e.g. Figure 5.2b). The other new solution, mode 6, has a smaller frequency than modes 3 and 4, but also displays acoustic behaviour ($W_r \alpha K$) for small K.

For comparison with the single Lorentz case (Figures 5.2) we have calculated the solutions of dispersion relation (5.38) for $V_d = 2$, $T_e/T_i = 1$ (Figures 5.7). Mode 3 is more strongly unstable than before,

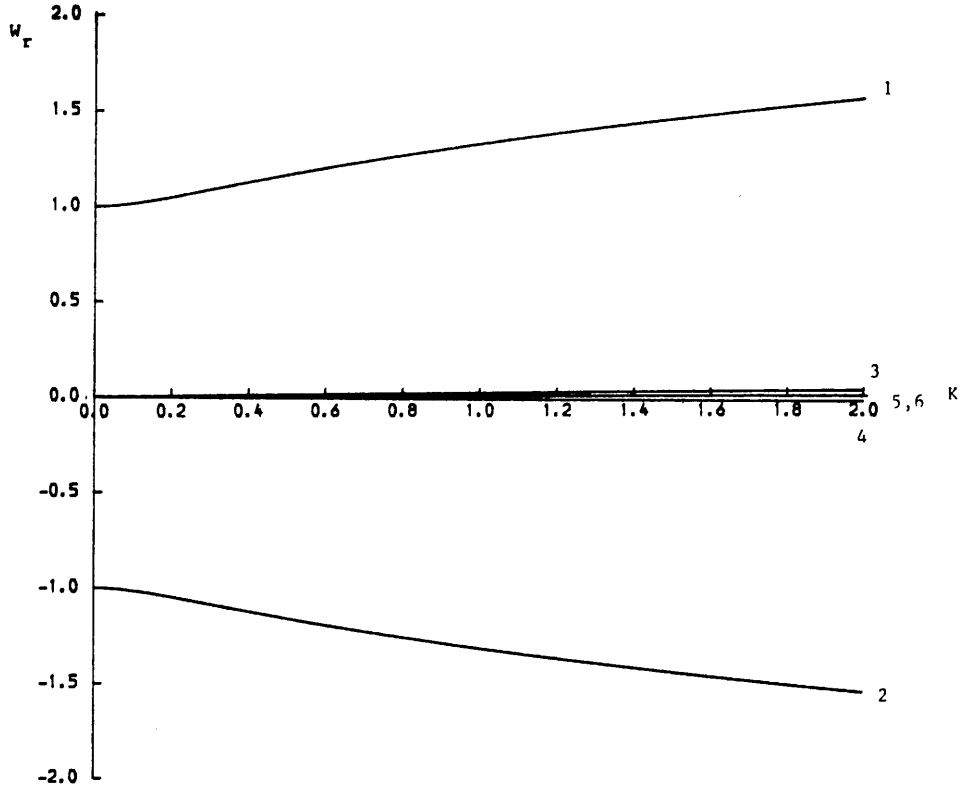

Figure 5.5a: Double Lorentz: W_r v. K for $V_d = 0$, $T_e/T_i = 1$

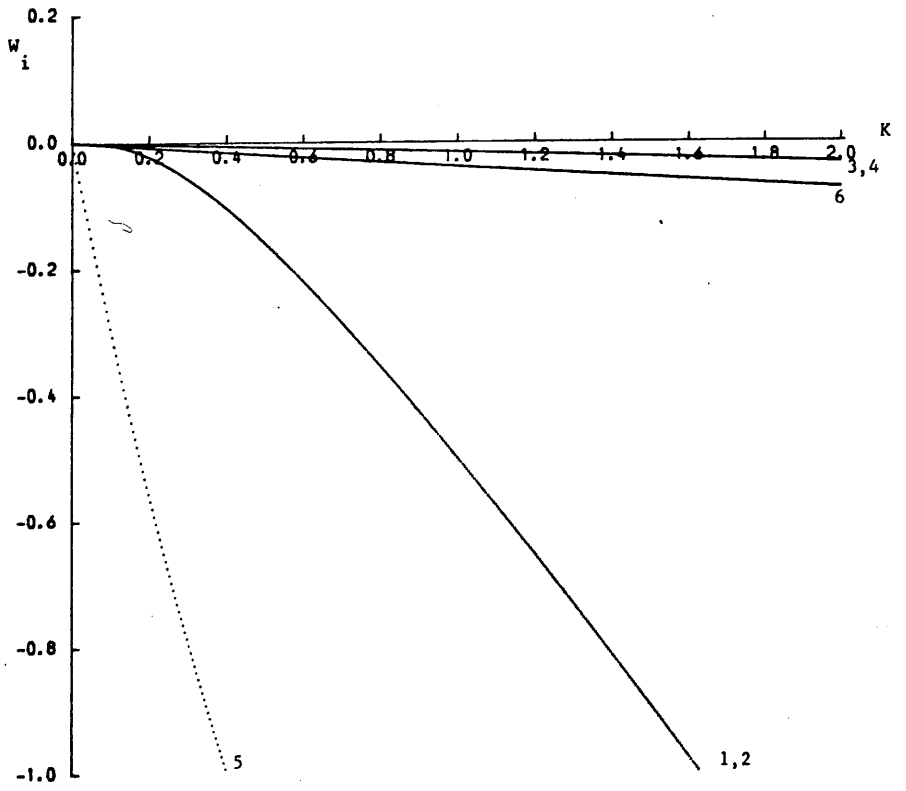

Figure 5.5b: Double Lorentz: W_i v. K for $V_d = 0$, $T_e/T_i = 1$

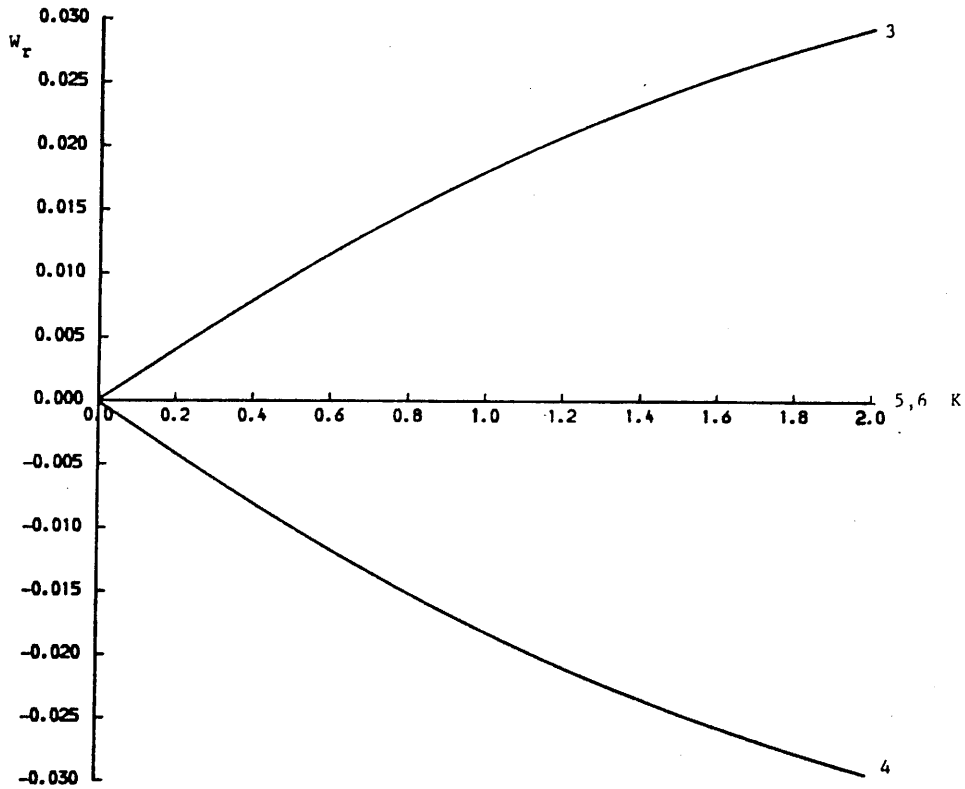

Figure 5.5c: Blow-up of Figure 5.5a.

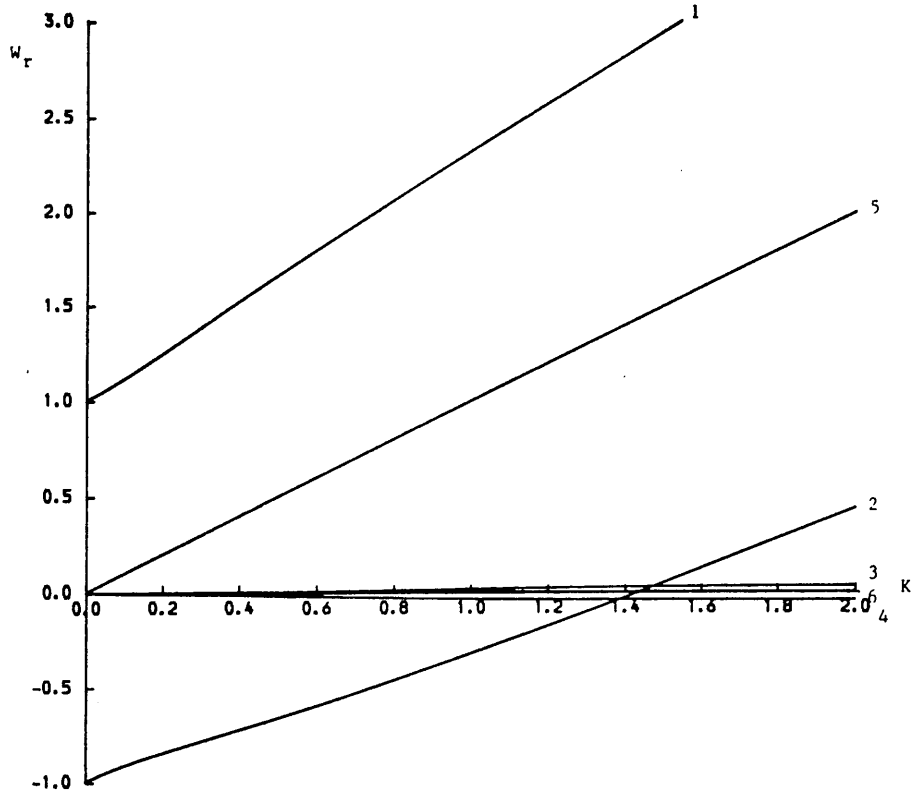

Figure 5.6a: Double Lorentz: W_r v. K for $V_d = 1$, $T_e/T_i = 1$

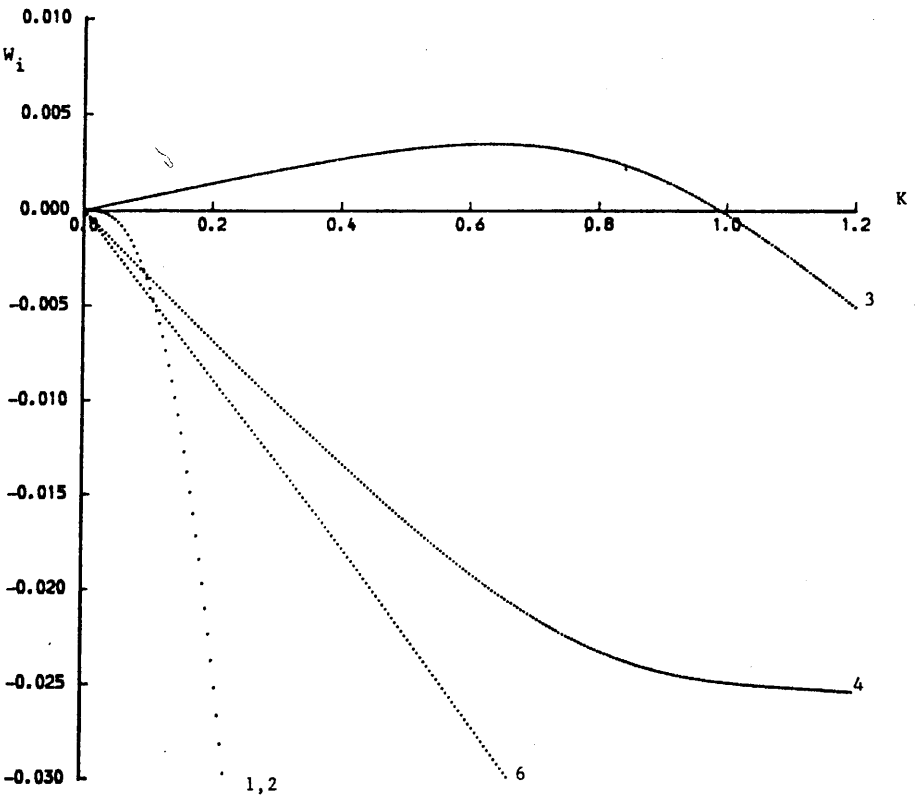

Figure 5.6b: Double Lorentz: W_i v. K for $V_d = 1$, $T_e/T_i = 1$

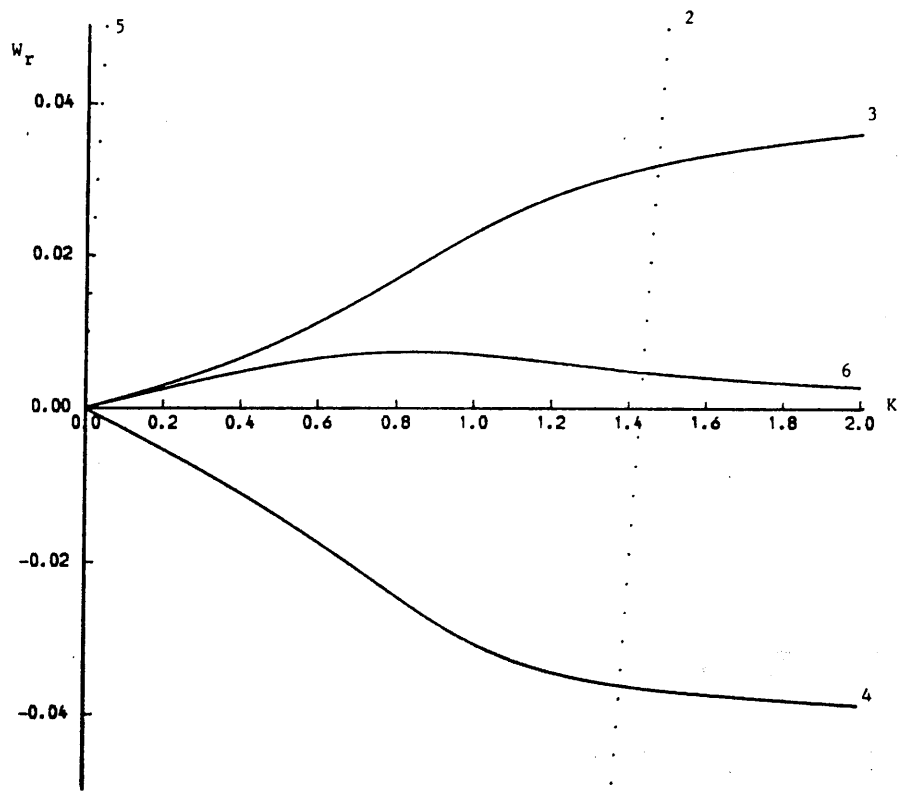

Figure 5.6c: Blow-up of Figure 5.6a.

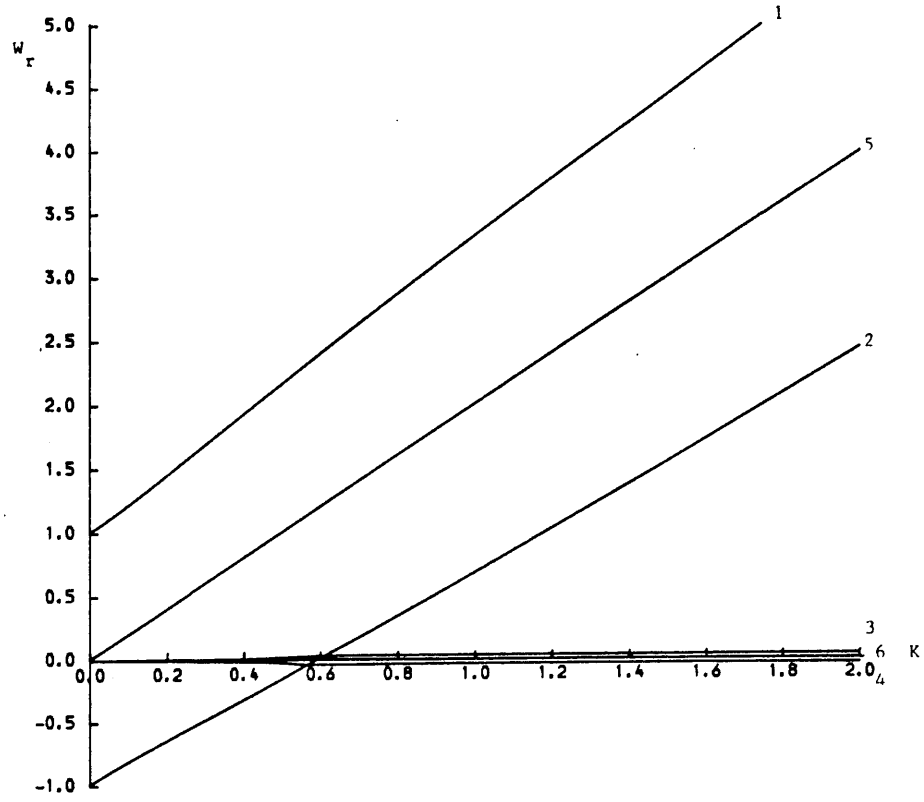

Figure 5.7a: Double Lorentz: W_r v. K for $V_d = 2$, $T_e/T_i = 1$

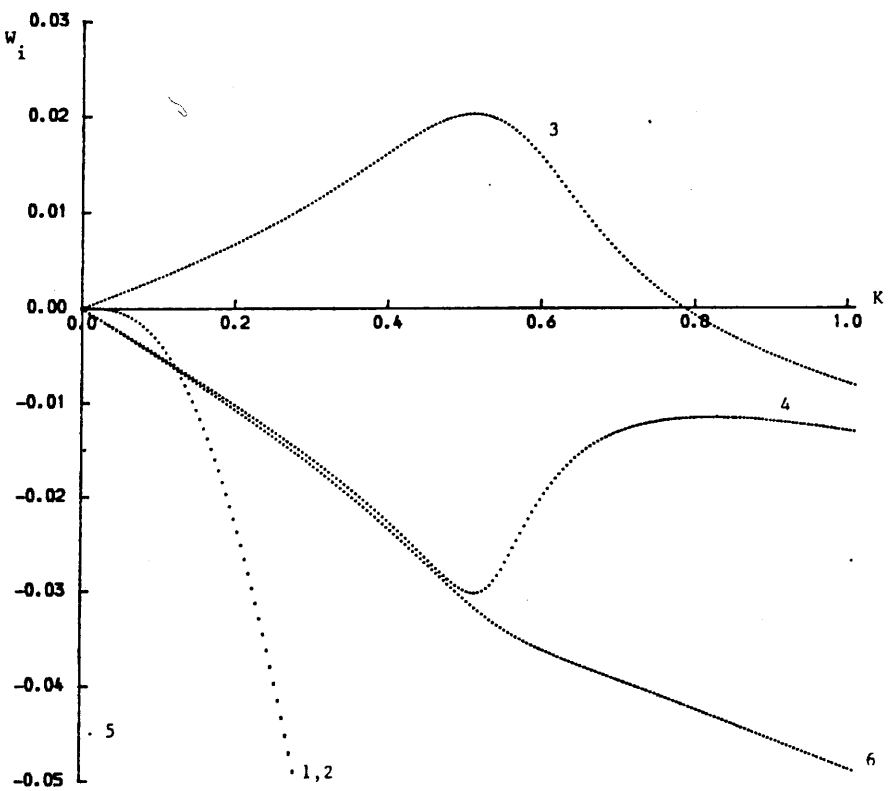

Figure 5.7b: Double Lorentz: W_i v. K for $V_d = 2$, $T_e/T_i = 1$

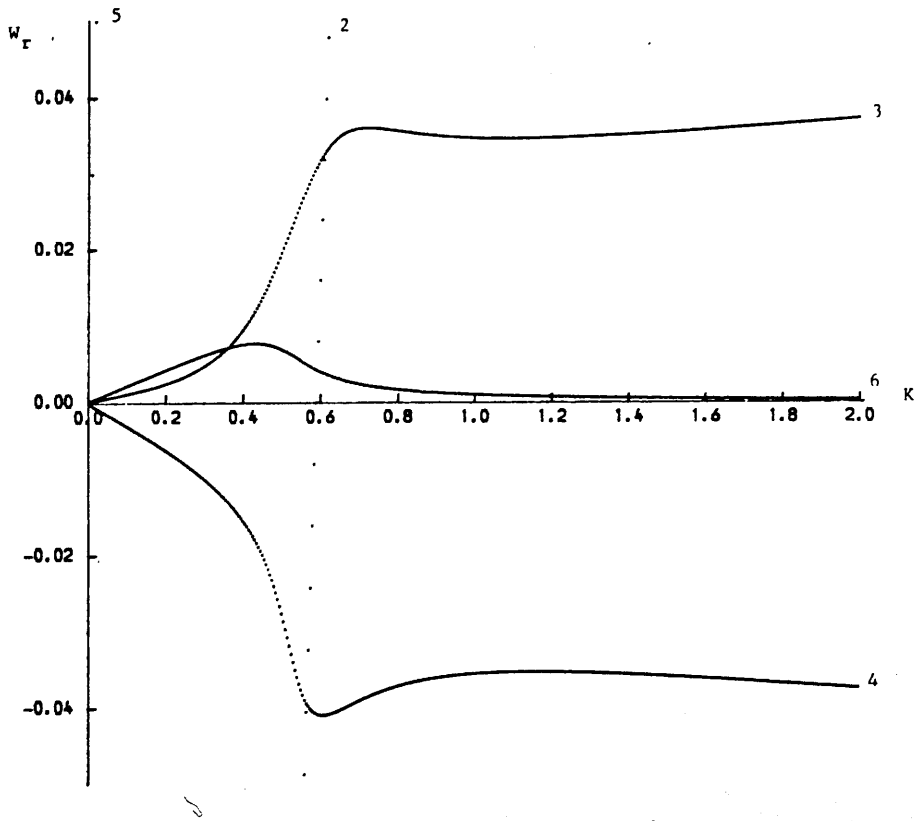

Figure 5.7c: Blow-up of Figure 5.7a.

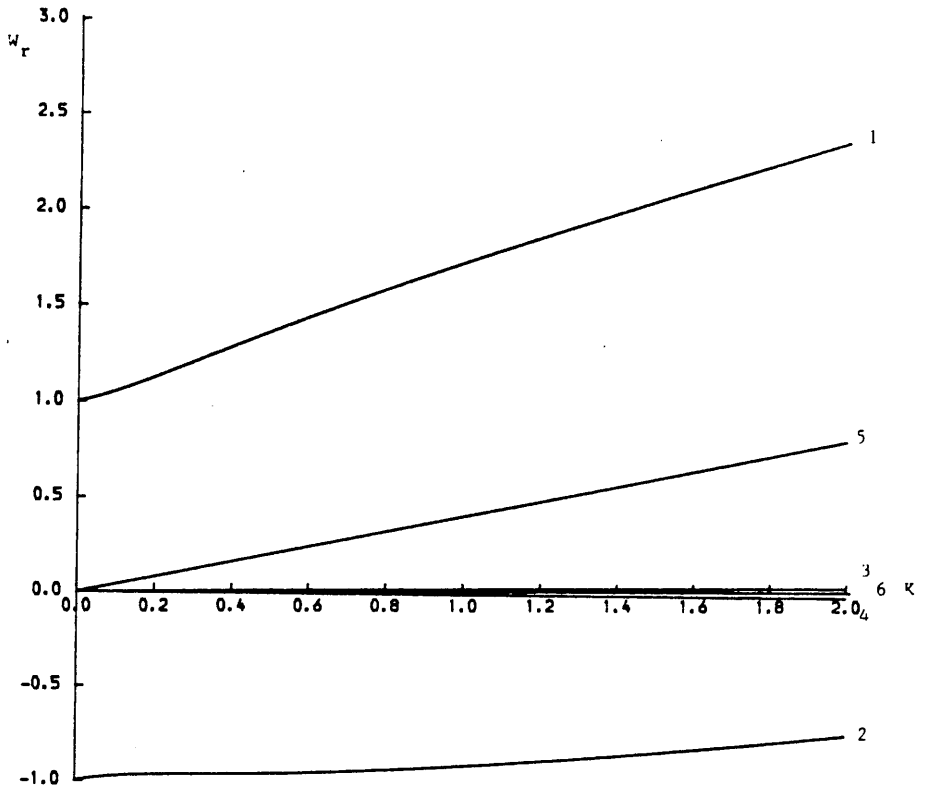

Figure 5.8a: Double Lorentz: W_r v. K for $V_d = 0.4$, $T_e/T_i = 5$

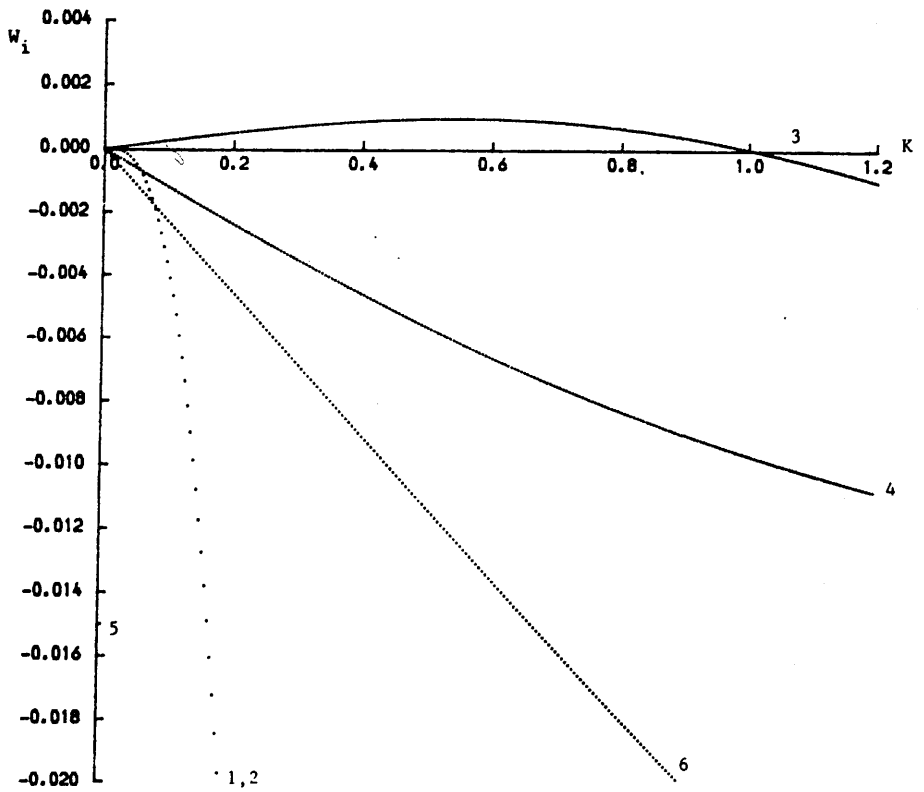

Figure 5.8b: Double Lorentz: W_i v. K for $V_d = 0.4$, $T_e/T_i = 5$

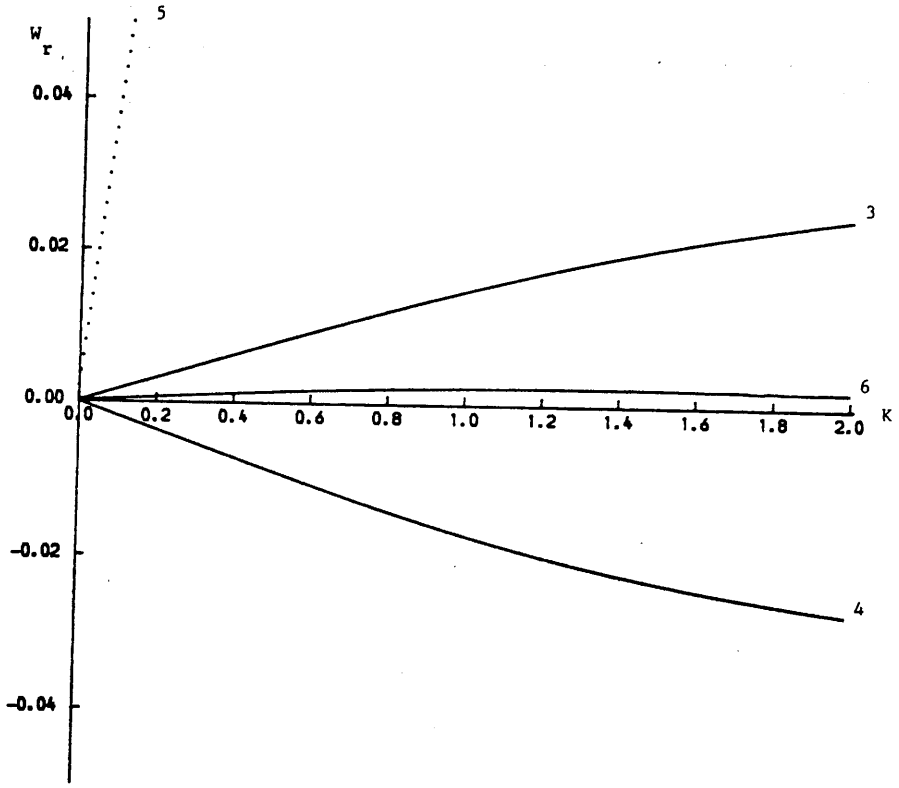

Figure 5.8c: Blow-up of Figure 5.8a.

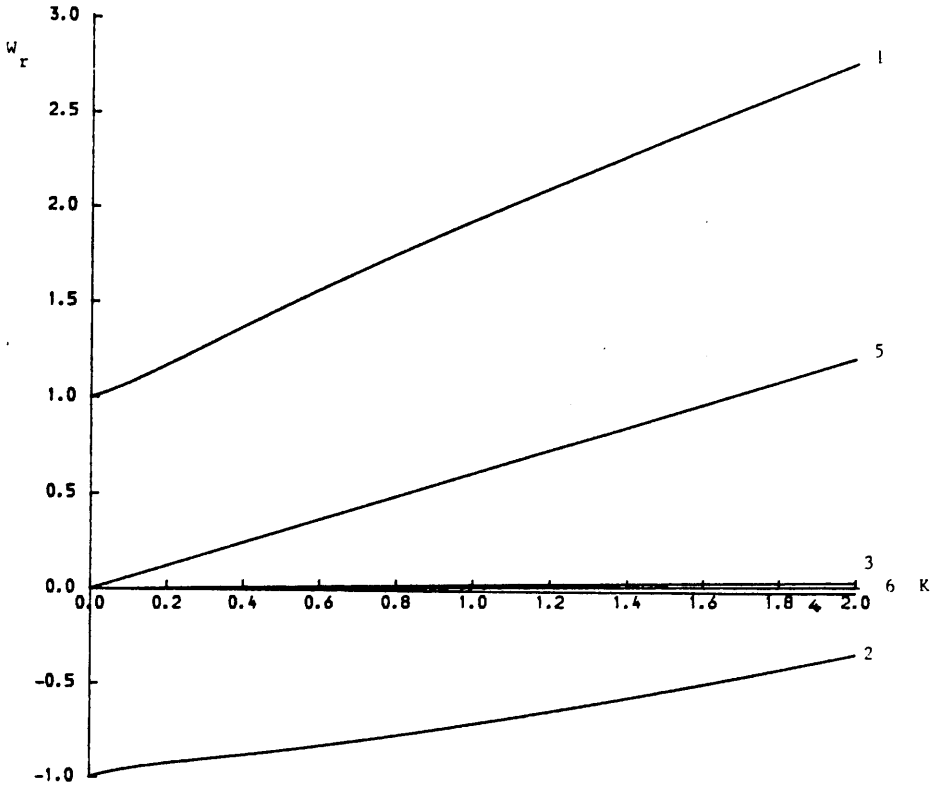

Figure 5.9a: Double Lorentz: W_r v. K for $V_d = 0.6$, $T_e/T_i = 5$

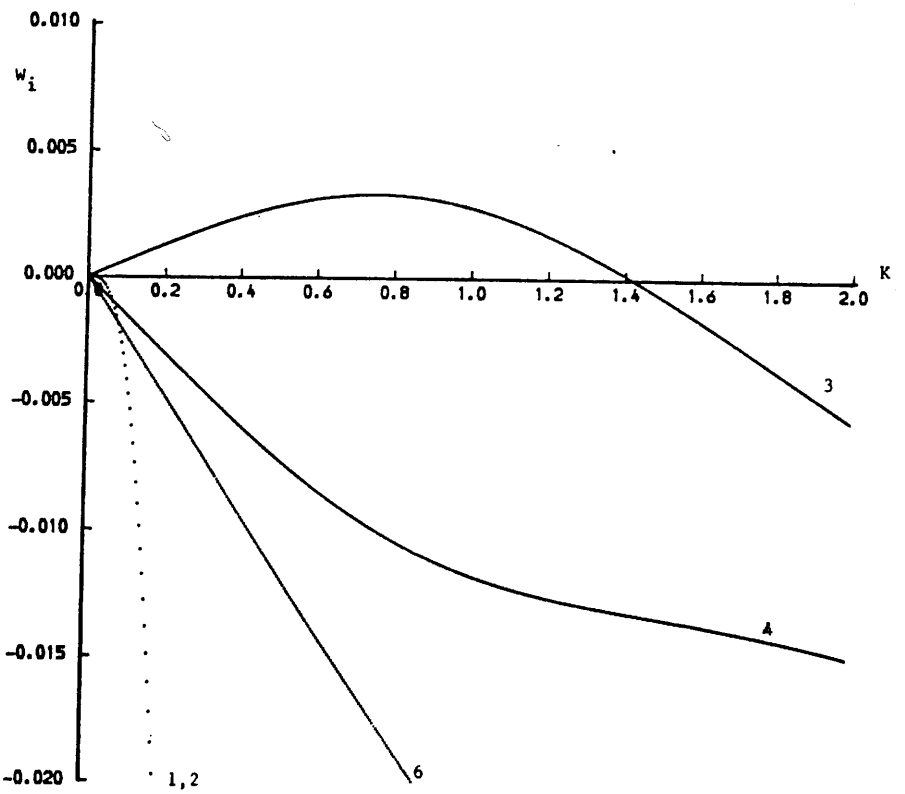

Figure 5.9b: Double Lorentz: W_i v. K for $V_d = 0.6$, $T_e/T_i = 5$

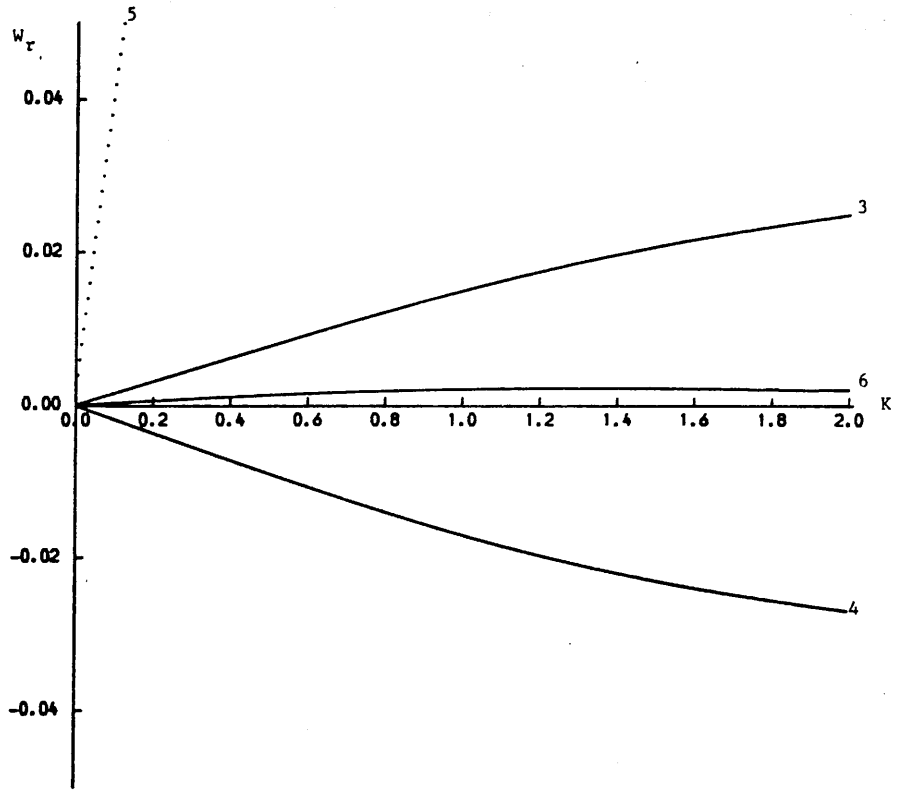

Figure 5.9c: Blow-up of Figure 5.9a.

having a larger range of unstable K: 0,0.8 and a larger growth rate: $\gamma \simeq 0.02$, at a slightly larger value of K:0.52. Also, for comparison, we present the results for $T_e/T_i = 5$ (i.e. $T = 0.2$) and $V_d = 0.4, 0.6$ (Figures 5.8 and 5.9 respectively). In both cases V_d exceeds the critical drift speed: mode 3 is unstable. When $V_d = 0.4$, we find that the range of unstable wave number is from K = 0, 1.0 with a maximum growth rate $\gamma \simeq 10^{-3}$ at $K \simeq 0.55$; for $V_d = 0.6$, the unstable K-range is 0,1.4 and $\gamma_{max} \simeq 3.5\ 10^{-3}$ at $K \simeq 0.75$ (cf. Figures 5.3, 5.4).

5.4 Discussion

In this chapter we have performed a dispersion relation analysis of a two-component field-free plasma of electrons and ions in which there is a relative drift speed, v_d. Our motivation was to investigate the behaviour of the unstable mode associated with return current instability in a field-free plasma. Adopting Lorentz velocity distributions for the particle species, algebraic dispersion relations were derived whose mathematical roots correspond to the possible modes of plasma oscillation (see Appendix A). We found that even in an isothermal plasma (i.e. $T_e/T_i \simeq 1.0$), instability of one (and only this one) of the modes occurred for $v_d \gtrsim v_e$. This mode may reasonably be term "ion-acoustic". McQuillan (1987) has shown that assuming Maxwellian distributions for the electrons and ions leads to a critical drift speed for ion-acoustic instability of $v_{crit} \simeq 1.34\ v_e$.

It is possible to utilise even higher-order Lorentz profiles, thus obtaining even more modes. However, these new modes are more heavily damped and are irrelevant to our investigations here. One then approaches the case of the dispersion relation associated with the

Maxwellian distribution which, for a single component electron plasma, yields the well-known weakly damped Langmuir wave and an infinite number of strongly-damped acoustic-like solutions, e.g. Montgomery (1971), McQuillan (1987). The so-called "electron-acoustic" mode has been investigated by Gary and Tokar (1985) who find that this mode only becomes weakly damped, or grows, when there exist two, or more, electron components at different temperatures.

In conclusion, we reaffirm that the unstable ion-acoustic mode can exist in an isothermal plasma, provided that the relative electron-ion drift is large enough: $v_d \gtrsim v_e$. This refutes claims occasionally made to the contrary in the literature (see Section 5.1). The reasons, then, for the failure of the marginal stability hypothesis if onset of ion-acoustic instability occurs below $T_e/T_i \simeq 5$ are as explained in detail in Section 4.5. We must therefore develop an alternative approach to beam-driven return current instability in this regime. This is attempted in the next chapter.

6. ION-ACOUSTIC INSTABILITY OF THE RETURN CURRENT: A WAVE GROWTH ANALYSIS

6.1 Introduction

As we saw in Chapter 4, the powerful tool of marginal stability is not applicable when onset of IA instability occurs at $T_e/T_i \lesssim 4.8$. In this regime, $v_d = v_{crit}\,(T_e/T_i)$ and $\chi = \chi_{IA}\,(T_e/T_i)$ are not consistent with $\eta > 0$. Put another way, the rate of growth, dW/dt, of the IA wave energy density cannot be neglected in this regime. A marginally stable plasma will respond to wave generation by adjusting T_e, T_i in such a way as to limit W, i.e. reduce dW/dt to very small values. However, for $T_e/T_i \lesssim 4.8$, the plasma is unable to adjust itself in this way and dW/dt is non-negligible. As a result, high levels of W are achieved (see Equation (4.27)). From Equation (B.51) we see that this corresponds to a high effective electron collision frequency, ν_{eff}, and, hence, a high effective plasma resistivity, η_{eff}. During this phase of plasma behaviour, as we shall see, the ohmic dissipation, $\eta_{eff} j^2$, is enhanced by orders of magnitude over classical values and very rapid heating occurs. It is apparent, therefore, that the concept of marginal stability implicitly assumes that $dW/dt = 0$; otherwise, the waves would heat the plasma on time scales far shorter than the beam rise time, t_r.

As an independent check on the validity of the marginal stability hypothesis, in Section 6.2 we apply a wave growth analysis to examples of marginally stable heating, i.e. where $(T_e/T_i)_{onset} \gtrsim 4.8$. We then utilise the wave growth approach to investigate an example of catastrophic heating (Section 6.3). Finally, a unified description incorporating both treatments is presented: the wave growth analysis tracks

the plasma evolution from onset of IA instability at $T_e/T_i \lesssim 4.8$ after which rapid heating takes place due to anomalous ohmic dissipation until the system relaxes to a state of marginal stability (for which $T_e/T_i \gtrsim 4.8$).

In Chapter 3 we demonstrated that the classical heating phase is completely specified as a function of time by the three parameters: $T_o/n_p^2 t_r$, $T_o/\mathcal{E}_o$ and $T_o^{3/2}/n_p$. Later, in Chapter 4, it was shown that for fixed T_o, n_p and $\mathcal{E}_o$, marginally stable heating occurs for large rise times, whereas catastrophic heating occurs for small rise times. In these chapters, for convenience, we chose the mean beam electron energy $\mathcal{E}_o$ to be 100 keV. If we now assume the more realistic value of $\mathcal{E}_o$ = 25 keV in our numerical codes we find that marginally stable heating results in cases where $t_r \gtrsim 1s$ and catastrophic heating takes place for $t_r \lesssim 1s$ (see Figure 6.1). It will be worthwhile bearing this in mind throughout this chapter.

6.2 A Wave Growth Treatment of Marginally Stable Heating

The marginal stability approach to plasma transport is, in a sense, an averaging of a more detailed kinetic description of the microscopic processes involved. The concept of the marginal stability description is relevant only on time scales (e.g. classical heating time) far longer than wave growth times. We can, however, compare the two types of analysis if a wave growth treatment is performed over a sufficiently long time interval, as described later in this section. Specifically, we would like to check that the values of anomalous resistivity obtained in both approaches are consistent in the regime where marginal stability is valid, i.e. $(T_e/T_i)_{onset} \gtrsim 4.8$.

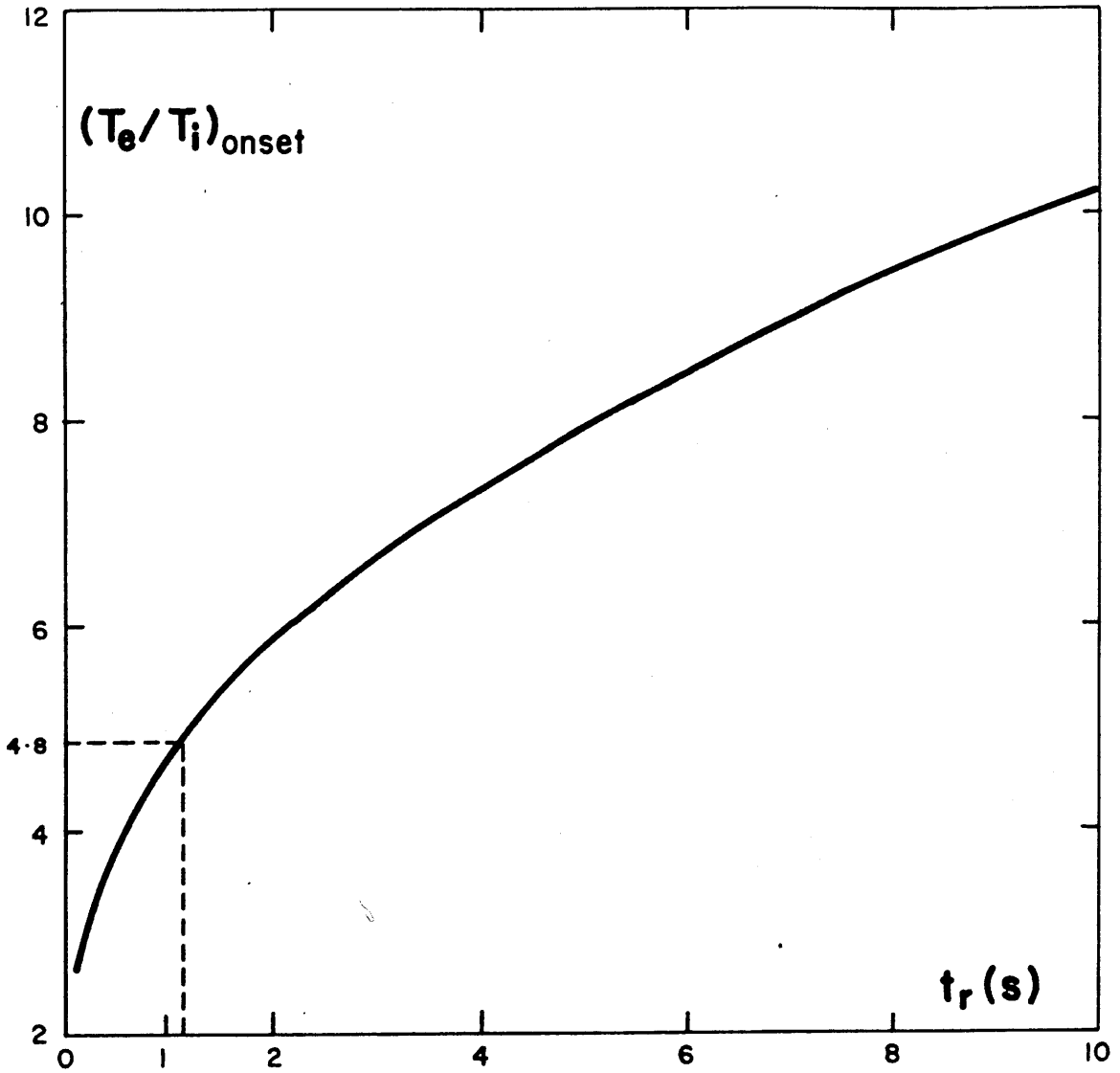

Figure 6.1: Value of T_e/T_i at onset of IA instability versus rise time, t_r (seconds), for the prescribed beam current evolution and $\mathcal{E}_o$ = 25 keV. Catastrophic heating results when $t_r \lesssim 1s$ and marginally stable heating takes place when $t_r \gtrsim 1s$.

We adopt the following equation for the evolution of W:

$$\frac{dW}{dt} = \gamma W \qquad (6.1)$$

where $\gamma = \gamma(v_d, T_e/T_i)$ is the linear growth rate for IA waves. Note that, in reality, an IA wave spectrum W(k) will exist in the plasma with a distribution of growth rates. The above equation assumes that the variation of the total IA wave energy density $W \equiv \int W(k)dk$ can be described by a single γ . Equation (6.1) leads to unlimited growth of W unless one of the following occurs:

(a) Saturation of wave growth (see Section 2.3).

(b) T_e rises sufficiently such that v_{crit} catches up with v_d and the IA waves are "switched off".

Strictly speaking, γ should be calculated self-consistently from the dispersion relation describing the possible modes of plasma oscillation in our return current system (see Chapter 5 and Appendix A). However, to incorporate such a rigorous instability analysis at each time step of the plasma evolution would dramatically increase the complexity of the problem and result in prohibitively long computing times for the numerical modelling. For ease of calculation, then, we make the simplifying assumption that γ remains constant during IA wave growth. In our dispersion relation analyses of Chapter 5 we found that, unless v_d was vastly in excess of v_{crit} (e.g. $v_d = 2v_{crit}$), typically $\gamma_{max} \sim (0.1 - 1.0)\ \omega_{pi}$ (e.g. Figures 5.6b, 5.8b, 5.9b; see also Figure 2 of Stringer (1964)). Given that the growth rate will, on the average, be less than this during the unstable phase of the plasma evolution we choose $\gamma = 10^{-2}\ \omega_{pi}$. In actual fact, we will see later that the assumed constant value of γ is not critically important

(by comparing with the cases $\gamma = 0.5\ 10^{-2}\omega_{pi}$ and $\gamma = 2.0\ 10^{-2}\omega_{pi}$).

The plasma resistivity may be obtained quite simply from the wave level, W, at any time by making use of the following relations:

$$\nu_{eff} \simeq \omega_{pe} \frac{W}{n_p T_e} \qquad \text{(Equation (B.51))}$$

and

$$\eta \simeq \frac{0.51\ m_e \nu_{eff}}{n_p e^2} \qquad \text{(from Equation (B.26))}$$

Combining these two equations gives the resistivity in terms of the "normalised" wave level as

$$\eta \simeq 2.80\ 10^7 \frac{W}{n_p T_e}\ \eta_{cl,o} \qquad (6.2)$$

using $\omega_{pe}^2 = 4\pi n_p e^2/m_e$. We can, therefore, solve the electron and ion temperature Equations (3.4) numerically in conjunction with Equations (6.1) and (6.2).

At onset of instability, the wave level grows from the random fluctuation or "noise" level obtained by substituting the Spitzer resistivity in the left hand side of Equation (6.2). We postulate that this growth occurs linearly (Equation (6.1) with constant γ) until either some saturation level $W^{sat}(T_e,T_i)$ is reached, at which point the growth is discontinued, or v_d drops below v_{crit}. If the condition $v_d < v_{crit}$ is attained following a period of anomalous ohmic dissipation then wave damping proceeds until the wave level drops to the random noise level. Once again, a dispersion relation analysis would be required, in this case to determine the correct wave damping rate. Note, however, that $\gamma = \gamma(k)$. For example, if we were to model

the damping of mode 3 of Figure 5.3b what values of $k,\gamma(k)$ would we adopt? A reasonable procedure might be to take the value of k at which the growth rate had previously been a maximum during the earlier phase of wave growth and then choose the corresponding damping rate γ to describe the decay of the IA waves. However, as before, to perform such a complete analysis, desirable as it may be, would require a very sophisticated numerical code and considerable computing time. In our simplified treatment here, we make the reasonable assumption that the IA waves damp on the same time scale as they grow and adopt a damping rate $\gamma = 10^{-2}\ \omega_{pi}$ (or $0.5\ \ 10^{-2}\omega_{pi}$, $2.0\ \ 10^{-2}\ \omega_{pi}$ in the respective comparison runs; see below).

In our discussion of Section 2.3 we nominated the nonlinear two-wave interaction investigated by Tsytovich (1971) as a likely mechanism for IA wave saturation. Whether saturation actually occurs, however, has to be determined; the tendency of the plasma to heat up raises the threshold drift speed for instability, v_{crit}, such as to keep pace with the imposed linearly increasing v_d. In other words, we anticipate that, during the IA heating phase, v_d/v_e decreases due to the rapid increase in T_e until the system drops below the marginal stability curve. If this happens, the waves become damped and we enter a regime of classical heating once again in which v_d/v_e rises until the next onset of turbulence. We might anticipate that many rapid cycles of such behaviour will be exhibited in the marginal stability regime with values of W remaining well below saturation amplitudes. On the other hand, in the case of catastrophic heating (see Section 4.5), we might expect that saturation wave levels would be attained. We will see later that in this regime ($T_e/T_i \lesssim 4.8$) IA wave heating rapidly raises T_e/T_i into the marginally stable regime

by the time v_{crit} has caught up with v_d.

At each numerical timestep our code checks to see whether or not v_d exceeds v_{crit} and then calls the relevant subroutine (depending on v_d/v_e and on the previous history): classical, IA wave growth, IA saturation or IA wave decay. A variable timestep is employed to retain accuracy in each regime: $\Delta t = 5.10^{-3}$ s(< classical heating time) in the classical phase, and $\Delta t = 10^{-7}$ s ($\lesssim 1/\gamma$) during IA wave growth, saturation or decay.

We are now in a position to present examples of the wave growth procedure described above, as applied to cases of marginally stable heating. The chosen parameters are:

(a) $T_o = 5.10^6$ K, $n_p = 10^{11}cm^{-3}$, $\mathcal{E}_o = 25$ keV, $t_r = 10s$.
- Figures 6.2a, 6.3a, 6.4a, 6.5a, 6.6, 6.7.

(b) $T_o = 5.10^6$ K, $n_p = 10^{11}cm^{-3}$, $\mathcal{E}_o = 25$ keV, $t_r = 2s$.
- Figures 6.2b, 6.3b, 6.4b, 6.5b, 6.8, 6.9, 6.10.

In case (a) we find that $(T_e/T_i)_{onset} \simeq 10.2$, while for case (b) which is somewhat closer to the catastrophic regime, $(T_e/T_i)_{onset} \simeq 5.8$. For each case we have chosen three different constant values of γ which are, in units of $10^{-2}\omega_{pi}$:

(i) $\gamma = 0.5$ - Figures 6.6i, 6.7i, 6.8i, 6.9i

(ii) $\gamma = 1.0$ - Figures 6.6ii, 6.7ii, 6.8ii, 6.9ii

(iii) $\gamma = 2.0$ - Figures 6.6iii, 6.7iii, 6.8iii, 6.9iii

The general forms of Figures 6.2 - 6.5 are already familiar to us (cf. Figures 4.5 - 4.8) and depict respectively:

2 - evolution of the plasma in the v_d/v_e: T_e/T_i plane.

3 - variation of the normalised resistivity with time.

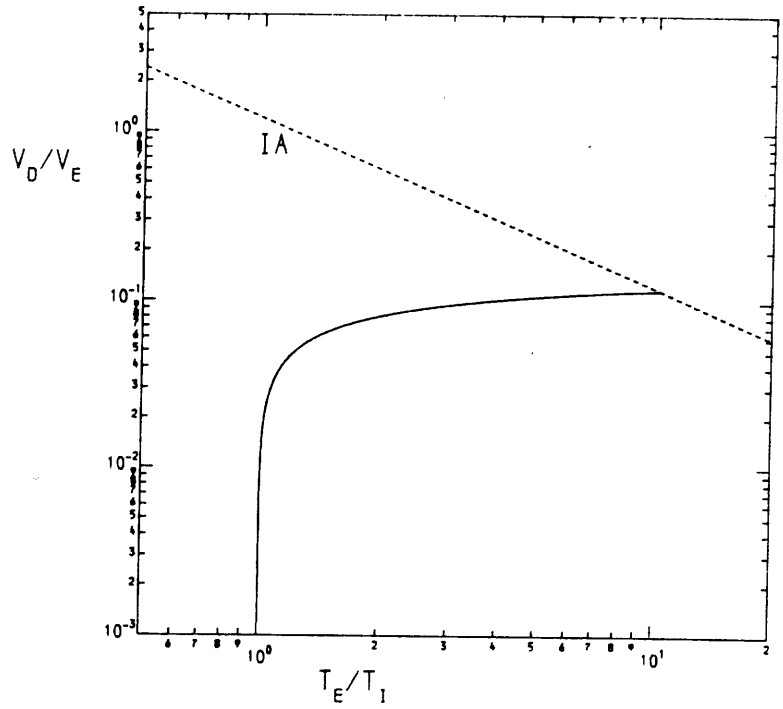

Figure 6.2a: Evolution of the plasma in the $(v_d/v_e, T_e/T_i)$ plane for wave growth case (a) (see text).

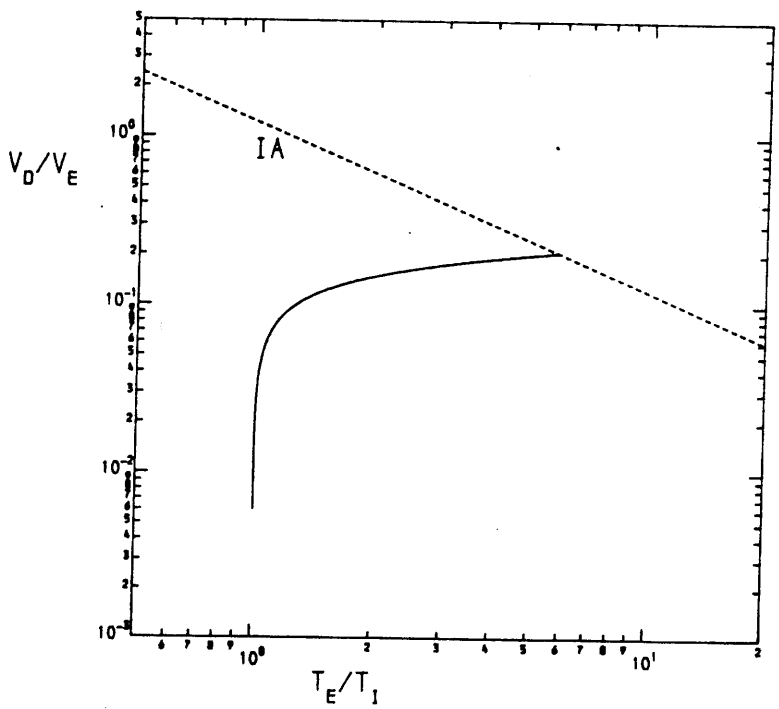

Figure 6.2b: Evolution of the plasma in the $(v_d/v_e, T_e/T_i)$ plane for wave growth case (b) (see text).

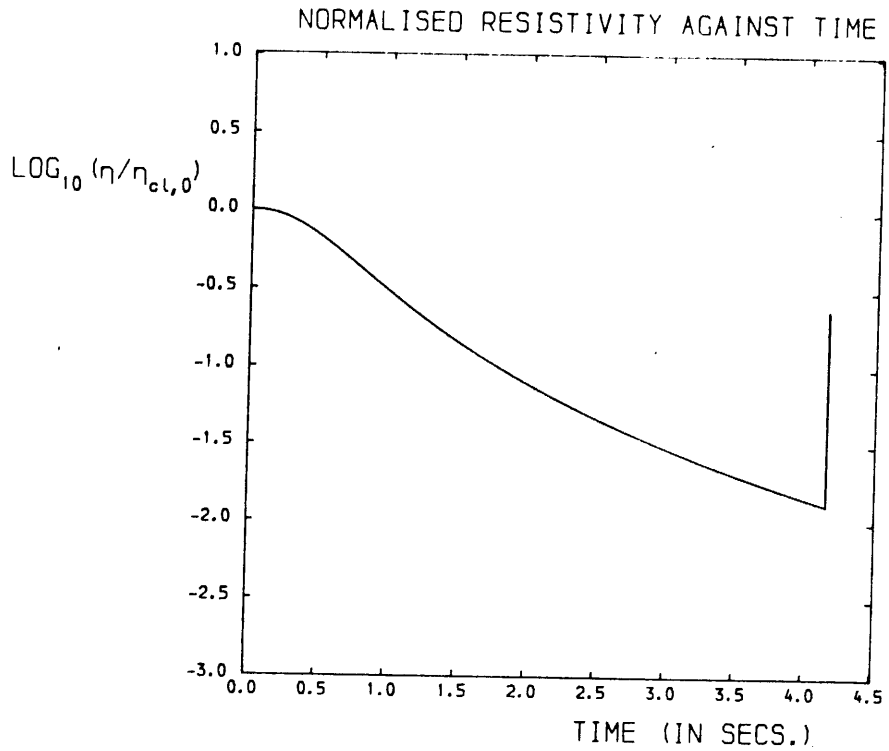

Figure 6.3a: Variation of the normalised resistivity with time for case (a).

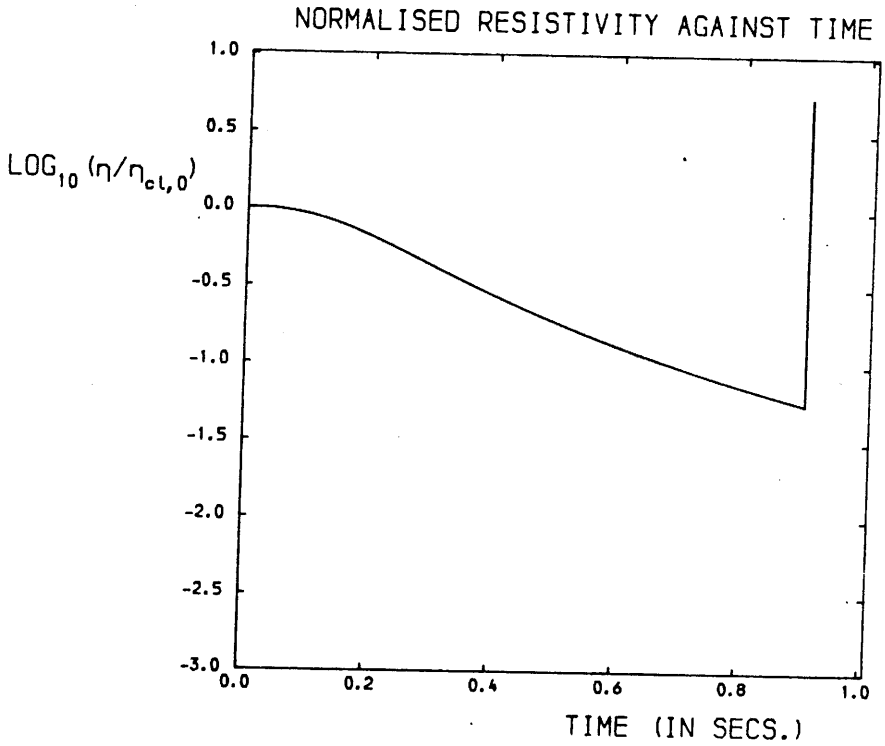

Figure 6.3b: Variation of the normalised resistivity with time for case (b).

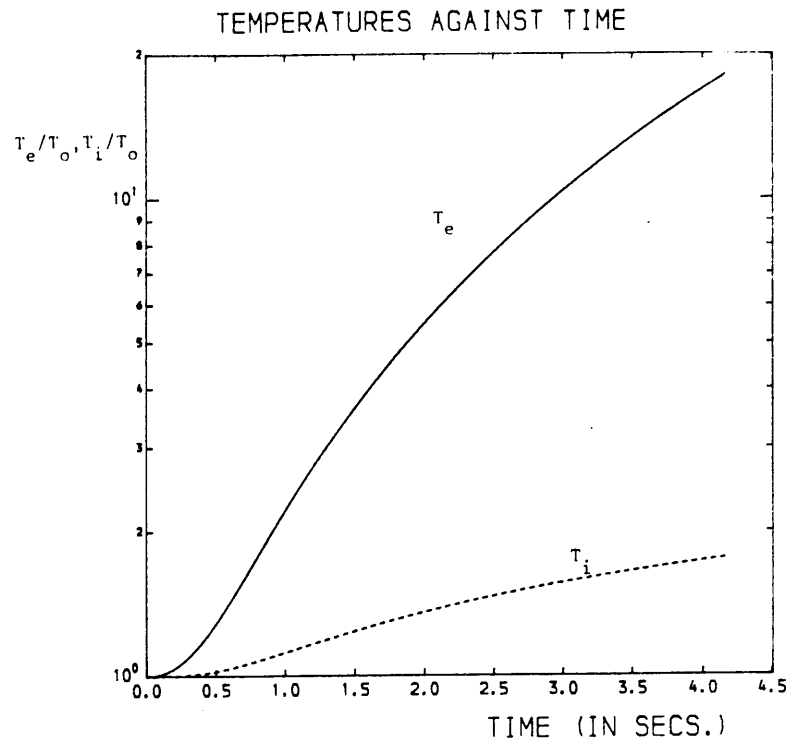

Figure 6.4a: The electron and ion temperature profiles for case(a).

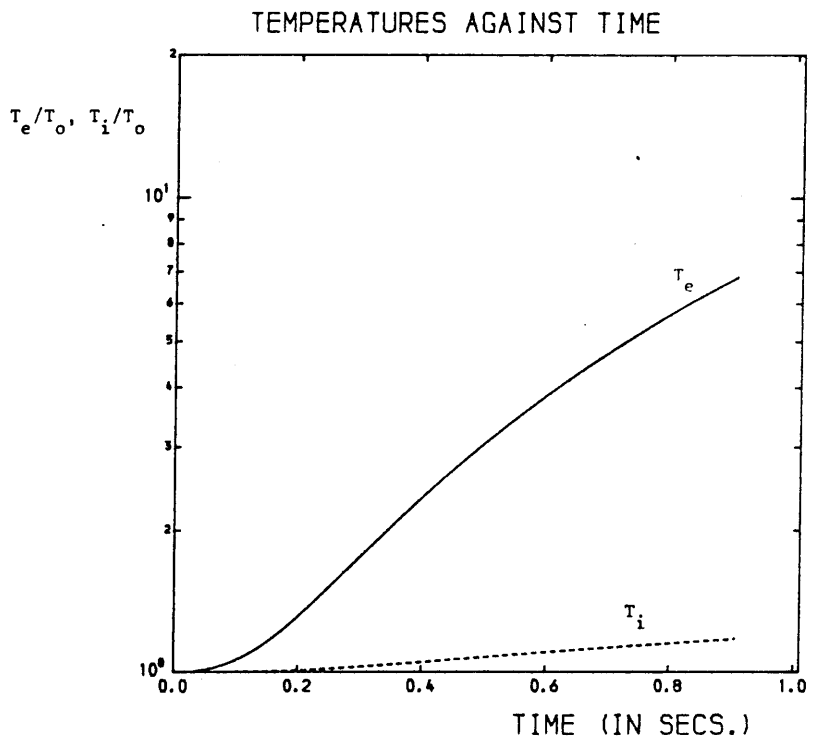

Figure 6.4b: The electron and ion temperature profiles for case (b).

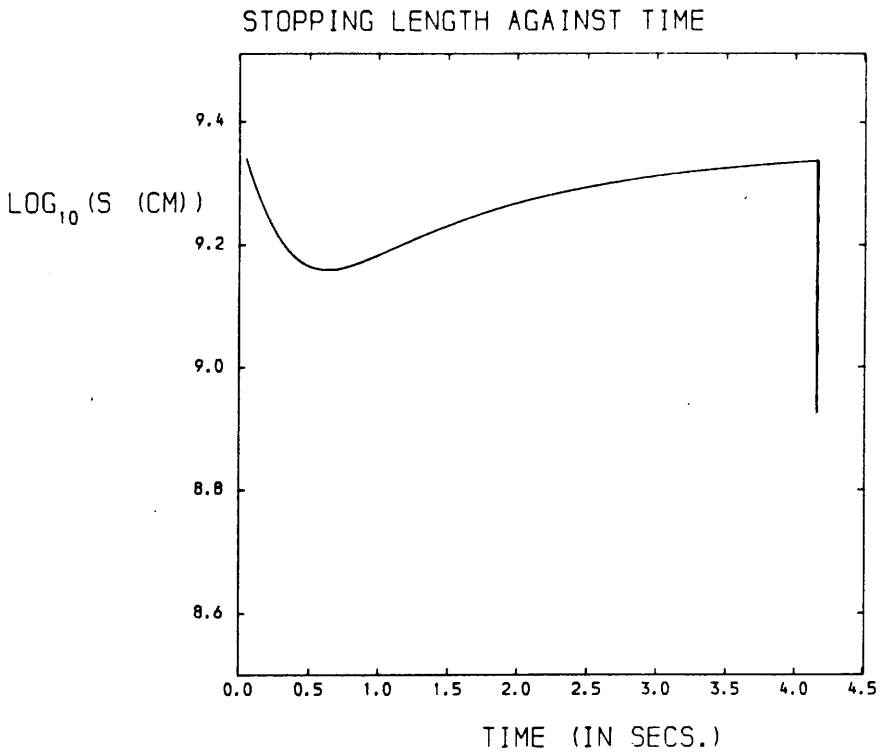

Figure 6.5a: Electron beam stopping length v. time for case (a)

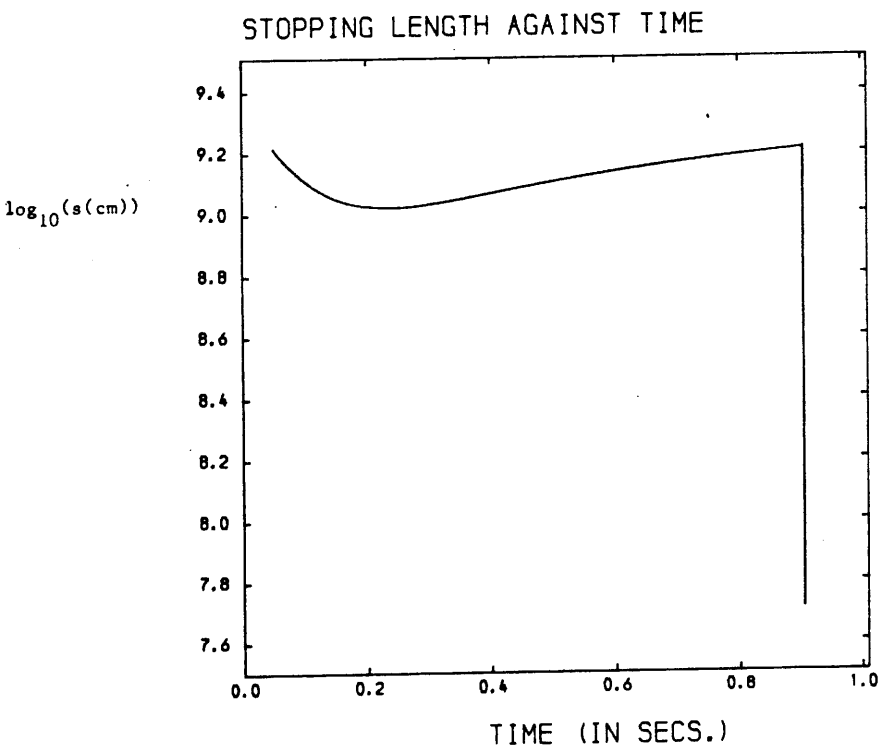

Figure 6.5b: Electron beam stopping length v. time for case (b)

4 - the normalised electron and ion temperature profiles.

5 - variation of beam stopping length with time.

Figures 6.6 show the variation in resistivity against the time interval $(t - t_{onset})$ measured in units of $(10^{-2}\omega_{pi})^{-1}$. Equivalently, Figures 6.6 illustrate the time profile of the normalised wave level, $W/n_p T_e$ (see Equation 6.2)). Note the rapid switching on and off of the IA waves. This is a natural consequence of the fast oscillations about the marginally stable drift speed which is exhibited most clearly for the case $t_r = 2s$, $\gamma = 2.0$, as depicted in Figure 6.10. Obviously, the faster the growth rate of the waves, the more rapidly do the waves switch on and off: compare Figures 6.6i,ii,iii. For example, in units of $(10^{-2}\omega_{pi})^{-1}$, the period of this cyclic behaviour is $\simeq 17$ for $t_r = 10s$, $\gamma = 0.5$ and $\simeq 8$ for $t_r = 10s$, $\gamma = 2.0$. In all cases the IA wave levels remain well below saturation levels ($W^{sat}/n_p T_e \simeq 10^{-3}$; $\eta^{sat}/\eta_{cl,o} \simeq 10^5$).

We have, therefore, demonstrated the rapid oscillatory plasma behaviour implicit in the marginal stability hypothesis. How does marginal stability fare, though, in predicting values of transport coefficients, in particular, the resistivity? To investigate this, note that several cycles of periodic behaviour occur within an interval of 100 time units for all three cases $\gamma = 0.5$, 1.0, 2.0 (Figures 6.6, 6.8). For each case, following the onset of instability, we calculate the mean wave growth resistivity, $\overline{\eta}_{WG}$, at time t_n:

$$\overline{\eta}_{WG}(t_n) = \frac{\int_{t_{n-1}}^{t_n} \eta_{WG}\, dt}{\int_{t_{n-1}}^{t_n} dt} \qquad n=1,2,\ldots,20 \qquad (6.3)$$

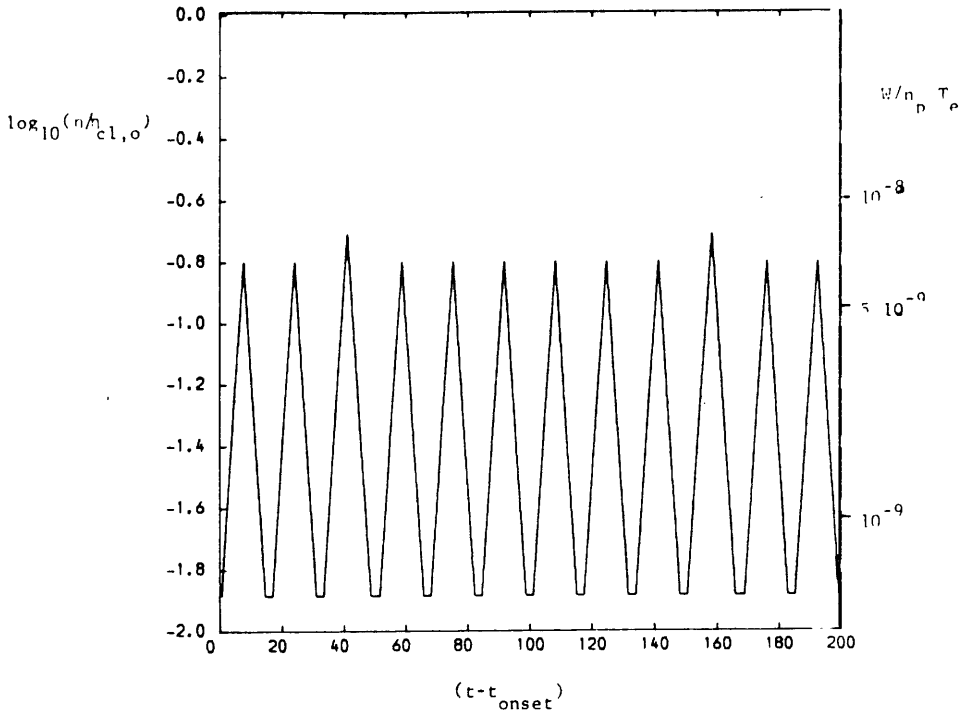

Figure 6.6i: Variation of the normalised resistivity with time after onset of instability, in case (a), for $\gamma = 0.5$. Time is in units of $(10^{-2}\ \omega_{pi})^{-1}$

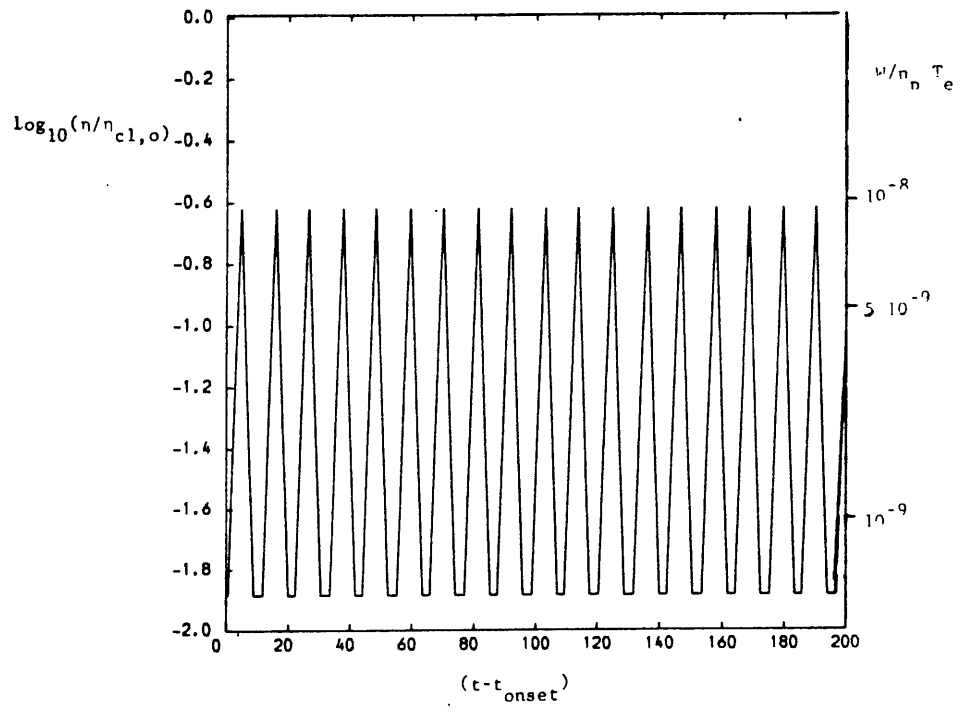

Figure 6.6ii: Variation of the normalised resistivity with time after onset of instability, in case (a), for $\gamma = 1.0$. Time is in units of $(10^{-2}\ \omega_{pi})^{-1}$

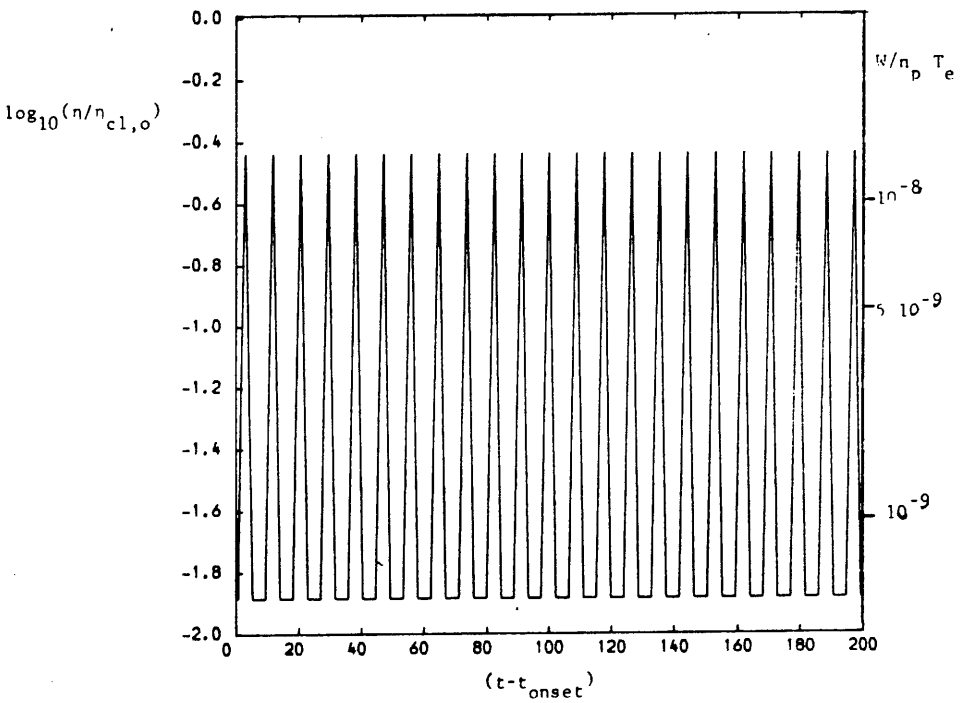

Figure 6.6iii: Variation of the normalised resistivity with time after onset of instability, in case (a), for $\gamma = 2.0$. Time is in units of $(10^{-2}\ \omega_{pi})^{-1}$

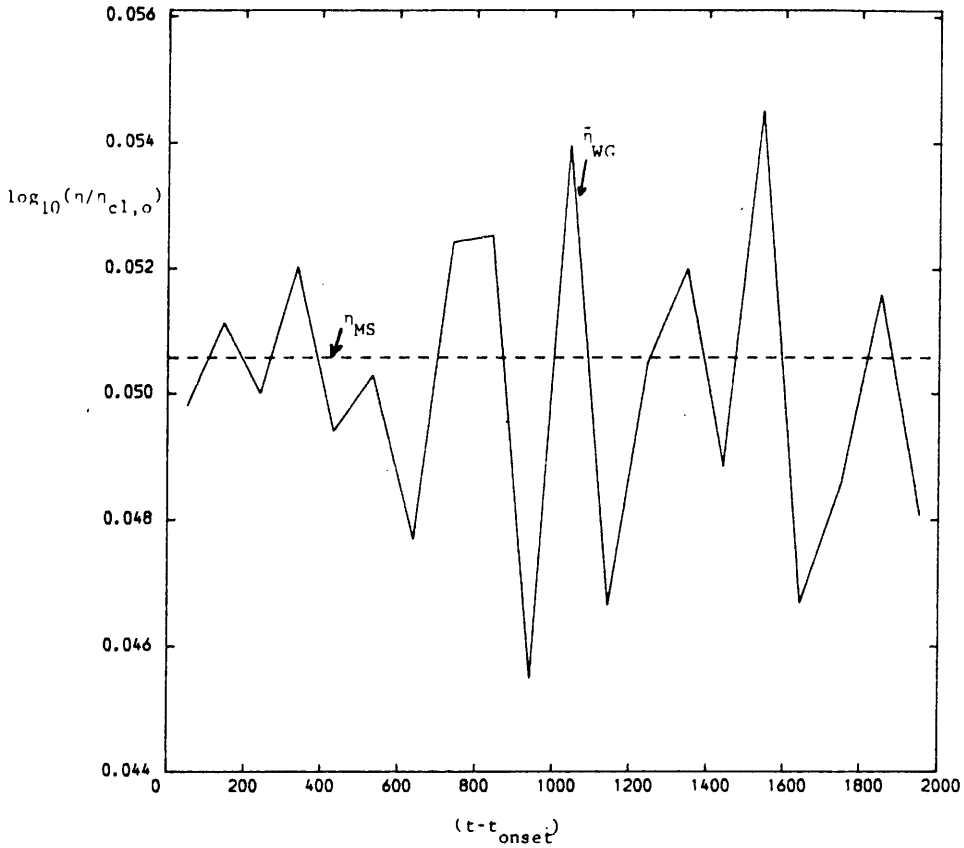

Figure 6.7i: A comparison of the mean wave growth resistivity, $\bar{\eta}_{WG}$, with the marginally stable resistivity, η_{MS}, in case (a), for $\gamma = 0.5$.

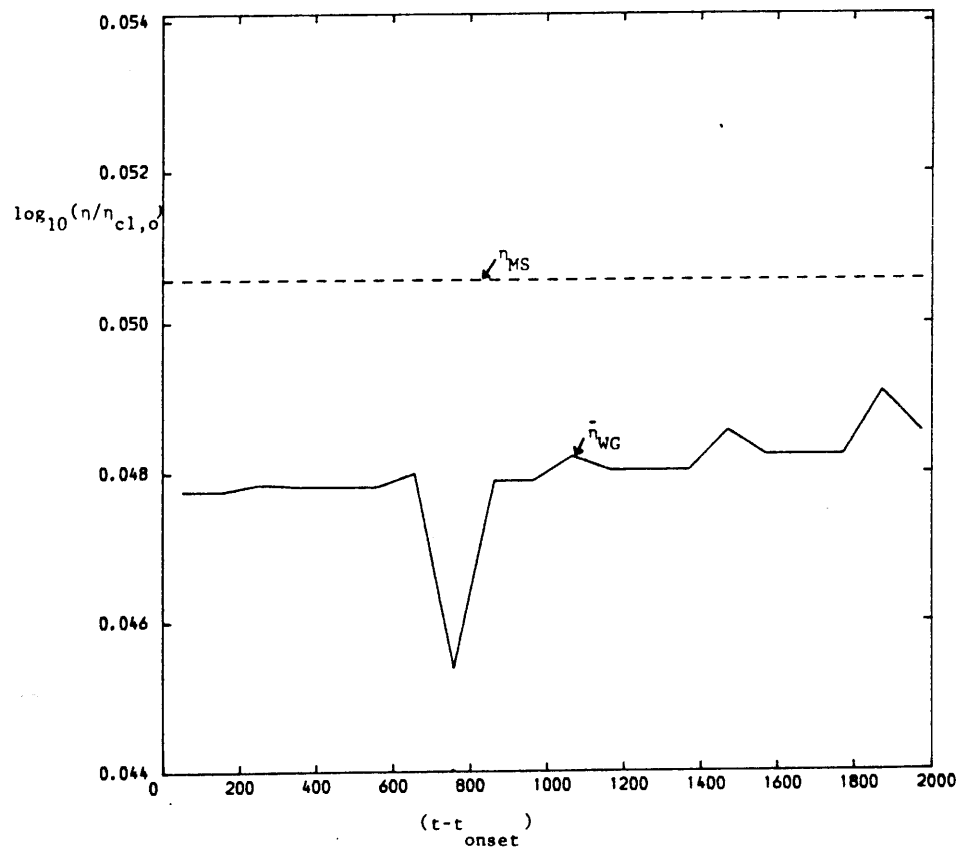

Figure 6.7ii: A comparison of the mean wave growth resistivity, $\bar{\eta}_{WG}$, with the marginally stable resistivity, η_{MS}, in case (a), for $\gamma = 1.0$.

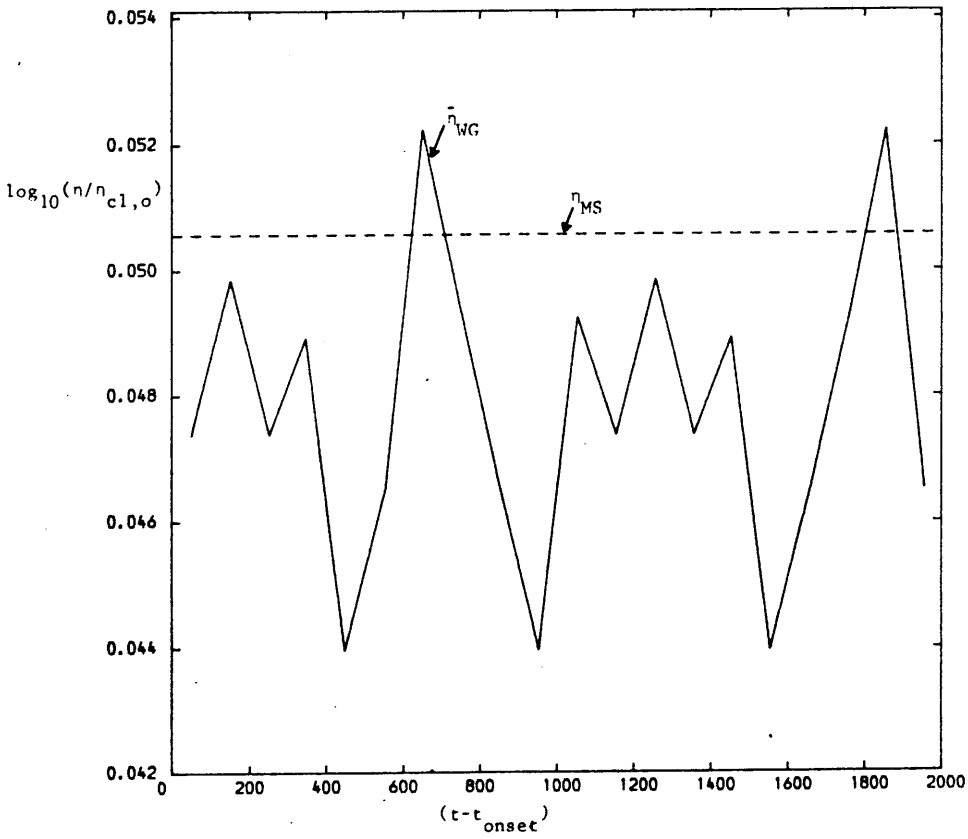

Figure 6.7iii: A comparison of the mean wave growth resistivity, $\bar{\eta}_{WG}$, with the marginally stable resistivity, η_{MS}, in case (a), for $\gamma = 2.0$.

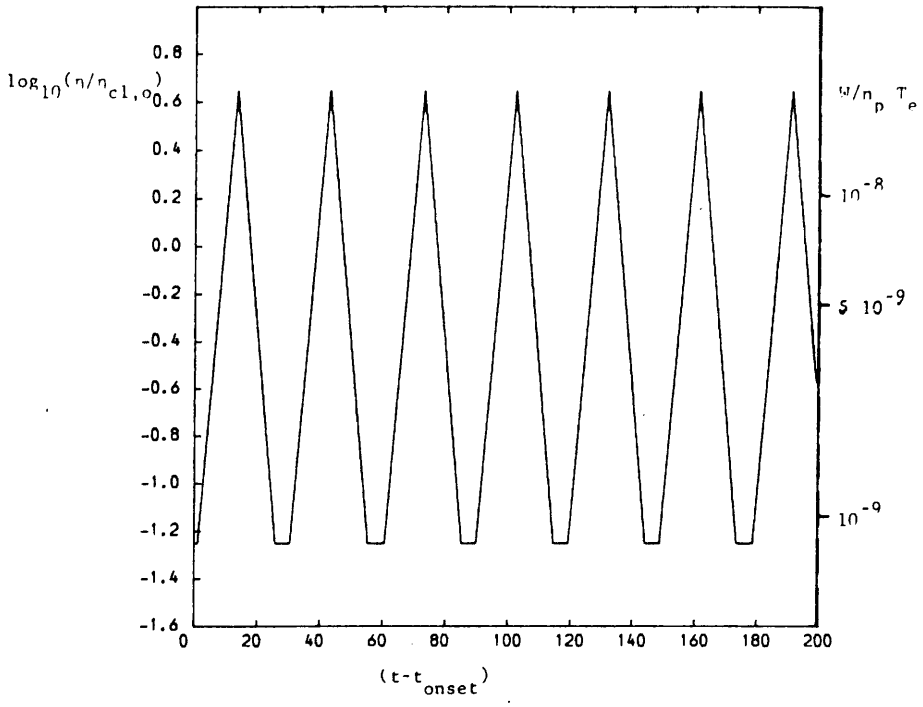

Figure 6.8i: Variation of the normalised resistivity with time after onset of instability, in case (b) for $\gamma = 0.5$. Time is in units of $(10^{-2}\ \omega_{pi})^{-1}$.

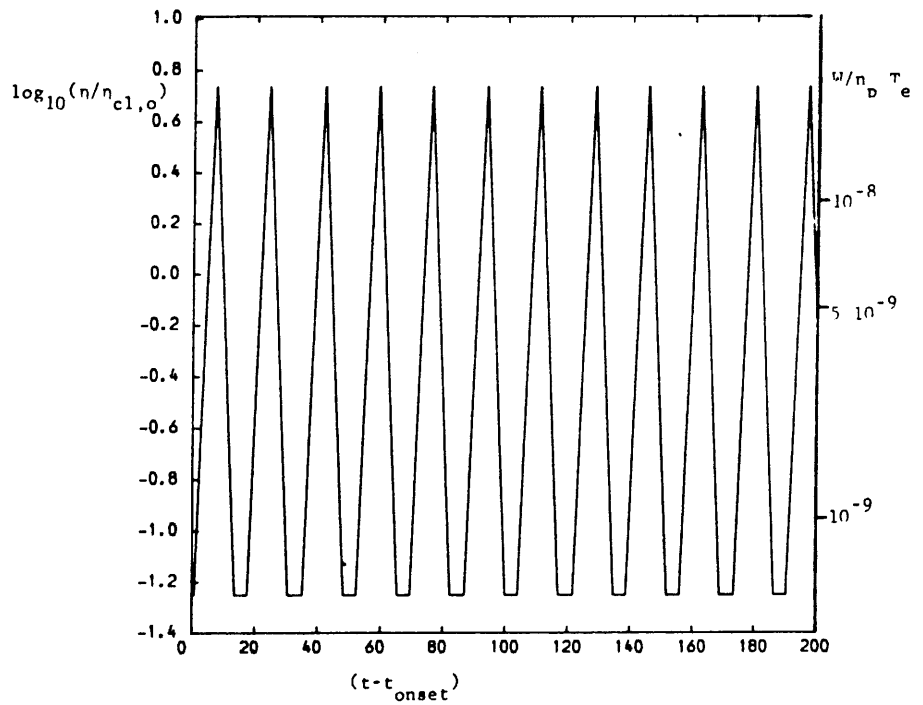

Figure 6.8ii: Variation of the normalised resistivity with time after onset of instability, in case (b), for $\gamma = 1.0$. Time is in units of $(10^{-2}\ \omega_{pi})^{-1}$.

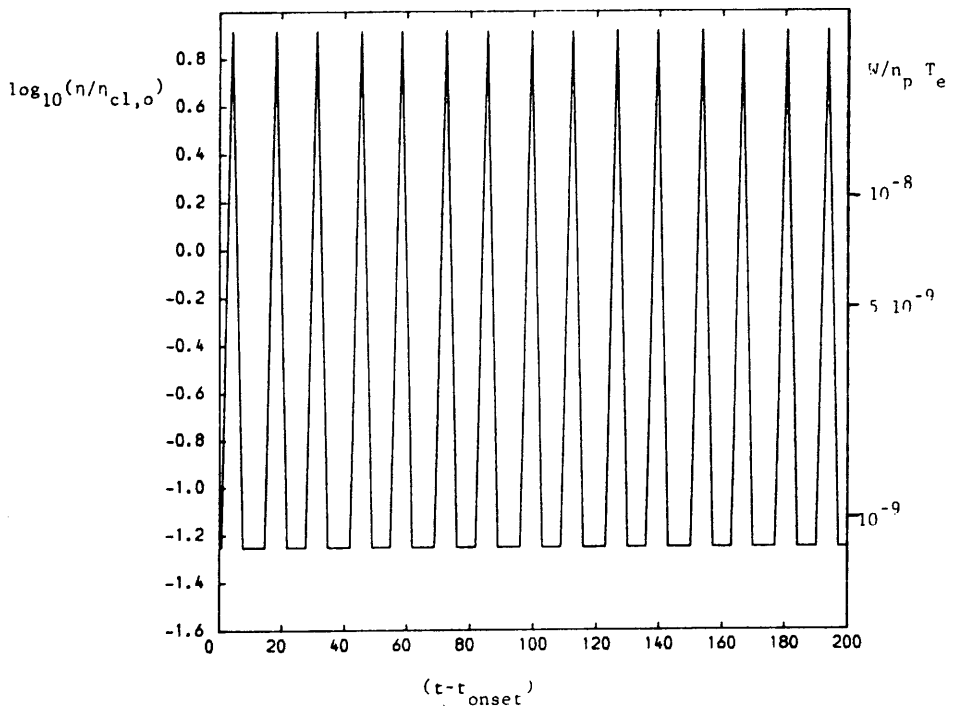

Figure 6.8iii: Variation of the normalised resistivity with time after onset of instability, in case (b), $\gamma = 2.0$. Time is in units of $(10^{-2}\ \omega_{pi})^{-1}$.

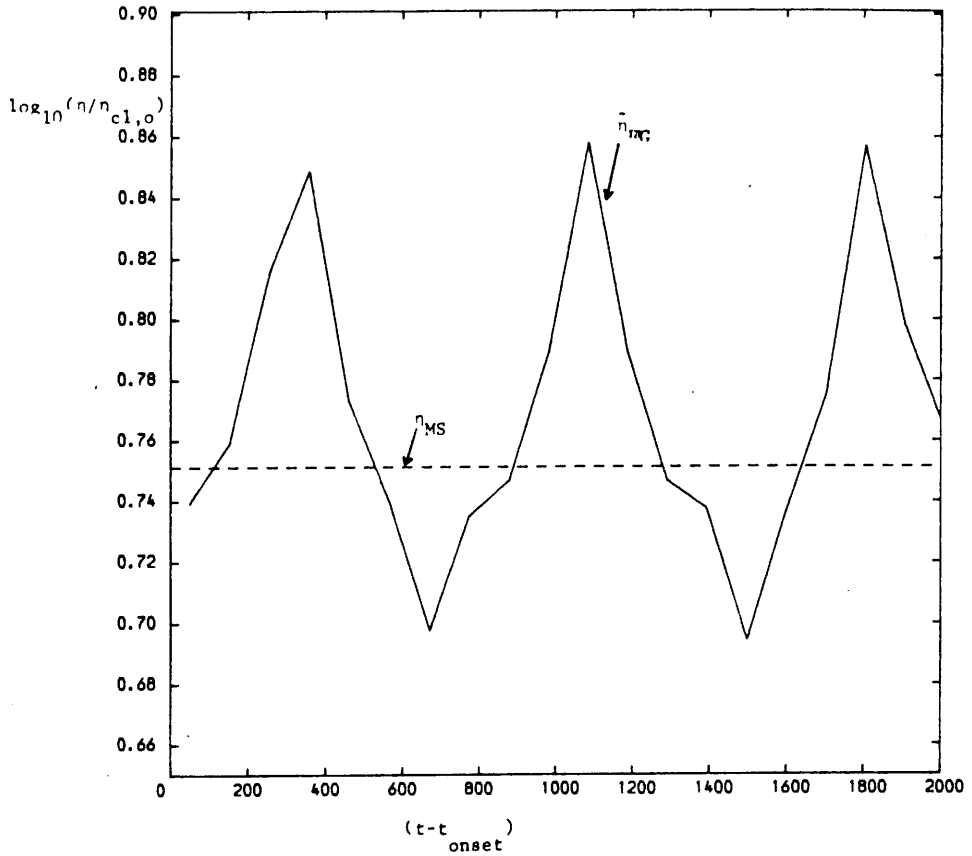

Figure 6.9i: A comparison of the mean wave growth resistivity, $\bar{\eta}_{WG}$, with the marginally stable resistivity, η_{MS}, in case (b) for $\gamma = 0.5$.

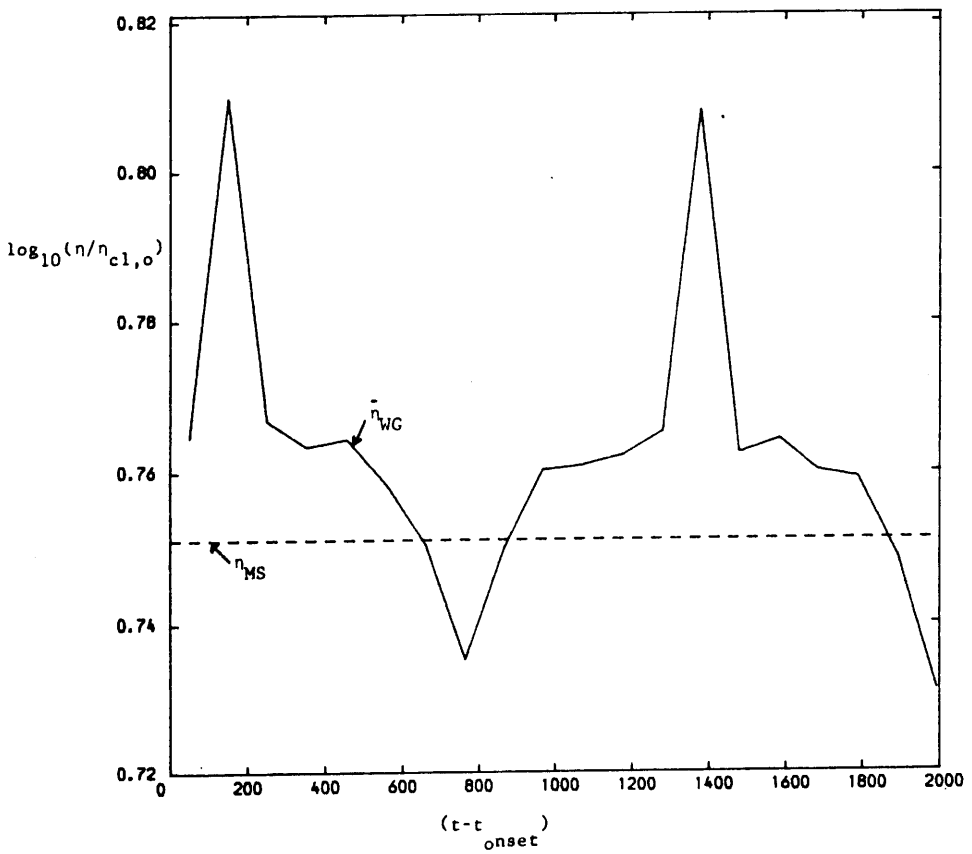

Figure 6.9ii: A comparison of the mean wave growth resistivity, $\bar{\eta}_{WG}$, with the marginally stable resistivity, η_{MS}, in case (b) for $\gamma = 1.0$.

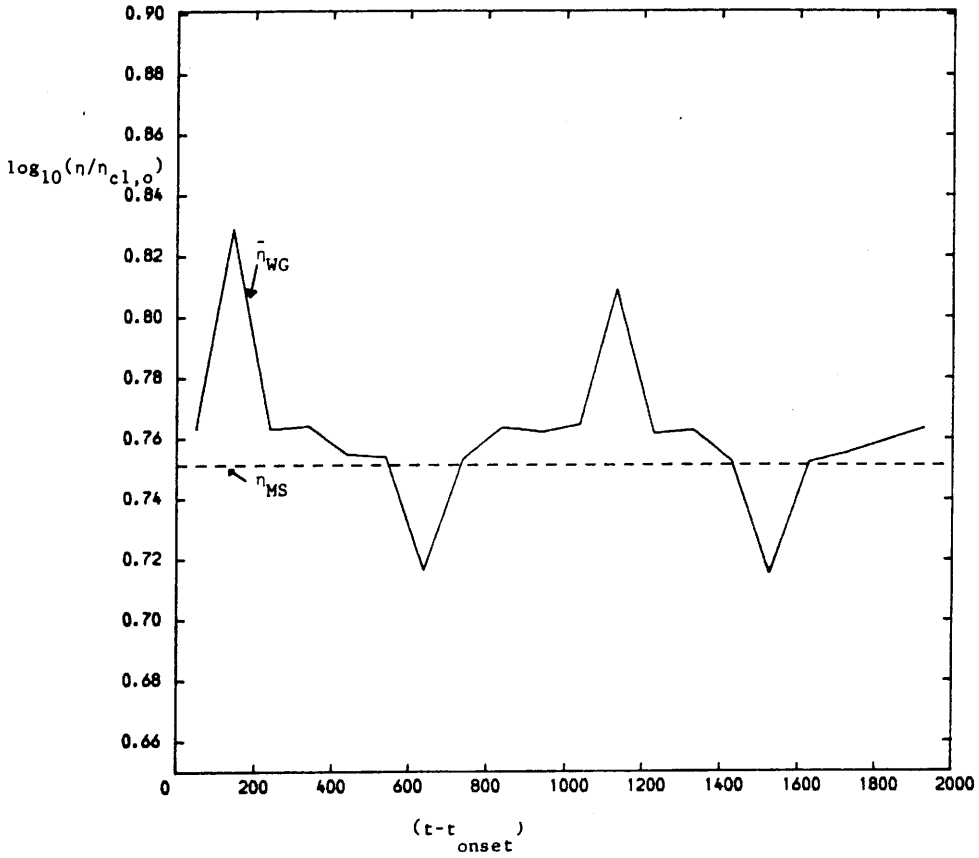

Figure 6.9iii: A comparison of the mean wave growth resistivity, $\bar{\eta}_{WG}$, with the marginally stable resistivity, η_{MS} in case (b) for $\gamma = 2.0$.

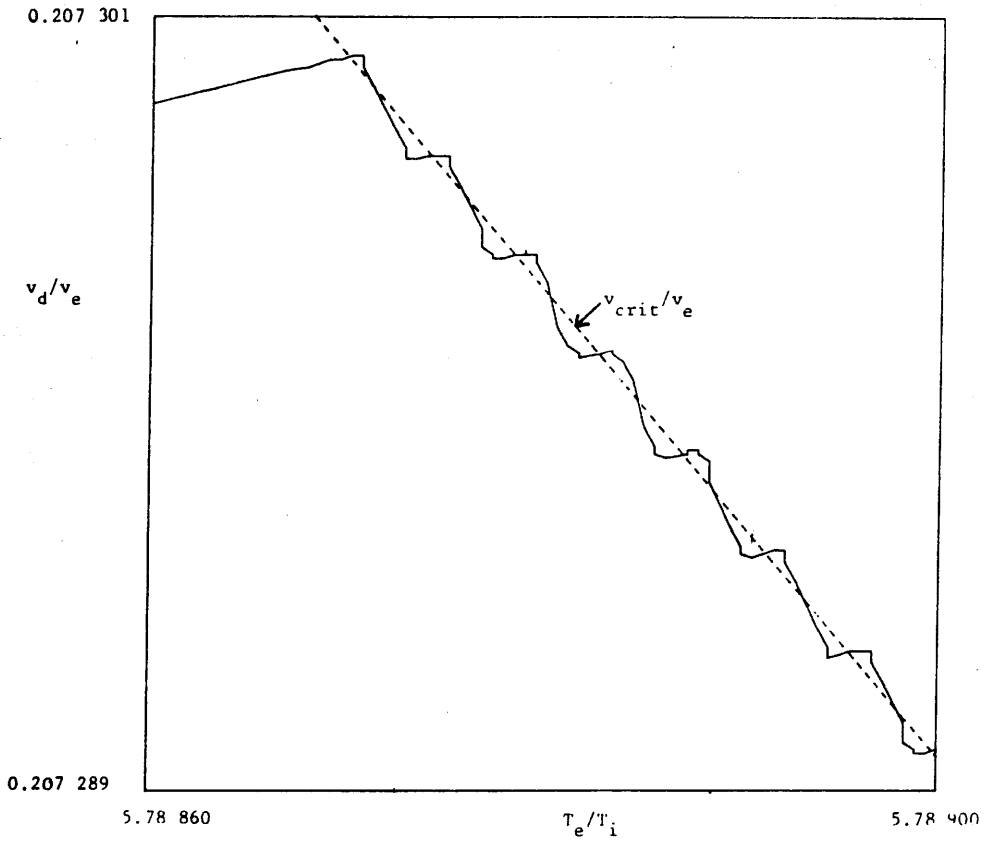

Figure 6.10: Rapid oscillations occur about the IA marginal stability curve (dashed line) after onset of instability. The case depicted here is t_r = 2s, γ = 2.0.

where t_o is the time of onset and $\int_{t_{n-1}}^{t_n} dt \equiv (t_n - t_{n-1}) = 100$ time units $\simeq 1.7\ 10^{-5}$ s. The time interval covered is 2000 units ($\simeq 3.4\ 10^{-4}$ s) during which time the plasma quantities (T_e, T_i, η) in our marginal stability analysis remain unchanged.

Figures 6.7 and 6.9 depict the results for $t_r = 10s$ and $t_r = 2s$ respectively. We note the excellent agreement between the marginal stability and wave growth analyses. In addition, particularly in the case of $t_r = 2s$, the values of $\bar{\eta}_{WG}$ are not especially sensitive to the assumed constant value of γ. This justifies a *posteriori* our simple modelling of IA wave turbulence. Consistent values of η and, therefore, the ohmic heating rate, ηj^2, are found in both approaches. The validity of the marginal stability hypothesis for $(T_e/T_i)_{onset} \gtrsim 4.8$ has thus been verified.

6.3 A Wave Growth Treatment of Catastrophic Heating

For sufficiently small rise times, t_r, at fixed values of T_o, n_p and $\mathcal{E}_o$, a marginally stable plasma configuration is not possible. We are therefore compelled to adopt a wave growth analysis in our approach to return current instability in this regime. For the parameter values $T_o = 5.10^6$ K, $n_p = 10^{11} cm^{-3}$ and $\mathcal{E}_o = 25$ keV, Figure 6.1 shows that, in our return current model (see Chapter 3), $(T_e/T_i)_{onset} \gtrsim 4.8$ for $t_r \gtrsim 1s$ and $(T_e/T_i)_{onset} \lesssim 4.8$ for $t_r \lesssim 1s$ (cf. Figure 4.3 which applies to $T_o = 5.10^6$ K, $n_p = 10^{11} cm^{-3}$ and $\mathcal{E}_o = 100$ keV). In other words, a wave growth approach is required in cases of return current heating where the beam rise time $t_r \lesssim 1s$.

As an example of a wave growth description of catastrophic heating we consider the case $t_r = 0.5s$ (with the same values of T_o, n_p and $\mathcal{E}_o$

as before). Again we take three different constant values of γ to describe the growth (and damping) of the IA waves. Figures 6.11, 6.13, 6.14 and 6.15 are the, by now, familiar set of four diagrams common to our return current heating analyses. They actually relate to the case $\gamma = 0.5$ but, as all three values of γ give virtually identical sets of four figures (on these scales), they can be considered to be a representative collection.

The slightly different plasma evolution profiles for each γ are seen in Figures 6.12i ($\gamma = 0.5$), 6.12ii ($\gamma = 1.0$) and 6.12iii ($\gamma = 2.0$). These are "blow-ups" of the boxed area around the marginal stability curve of Figure 6.11. Onset of instability occurs at $T_e/T_i \simeq 3.8$ and the subsequent period of heating is catastrophic. The IA waves grow linearly and saturation wave levels ($W/n_p T_e \simeq 10^{-3}$) are attained as shown in Figures 6.16. Since $\bar{\chi}_{ia}(T_e/T_i) > 0.5$ (Section 2.3), the electrons are preferentially heated over the ions; the electron-ion temperature ratio increases especially rapidly during this catastrophic phase.

In all the cases of catastrophic heating which we have examined, v_{crit} rises sufficiently rapidly (or, equivalently, v_d/v_e drops with the rapid increase in T_e) that the saturated IA waves become damped. A short period of classical heating then follows, with v_d/v_e once again rising, until the threshold drift speed for instability is reached for the second time. This second onset of turbulence occurs at $(T_e/T_i)_{onset} > 4.8$ and, as in Section 6.2, we observe rapid oscillations about marginal stability. This is illustrated in Figure 6.12iv, which is an enlargement of the small boxed section of Figure 6.12iii ($\gamma = 2.0$).

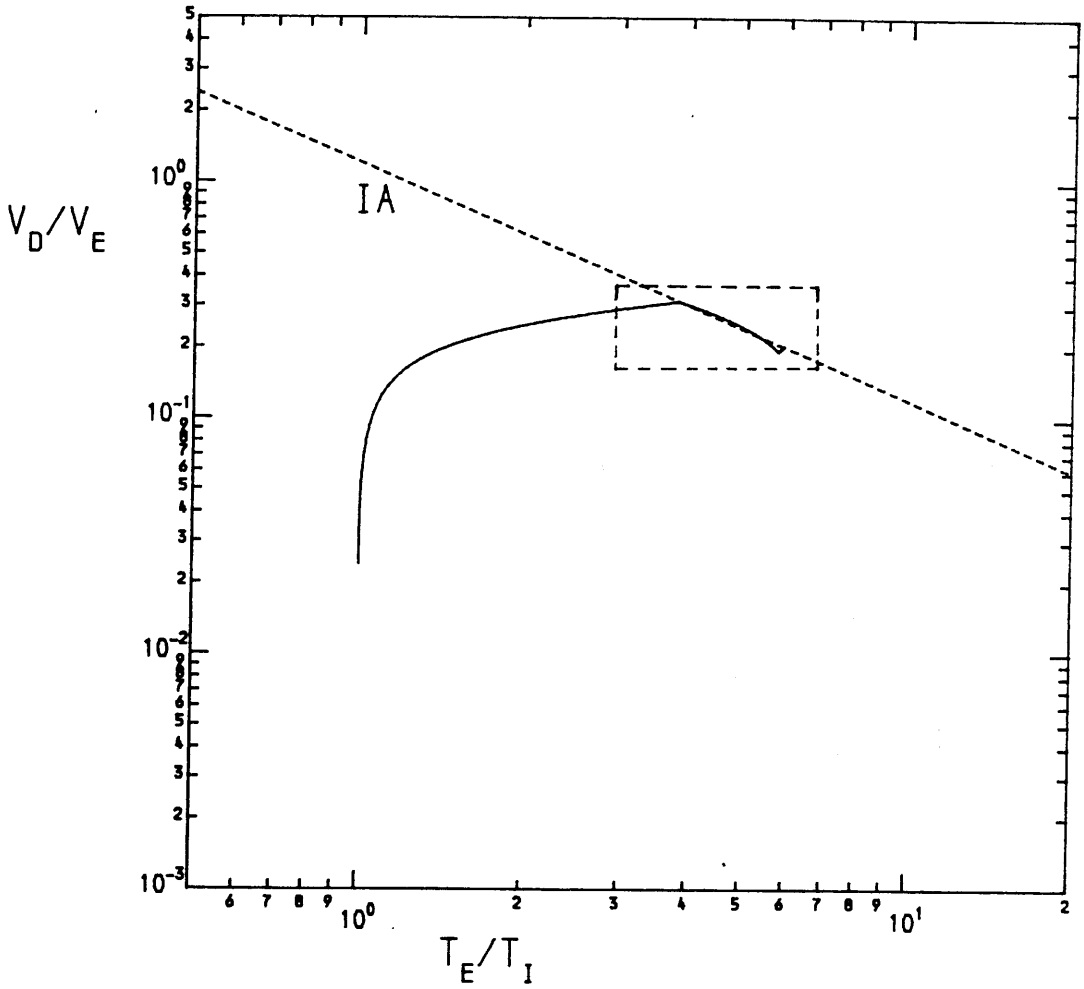

Figure 6.11: Evolution of the plasma in the (v_d/v_e, T_e/T_i) plane for the cases of catastrophic heating discussed in the text. The boxed area is enlarged in Figures 6.12i,ii,iii for the cases γ = 0.5, 1.0, 2.0 respectively.

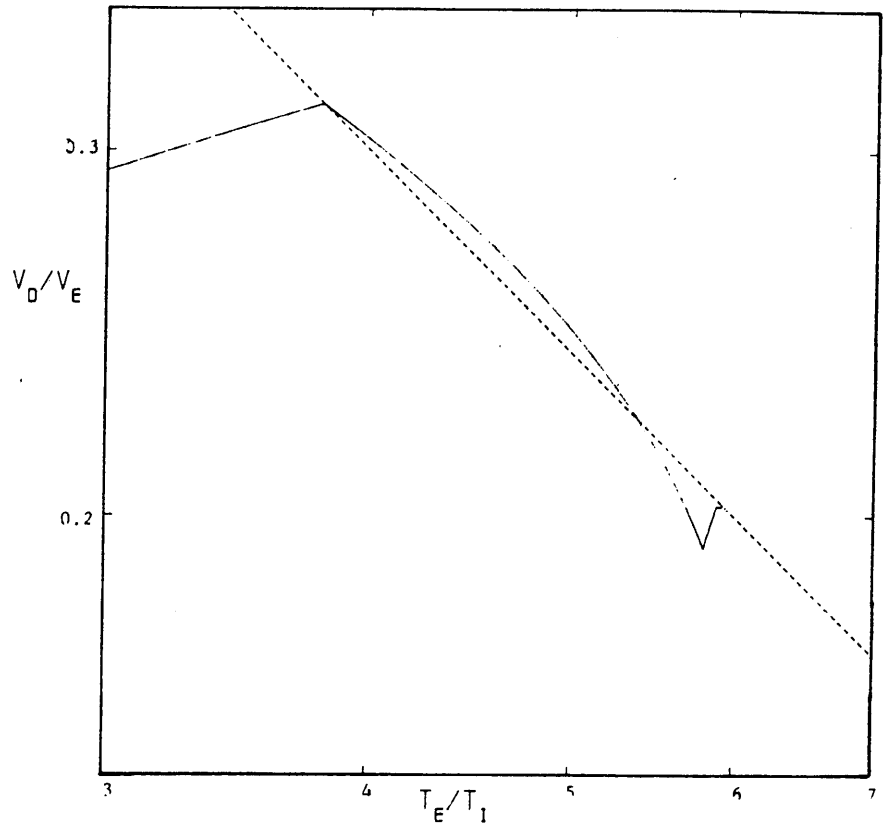

Figure 6.12i: Blow-up of the boxed area in Figure 6.11 for $\gamma = 0.5$

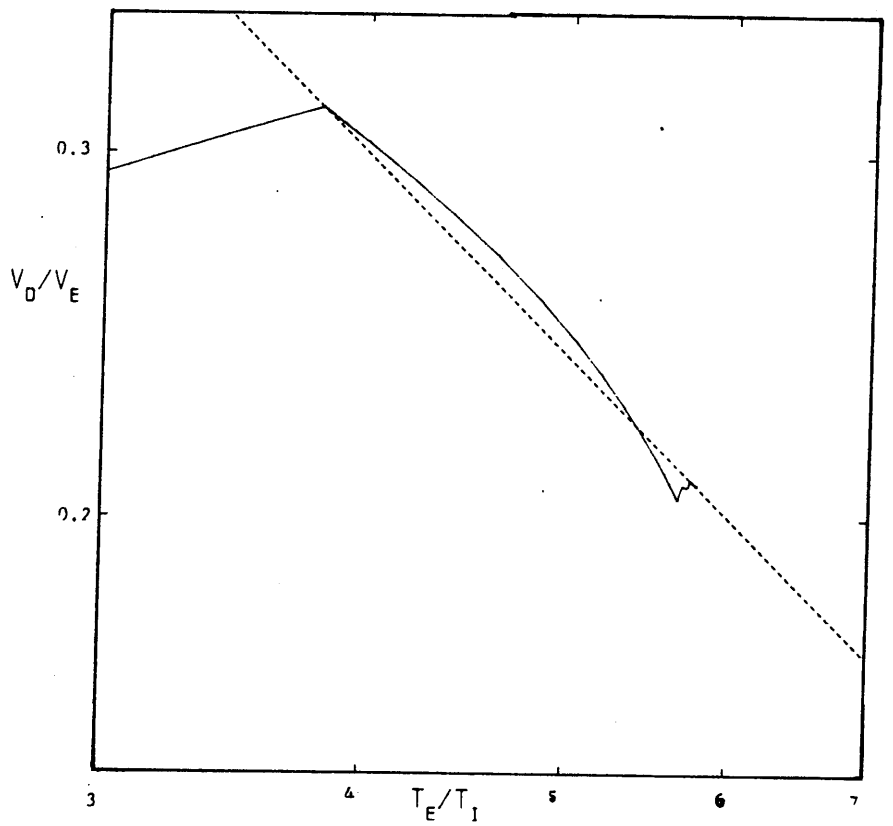

Figure 6.12ii: Blow-up of the boxed area in Figure 6.11 for $\gamma = 1.0$.

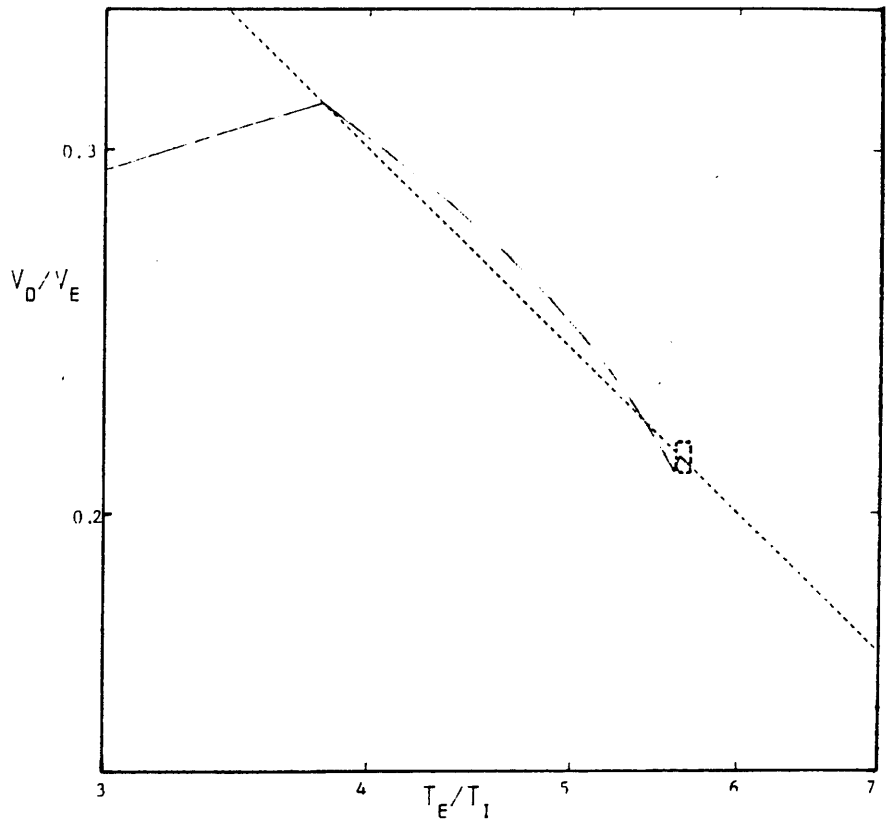

Figure 6.12iii: Blow-up of the boxed area in Figure 6.11 for $\gamma = 2.0$.

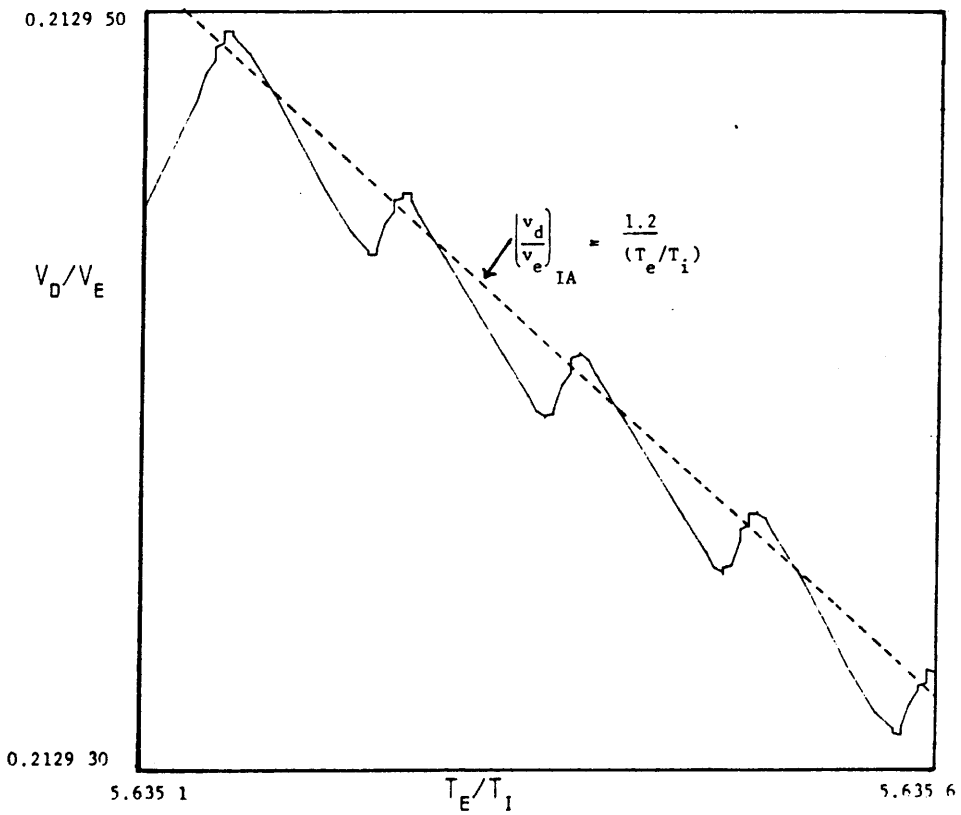

Figure 6.12iv: Blow-up of the boxed area in Figure 6.12iii showing the rapid oscillations around marginal stability at the second onset of IA turbulence.

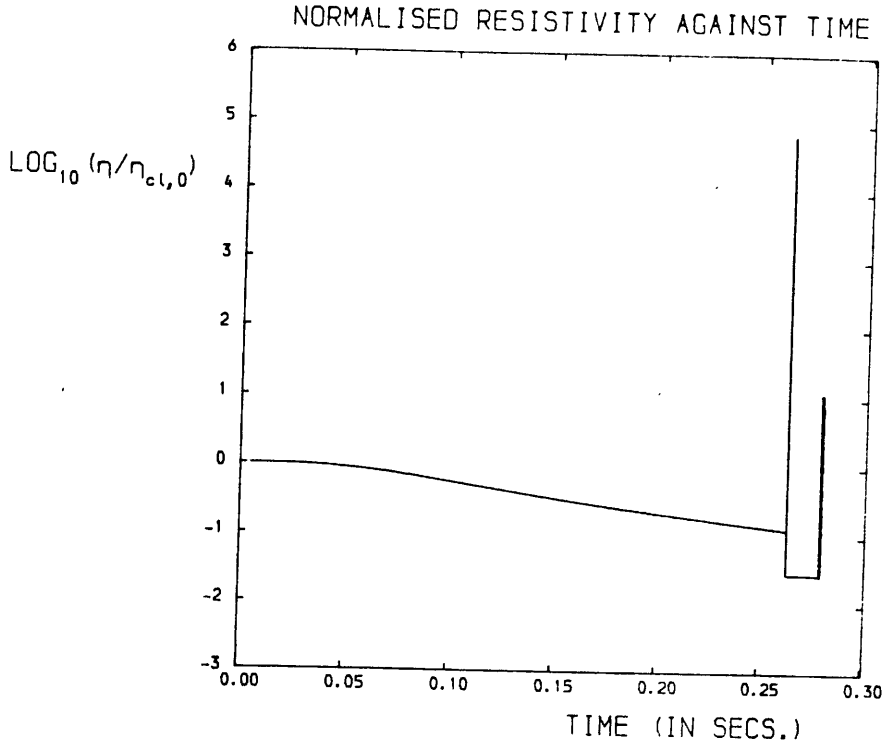

Figure 6.13: Variation of the normalised resistivity with time for the sample case of catastrophic heating (see text). Note the two peaks corresponding to the two onsets of IA turbulence.

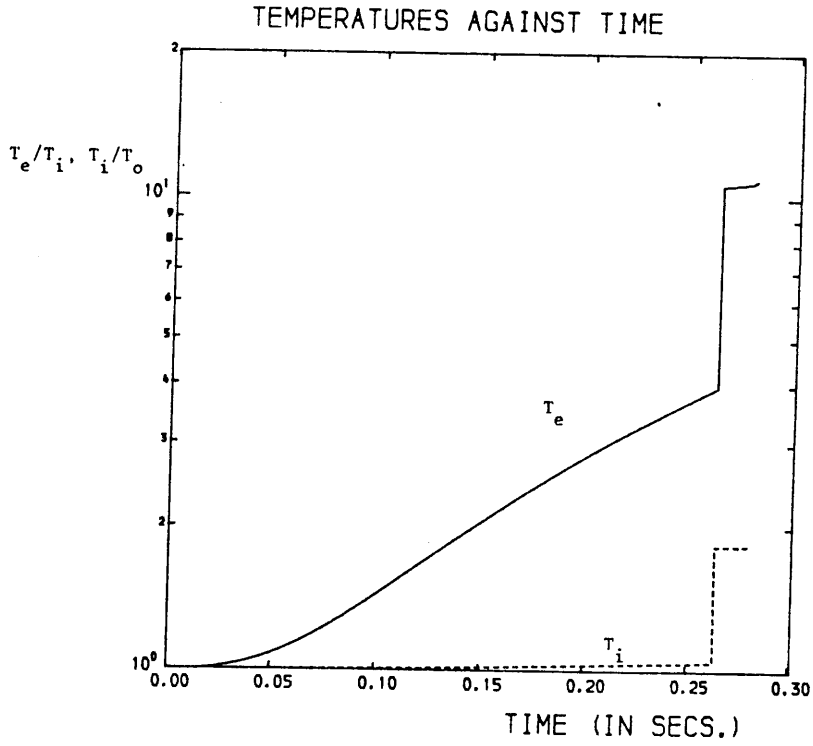

Figure 6.14: Electron and ion temperature profiles for the sample case of catastrophic heating.

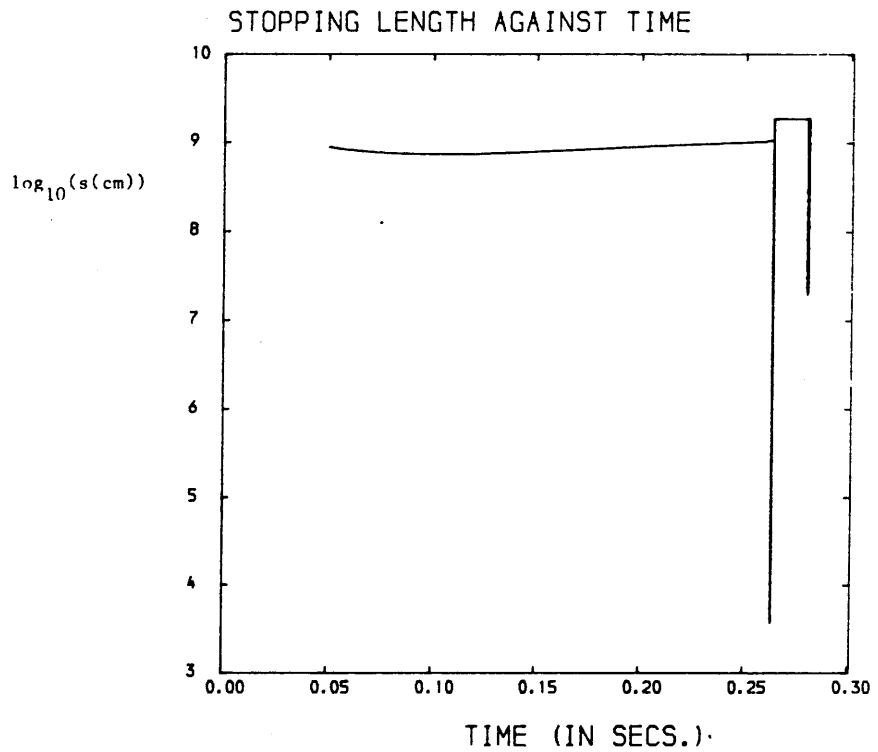

Figure 6.15: Electron beam stopping length v. time for the sample case of catastrophic heating.

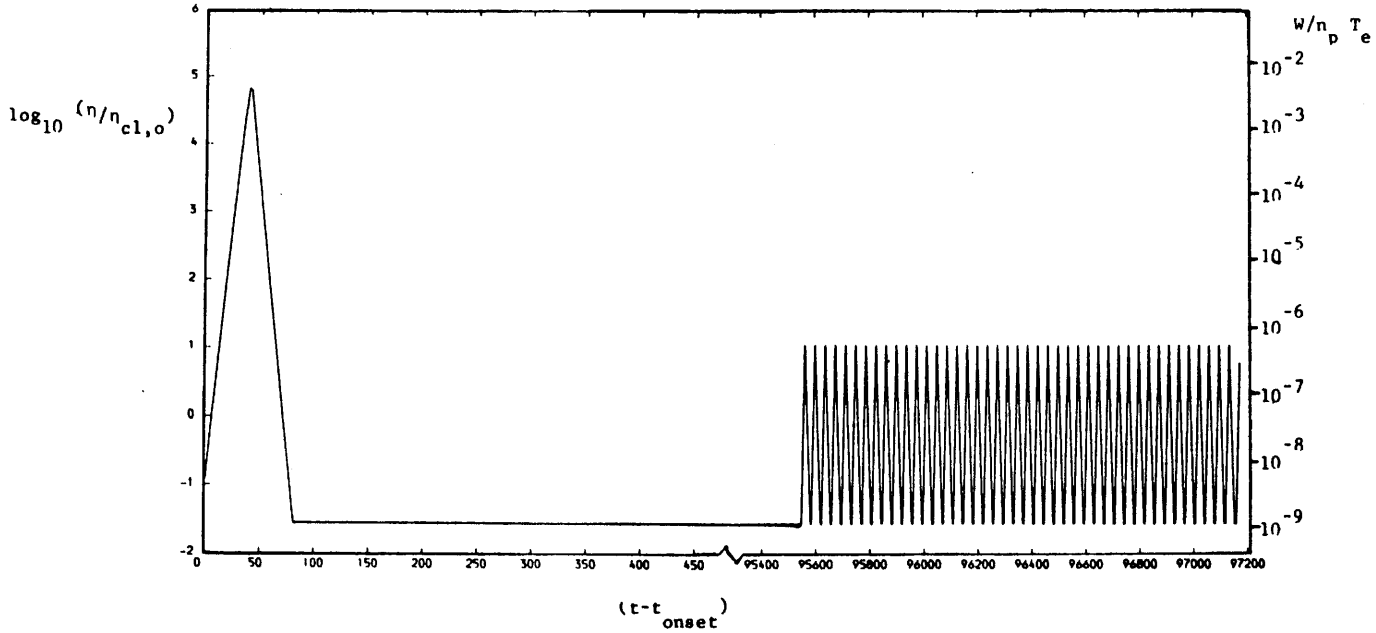

Figure 6.16i: Variation of normalised resistivity with time for the sample case of catastrophic heating, with $\Upsilon = 0.5$ (see text). Time is in units of $(10^{-2}\ \omega_{pi})^{-1}$.

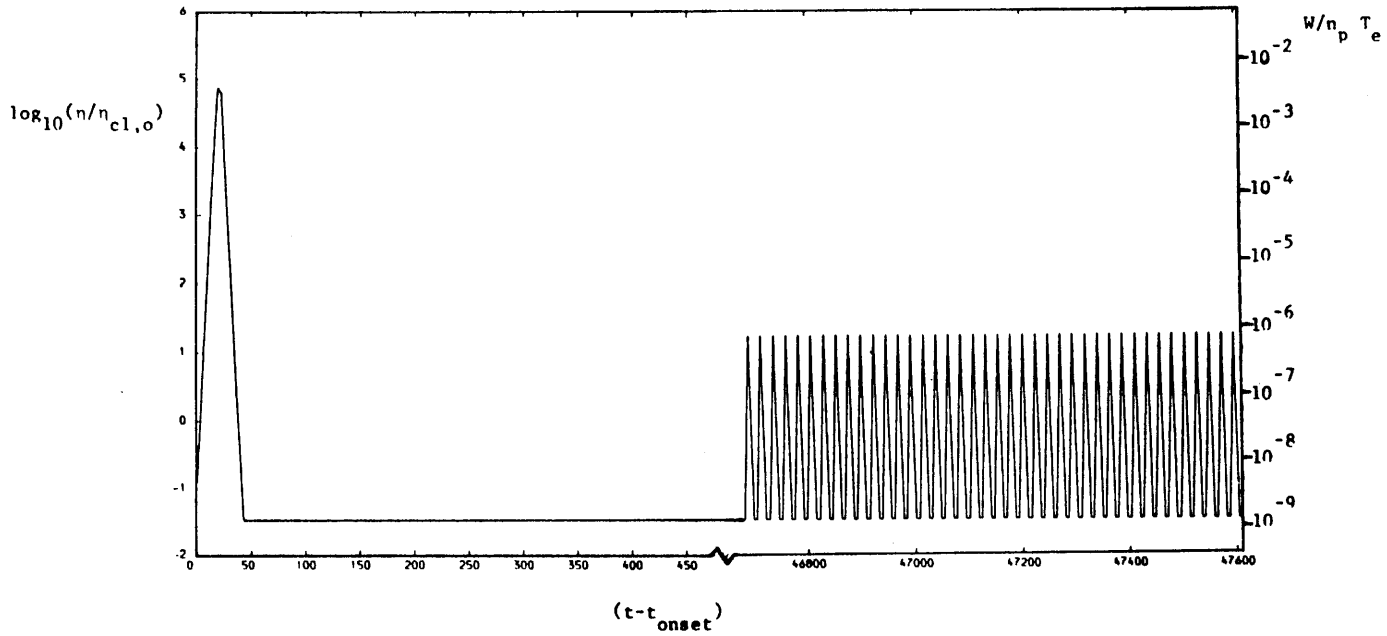

Figure 6.16ii: Variation of normalised resistivity with time for the sample case of catastrophic heating, with $\gamma = 1.0$ (see text). Time is in units of $(10^{-2}\ \omega_{pi})^{-1}$.

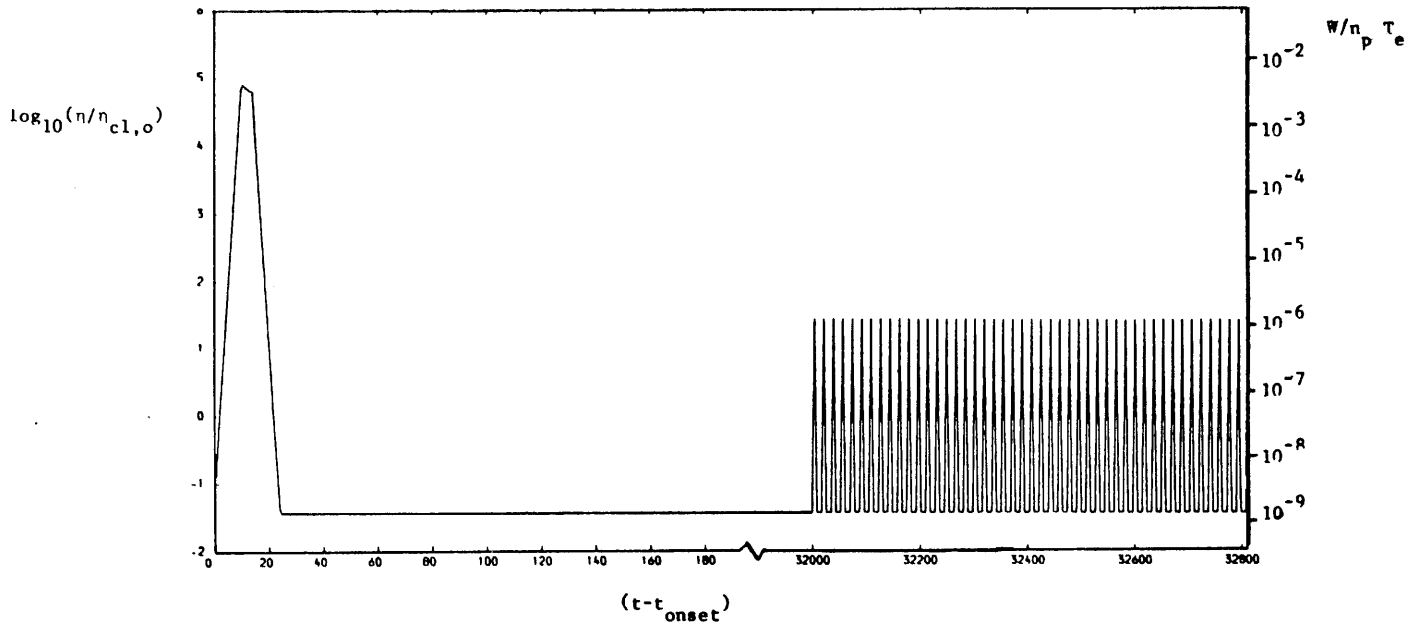

Figure 6.16iii: Variation of normalised resistivity with time for the sample case of catastrophic heating, with $\Upsilon = 2.0$ (see text). Time is in units of $(10^{-2}\ \omega_{pi})^{-1}$.

As Figures 6.16 indicate, this second period of turbulence occurs many time units after the first (note the change in scale in the abscissa after the break-point). The peak wave amplitudes (and resistivities) during this marginally stable turbulent state are around four orders of magnitude smaller than those reached in the catastrophic phase (cf. Figures 6.6, 6.8). As we might expect, the time interval between the first and second onset of turbulence is less for larger values of γ ; Figures 6.12i - iii indicate that the plasma does not drop far below the marginal stability curve if the waves are rapidly damped. The threshold for instability is therefore reached quickly once v_d/v_e begins to rise again.

6.4 A Combined Wave Growth/Marginal Stability Analysis

The previous section showed that a simple wave growth approach can describe the phase of catastrophic heating at onset of IA turbulence for $T_e/T_i \lesssim 4.8$. Moreover, such heating is always followed by a negligibly short period of classical ohmic dissipation before turbulence is generated once again, this time in a marginally stable state. It is immediately apparent, then, that a unified treatment may be adopted, incorporating both wave growth and marginal stability techniques.

We have therefore developed a numerical code embodying this approach: for large rise times IA turbulence switches on at $T_e/T_i > 4.8$. The concept of marginal stability can then be applied with great success in describing the ohmic dissipation of the unstable return current. On the other hand, for small rise times such that $(T_e/T_i)_{onset} \lesssim 4.8$, the first period of turbulence is catastrophic and must be tracked via the wave growth method. This phase of the heating process ends rapidly

when v_{crit} rises to the same value as v_d at which point marginal stability applies (since, by now, $T_e/T_i \gtrsim 4.8$). With this combined approach we are able to investigate return current instability for any beam rise time.

Two examples of the success of this method are presented in Figures 6.17 - 6.21 for $t_r = 0.5s$ (case (a)) and $t_r = 0.1s$ (case (b)). During the phase of catastrophic heating we assume a constant growth rate $\gamma = 10^{-2}\omega_{pi}$. As Figures 6.17 indicate, the plasma remains in a state of marginal stability following the catastrophic regime. In both cases the resistivity rises by nearly six orders of magnitude at onset of catastrophic turbulence (Figures 6.18). The final temperatures reached after evolution times of $2t_r$ are: case (a) : $T_e \simeq 182\ T_o, T_i \simeq 26.8\ T_o$ and case (b): $T_o \simeq 179\ T_o$, $T_i \simeq 26.6\ T_o$ (Figures 6.19).

With the very high resistivities attained, anomalous ohmic dissipation is considerable and the minimum beam stopping lengths are very short (in comparison to coronal loop lengths). In case (a), $s_{min} \simeq 1.2\ 10^4$ cm and, in case (b), $s_{min} \simeq 8.8\ 10^3$ cm (Figures 6.20). As explained in Chapters 3 and 4, the electron and ion temperature equations (Eqns. (3.4)) are solved for the plasma volume bounded by the minimum beam stopping length. Outside this region the heating is not taken account of in our numerical simulation. For example, after $t \simeq 6.5\ \ 10^{-2}$ s, in case (b), our description only applies to a thin layer $\sim$ 100m in thickness. The way in which this "boundary" layer might progress through the plasma is considered qualitatively in Chapter 8.

Despite this limitation we perform, for completeness, the same

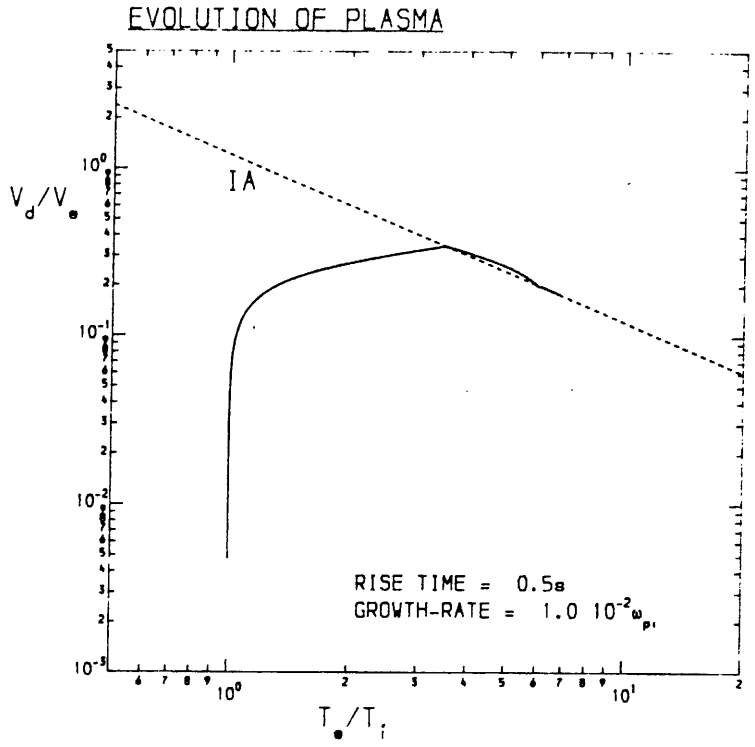

Figure 6.17a: Evolution of the plasma for the combined wave growth/marginal stability analysis of case (a) (see text).

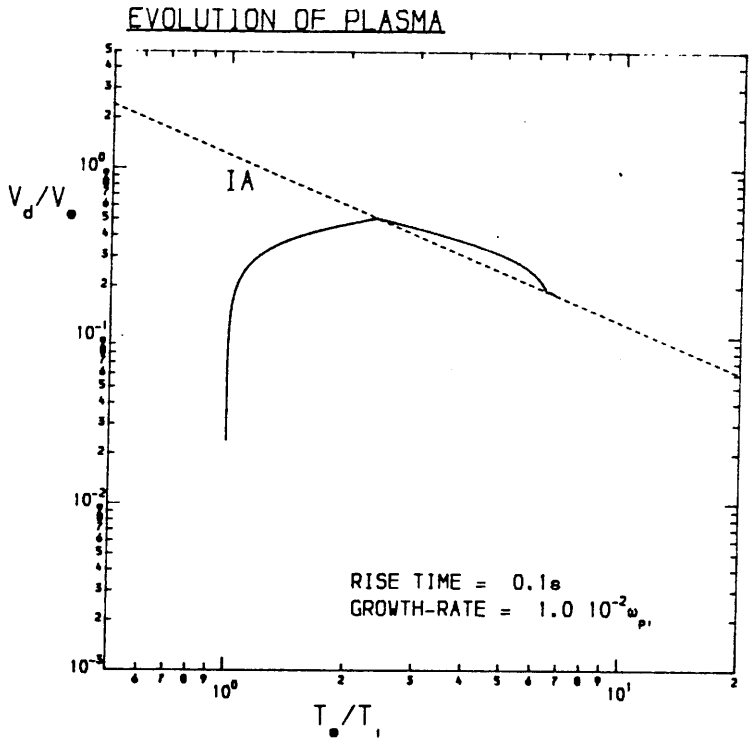

Figure 6.17b: Evolution of the plasma for the combined wave growth/marginal stability analysis of case (b).

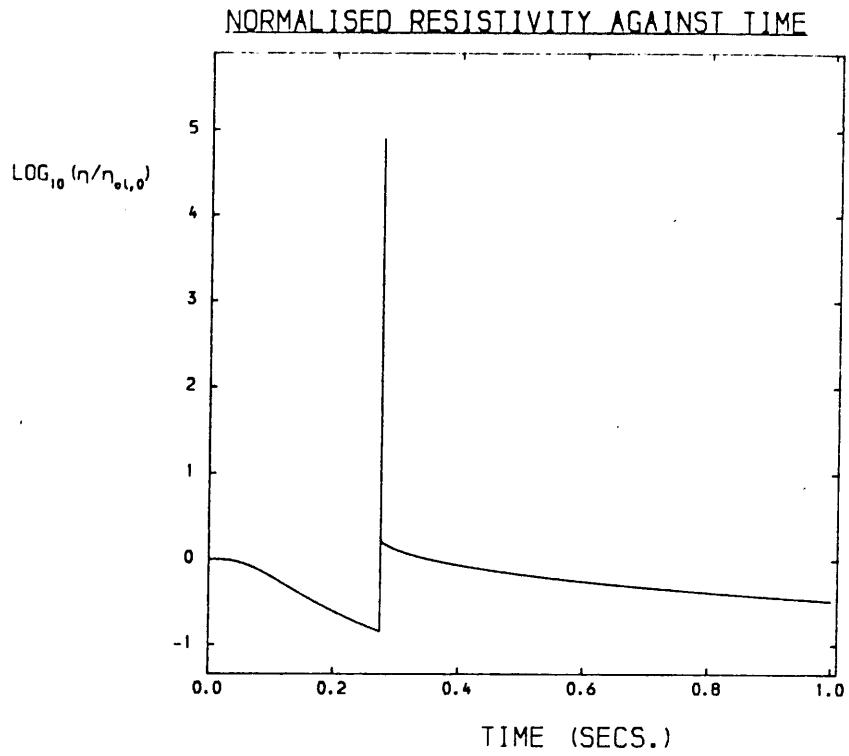

Figure 6.18a: Variation of the normalised resistivity with time for the combined wave growth/marginal stability analysis of case (a).

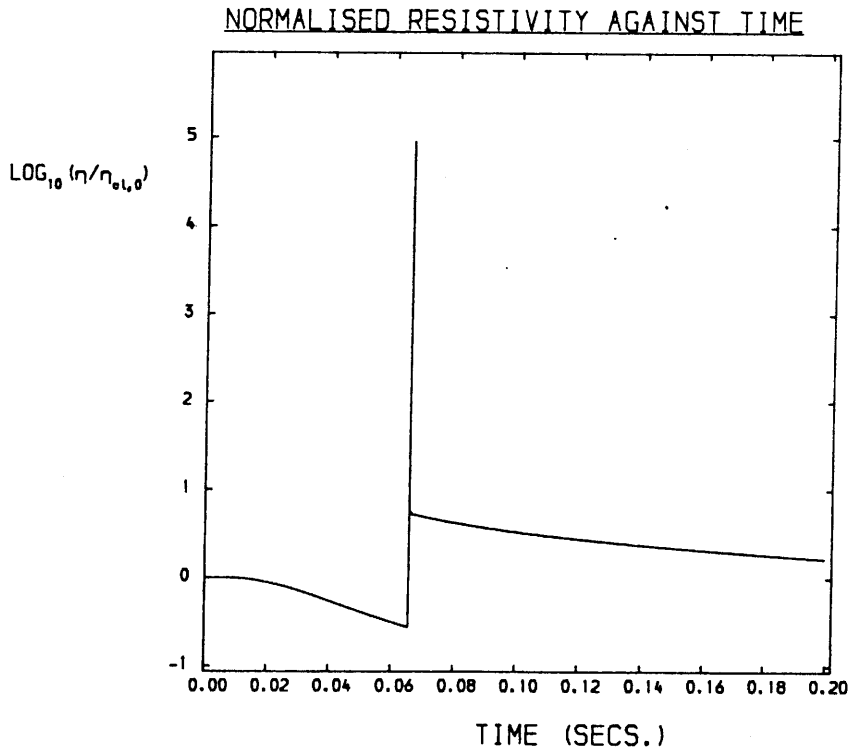

Figure 6.18b: Variation of the normalised resistivity with time for the combined wave growth/marginal stability analysis of case (b).

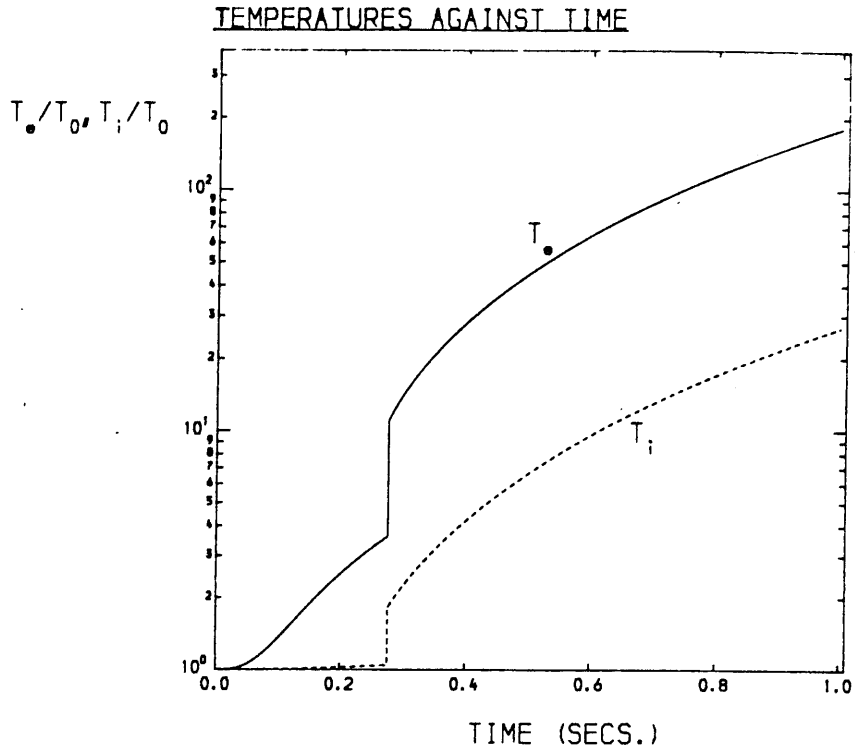

Figure 6.19a: Electron and ion temperature profiles for the combined wave growth/marginal stability analysis of case (a).

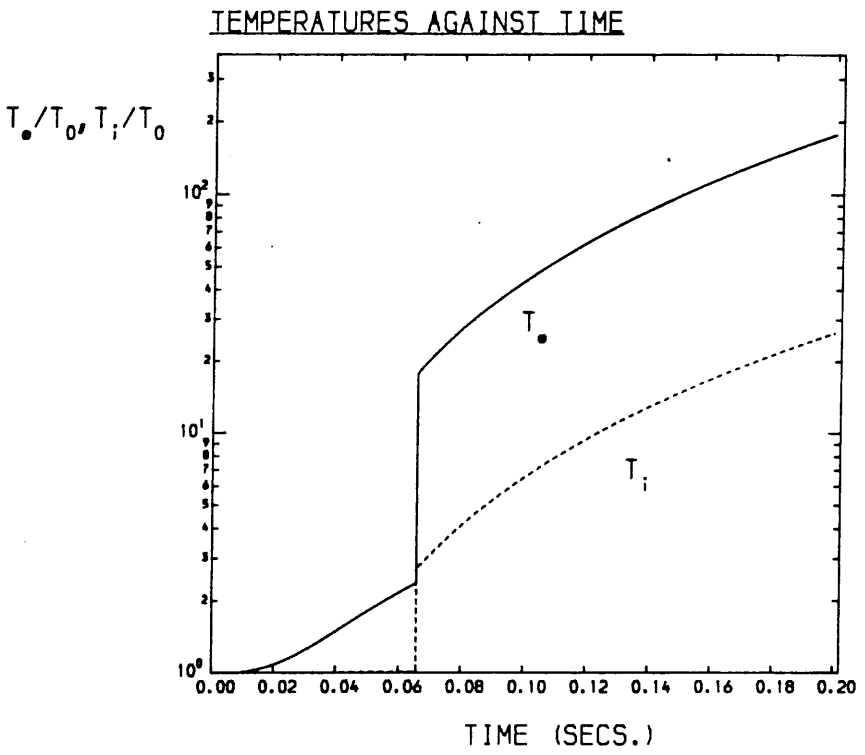

Figure 6.19b: Electron and ion temperature profiles for the combined wave growth/marginal stability analysis of case (b).

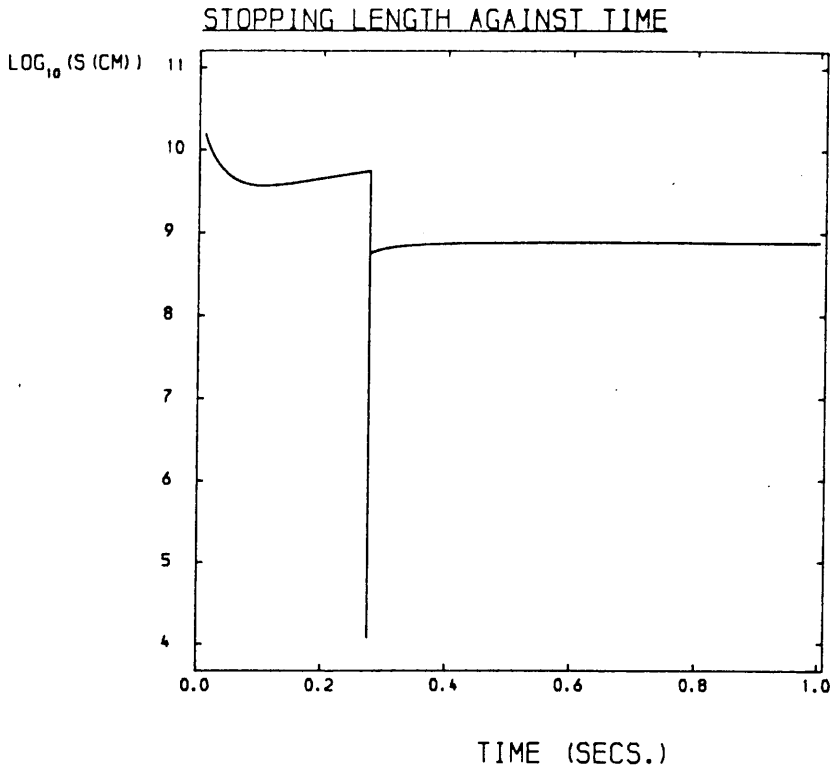

Figure 6.20a: Electron beam stopping length v. time for the combined wave growth/marginal stability analysis of case (a).

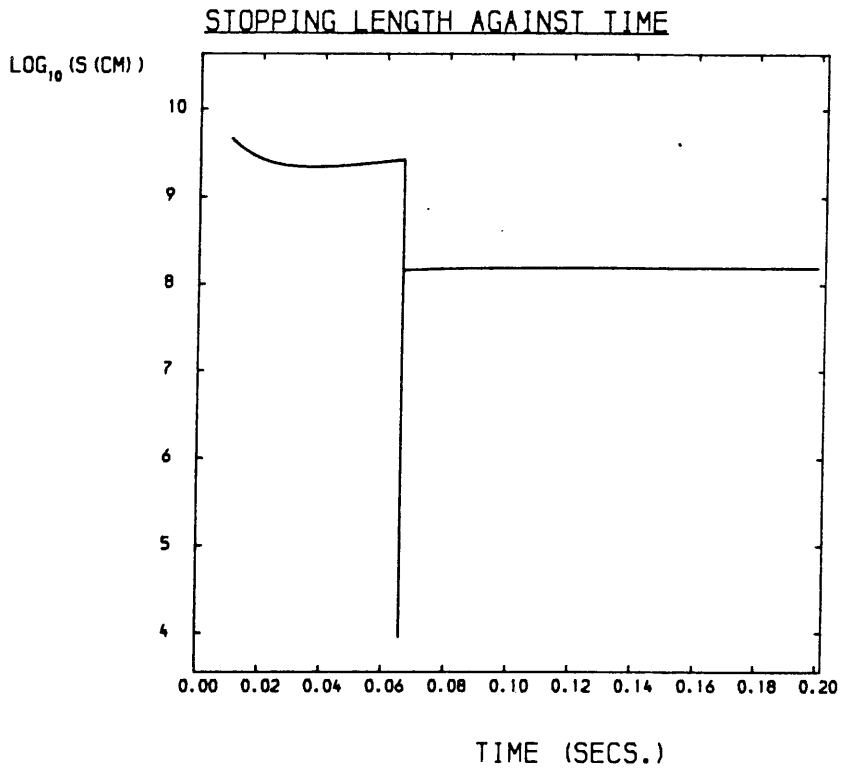

Figure 6.20b: Electron beam stopping length v. time for the combined wave growth/marginal stability analysis of case (b).

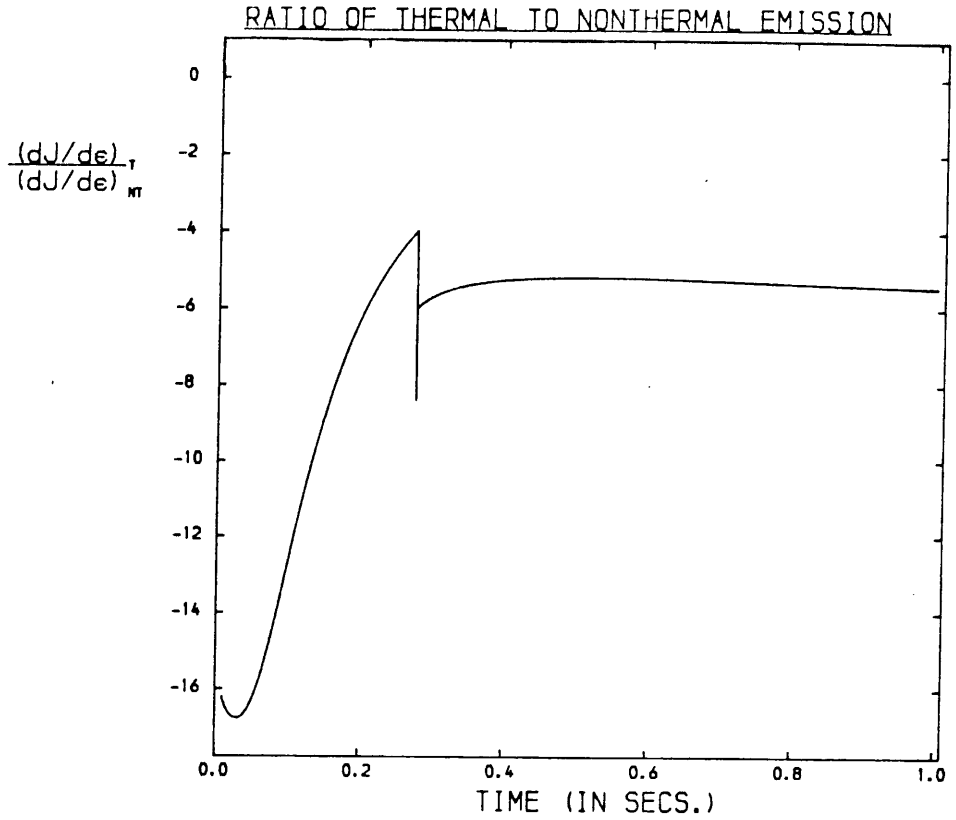

Figure 6.21a: Ratio of thermal/non-thermal bremsstrahlung yields (in logarithmic units, base 10) v. time at a photon energy ε = 20 keV for case (a).

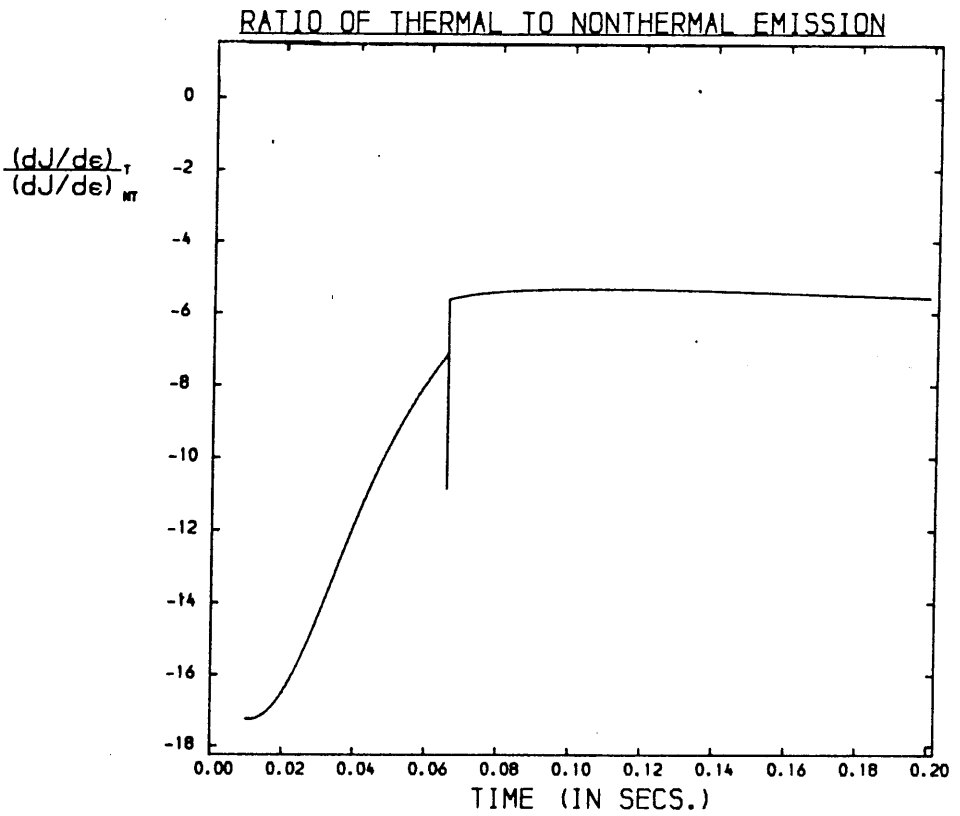

Figure 6.21b: Ratio of thermal/non-thermal bremsstrahlung yields (in logarithmic units, base 10) v. time at a photon energy ε = 20 keV for case (b).

calculation as in Section 4.4 to evaluate the ratio of thermal to (thick-target) non-thermal bremsstrahlung yields (Figures 6.21). At onset of turbulence the beam stopping length is reduced and so our calculated thermal yield drops. This rises again, however, with the rapid increase in T_e and, during marginal stability, values of $(dJ/d\varepsilon)_T/(dJ/d\varepsilon)_{NT} \sim 10^{-6}$ are obtained (cf. Figures 4.10). It is probable that a large plasma volume $V = As_{min} \simeq 10^{16}.10^8 cm^3 = 10^{24} cm^3$ is heated to large temperatures during marginal stability; the actual thermal emission will therefore be much larger than that calculated here. To properly estimate these temperatures and thermal emission would, however, require the development of a beam-plasma model with spatial, as well as temporal, variation in T_e, T_i and n. Such a treatment is outwith the scope of this thesis.

6.5 Discussion

In this chapter we have demonstrated the soundness of the marginal stability hypothesis for $T_e/T_i \gtrsim 4.8$, as applied to beam-driven return current instability. We did this by adopting a straightforward plasma wave analysis which modelled the growth, saturation and decay of IA waves. This method revealed the rapid oscillations which occur around the threshold curve for instability, a feature implicit in the concept of marginal stability. The values of resistivity determined in both approaches were found to be consistent.

An example of the success of the wave growth technique to describe the rapid catastrophic heating for $(T_e/T_i)_{onset} \lesssim 4.8$ was given. Saturation wave levels of $W/n_p T_e \simeq 10^{-3}$ were found. This satisfies our requirement for weak turbulence ($W/n_p T_e \ll 1$: see Appendix B) and

justifies our use of the effective electron collision frequency ν_{eff} to determine η .

A synthesis of the two approaches was then made to describe the cases where catastrophic heating is followed by a phase of marginally stable dissipation, i.e. cases where $(T_e/T_i)_{onset} \leq 4.8$. For the typical flaring corona parameters $T_o = 5.10^6$ K, $n_p = 10^{11} cm^3$ and $\mathcal{E}_o$ = 25 keV, this type of behaviour occurs in beam-plasma systems where the rise time $t_r \lesssim$ 1s.

7. ION-ACOUSTIC AND/OR ION-CYCLOTRON INSTABILITY OF THE RETURN CURRENT: A MARGINAL STABILITY ANALYSIS

7.1 Introduction

Up till now we have investigated beam-driven return current instability in an unmagnetised plasma. The generation of only ion-acoustic (IA) waves was considered and we found that, for certain parameters, an electron beam will emit more hard X-rays by anomalous joule dissipation of its return current than by direct thick-target interaction with the solar atmosphere (Section 4.4). By treating the simpler case of an unmagnetised plasma we were able to develop an understanding of return current instability through the twin approaches of marginal stability (Chapter 4) and a wave growth analysis (Chapter 6). We argued that, although, in a magnetised plasma, ion-cyclotron (IC) waves will be excited first when $T_e/T_i \lesssim 8$ (Kindel and Kennel (1971)), the anomalous ohmic dissipation would be dominated by the IA wave level (Duijveman et al. (1981); Pritchett et al. (1981)). Consequently, we could neglect the effect of IC waves. In the following sections, however, we explicitly include the production of IC waves in a magnetised plasma.

We mentioned in Chapter 5 that there could only exist one unstable mode in an unmagnetised two-component plasma. In the presence of a magnetic field, however, the plasma can also support the transverse IC mode in addition to the longitudinal IA oscillations. We do not wish to become involved here in a discussion of the number of unstable modes which may be excited in a magnetised plasma, given the distributions of particle species; we would simply like to stress that the total plasma resistivity, η, has components due to IA and IC turbulence (η_{IA}, η_{IC} respectively) as well as a classical, i.e.

Spitzer, part (η_{cl}): e.g. Duijveman et al. (1981). The work of this chapter is an attempt to gain some understanding of beam-driven return current instability in the flaring magnetised corona. Since this is a difficult problem, one must regard the approach as exploratory; it cannot be claimed that all of the results are entirely explained or, indeed, that the behaviour found here would actually occur in the highly complex natural phenomenon of a solar flare. Despite this caveat we believe that our analysis yields useful information and demonstrates what may happen when a beam-driven return current goes unstable.

The new electron and ion temperature equations, including the effect of IC ohmic dissipation, are presented in Section 7.2. We also show, by means of a flow diagram, the possible regimes of return current heating which may occur. Previously, in Section 4.4, we derived an expression for the ratio of thermal to non-thermal hard X-ray yields assuming non-thermal emission by thick-target Coulomb collisions with the ambient plasma. In Section 7.3 we calculate this ratio for two other cases: non-thermal emission through return current losses only, and non-thermal emission through both ohmic dissipation of the return current and thick-target interaction. Illustrative cases of beam-driven return current instability in the magnetised corona are given in Section 7.4; these are for different rise times and postulated IC and IA saturation wave levels. Finally, in Section 7.5, we offer an overview of the main conclusions from this work.

7.2 Solution of the Heating Equations

The effect of IC ohmic dissipation on the electron and ion tempera-

tures is introduced in exactly the same way as for IA waves. Adopting the same dimensionless variables as before (Section 3.3) the heating equations become:

$$\frac{dx}{d\tau} = \frac{(y-x)}{x^{3/2}} + B\tau + C\tau^2 \left(\frac{1}{x^{3/2}} + \chi_{IA} Z_{IA} + \chi_{IC} Z_{IC}\right) \qquad (7.1a)$$

$$\frac{dy}{d\tau} = \frac{(x-y)}{x^{3/2}} + C\tau^2 \{ (1 - \chi_{IA})Z_{IA} + (1 - \chi_{IC})Z_{IC} \} \qquad (7.1b)$$

where $Z_{IC} \equiv \chi_{IC}/\eta_{cl,o}$ and $\chi_{IC} = \chi_{IC}(T_e/T_i)$ is as given in Equation (2.49). As before, we have the initial conditions $x=y=1$ at $\tau=0$.

The threshold relative electron-ion drift speed at which the IA instability is excited is:

$$v_{IA} = \frac{1.2\, T_i}{T_e} \left(\frac{T_e}{m_e}\right)^{\frac{1}{2}} \qquad (7.2)$$

(see Equation (3.14)). From the work of Kindel and Kennel (1971) we know that v_{IA} and v_{IC}, the critical IC drift speed, intersect $T_e/T_i \simeq 8$. We therefore take the following fit for v_{IC}:

$$v_{IC} = 0.6 \left(\frac{T_e}{T_i}\right)^{-\frac{2}{3}} \left(\frac{T_e}{m_e}\right)^{\frac{1}{2}} \qquad (7.3)$$

(The slightly more accurate form used earlier, Equation (2.46), does not intersect at $T_e/T_i \simeq 8$ with the simple form for v_{IA}, Equation (7.2); however, this invalidates neither the results of Section 2.4 nor this chapter).

In Section 4.2 we found the following relationship between the normalised electron and ion temperatures, x and y respectively, during a state of IA marginal stability:

$$y = D\tau x^{\frac{1}{2}} \qquad (7.4)$$

where $D = 2.62\ 10^{7}\ \tau_{eq}(o)/(n_p\ t_r\ T_o^{\frac{1}{2}})$ is a constant. Taking Equation (7.3) and performing the same type of algebraic manipulation leads to the following expression during IC marginal stability:

$$y = E\tau^{3/2}\ x^{\frac{1}{2}} \qquad (7.5)$$

where $E = 1.20\ 10^{10}\ (\tau_{eq}(o)/(n_p\ t_r\ T_o^{\frac{1}{2}}))^{3/2}$ is a constant.

In either state of marginal stability the anomalous resistivity is derived by differentiating Equation (7.4) or (7.5), as appropriate, and then using heating equations (7.1) to eliminate $\frac{dx}{d\tau}$ and $\frac{dy}{d\tau}$. Specifically, during IA marginal stability, the normalised IA resistivity is

$$Z_{IA} = \frac{Dx^{\frac{1}{2}}+0.5\ D\tau x^{-\frac{1}{2}}\ \{(y-x) + C\tau^2(1+x^{3/2}\chi_{IC}\ Z_{IC}) + B\tau\ x^{3/2}\ \}}{-C\tau^2(1-\chi_{IC})Z_{IC} - (x-y)x^{-3/2}} \qquad (7.6)$$
$$C\tau^2\ \{1 - \chi_{IA}(1 + \frac{y}{2x})\ \}$$

The value of Z_{IC} is known and depends on the previous history of the plasma; it is either zero, or equal to Z_{IC}^{sat} if the IC instability has already been excited. We note that the denominator is the same as before (Equation (4.7)); hence $Z_{IA} > 0 \Longleftrightarrow T_e/T_i > 4.8$. Including IC waves does not remove the failure of IA marginal stability for $T_e/T_i < 4.8$.

In the case of IC marginal stability, we may derive the following general expression for the normalised IC resistivity:

$$Z_{IC} = \frac{1.5E\tau^{\frac{1}{2}}x^{\frac{1}{2}} + 0.25E\tau^{3/2}x^{-9/4}\{(y-x)+ C\tau^2(1+x^{3/2}\chi_{IA}Z_{IA})+B\tau x^{3/2}\ \}}{- C\tau^2(1-\chi_{IA})Z_{IA} - (x-y)x^{-3/2}} \qquad (7.7)$$
$$C\tau^2\{(1-\chi_{IC}) - 0.25\ \frac{y}{x}\chi_{IC}\ \}$$

The value of Z_{IA} is also known. One may be tempted to state, in analogy to the above, that Z_{IA} is either zero, or equal to Z_{IA}^{sat} if the IA instability has previously been turned on. In practice, however, it is found that a state of IC marginal stability is not attainable if there already exists a turbulent IA wave level. We return to this point in Section 7.4.

The important feature of Equation (7.7) lies in determining the range of T_e/T_i for which a state of IC marginal stability is possible. Using the form of $\chi_{IC}(T_e/T_i)$ from Equation (2.49) it is straightforward to show that $Z_{IC} > 0 \iff T_e/T_i \gtrsim 0.15$. Conversely, the concept of marginal stability fails for the IC instability when $T_e/T_i \lesssim 0.15$. In these cases we would require an IC wave growth treatment similar to the IA wave analysis developed in the previous chapter. However, these values of T_e/T_i are never attained in our simulations and, although the failure of marginal stability as applied to IC turbulence may occur for a given set of input parameters ($\mathcal{E}_o$, n_p, etc.), we merely point this out for completeness.

As explained in Chapter 2, the expressions for χ_{IA} and χ_{IC} (Equations (2.34) and (2.49) respectively), are, strictly, applicable only in marginal stability. However, assuming continuity in T_e/T_i we may write:

$$\chi_{IC}^{sat} = 1 - \frac{v_{IC}}{v_e}\,(1 - \chi_{IC}^{sat})\,\frac{v_e}{v_d} \qquad (7.8)$$

$$\text{i.e.} \qquad \chi_{IC}^{sat} = 1 - 0.6\,\left(\frac{T_e}{T_i}\right)^{-2/3}\left[1 - 0.14\,\left(\frac{T_e}{T_i}\right)^{-\frac{1}{2}}\right]\frac{v_e}{v_d} \qquad (7.9)$$

(cf. Equation (2.50)). Assuming that χ_{IA} is also continuous in T_e/T_i we have, analogously to (7.8):

$$\chi_{IA}^{sat} = 1 - 1.2 \left(\frac{T_e}{T_i}\right)^{-1} \left(\frac{T_e/T_i}{51.4}\right) \frac{v_e}{v_d}$$

i.e.
$$\chi_{IA}^{sat} = 1 - \frac{1}{43} \frac{v_e}{v_d} \qquad (7.10)$$

Before we present a flow chart which demonstrates all possible paths of plasma evolution one additional point must be made. For given combinations of rise time and IC saturation wave level it is possible for IA onset to occur at $(T_e/T_i) \lesssim 4.8$. A completely rigorous analysis would describe the growth phase of the IA wave spectrum to saturation levels. However, given that this is likely to occur extremely rapidly, and simply for tractability, we neglect this phase and postulate immediate IA saturation. Adopting this approach allows us to continue tracking the evolution of the flaring plasma. Figure 7.1 displays all the possible behaviour of the coronal plasma during beam-driven return current instability and is essentially a synopsis of the numerical code utilised to investigate the sample case studies of Section 7.4.

7.3 Thermal and Non-thermal X-Ray Radiation Signatures

One of the major objectives of this thesis is to determine the thermal X-ray bremsstrahlung emission from the plasma volume which is heated via ohmic dissipation of a beam-driven return current. In Section 4.4 we compared this emission to that from a standard thick-target beam of sufficiently large cross-sectional area, A, that return current losses were negligible. The ratio of thermal to non-thermal bremsstrahlung yields in this case was found to be:

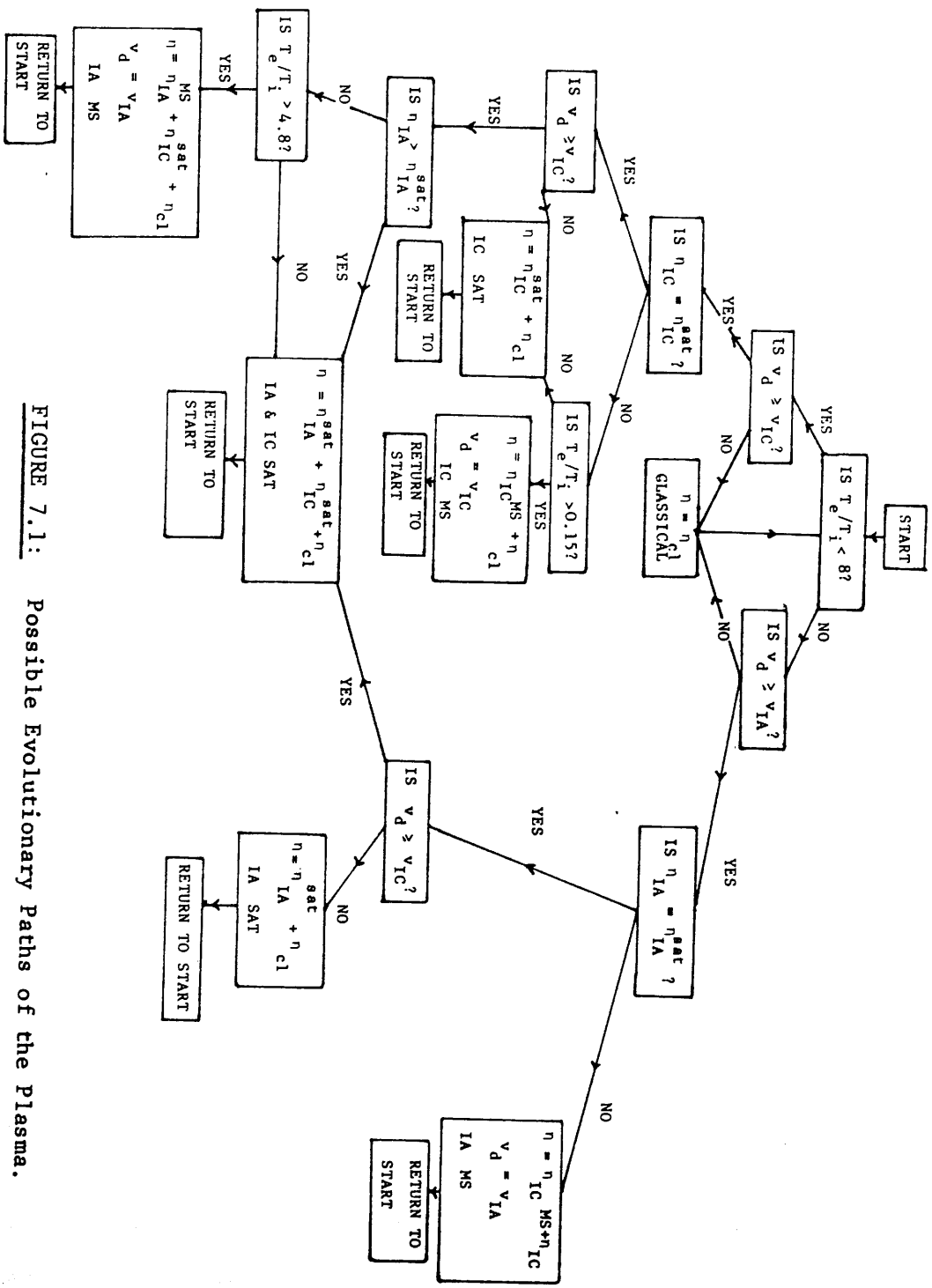

FIGURE 7.1: Possible Evolutionary Paths of the Plasma.

$$\frac{(dJ/d\varepsilon)_T}{(dJ/d\varepsilon)_{\substack{NT \\ TT}}} = \left(\frac{8}{\pi m_e T_e}\right)^{\frac{1}{2}} \frac{n_p^2 \, As_{min}}{F_b(\mathcal{E}_o - \varepsilon)} \exp(-\frac{\varepsilon}{T_e}) \quad (7.11)$$

(see Equation (4.17); TT denotes thick-target losses only).

Going to the other extreme, we may evaluate the non-thermal emission from the beam electrons assuming return current losses of the electron beam to dominate Coulomb collisional losses with the background plasma. As suggested by Emslie (1980), in the context of classical resistivity only, this may be the case in the initial stages of a solar flare (see Section 1.5). If η is anomalous then this is even more likely to be true. Assuming return current losses only, then, the energy loss equation for beam electrons is:

$$\frac{d\mathcal{E}_*}{dt} = - eEv(\mathcal{E}_*) \quad (7.12)$$

i.e.
$$\frac{d\mathcal{E}_*}{dt} = - e^2\eta \frac{F_b}{A} v(\mathcal{E}_*) \quad (7.13)$$

with notation as in Section 4.4. We evaluate $(dJ/d\varepsilon)_{NT}$ in this case in a similar manner to before, substituting Equation (7.13) into Equation (4.13). The resultant non-thermal yield is:

$$(\frac{dJ}{d\varepsilon})_{\substack{NT \\ RC}} = \frac{n_p Q_o A m_e c^2}{e^2\eta\varepsilon} \ln(\frac{\mathcal{E}_o}{\varepsilon}) \quad (7.14)$$

where RC denotes return current losses only. Note that the non-thermal emission is independent of the electron beam flux: the greater the electron flux, the greater is the energy loss rate. The thermal/non-thermal ratio in this case is:

$$\frac{(dJ/d\varepsilon)_T}{(dJ/d\varepsilon)_{NT}^{RC}} = \left(\frac{8}{\pi m_e T_e}\right)^{\frac{1}{2}} \frac{e^2 \eta n_p S_{min}}{\ell n \left(\frac{\mathcal{E}_o}{\varepsilon}\right)} \exp\left(-\frac{\varepsilon}{T_e}\right) \qquad (7.15)$$

Of course, by writing down the complete energy loss rate for beam electrons, we may evaluate the non-thermal emission from the beam assuming <u>both</u> thick-target and return current losses. The energy loss equation is then:

$$\frac{d\mathcal{E}_*}{dt} = -\frac{Kn_p v(\mathcal{E}_*)}{\mathcal{E}_*} - n_p e^2 v^2(\mathcal{E}_*)\eta \qquad (7.16)$$

From Equation (4.16), the number of photons of energy ε emitted by an electron with initial energy, $\mathcal{E}$, is

$$\nu(\varepsilon,\mathcal{E}) = \frac{Q_o m_e c^2}{\varepsilon K} \int_{\mathcal{E}_* = \varepsilon}^{\mathcal{E}_* = \mathcal{E}} \frac{d\mathcal{E}_*}{1 + \frac{e^2 \eta v(\mathcal{E}_*)\mathcal{E}_*}{K}} \qquad (7.17)$$

Now, for non-relativistic electrons, $v(\mathcal{E}_*) = (2\mathcal{E}_*/m_e)^{\frac{1}{2}}$. Let $a \equiv Q_o m_e c^2/\varepsilon K$; $b \equiv e^2\eta(2/m_e)^{\frac{1}{2}}/K$. Then

$$\nu(\varepsilon,\mathcal{E}) = a \int_{\mathcal{E}_* = \varepsilon}^{\mathcal{E}_* = \mathcal{E}} \frac{d\mathcal{E}_*}{1 + b\,\mathcal{E}_*^{3/2}} \qquad (7.18)$$

Now, since the injected beam spectrum is $F(\mathcal{E}) = F_b \delta(\mathcal{E} - \mathcal{E}_o)$, the non-thermal emission is simply

$$\left(\frac{dJ}{d\varepsilon}\right)_{NT} = F_b \nu(\varepsilon,\mathcal{E}_o) \qquad (7.19)$$

i.e.
$$\left(\frac{dJ}{d\varepsilon}\right)_{NT} = \frac{Q_o F_b m_e c^2}{\varepsilon K} \int_{\mathcal{E}=\varepsilon}^{\mathcal{E}=\mathcal{E}_o} \frac{d\mathcal{E}}{1 + \frac{e^2\eta(2/m_e)^{\frac{1}{2}}}{K}} \qquad (7.20)$$

Hence,

$$\frac{(dJ/d\varepsilon)_T}{(dJ/d\varepsilon)_{NT}} = \left(\frac{8}{\pi m_e T_e}\right)^{\frac{1}{2}} \frac{n_p^2 V K}{F_b I} \exp(-\frac{\varepsilon}{T_e}) \qquad (7.21)$$

where the integral, I, is

$$I = \int_{\mathcal{E}=\varepsilon}^{\mathcal{E}=\mathcal{E}_o} \frac{d\mathcal{E}}{1 + b\mathcal{E}^{3/2}} \quad ; \quad b = \frac{e^2 \eta}{K}\sqrt{\frac{2}{m_e}} \qquad (7.22)$$

and is readily evaluated using the relevant NAG subroutine.

Equations (7.11), (7.15) and (7.21) will be used to calculate the thermal/non-thermal emission yields at ε = 20 keV for the three cases: thick-target dominated, return current dominated, and combined thick-target and return current losses respectively (e.g. Figure 7.8).

7.4 Results

As Figure 7.1 shows, there are many different ways in which the flaring plasma can respond to a prescribed injected beam flux; the rise time, t_r, is a very important parameter in determining the plasma behaviour, as are the assumed saturation wave levels for the IC and IA instabilities. In this section we present a broad sample of possible cases of anomalous ohmic dissipation by a beam-driven return current.

Throughout this section we assume the following parameters for the flaring corona: $T_o = 5.10^6$ K, $n_p = 10^{11}$ cm^{-3}, $\mathcal{E}_o$ = 25 keV (as in Chapter 6). The work of Sections 2.3 and 2.4 will be referred to in the context of choosing plausible saturation amplitudes for IC/IA waves. The third variable (in addition to W_{IC}^{sat}, W_{IA}^{sat}), as already mentioned, is the electron beam rise time, t_r. Generally, we adopt an evolution

time for our simulations of $t_e = 20s$, unless $t_r \lesssim 2s$, in which case we take $t_e = 10\ t_r$; otherwise, the beam-plasma density ratio n_b/n_p exceeds 1, as we now show, and we would no longer have a dilute beam propagating in the corona:

$$\frac{n_b(t)}{n_p} = \frac{j_b(t)/ev_b}{n_p}$$

i.e. $$\frac{n_b(t)}{n_p} = \frac{5.10^{10}(t/t_r)/(e\sqrt{2\mathcal{E}_o/m_e})}{n_p}$$

i.e. $$\frac{n_b(t)}{n_p} \simeq 0.1\ \frac{t}{t_r} \qquad (7.23)$$

In Section 2.3 it was suggested that saturation of IA wave growth occurred by Tsytovich's mechanism. From Equations (2.38) and (2.39) we obtain the following simple expression for the IA saturation wave level:

$$\frac{W_{IA}^{sat}}{n_p\ T_e} \simeq 1.0\ 10^{-2}\ \frac{v_d}{v_e} \qquad (7.24)$$

IC saturation is thought to take place by ion resonance broadening (as discussed in Section 2.4) at a wave level:

$$\frac{W_{IC}^{sat}}{n_p\ T_e} \simeq 7.4\ 10^{-7}\ \frac{B_2^2}{n_{p_{\parallel}}} \cdot \frac{T_e}{T_i} \qquad (7.25)$$

Assuming a coronal magnetic field of B = 500 gauss, a typical deduced value (e.g. Brown, Melrose and Spicer (1981)), then Equation (7.25) becomes:

$$\frac{W_{IC}^{sat}}{n_p\ T_e} \simeq 1.85\ 10^{-5}\ \frac{T_e}{T_i} \qquad (7.26)$$

We assume these saturation wave levels for the first two examples of return current heating: $t_r = 4s$ (Figures 7.2 - 7.8) and $t_r = 10s$ (Figures 7.9 - 7.15). It is useful to note, from Figure 6.1, that $(T_e/T_i)_{onset} = 8$ for $t_r \simeq 5.2s$. Therefore, our prescribed current density (Equation (3.3)) leads to the IA instability being excited first for rise times $t_r \gtrsim 5.2s$; conversely, the IC threshold will be reached first for rise times $t_r \lesssim 5.2s$.

Case 1. $t_r = 4s$; W_{IC}^{IRB} ; W_{IA}^{TSYT}

(W_{IC}^{IRB} denotes IC saturation wave level via ion resonance broadening; W_{IA}^{TSYT} denotes IA saturation wave level via Tsytovich's mechanism). From Figures 7.2, 7.3 we note that the IC instability is triggered at $T_e/T_i \simeq 7$ and that the plasma remains in a state of marginal stability with T_e/T_i decreasing due to preferential heating of the ions. The total resistivity, η, together with the components due to scattering by IC waves (η_{IC}) and Spitzer resistivity (η_{cl}) are plotted in Figure 7.4. As shown in Figure 7.5, saturation of IC turbulence never occurs; the IC wave level remains at least five orders of magnitude below saturation values. The electron and ion temperature profiles are displayed in Figure 7.6: note the rapid increase in T_i at $t \simeq 1.7s$ when the IC threshold is reached ($v_d = v_{IC}$). The final normalised (w.r.t. T_o) temperatures are $T_{e_f} \simeq 870$; $T_{i_f} \simeq 170$. These temperatures are attained in the cylindrical plasma volume of thickness $S_{min} \simeq 1.2\ 10^9$ cm (Figure 7.7). Finally, we have graphed the thermal/non-thermal bremsstrahlung yields for the three cases described in the previous section. (Note that the thermal emission is the same in each case; it is the non-thermal emission from the beam electrons which is calculated differently in the three cases). In each instance

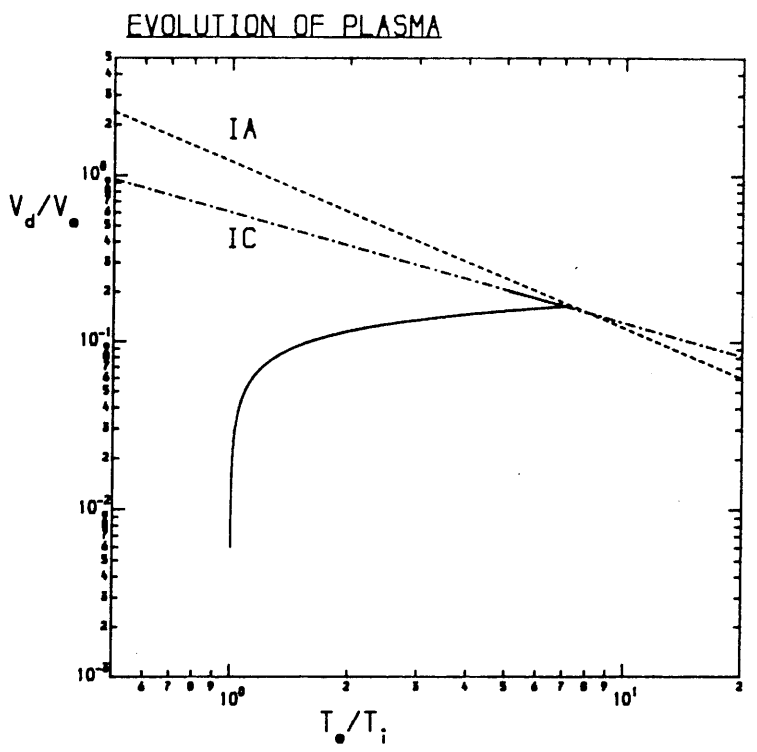

Figure 7.2: Evolution of the plasma in the (v_d/v_e, T_e/T_i) plane for case 1 (see text).

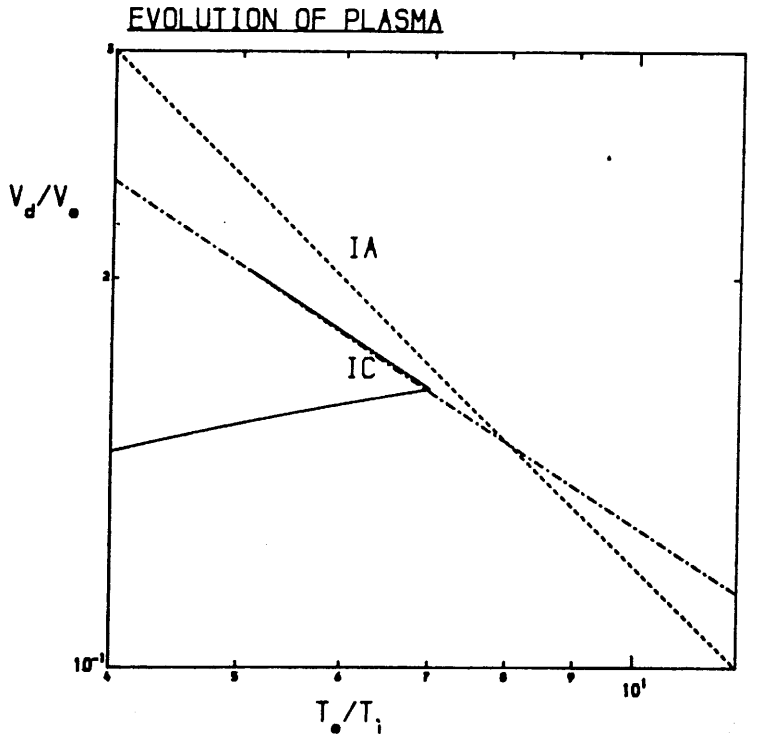

Figure 7.3: Blow-up of Figure 7.2

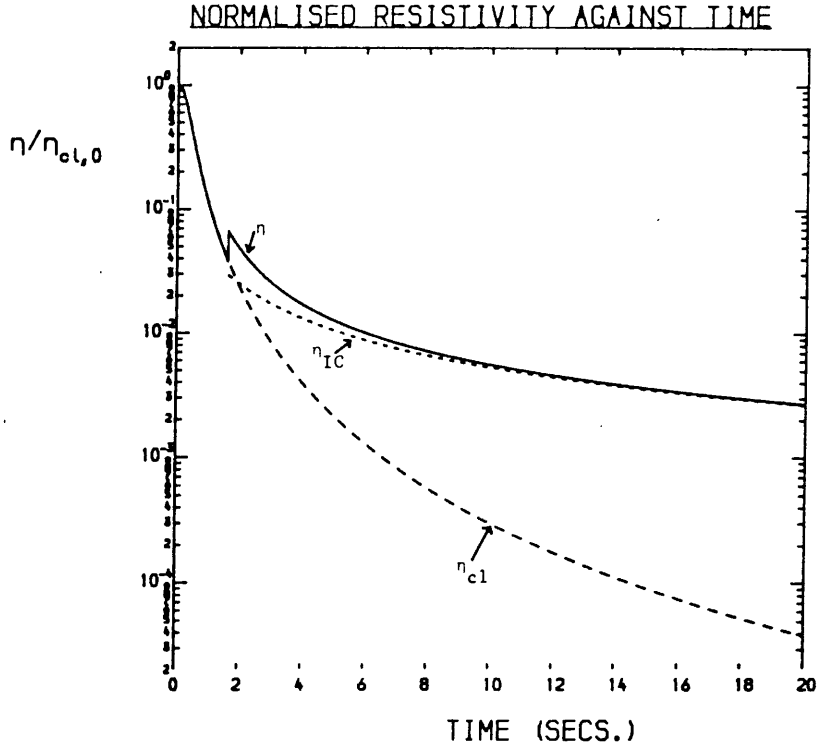

Figure 7.4: Variation of the resistivities with time (case 1).

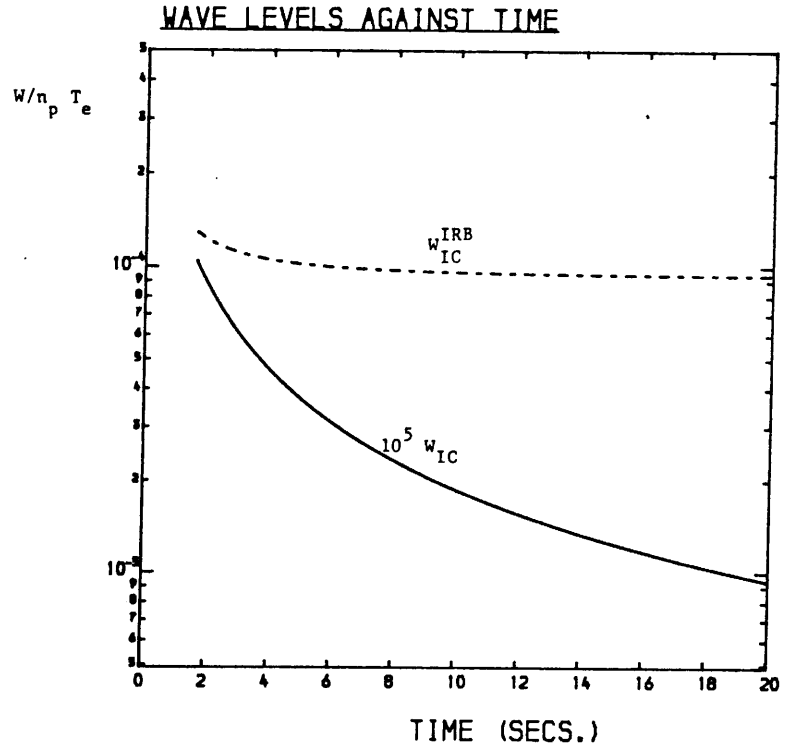

Figure 7.5: Variation of the wave level with time (case 1).

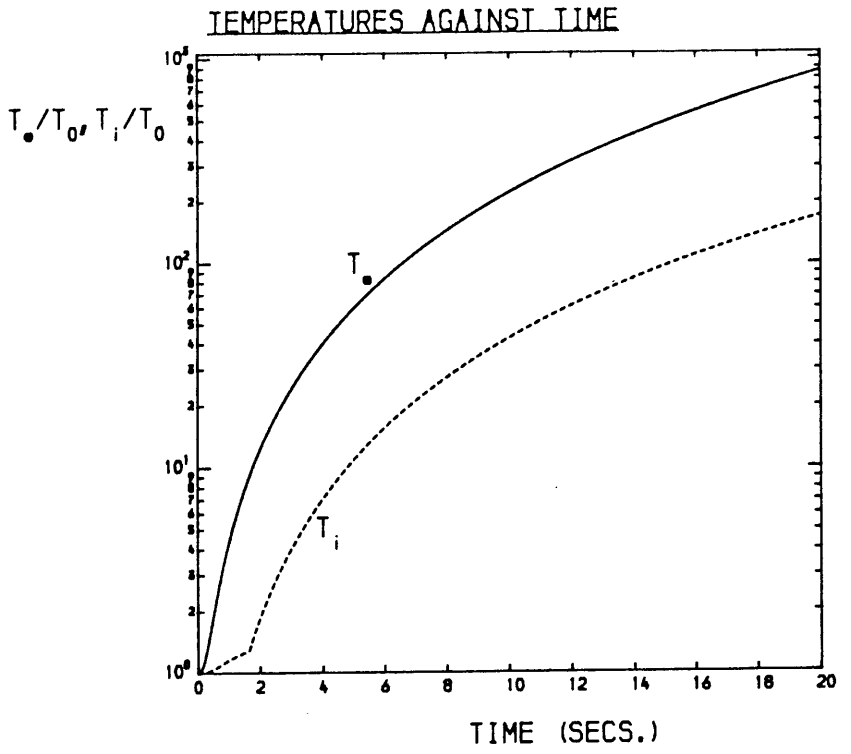

Figure 7.6: Electron and ion temperature profiles (case 1)

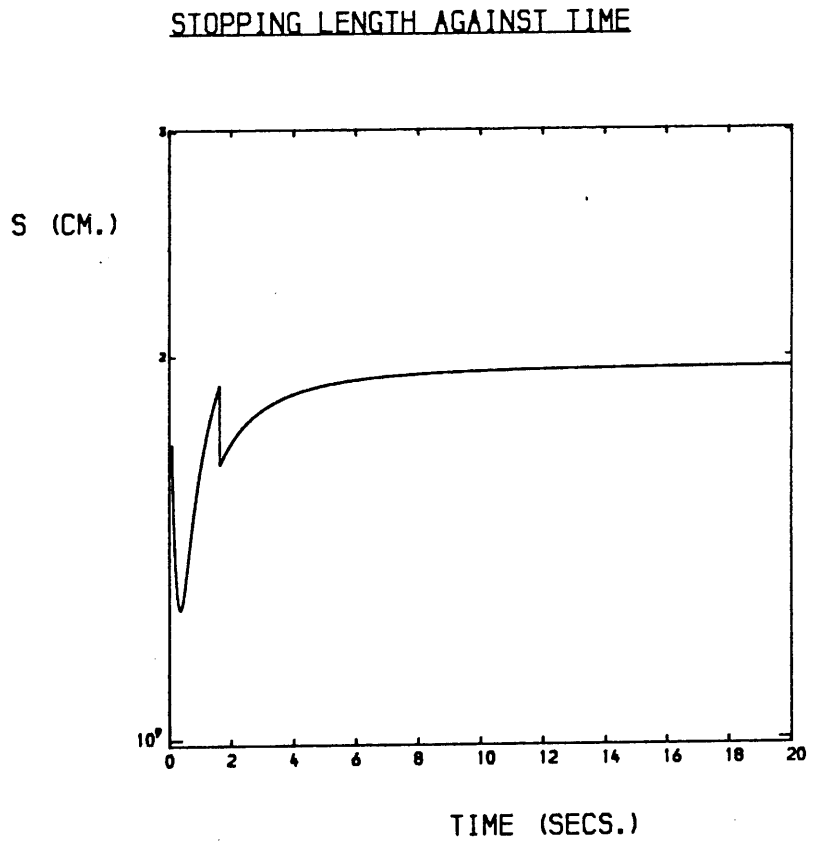

Figure 7.7: Electron beam stopping length v. time (case 1).

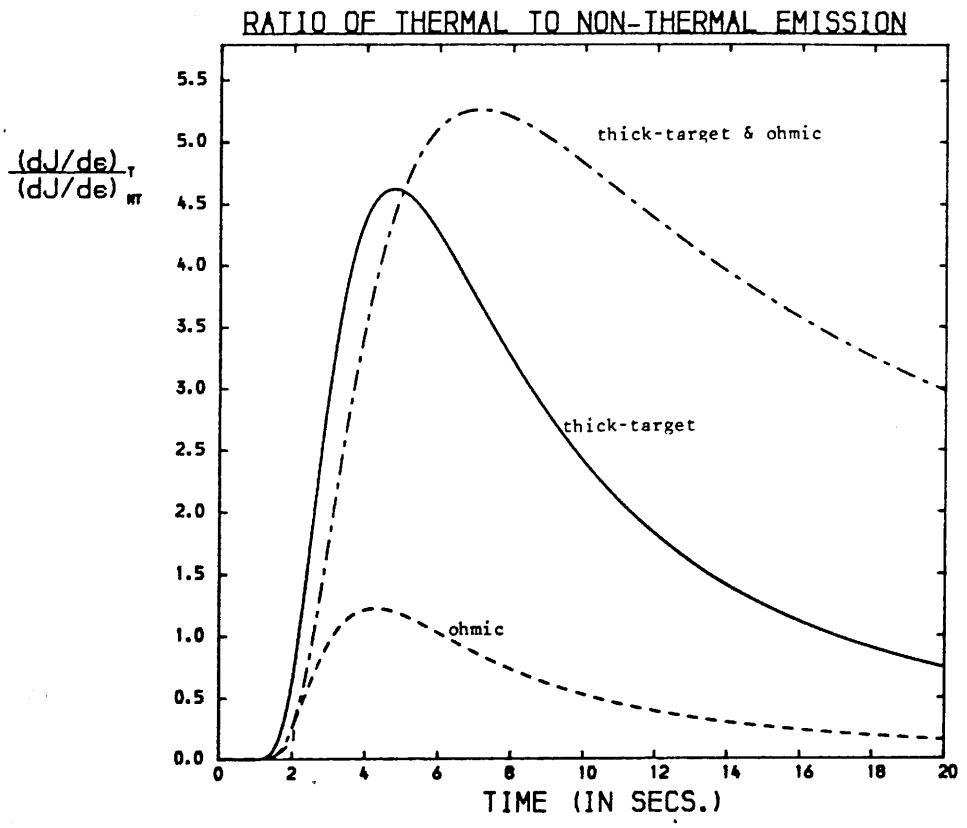

Figure 7.8: Variation of thermal/non-thermal bremsstrahlung yields at ε = 20 keV. (case 1).

the ratios rise sharply and decay slowly, peaking at values $\gtrsim 1$: the solid curve indicates that the beam generates more hard X-rays (at $\varepsilon = 20$ keV) through anomalous ohmic dissipation of its return current than by thick-target bombardment of the atmosphere. It is interesting to note that, in the case of combined thick-target and ohmic losses, the peak is greatest and occurs last. We also see that non-thermal emission due to ohmic losses dominate non-thermal emission via Coulomb losses throughout the 20s.

Case 2. $t_r = 10s$; W_{IC}^{IRB} ; W_{IA}^{TSYT}

For $t_r = 10s$, the IA threshold curve is reached first, as the injected beam flux rises. Onset occurs at $T_e/T_i \simeq 10$ and the plasma stays IA marginally stable with T_e/T_i increasing (Figures 7.9 and 7.10). The total resistivity rises by around an order of magnitude when the IA waves are generated (Figure 7.11); however, as seen in Figure 7.12, the wave level, W_{IA}, remains five or six orders of magnitude below W_{IA}^{TSYT}. The gradients in the variations of T_e, T_i rise sharply at IA onset ($t \simeq 4s$) and the final temperatures are $T_{e_f} \simeq 490$, $T_{i_f} \simeq 44$ (Figure 7.13). The heated volume is $A.s_{min} \simeq 10^{16}.1.4\ 10^{9} cm^3$, i.e. $1.4\ 10^{25} cm^3$ (emission measure $n_p^2\ V \simeq 1.4\ 10^{47}\ cm^{-3}$) - Figure 7.14. For $t_r = 10s$, the thermal/non-thermal ratio is largest for the case of thick-target losses only, attaining values $\simeq 7$ (Figure 7.15).

Cases 1 and 2 above are typical examples of return current heating which we have investigated using different rise times. It is found that neither IC saturation (IC onset: $t_r \lesssim 5.2s$) nor IA saturation (IA onset: $t_r \gtrsim 5.2s$) ever occurs. However, it is by no means certain that the above saturation mechanisms would actually

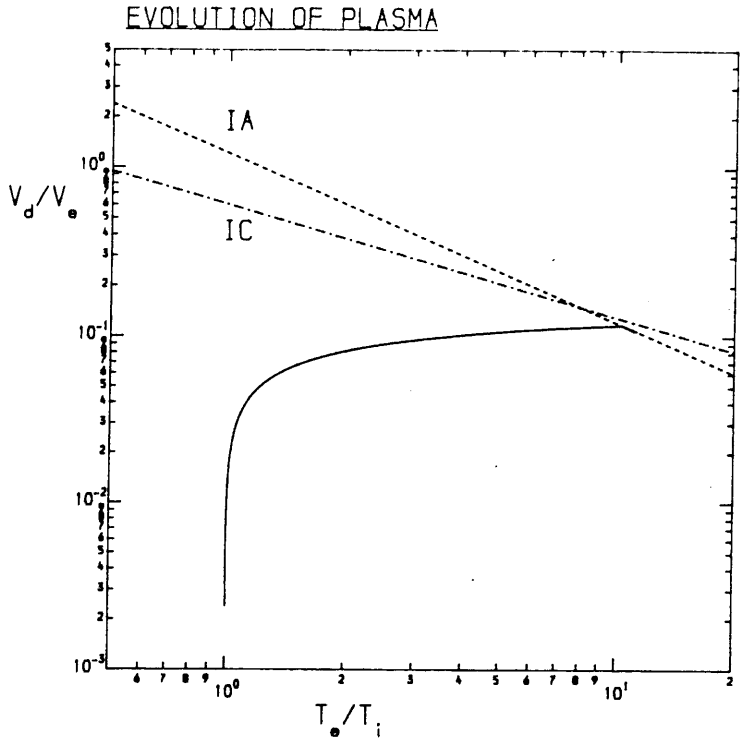

Figure 7.9: Evolution of the plasma in the (v_d/v_e, T_e/T_i) plane for case 2 (see text).

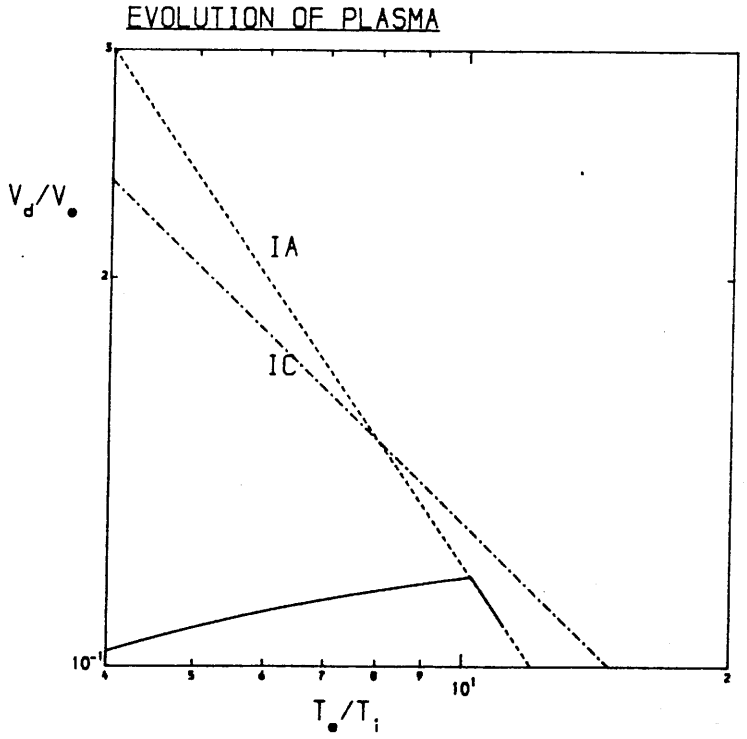

Figure 7.10: Blow-up of Figure 7.9.

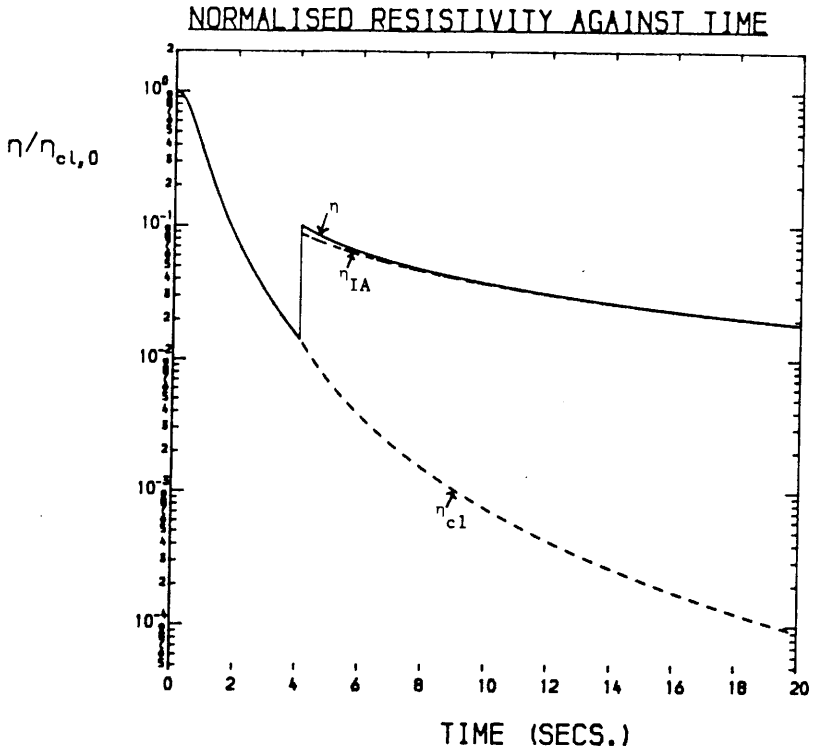

Figure 7.11: Variation of the resistivities with time (case 2).

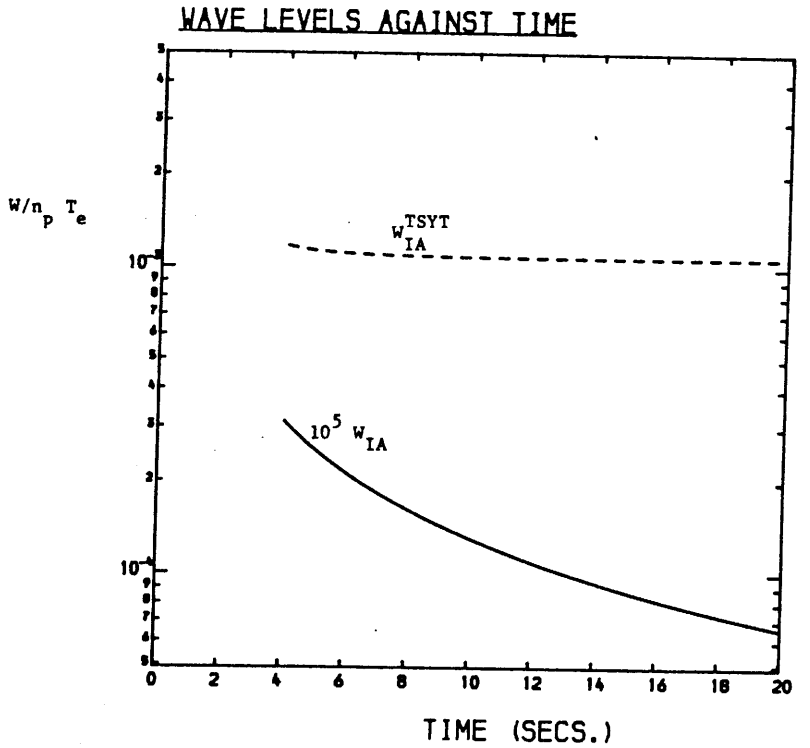

Figure 7.12: Variation of the wave level with time (case 2).

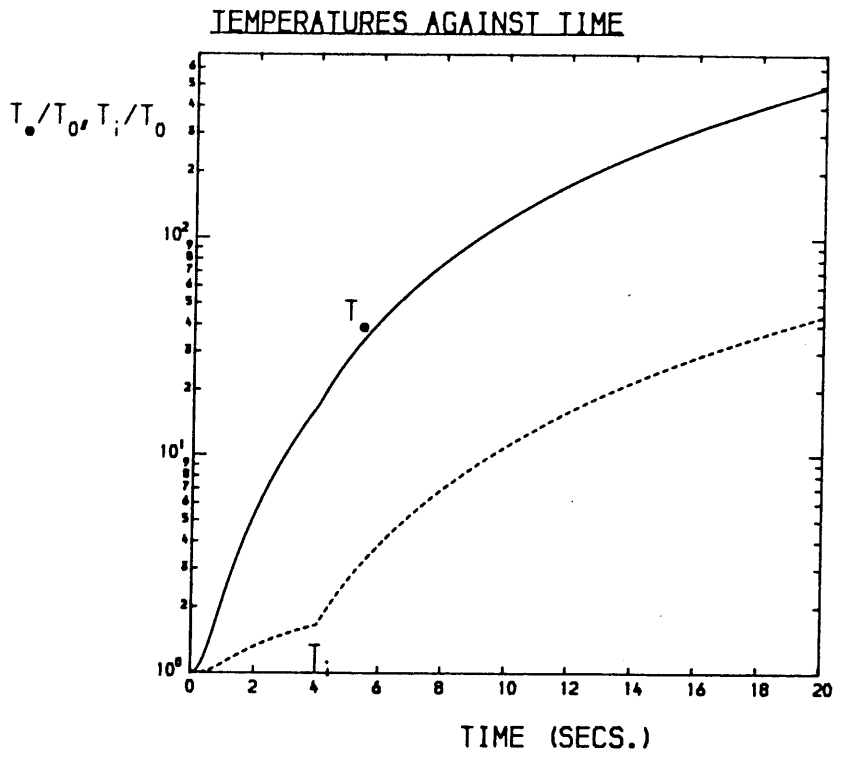

Figure 7.13: Electron and ion temperature profiles (case 2).

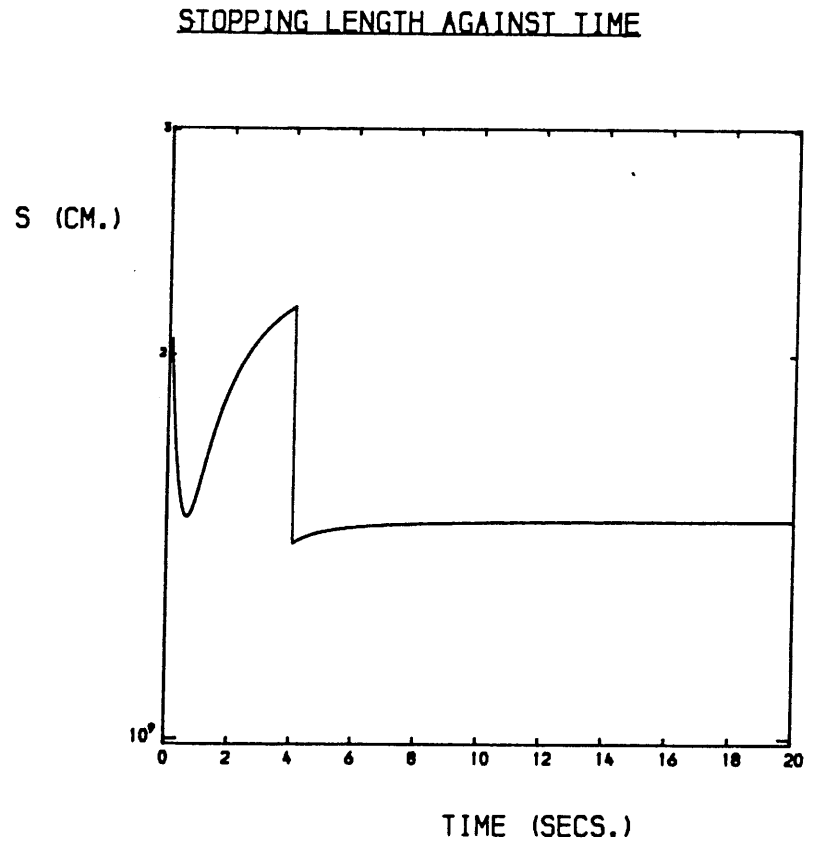

Figure 7.14: Electron beam stopping length v. time (case 2).

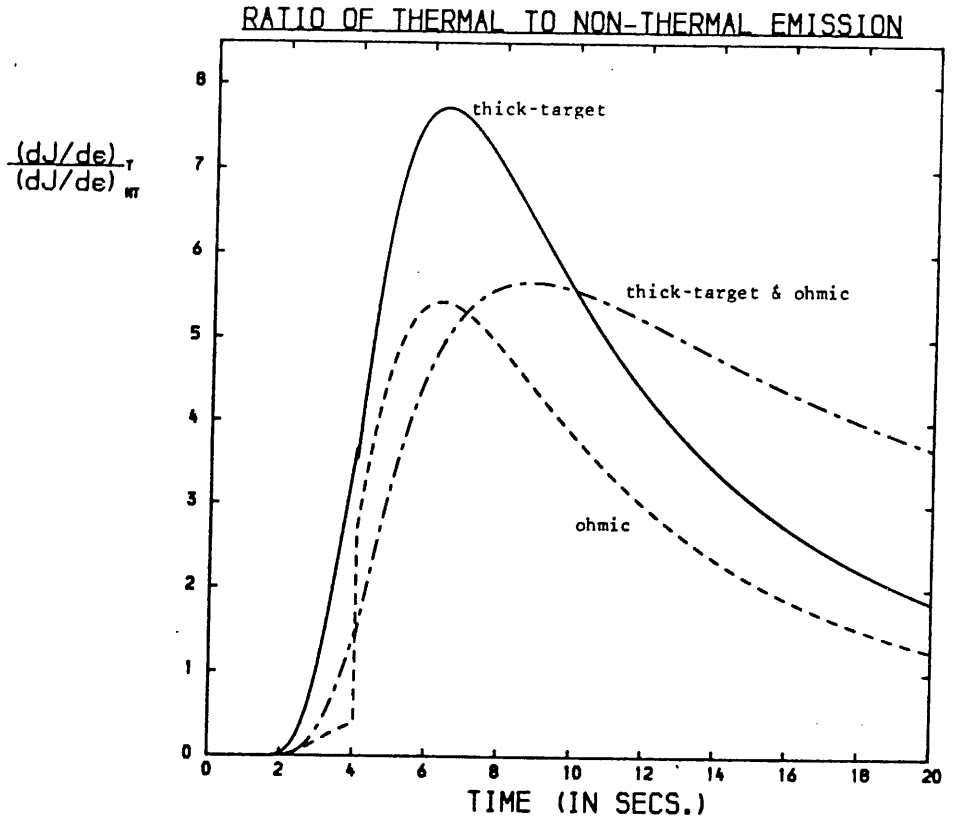

Figure 7.15: Variation of thermal/non-thermal bremsstrahlung yields at ε = 20 keV (case 2)

occur in the flaring solar atmosphere. Even though there is support in the plasma literature for the saturation wave levels adopted above (particularly in the case of the IC instability) it would be prudent to allow for the possibility of saturation taking place at much lower levels. As discussed in Chapter 2, the subject of non-linear plasma kinetic theory and, in particular, the topic of saturation mechanisms for particular microinstabilities, is very complex. Rather than becoming embroiled in such issues we prefer to follow the approach of Duijveman et al. (1981) in postulating, as parameters in our models, various saturation wave levels for the IA/IC instabilities. By doing this we are able to examine the possible effects of wave saturation on anomalous return current heating of the corona without becoming ensnared in the detailed theories of the mechanisms.

We first of all turn our attention to IC saturation. There is some evidence that IC turbulence may saturate at low levels due to quasi-linear plateau formation in the electron distribution function (Drummond and Rosenbluth (1962)). The IC resistivity at saturation is then:

$$\eta_{IC}^{sat} \simeq \eta_{cl} \left(1 + \frac{v_d}{v_e}\right) \qquad (7.27)$$

(from Equation (2.51)). Now, from Equation (6.2),

$$\frac{W_{IC}^{sat}}{n_p T_e} \simeq 3.6\ 10^{-8}\ \frac{\eta_{IC}^{sat}}{\eta_{cl,o}} \qquad (7.28)$$

Substituting η_{IC}^{sat} from Equation (7.27) we obtain

$$\frac{W_{IC}^{sat}}{n_p T_e} \simeq 3.6\ 10^{-8}\ x^{-3/2} \left(1 + \frac{v_d}{v_e}\right) \qquad (7.29)$$

(Note that this is independent of the magnetic field, B; cf. Equation (7.26)).

Case 3. $t_r = 4s$; W_{IC}^{PF}; W_{IA}^{TSYT}

(W_{IC}^{PF} denotes IC saturation wave level by plateau formation in the electron distribution function). Figures 7.16 - 7.21 comprise the results for the above parameters. Onset of IC turbulence is at $T_e/T_i \simeq 7$ (as in case 1, of course) followed by a period of marginally stable heating until IC saturation occurs at $T_e/T_i \simeq 6.5$ and $t \simeq 2.3s$ (see also Figure 7.18). This phase of saturated IC heating proceeds, with T_e/T_i first of all decreasing then increasing when classical heating dominates, until the IA threshold is reached at which $v_d = v_{IA}$ (see flow diagram of Figure 7.1). The value of T_e/T_i rises until, at $T_e/T_i \simeq 8$, v_d drops below v_{IC} and the saturated IC waves are switched off. At this point, the IA resistivity/wave level increases slightly, while still remaining marginally stable, as though over-compensating for the switching off of the IC waves. As before (case 2), the IA wave levels remain far below saturation amplitudes. The final temperatures reached (after 20s) are $T_{e_f} \simeq 1900$; $T_{i_f} \simeq 220$ (Figure 7.19) in a plasma layer of thickness $s_{min} \simeq 8.7\ 10^8$ cm. Figure 7.20 reflects the behaviour of the plasma through its different phases: classical heating, IC onset (with a reduction in s), a period of IC marginally stable heating followed by IC saturation (indicated by the "knee" in the plot), IA onset (when s is reduced by half) and then IA marginal stability, including a slight drop in s when the IC waves switch off. Note that it is this phenomenon that determines the value of s_{min}. For this case the ratio $(dJ/d\varepsilon)_T/(dJ/d\varepsilon)_{NT}$ is greatest

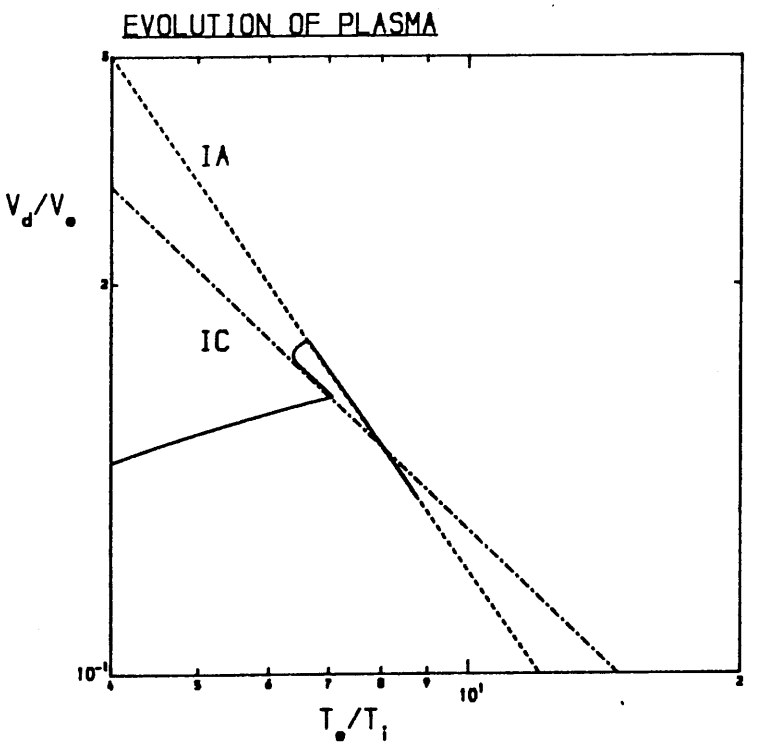

Figure 7.16: Evolution of the plasma in the (v_d/v_e, T_e/T_i) plane for case 3 (see text).

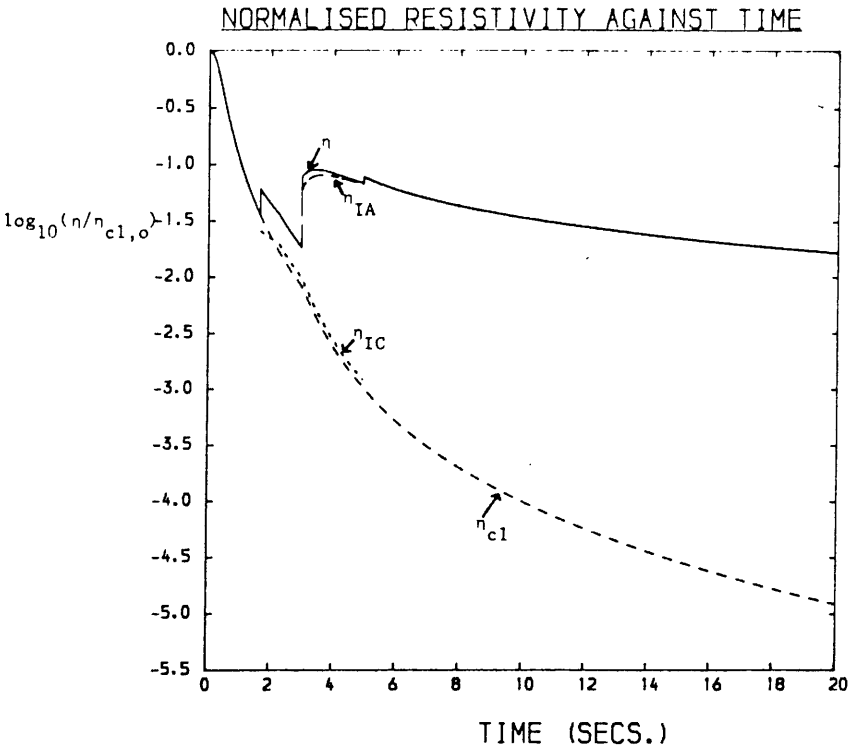

Figure 7.17: Variation of the resistivities with time (case 3).

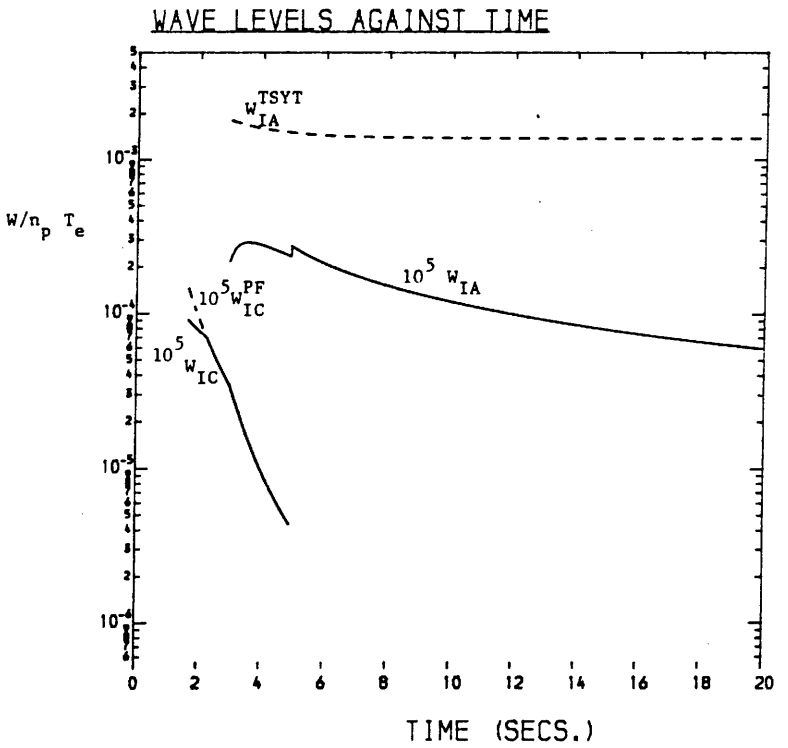

Figure 7.18: Variation of the wave levels with time (case 3).

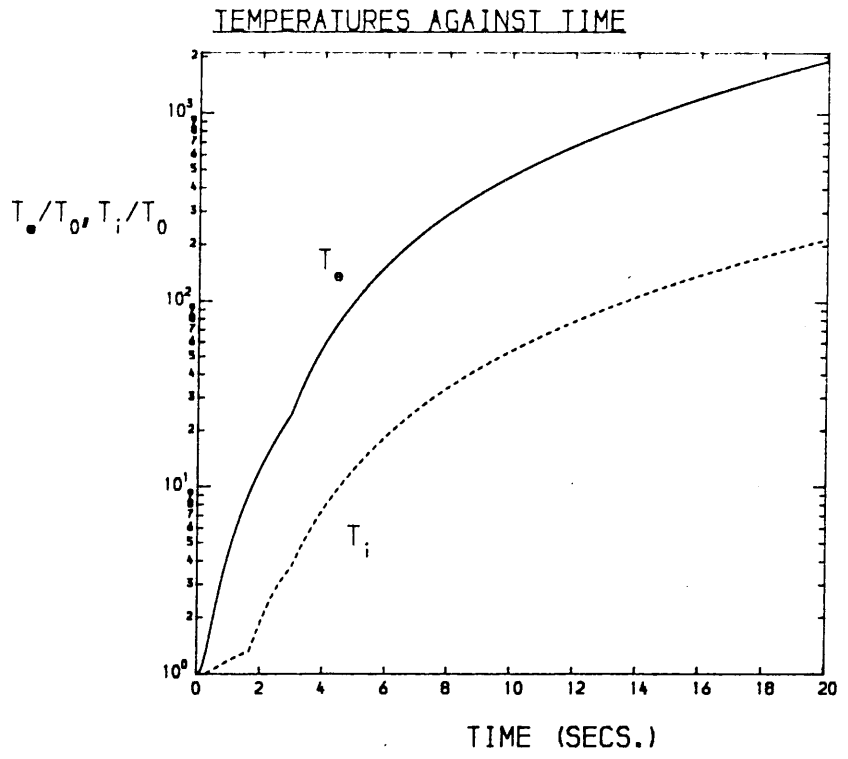

Figure 7.19: Electron and ion temperature profiles (case 3).

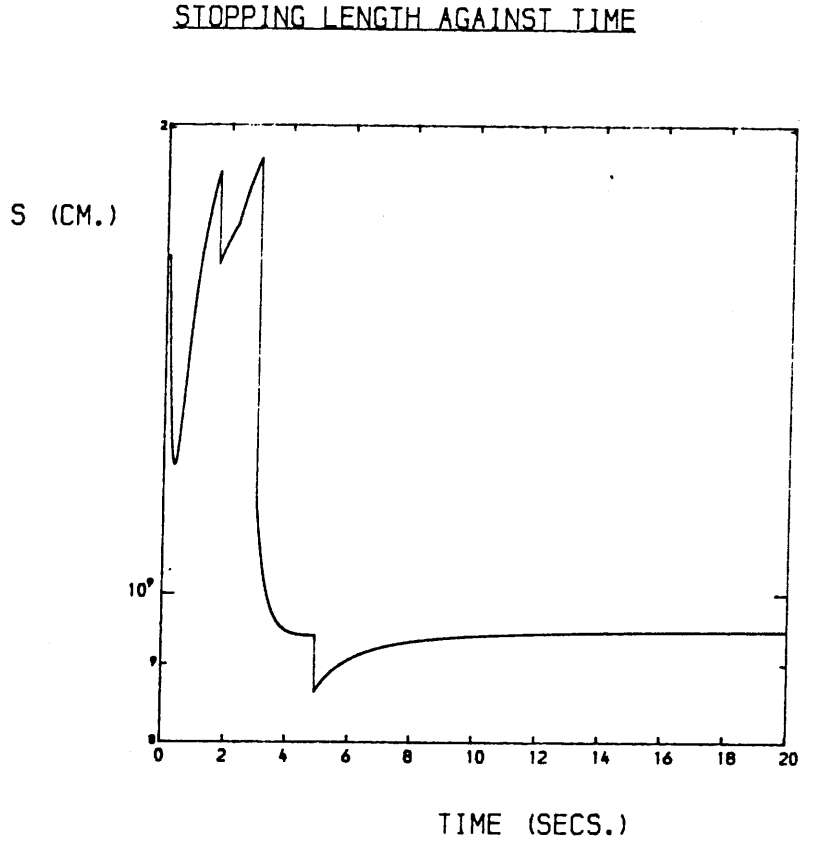

Figure 7.20: Electron beam stopping length v. time (case 3).

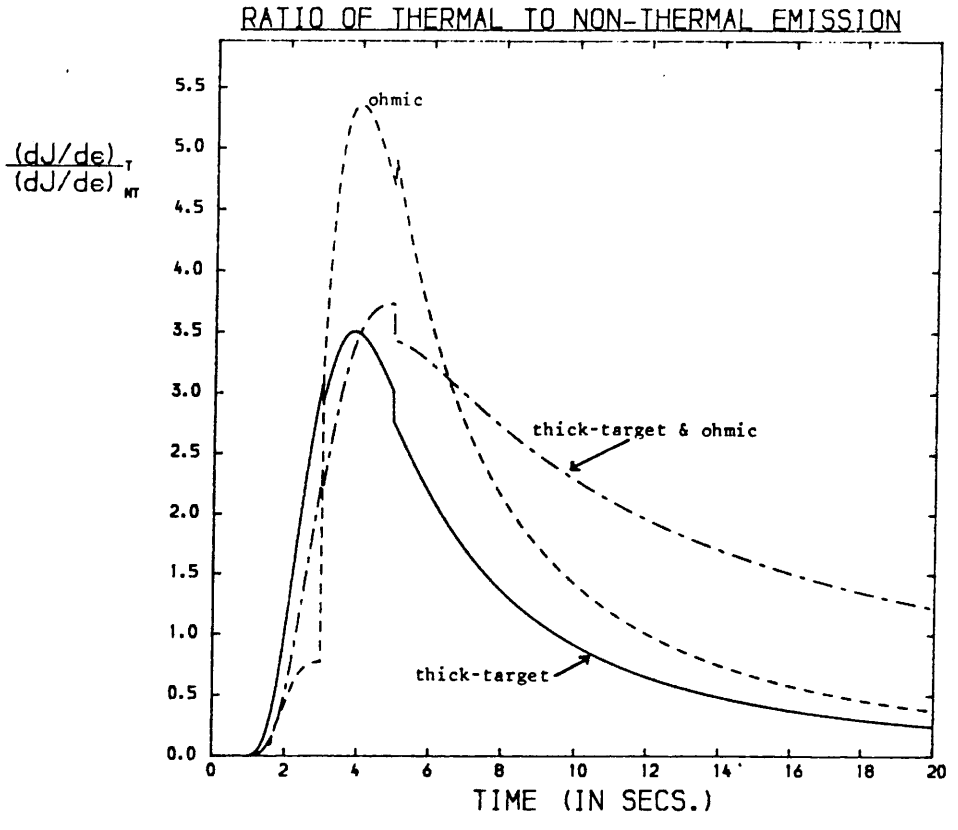

Figure 7.21: Variation of thermal/non-thermal bremsstrahlung yields at ε = 20 keV (case 3).

when ohmic losses are dominant; for thick-target interaction the thermal emission from the hot, return current heated plasma exceeds the non-thermal beam bremsstrahlung (peak ratio $\sim$ 3).

In cases 2 and 3 above we found that the values of W_{IA} were around factors of 10^5 to 10^6 smaller than W_{IA}^{sat}. To examine the effect of IA saturation on the plasma behaviour we adopt a saturation level $W_{IA}^{sat} \equiv 10^{-6}\ W_{IA}^{TSYT}$, i.e.

$$\frac{W_{IA}^{sat}}{n_p T_e} \simeq 1.0 \quad 10^{-8} \quad \frac{v_d}{v_e} \qquad (7.30)$$

(from Equation (7.24)). We take the same rise time as above.

Case 4. $t_r = 4_s$; W_{IC}^{PF}; $10^{-6}\ W_{IA}^{TSYT}$

Figure 7.22 displays the evolution of the plasma in the region of interest in the v_d/v_e: T_e/T_i plane. As before, classical heating takes place followed by IC onset, IC saturation and then IA onset at $T_e/T_i \simeq 6.6$. It is found that IA saturation takes effect immediately and v_d rises above v_{IA}. A maximum value of $T_e/T_i \sim 10$ is attained during IA saturation but then the ratio decreases and v_d drops below v_{IC} at $t \simeq 10.9s$ (see Figures 7.23, 7.24). A little later, at $t \simeq 11.7s$, v_d drops down to v_{IA} and the plasma resides in a state of IA marginal stability. The IA waves "de-saturate" and drop to marginally stable values (Figure 7.24). During IA marginal stability the value of T_e/T_i increases only very slightly, from 8.72 to 8.74. The temperatures reached at t = 20s are the same values as in case 3: $T_{e_f} \simeq 1900$; $T_{i_f} \simeq 220$ (Figure 7.25). However, the volume heated is slightly smaller: $s_{min} \simeq 7.8\ \ 10^8$ cm (Figure 7.26). The plots of $(dJ/d\varepsilon)_T/(dJ/d\varepsilon)_{NT}$ are also different (Figure 7.27); combined ohmic and thick-

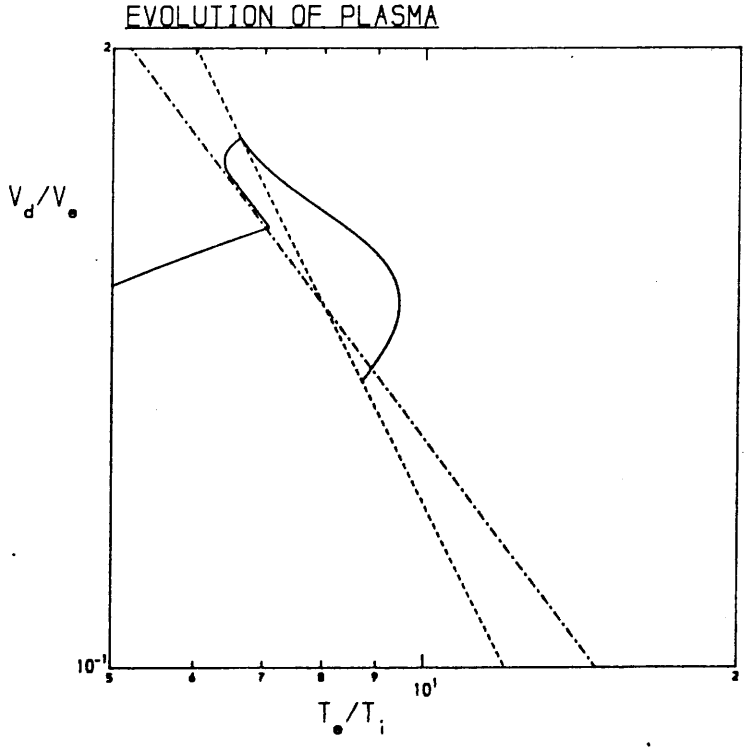

Figure 7.22: Evolution of the plasma in the (v_d/v_e, T_e/T_i) plane for case 4 (see text).

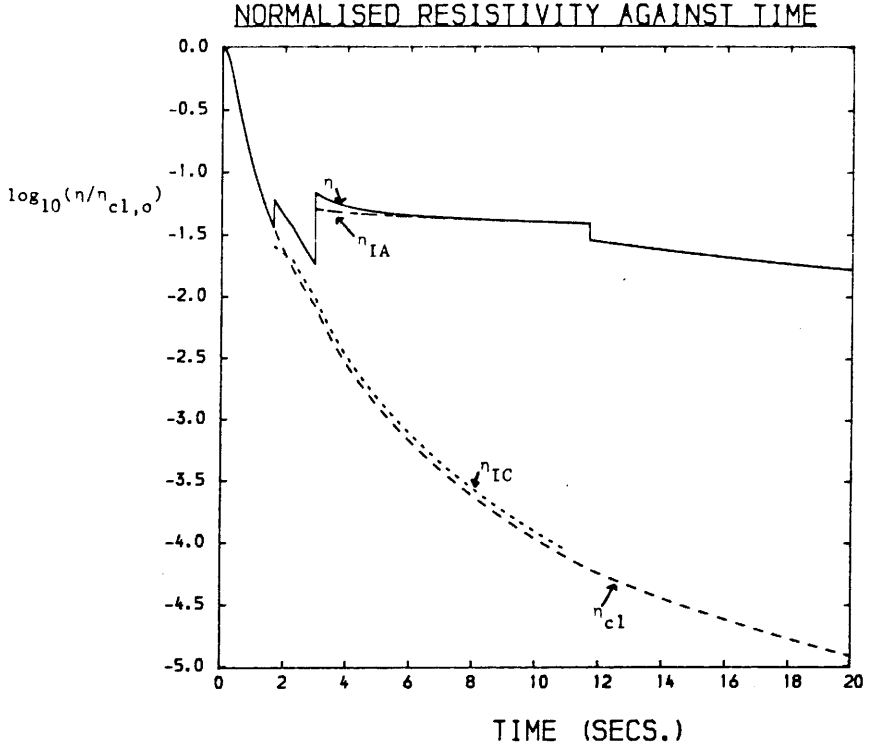

Figure 7.23: Variation of the resistivities with time (case 4).

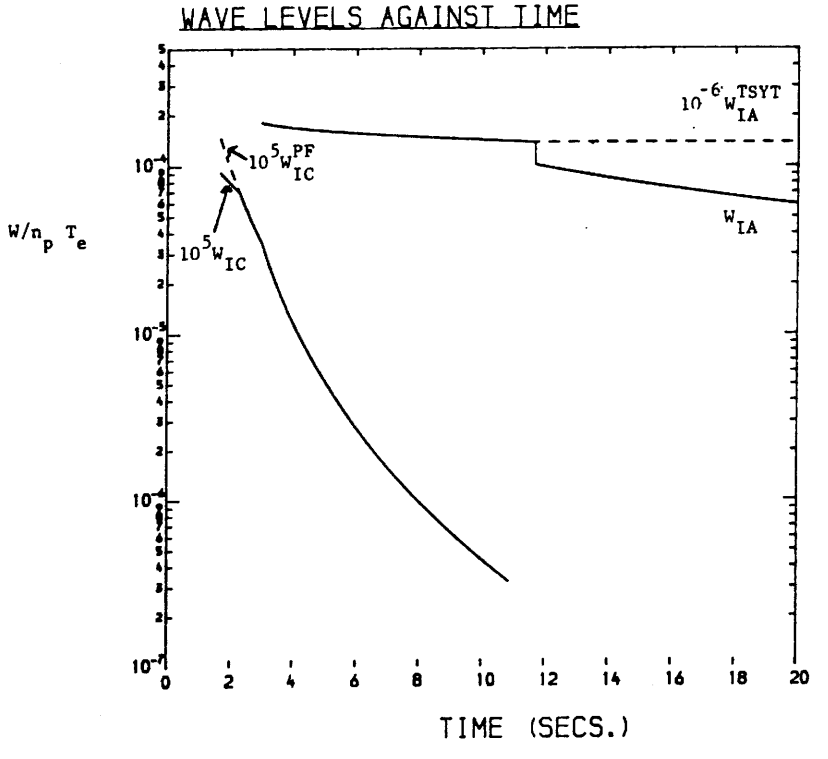

Figure 7.24: Variation of the wave levels with time (case 4).

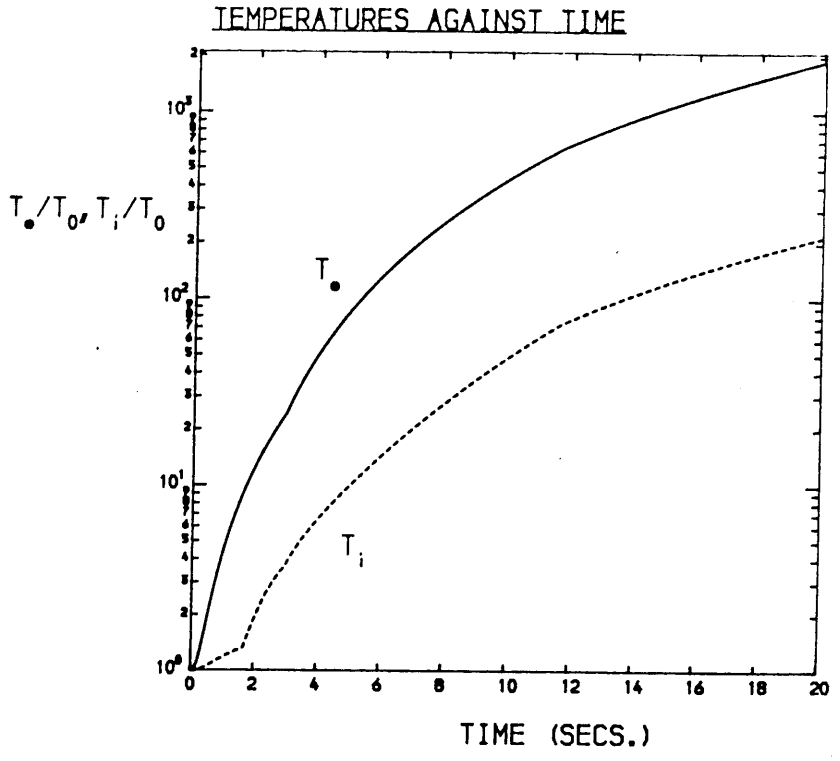

Figure 7.25: Electron and ion temperature profiles (case 4).

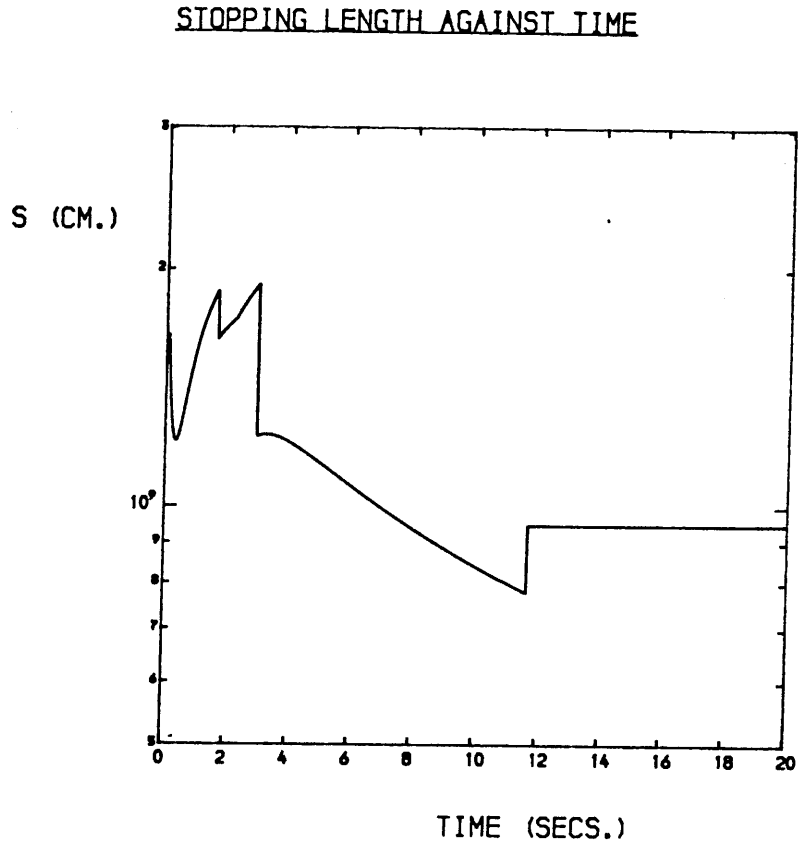

Figure 7.26: Electron beam stopping length v. time (case 4).

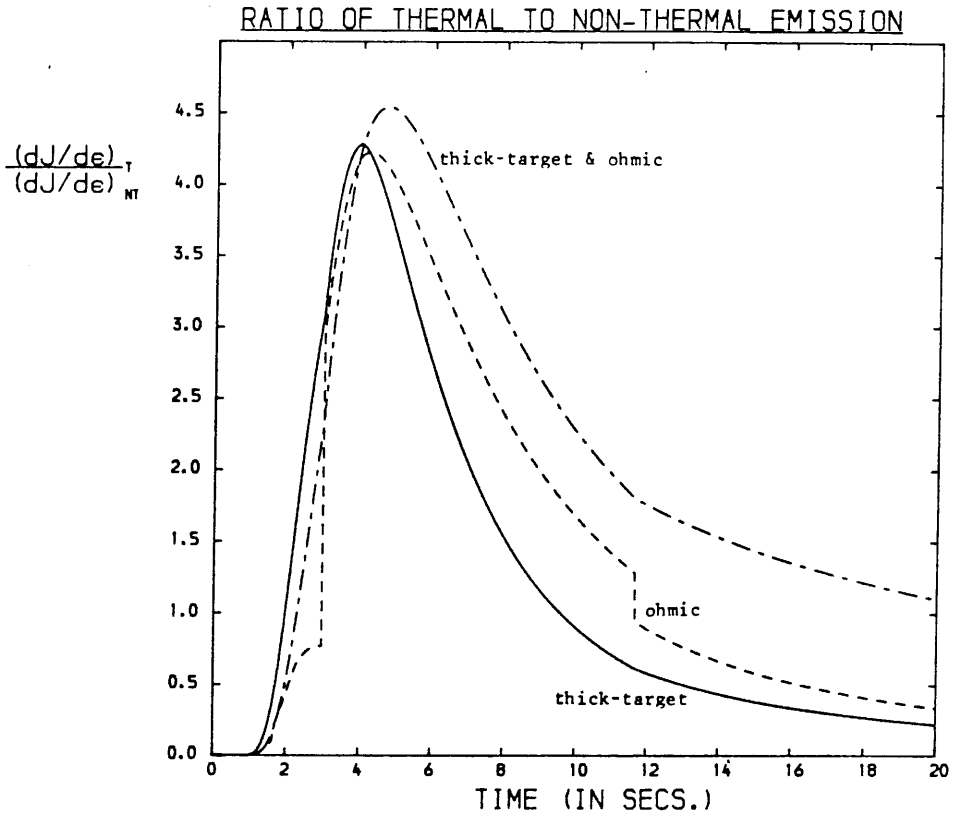

Figure 7.27: Variation of thermal/non-thermal bremsstrahlung yields at ε = 20 keV (case 4).

target losses produce the largest peak and, in the thick-target model, even more thermal emission is generated than in case 3.

Case 5. $t_r = 10s$; W_{IC}^{PF} ; $10^{-6}\, W_{IA}^{TSYT}$

Here we investigate a case in which the IA instability is triggered, followed by wave saturation and then onset of IC turbulence. From simulations of such return current heating we have found that it is not possible for the plasma to remain in an IC marginally stable state if a turbulent IA wave level exists. Since $W_{IA} >> W_{IC}$, scattering off IA waves dominates the process of ohmic dissipation. As IA waves, in general, preferentially heat electrons over ions (see Section 2.3) we would find that T_e/T_i rises along the threshold curve $v_d = v_{IC}$ (Figure 7.28). However, this is inconsistent with the form of $\chi_{IC}(T_e/T_i)$ and the physical requirement that $\eta_{IC} > 0$: negative values of resistivity arise on application of the marginal stability hypothesis. Since $\chi_{IC} < 0.5$ (Section 2.4), IC marginal stability will only occur in a realistic system ($\eta_{IC} > 0$) if T_e/T_i decreases.

To circumvent the failure of marginal stability would require developing an IC wave growth technique along the lines of the method for IA waves presented in the previous chapter. Instead, we make the physically plausible assumption that IC saturation occurs very rapidly and track the plasma evolution given that both the IA and IC waves are saturated (the interested reader might like to work out the route using Figure 7.1). Figure 7.29 shows the path in the v_d/v_e: T_e/T_i plane and Figure 7.30 shows the changing resistivity with time. Note that v_d remains very close to v_{IC} for a period of time (from $t \simeq 5s$ to $t \simeq 8.5s$). During this phase v_d rapidly oscillates about v_{IC}, with a period of a few hundredths of a second, with the IC wave level

alternately switching on and off. This cyclic behaviour is most easily seen in the form of Figure 7.31 which shows the variation in the total resistivity as the IC contribution, η_{IC}, switches on and off. As T_e/T_i rises, the excursions in v_d about v_{IC} occur less frequently and with smaller jumps in η_{IC} (Figure 7.31) until v_d drops below v_{IC} and the IC resistivity remains zero. During the subsequent phase of IA heating, T_e/T_i actually drops. We believe that this is directly related to the existence of an equilibrium value of T_e/T_i for IA dissipation: IA turbulence does not necessarily cause T_e/T_i to increase (see Section 2.3 for more detailed discussion of this point). A state of IA marginal stability ensues at $t \simeq 14$s when $v_d = v_{IA}$; the value of T_e/T_i remains very nearly constant at 11.1.

The final electron and ion temperatures are, at $t = 20$s, $T_{e_f} \simeq 490$, $T_{i_f} \simeq 44$ (Figure 7.33) and $s_{min} \simeq 1.3\ 10^9$ cm (Figure 7.34). With the varying resistivity, as the saturated IC waves switch on and off, the electric field, $E = \eta j$, decelerating the beam electrons oscillates in magnitude. As a result, the stopping length of the beam-return current system during this time varies rapidly (Figure 7.34). This is also manifest in the X-ray signature for ohmic loss-dominated flaring electron beams (Figure 7.35). If real, these oscillations would, of course, be observationally interesting.

We might add that, for different rise times $t_r \gtrsim 5.2$ s, it is not always the case that v_d remains close to v_{IC}. For $t_r = 6$s, for example (not shown here), some oscillations do occur but v_d quickly rises above v_{IC} for a short time before dropping back down to v_{IC} at which point the IC waves switch off; v_d continues to fall until at $v_d = v_{IA}$ a state of IA marginal stability ensues.

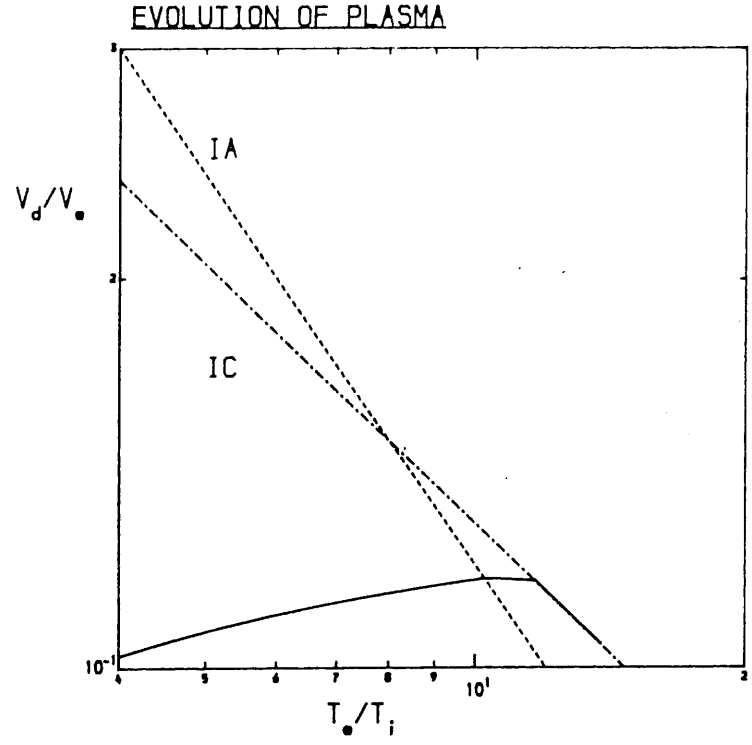

Figure 7.28: Evolution of the plasma in the $(v_d/v_e, T_e/T_i)$ plane when marginal stability is (wrongly) assumed for case 5 (see text).

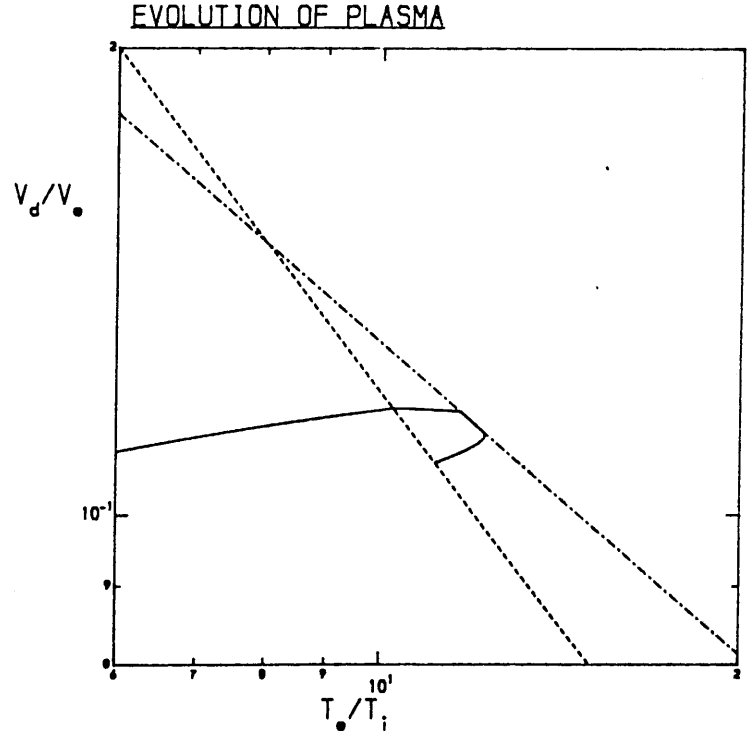

Figure 7.29: Actual evolution of the plasma in the $(v_d/v_e, T_e/T_i)$ plane for case 5.

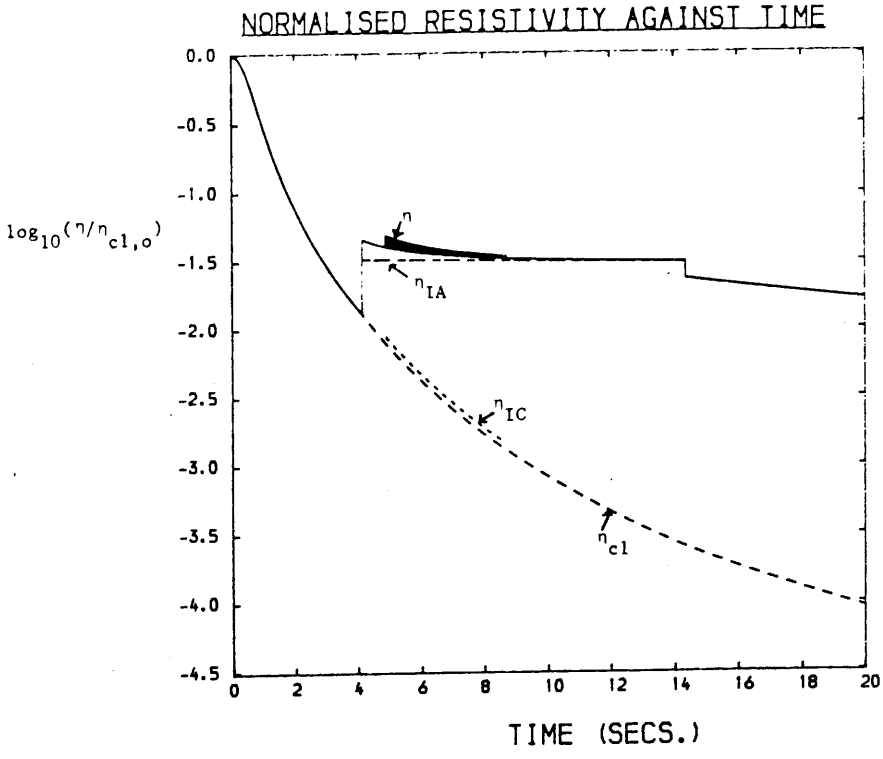

Figure 7.30: Variation of the resistivities with time (case 5).

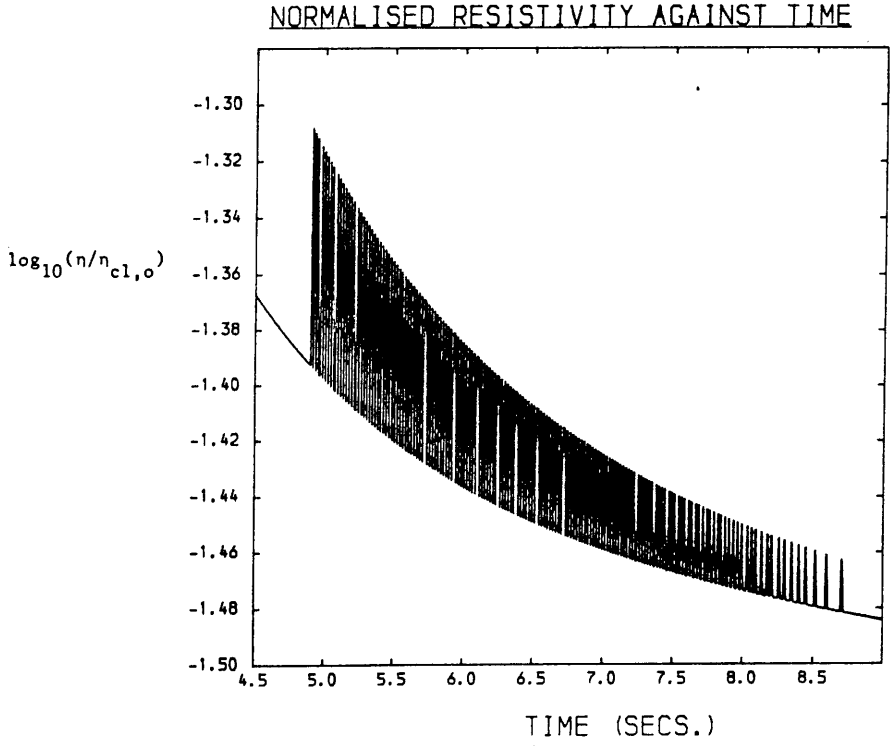

Figure 7.31: Variation of the total normalised resistivity with time showing the rapid oscillations as IC turbulence switches on and off with a period $\sim 10^{-2}$ s.

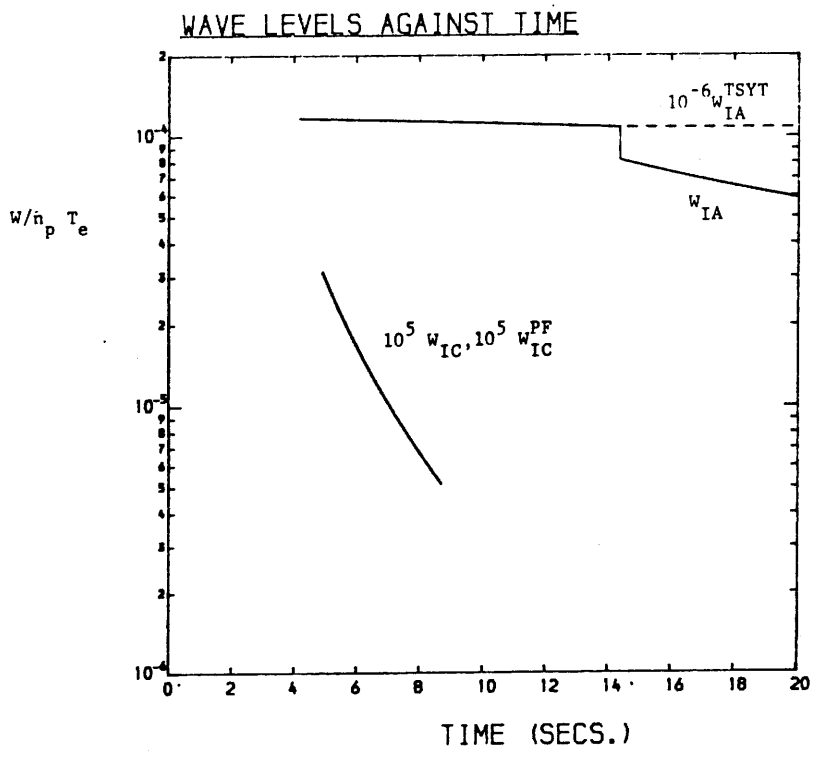

Figure 7.32: Variation of the wave levels with time (case 5).

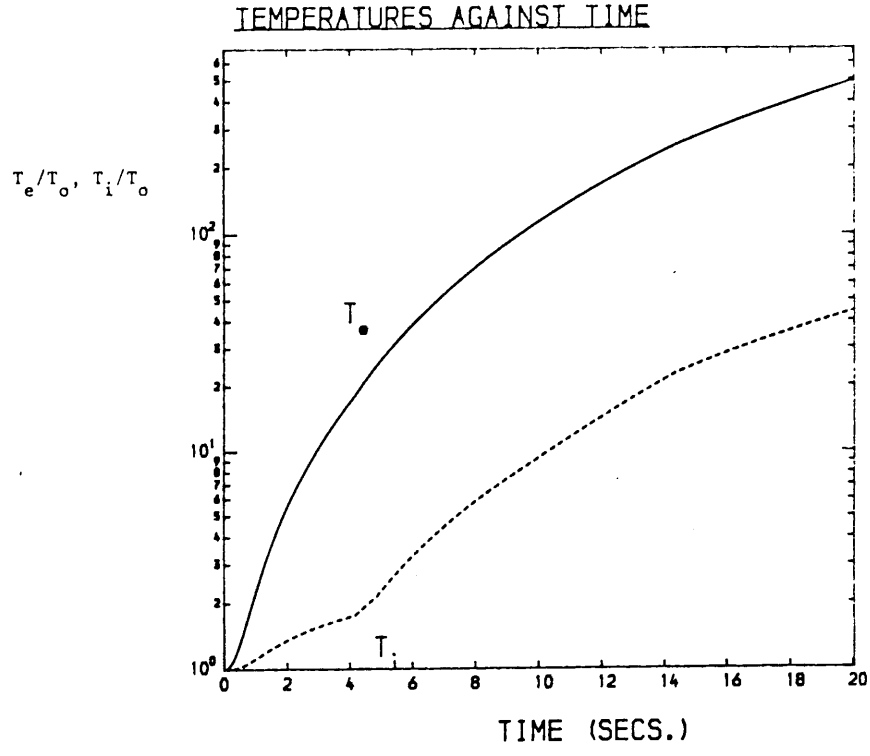

Figure 7.33: Electron and ion temperature profiles (case 5).

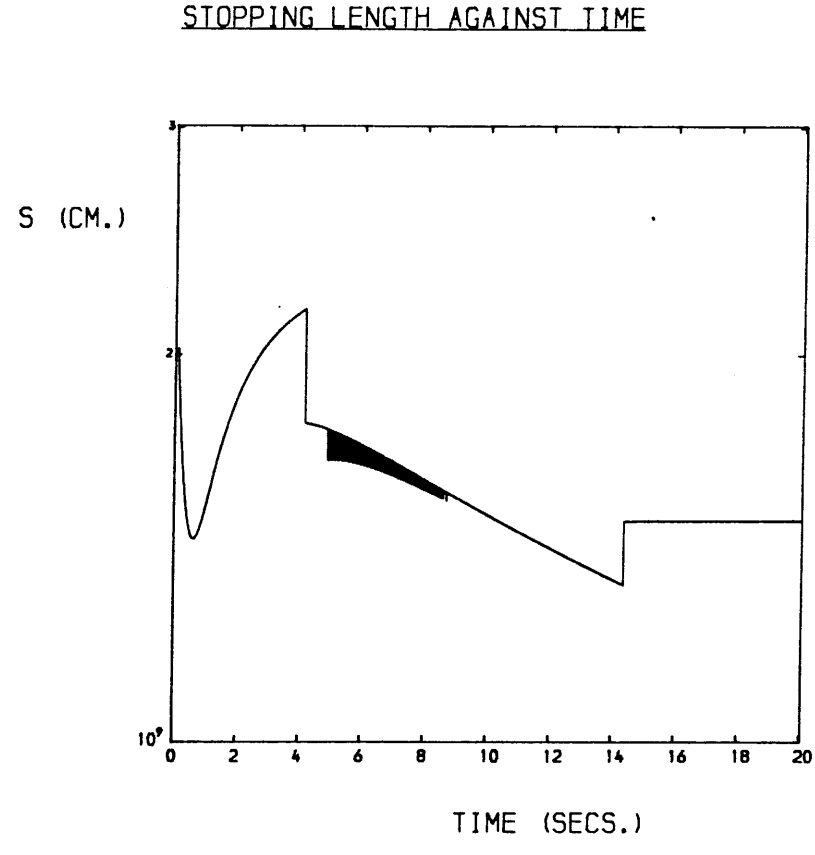

Figure 7.34: Electron beam stopping length v. time (case 5).

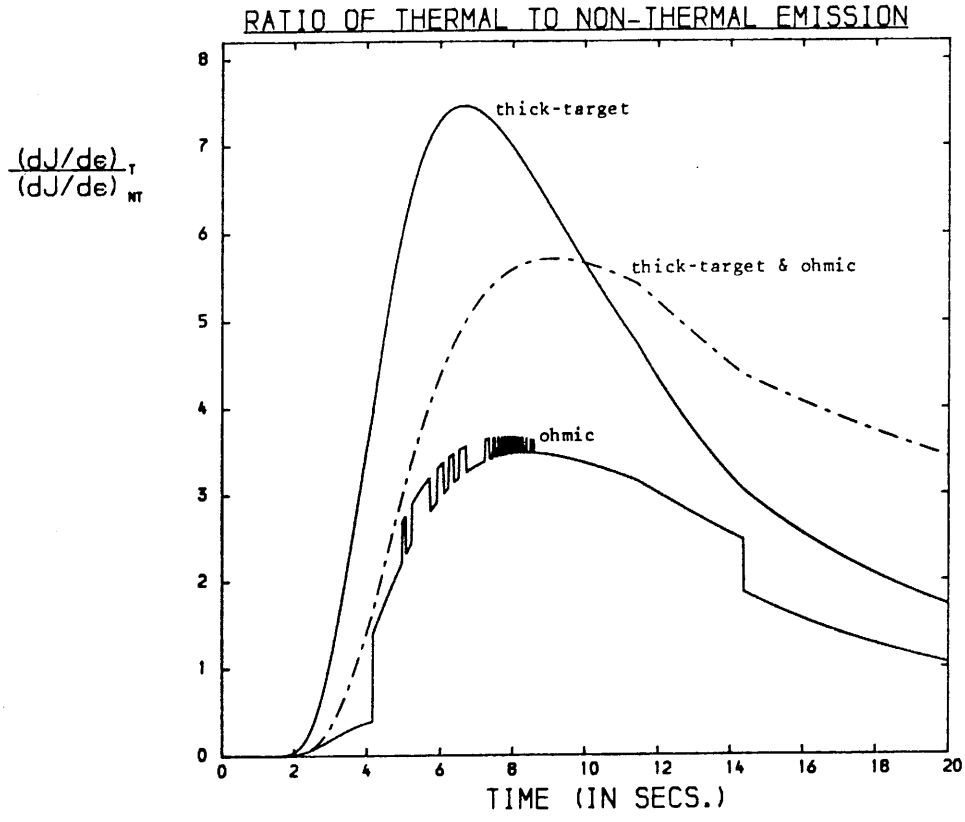

Figure 7.35: Variation of thermal/non-thermal bremsstrahlung yields at ε = 20 keV (case 5). Note the oscillations in the case where the beam electron energy losses are dominated by ohmic dissipation of the return current.

For $t_r = 4s$; $W_{IC}^{sat} \equiv W_{IC}^{PF}$; $W_{IA}^{sat} \equiv 10^{-6} W_{IA}^{TSYT}$ (i.e. case 4) we found that during the phase of combined IA and IC saturation T_e/T_i increases beyond 8 before v_d drops to one of the threshold curves (Figure 7.22). The drift velocity v_d falls back to, firstly, v_{IC} then v_{IA}. This behaviour occurs for $t_r \gtrsim 2.1s$, according to the many simulations we have run. For smaller rise times, $t_r \lesssim 2.1s$, we have found that after a period of IA and IC saturation, v_d falls back to v_{IA} and a state of marginal stability is achieved. We always find that, at the first onset of IA instability, saturation occurs immediately. In fact, for $t_r \lesssim 1.9s$, IA onset occurs at $T_e/T_i \lesssim 4.8$ at which point a marginal stability treatment would, in fact, fail (see Figure 7.1 and earlier discussion of Section 7.2). Case 6 is an example of return current heating for small rise times $t_r \lesssim 2.1s$.

Case 6. $t_r = 1.5s$; W_{IC}^{PF} ; $10^{-6} W_{IA}^{TSYT}$

Here, we restrict the evolution time, t_e, to 15s (see Equation (7.23)). Figure 7.36 shows that during the period of IA and IC saturation heating, in which the IA turbulence dominates, the value of T_e/T_i increases at first, then decreases. This decrease in T_e/T_i continues during the phase of IA marginal stability. Figures 7.36 - 7.41 comprise the complete set of results for case 6; the final temperatures are $T_{e_f} \simeq 5800$, $T_{i_f} \simeq 760$ (Figure 7.39) and these occur in the plasma cylinder of thickness $s_{min} \simeq 3.4\ 10^8$ cm (Figure 7.40). The largest peak in $(dJ/d\varepsilon)_T/(dJ/d\varepsilon)_{NT}$ is attained in the case of ohmic dominated beam losses; however, in the thick-target case the thermal emission still exceeds the non-thermal emission for the time interval

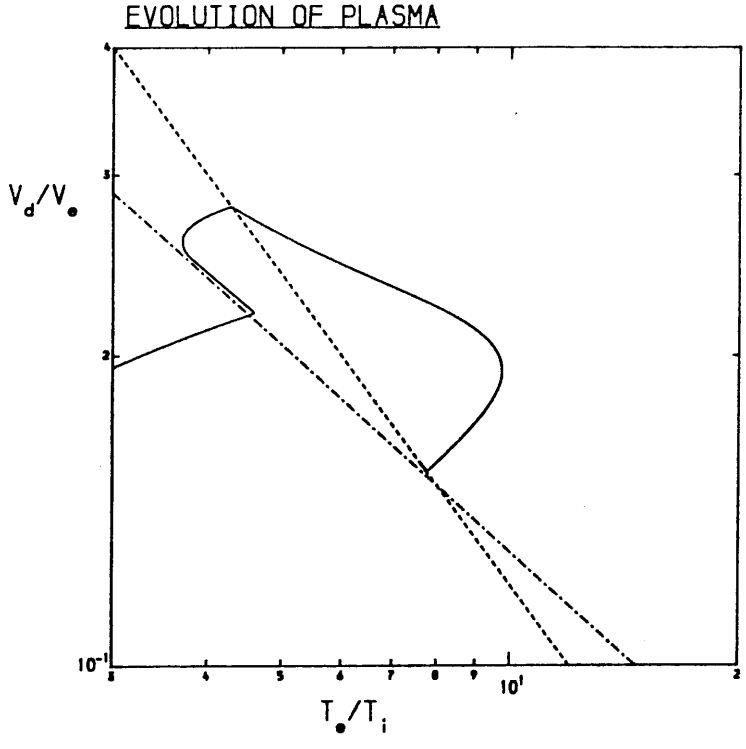

Figure 7.36: Evolution of the plasma in the $(v_d/v_e, T_e/T_i)$ plane for case 6 (see text).

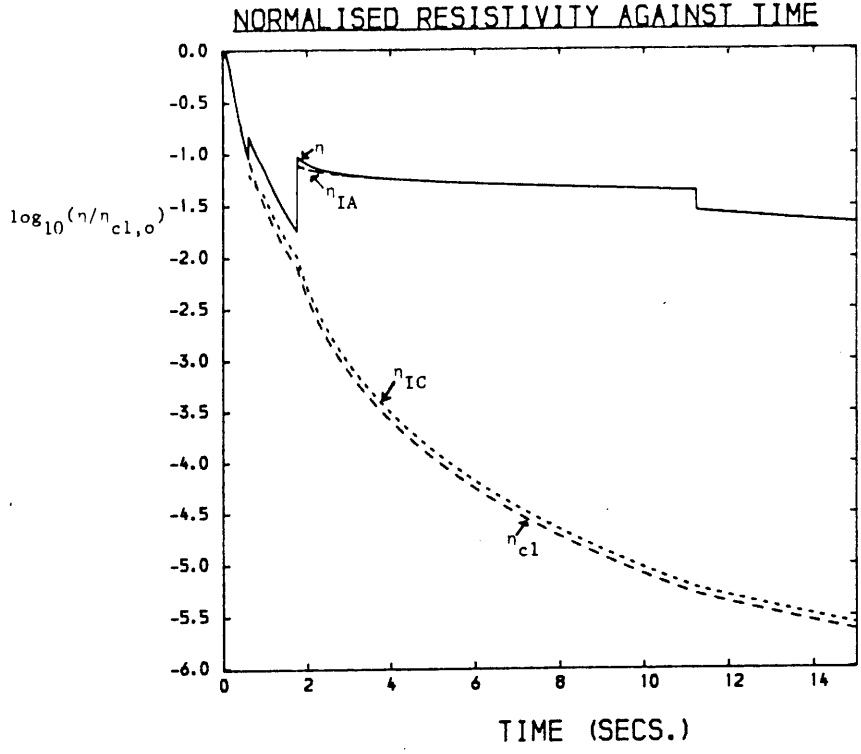

Figure 7.37: Variation of the resistivities with time (case 6).

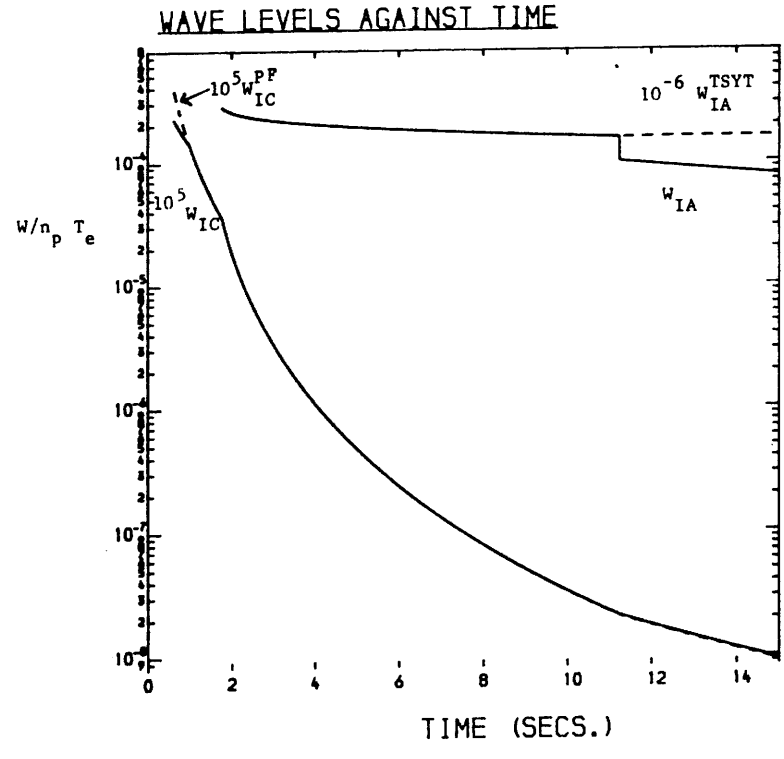

Figure 7.38: Variation of the wave levels with time (case 6).

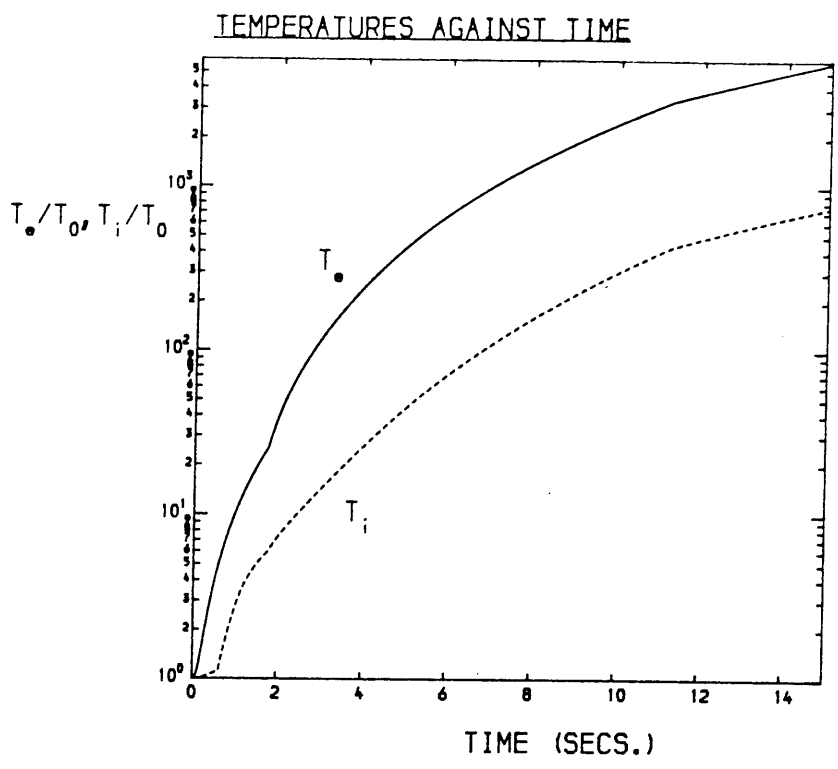

Figure 7.39: Electron and ion temperature profiles (case 6).

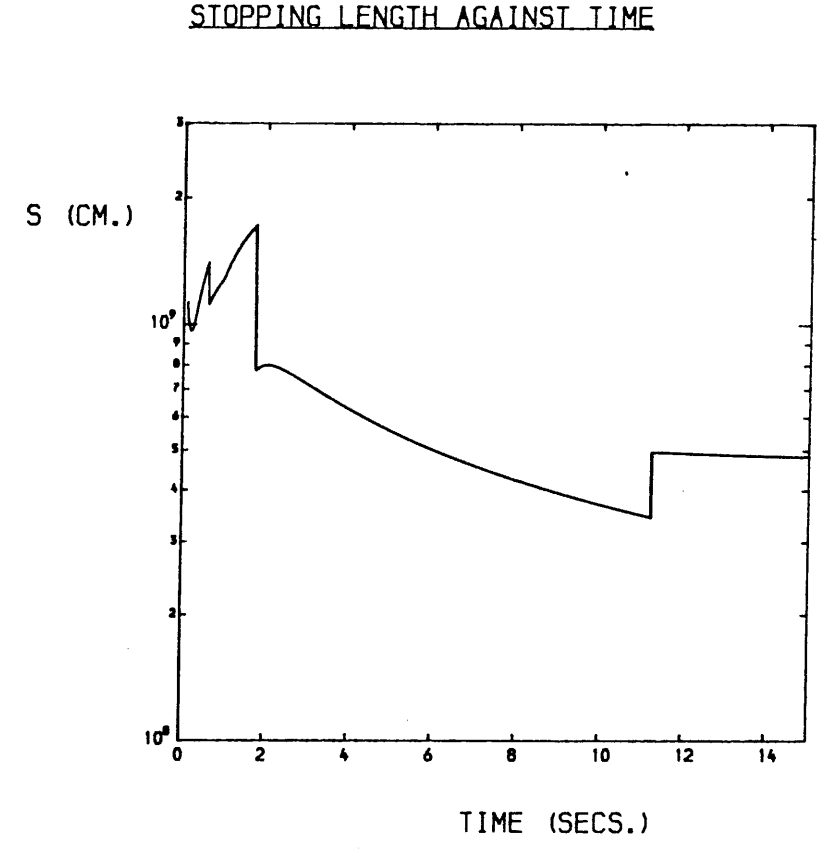

Figure 7.40: Electron beam stopping length v. time (case 6).

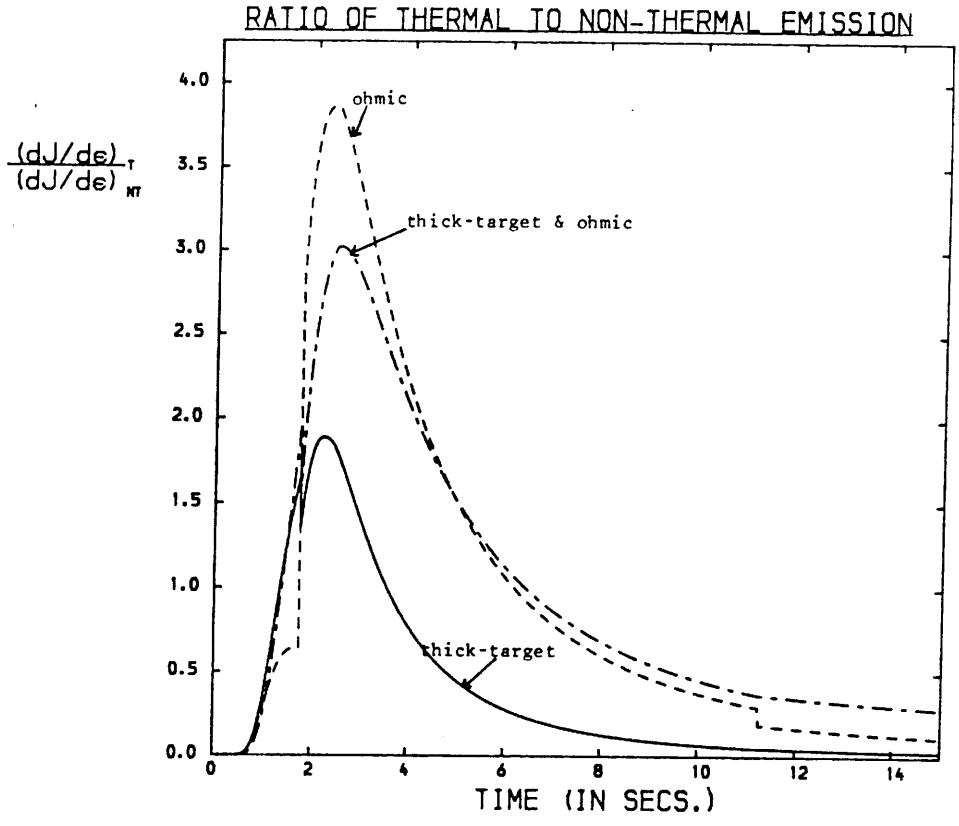

Figure 7.41: Variation of thermal/non-thermal bremsstrahlung yields at ε = 20 keV (case 6).

CASE	t_r(s)	W_{IC}^{sat}	W_{IA}^{sat}	T_{e_f}	T_{i_f}	$(T_e/T_i)_f$	S_{min}(cm)	$(T_e/T_i)_{IC\ onset}$	$(T_e(T_i)_{IC\ sat}$	$(T_e/T_i)_{IA\ onset}$	$(T_e/T_i)_{IA\ MS}$
1	4	IRB	TSYT	870	170	5.1	$1.2\ 10^9$	7.0	-	-	-
2	10	IRB	TSYT	490	44	11.2	$1.4\ 10^9$	-	-	10.3	10.3
3	4	PF	TSYT	1900	220	8.8	$8.7\ 10^8$	7.0	6.5	6.6	6.6
4	4	PF	10^{-6}TSYT	1900	220	8.74	$7.8\ 10^8$	7.0	6.5	6.6	8.72
5	10	PF	10^{-6}TSYT	490	44	11.1	$1.3\ 10^9$	11.7 (oscillations)	11.7	10.3	11.1
6	1.5	PF	10^{-6}TSYT	5800	760	7.6	$3.4\ 10^8$	4.6	3.8	4.3	7.8

TABLE 7.1 Summary of results obtained for the cases 1-6, described in the text. IRB denotes ion resonance broadening; TSYT - Tsytovich's mechanism; PF - plateau formation; "f" - final; MS - marginal stability. Note that in cases 2 and 3, IA onset and IA MS occur concurrently; in case 5, IC onset and IC sat also occur together (with subsequent oscillations of W_{IC} - see Figure 7.31).

$t \simeq 1s$ to $t \simeq 4s$.

A summary of the results of cases 1-6 is presented in Table 7.1.

7.5 Discussion

In this chapter we have extended our model of beam-driven return current instability to that of a magnetised plasma by including the effect of IC ohmic dissipation. This problem is considerably more complex than the case of an unmagnetised plasma and the nature of our approach was, to some extent, speculative. We initially adopted what would appear to be the current generally accepted saturation mechanisms in the plasma literature for the IC and IA instabilities. With these mechanisms it was found that, in fact, saturation never occurred; for rise times $t_r \lesssim 5.2s$, IC ohmic dissipation took place (once $v_d = v_{IC}$) and, for rise times $t_r \gtrsim 5.2s$, IA ohmic dissipation took place (once $v_d = v_{IA}$). However, we considered it wise to take account of the possibility that wave saturation may occur at lower levels in the flaring corona. A representative set of results were presented showing the possible types of plasma response to our given injected beam flux for various saturation wave levels. The principal conclusion remains that an electron beam can emit more hard X-rays through anomalous ohmic dissipation, and subsequent rapid heating of the plasma, than by thick-target bombardment of the solar atmosphere.

8. FUTURE WORK

In this thesis we have investigated beam-driven return current instability during solar flares and the possible effects on the hard X-ray signature. We were especially interested in evaluating the thermal bremsstrahlung yield from the rapidly heated coronal plasma. This thermal emission was compared with the non-thermal bremsstrahlung generated by a thick-target electron beam. It was found that, contrary to previous expectations, more hard X-rays could be produced from the hot thermal plasma than from thick-target bombardment of the atmosphere by the electron beam.

In order to perform this work we initially adopted the hypothesis of marginal stability to examine the case of an unmagnetised plasma. This method was found to be a very powerful tool for describing ion-acoustic instability of the return current as long as the electron-ion temperature ratio $T_e/T_i \gtrsim 4.8$. Below this value, however, application of the marginal stability approach failed, as negative resistivities were obtained. Confusion exists in the plasma literature as to whether or not the ion-acoustic instability can, in fact, be excited for such low values of T_e/T_i. This led us to analyse the possible modes of plasma oscillations in our return current system. It was found that the ion-acoustic instability can be excited in this regime if the relative electron-ion drift speed is sufficiently large (e.g. $v_d \simeq v_e$ for $T_e/T_i \simeq 1.0$).

We then developed a technique to account for the rate of growth of the wave energy density, dW/dt, which is implicitly assumed to be zero in the marginal stability description. This was used to verify the validity of marginal stability for $T_e/T_i \gtrsim 4.8$. Subsequently, the

method was applied to cases of onset of ion-acoustic instability where $T_e/T_i \lesssim 4.8$, for which the heating is catastrophic. A combined treatment, incorporating both the marginal stability and wave growth methods, was then presented.

Finally, a tentative attack on the problem of return current instability in a magnetised plasma was made. This is a considerably more complex problem given that both ion-cyclotron and ion-acoustic turbulence must be included. The essential result found earlier, that thermal emission from the rapidly heated plasma exceeds the non-thermal yield from the beam, remained unaltered.

There are many ways of extending and refining the work contained in this thesis and some of the possibilities have been identified already. For example, one of our assumptions was that we could describe the injected electron beam by means of a single constant energy, $\mathcal{E}_o$. A more realistic approximation would be to postulate a spectral distribution of the form

$$\frac{dF_o}{d\mathcal{E}_o}(\mathcal{E}_o) = (\delta-1)\frac{F_b}{\mathcal{E}_1}\left(\frac{\mathcal{E}_o}{\mathcal{E}_1}\right)^{-\delta} \qquad (s^{-1} \text{ per unit } \mathcal{E}_o) \quad (8.1)$$

for kinetic energies $\mathcal{E}_o > \mathcal{E}_1$, the cutoff energy, where F_b is the total injected beam flux (Equation 3.2) and δ is a constant.

More significantly, we did not include the effect of thermal conduction in our heating equations (3.4) (although see the discussion of Section 4.6). This can be done, however, by adding a term

$$\frac{dF_e}{dz} \equiv \frac{d}{dz}\left(\kappa^e \frac{dT_e}{dz}\right) \quad (8.2)$$

to the RHS of Equation (3.4a) and by adding

$$\frac{dF_i}{dz} \equiv \frac{d}{dz}\left(\kappa^i \frac{dT_i}{dz}\right) \tag{8.3}$$

to the RHS of Equation (3.4b) where F_e, F_i are the electron, ion heat fluxes respectively. The electron and ion thermal conductivities (κ^e, κ^i) can be evaluated for a classical plasma and also when microscopic turbulence exists, as described in Appendix B.

To properly include thermal conduction in our model requires a spatial, as well as temporal, dependence of the physical quantities; i.e. $T_e = T_e(z,t)$; $T_i = T_i(z,t)$; $\eta = \eta(z,t)$. (One could, of course, use a crude averaged conductive loss term of the form KT/s^2, where s is the beam stopping length, in a time-dependent treatment only. However, this can be quite inaccurate as T(z) often varies very nonlinearly over s (cf. Emslie (1985))). The new electron and ion heating equations would become respectively:

$$\frac{3}{2} n_p \frac{\partial T_e}{\partial t}(z,t) = \frac{3}{2} n_p \frac{\{T_i(z,t) - T_e(z,t)\}}{\tau_{eq}} + \frac{2\pi e^3 \ell n \Lambda n_p j_p(z,t)}{\mathcal{E}(z)}$$

$$+ \sum_i \chi_i \eta_i(z,t) j_p^2(z,t) + \frac{\partial}{\partial z}\left(\kappa^e \frac{\partial T_e}{\partial z}(z,t)\right) \tag{8.4a}$$

$$\frac{3}{2} n_p \frac{\partial T_i}{\partial t}(z,t) = \frac{3}{2} n_p \frac{\{T_e(z,t) - T_i(z,t)\}}{\tau_{eq}} + \sum_i (1-\chi_i)\eta_i(z,t) j_p^2(z,t)$$

$$+ \frac{\partial}{\partial z}\left(\kappa^i \frac{\partial T_i}{\partial z}(z,t)\right) \tag{8.4b}$$

Note that the plasma current density, j_p, is a function of space and time:

$$j_p(z,t) = \begin{cases} j_p(t), & 0 \leq z \leq s(t) \\ 0, & z > s(t) \end{cases} \tag{8.5}$$

where $j_p(t)$ is as given in Equation (3.3) and s(t) is the stopping length of the injected beam at time t. Also, in extending our model to include spatial variations in the plasma we have properly accounted for the inhomogeneous nature of collisional heating by the beam electrons (second term on RHS of Equation (8.4a), cf. Equation (3.4a)).

We may also include the effect of radiation losses on the electrons by incorporating a term of the form $-n_p^2 f(t_e)$ in the RHS of Equation (8.4a) (e.g. Summers and McWhirter (1979)), based on the assumption of the plasma being optically thin. To provide an initial equilibrium such modelling necessitates the inclusion of an electron heating function H_e. This is obtained by postulating an atmosphere in hydrostatic equilibrium (e.g. MacNeice et al. (1984)). However, we believe that including radiation losses will lead only to a minor refinement of the analysis: for the n_p, T_e values involved, $n_p^2 f(T_e)$ will be small compared to $\frac{dF_{cond.}}{dz}$.

We now discuss qualitatively how such a combined spatial and temporal analysis might be applied to the problem of beam-driven return current instability. Schematically, we may depict the plasma as shown in Figure 8.1.

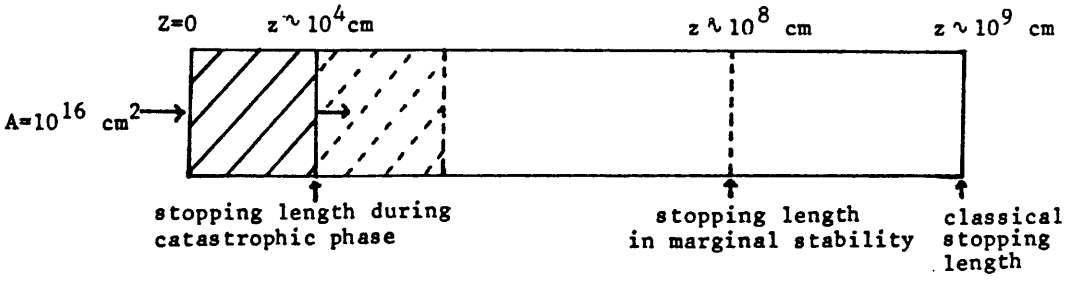

Figure 8.1 Different regions of a return current heated cylinder of coronal plasma.

Let us imagine that we wish to apply our analysis of return current instability to a cylindrical unmagnetised plasma volume of length $\sim 10^9$ cm, a typical beam stopping distance in the classical heating phase (e.g. Figure 6.5b). If onset of IA instability occurs for $T_e/T_i \gtrsim 4.8$ then a state of marginal stability is achieved. The resistivity rises due to the presence of turbulence and the beam-return current system is reduced in length (by a factor ~ 10). To evaluate the total thermal bremsstrahlung yield from the volume of Figure 8.1 would require tracking the plasma quantities T_e, T_i, η in the smaller region using marginal stability (Chapter 4) and, in the larger region, using the straightforward classical heating analysis (Chapter 3) with proper account taken of the electron and ion heat fluxes at the interface between these regions and at the plasma boundaries.

In the case of catastrophic heating the stopping length may be reduced by five orders of magnitude to $\sim 10^4$ cm (e.g. Figure 6.15). As shown in Chapter 6, this thin slab of plasma is rapidly heated (from $T_e/T_i \simeq 4$, say) until a state of marginal stability is achieved (in which $T_e/T_i \gtrsim 4.8$). The beam stopping length increases with the reduction in η to marginally stable levels and, as the beam begins to propagate through the neighbouring slab (which is still at $T_e/T_i \simeq 4$), catastrophic heating will once again take place, this time in slab 2 (see Figure 8.1).

This process will spread continuously with the gradual progression of a slab of catastrophically heated plasma through the flaring corona; at smaller depths the plasma will be in a state of marginal stability, while, at larger depths, the electron and ion temperatures evolve via

electron-ion equilibration and by heat flow between this and neighbouring regions. A detailed study of this kind, incorporating both spatial and temporal variations, would be highly desirable.

There is also scope for more sophisticated modelling of plasma wave turbulence excited by a beam-driven return current. Our approach in Chapter 6 was based on linear wave growth, at a constant rate γ , to saturation wave levels. As indicated earlier, a self-consistent solution of the appropriate dispersion relation is required to properly estimate γ . The issue of which saturation mechanisms operate in the flaring plasma to limit the growth of ion-acoustic and ion-cyclotron turbulence has barely been touched upon in the solar literature. We were therefore compelled, especially in Chapter 7, to treat W_{IC}^{sat} and W_{IA}^{sat} as input parameters in our model. More detailed understanding of this topic, possibly emerging from ongoing collaboration in the fields of natural and man-made plasmas, would certainly be of considerable importance in work such as this.

Recently there has been much interest in rapid fluctuations on sub-second time scales observed during solar flares at both microwave (e.g. Kaufmann et al. (1984)) and hard X-ray (Kiplinger et al. (1983)) energies. In fact, one of the series of NASA SMM workshops has been devoted to this subject alone (see Dennis et al. (1987)). We saw in Chapter 7 (case 5) that rapid hard X-ray oscillations, $\sim 10^{-2}$s in period, may occur for ohmic loss dominated flaring electron beams. Although this result is by no means conclusive, depending as it does on various assumed model parameters, such observations may well be placed on a firm theoretical footing using more rigorous methods developed from those presented in this thesis. Holman (1987) has also

attempted to model such rapid fluctuations by invoking two different instabilities in a current sheet.

The techniques we have applied in our analysis of beam-driven return current instability in solar flares also have wider applications. The role of anomalous current dissipation as a mechanism for coronal heating has been studied by several authors (e.g. Hinata (1979, 1980), Benford (1983)). It is generally agreed that ion-acoustic turbulence, although of some importance, is probably related more to the dynamic phenomenon of a solar flare than quiescent coronal heating (since it leads to large changes in transport coefficients in a very short time and rapid plasma heating). As a result, attention has been focussed on ion cyclotron turbulence. Misconceptions occur throughout such work on coronal heating, usually regarding the necessary conditions for onset of a particular instability. For example, Hinata (1979) takes the critical drift speed for the unstable ion-acoustic mode to be the ion sound speed, c_s. Benford (1983) actually neglects ion-acoustic turbulence on the grounds that "Ion acoustic models never become unstable, since T_e/T_i never exceeds 3." Needless to say, there is certainly scope for a more rigorous investigation of the role of anomalous ohmic dissipation in quiescent coronal heating.

We may end by pointing out that our work has applications to astrophysical beam-plasma systems in general, whether they occur in stellar flares or active galaxies, for example. As pointed out in the preface, however, advances in our understanding of such systems is likely to come from a cross-breeding of ideas from those studying laboratory, atmospheric and solar plasmas.

APPENDIX A: THE LANDAU INITIAL VALUE PROBLEM

In plasma kinetic theory, the particle distribution function $f_\alpha(\underset{\sim}{r},\underset{\sim}{v},t)$ gives the density of species α (e.g. electrons, ions) in a six-dimensional phase space, at the position with coordinates $(\underset{\sim}{r},\underset{\sim}{v})$ at time t. In other words, the number of particles of type α in the "six-volume" between $\underset{\sim}{r}$ and $\underset{\sim}{r}+d\underset{\sim}{r}$, and $\underset{\sim}{v}$ and $\underset{\sim}{v}+d\underset{\sim}{v}$, at time t, is $f_\alpha(\underset{\sim}{r},\underset{\sim}{v},t)d\underset{\sim}{r}\, d\underset{\sim}{v}$. Fluid (i.e. macroscopic) parameters are obtained as velocity moments of the distribution function. The number density is

$$n_\alpha(\underset{\sim}{r},t) = \int f_\alpha(\underset{\sim}{r},\underset{\sim}{v},t)d\underset{\sim}{v} \qquad (A.1)$$

the fluid velocity (i.e. mean particle velocity) is

$$\underset{\sim}{V}_\alpha(\underset{\sim}{r},t) = \frac{1}{n_\alpha} \int \underset{\sim}{v}\, f_\alpha(\underset{\sim}{r},\underset{\sim}{v},t)d\underset{\sim}{v} \qquad (A.2)$$

and the temperature is

$$T_\alpha(\underset{\sim}{r},t) = \frac{m_\alpha}{3n_\alpha} \int (\underset{\sim}{v}-\underset{\sim}{V}_\alpha)^2\, f_\alpha(\underset{\sim}{r},\underset{\sim}{v},t)d\underset{\sim}{v} \qquad (A.3)$$

The time evolution of f_α is described by a kinetic equation of the form

$$\frac{\partial f_\alpha}{\partial t} + \underset{\sim}{v}.\nabla f_\alpha + \frac{q_\alpha}{m_\alpha}(\underset{\sim}{E} + \frac{\underset{\sim}{v}}{c} \times B).\nabla_v f_\alpha = (\frac{\partial f_\alpha}{\partial t})_{coll} \qquad (A.4)$$

where $\nabla_v \equiv (\frac{\partial}{\partial v_x}, \frac{\partial}{\partial v_y}, \frac{\partial}{\partial v_z})$ and assuming that the particles (mass m_α and charge q_α) are subject to the Lorentz force; $\underset{\sim}{E}$ and $\underset{\sim}{B}$ are the macroscopic electric and magnetic fields, respectively. The quantity on the RHS of (A.4) is a collision term; for example, in the case of an ensemble of particles undergoing a series of small-angle scatterings, (A.4) takes the form of the Fokker-Planck equation, with $(\frac{\partial f_\alpha}{\partial t})_{coll}$ representing the Landau collision integral (e.g. Chapter 6 of Krall and Trivelpiece (1977)).

If we restrict our attention to timescales short in comparison to

collision times, we obtain the lowest-order approximation in a kinetic description, the Vlasov equation:

$$\frac{\partial f_\alpha}{\partial t} + \underset{\sim}{v}.\underset{\sim}{\nabla} f_\alpha + \frac{q_\alpha}{m_\alpha}\left(\underset{\sim}{E} + \frac{\underset{\sim}{v}}{c} \times \underset{\sim}{B}\right).\underset{\sim v}{\nabla} f_\alpha = 0 \qquad (A.5)$$

Equivalently, we may say that in a sufficiently hot plasma collisions can be neglected.

The most important use of Vlasov theory is in the study of electrostatic oscillations of a collisionless plasma, in which a small-amplitude perturbation is applied to a field-free equilibrium at time t=0. This is the so-called "initial value problem" which was first correctly treated by Landau (1946). As an understanding of dispersion relations and plasma instabilities is essential to the work of this thesis, we present below an account of this problem, along the lines of Krall and Trivelpiece (1977), sections 8.3 and 8.4.

The plasma equilibrium has the properties

$$\underset{\sim}{E}_o = \underset{\sim}{B}_o = 0 \quad ; \quad f_{\alpha_o} = f_{\alpha_o}(\underset{\sim}{v}) \qquad (A.6)$$

Hence, by Maxwell's equations, there is no net charge and no net current:

$$\rho_q \equiv \sum_\alpha q_\alpha \int f_{\alpha_o}\, d\underset{\sim}{v} = 0 \qquad (A.7)$$

$$\underset{\sim}{j} \equiv \sum_\alpha q_\alpha \int \underset{\sim}{v}\, f_{\alpha_o}\, d\underset{\sim}{v} = 0 \qquad (A.8)$$

A small-amplitude electrostatic perturbation is applied to the equilibrium by displacing a small amount of charge at t=0. Therefore, for the perturbed electric field, $\underset{\sim}{E}_1$,

$$\underset{\sim}{\nabla} \times \underset{\sim}{E}_1 = 0 \qquad (A.9)$$

$$\underset{\sim}{E}_1 = -\underset{\sim}{\nabla}\phi_1 \qquad (A.10)$$

where $\phi_1 = \phi_1(\underset{\sim}{r},t)$ is the perturbed electrostatic potential. The time evolution of the perturbed distribution function $f_{\alpha_1}(\underset{\sim}{r},\underset{\sim}{v},t)$ is found by solving

$$\left(\frac{\partial}{\partial t} + \underset{\sim}{v}.\underset{\sim}{\nabla}\right) f_{\alpha_1} = \frac{q_\alpha}{m_\alpha} \underset{\sim}{\nabla}\phi_1 . \underset{\sim}{\nabla}_v f_{\alpha_o} \qquad (A.11)$$

(the linearised Vlasov equation) together with

$$\underset{\sim}{\nabla}^2\phi_1 = -4\pi \sum_\alpha q_\alpha \int f_{\alpha_1}\, d\underset{\sim}{v} \qquad (A.12)$$

(from Poisson's equation).

We assume that perturbed quantities vary as $e^{i(\underset{\sim}{k}.\underset{\sim}{r}-\omega t)}$ and proceed by taking Fourier transforms with respect to the spatial variables and Laplace transforms in time. For convenience, we also take u to be the velocity component in the direction of the wave vector $\underset{\sim}{k}$ and define $F(u)$ as the integral of $f(\underset{\sim}{v})$ along the other two coordinates, i.e.

$$F_\alpha(u) = \int f_\alpha(\underset{\sim}{v})\, \delta\left(u - \frac{\underset{\sim}{k}.\underset{\sim}{v}}{|k|}\right) d\underset{\sim}{v} \qquad (A.13)$$

Equations (A.11) and (A.12), under these transforms, become

$$(\bar{p}+iku)\, \tilde{F}_{\alpha_{1k}} = F_{\alpha_{1k}}(t=0) + \frac{q_\alpha}{m_\alpha} .ik\, \frac{\partial F_{\alpha_o}}{\partial u}\, \tilde{\phi}_k \qquad (A.14)$$

$$k^2\tilde{\phi}_k = 4\pi \sum_\alpha q_\alpha \int \tilde{F}_{\alpha_{1k}}\, du \qquad (A.15)$$

where the Fourier transform is

$$A_k(u,t) = \frac{1}{(2\pi)^3} \int A(\underset{\sim}{r},u,t) e^{-i\underset{\sim}{k}.\underset{\sim}{r}}\, d\underset{\sim}{r} \qquad (A.16)$$

and the Laplace transform is

$$\tilde{A}(\underset{\sim}{r},u,p) = \int_o^\infty A(\underset{\sim}{r},u,t) e^{-pt}\, dt, \quad R_e(p) \geq p_o \qquad (A.17)$$

where the constant p_o is such that the integral converges. After some algebraic manipulation,

$$\tilde{\phi}_k(p) = \frac{\left(\frac{-i}{k^3}\right) 4\pi \sum_\alpha q_\alpha \int \frac{F_{\alpha_{1k}}(t=0)}{u-(ip/k)}\, du}{D(k,ip)}, \quad R_e(p) \geq p_o \qquad (A.18)$$

where the plasma dielectric function

$$D(k,ip) = 1 - 4\pi \sum_\alpha \frac{q_\alpha^2}{m_\alpha k^2} \int \frac{\frac{\partial F_{\alpha_o}}{\partial u}\, du}{u-(ip/k)} \qquad (A.19)$$

The perturbed distribution function is, from (A.13),

$$\tilde{F}_{\alpha_{1k}} = \frac{1}{(p+iku)} \left[F_{\alpha_{1k}}(t=0) + \frac{q_\alpha}{m_\alpha} ik \frac{\partial F_{\alpha_o}}{\partial u} \tilde{\phi}_k \right] \qquad (A.20)$$

To see how ϕ_1 and F_{α_1} evolve with time requires inverting their transforms (A.18) and (A.20). The inverse of the Laplace transform is

$$A(t) = \frac{1}{2\pi i} \int_C \tilde{A}(p) e^{pt}\, dp \qquad (A.21)$$

where C is a contour parallel to the imaginary axis lying to the right of all singularities of $\tilde{A}(p)$ in the complex p-plane. Figure A.1 shows a possible set of poles of $\tilde{\phi}_k$ corresponding to zeroes of D(k,ip).

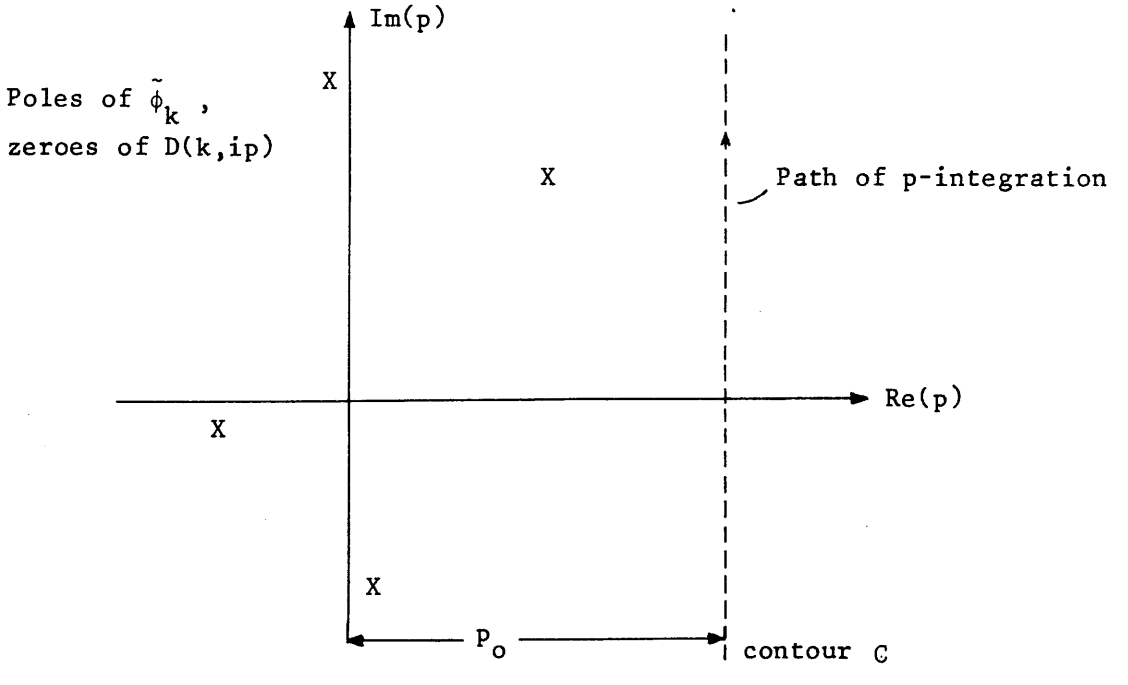

Figure A.1: Contour for the Inverse Laplace Transform of $\tilde{\phi}_k(p)$

It is difficult to find a general solution for $\phi_1(t), F_{\alpha_1}(t)$; however, we can find the long-time/asymptotic ($t \to \infty$) solution by deforming the contour C as shown in Figure A.2.

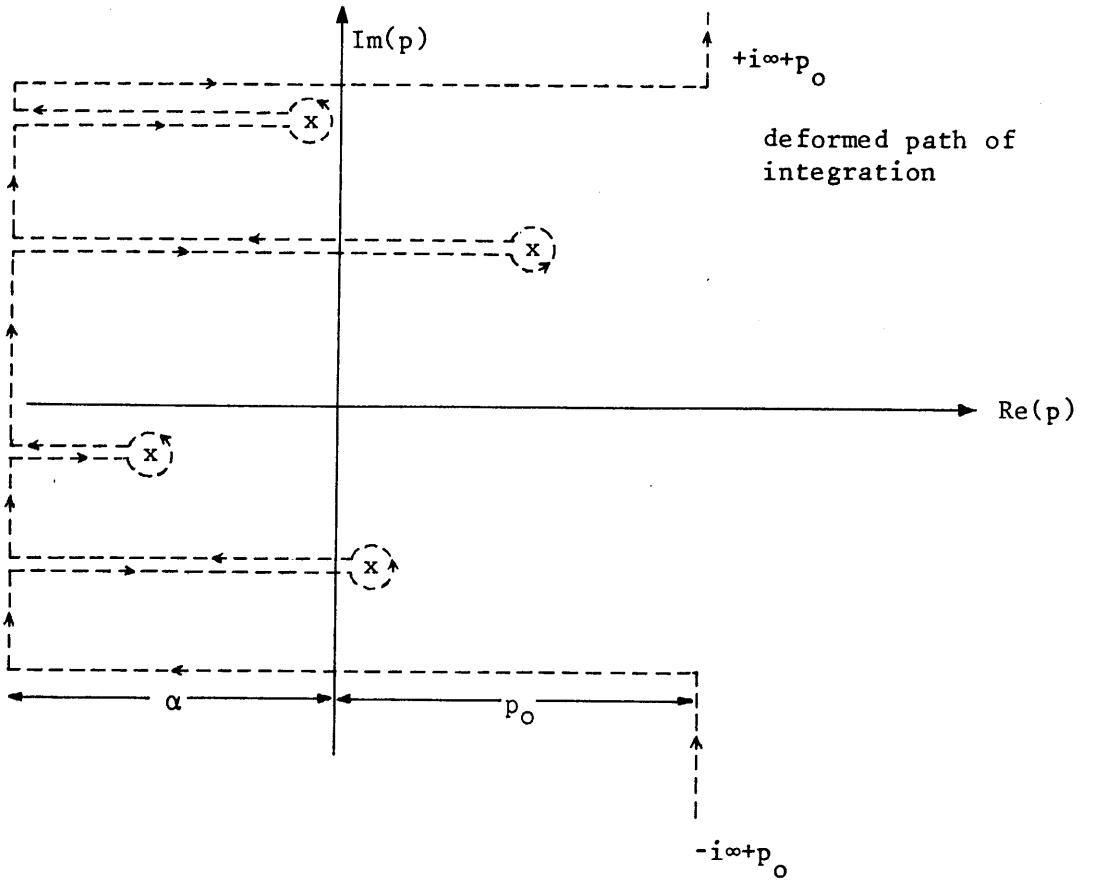

Figure A.2: Deformed Contour for the Inverse Laplace Transform of $\tilde{\phi}_k(p)$

With this change of contour, the theory of complex analysis yields:

$$\phi_k(t) = \underbrace{\sum_j R_j e^{p_j(k)t}}_{(1)} + \underbrace{\int_{-i\infty+p_o}^{-i\infty-\alpha} \frac{\tilde{\phi}_k(p)e^{pt}}{2\pi i}\,dp}_{(2)} + \underbrace{\int_{-\alpha-i\infty}^{-\alpha+i\infty} \frac{\tilde{\phi}_k(p)e^{pt}}{2\pi i}\,dp}_{(3)} + \underbrace{\int_{i\infty-\alpha}^{i\infty+p_o} \frac{\tilde{\phi}_k(p)e^{pt}}{2\pi i}\,dp}_{(4)} \qquad (A.22)$$

where

$$D[k, ip_j(k)] = 0 \qquad (A.23)$$

gives the poles p_j of $\tilde{\phi}_k(p)$ and R_j is the residue

$$R_j = \lim_{p \to p_j} (p-p_j)\,\tilde{\phi}_k(p) \qquad (A.24)$$

Terms (2) and (4) are negligible if $\tilde{\phi}_k(p) \to 0$ quickly as $|p| \to \infty$, while terms (3) $\to 0$ rapidly as $t \to \infty$. In other words, the contributions from the poles, particularly those furthest to the right, dominate the behaviour of $\phi_k(t)$.

The deformation of contour C from Figure A.1 to Figure A.2 requires the analytic continuation of $\phi_k(p)$, defined for $Re(p) \geq p_o$, into that part of the complex p-plane in which $Re(p) < p_o$. This requires analytic continuation of velocity integrals of the form

$$h(p) = \int_{-\infty}^{\infty} \frac{g(u)}{u-(ip/k)}\, du \qquad Re(p) \geq p_o \qquad (A.25)$$

to values of $Re(p) < p_o$. If g(u) is sufficiently well-behaved that it can be continued off the real axis as an analytic function of a complex variable u, then analytic continuation is satisfied by utilising the Landau contours for various values of Re(p) as shown in Figure A.3.

The function h(p) defined by

$$h(p) = \begin{cases} \displaystyle\int_{-\infty}^{\infty} \frac{g(u)}{u-(ip/k)}\, du & Re(p) \geq 0 \qquad (A.26) \\ \displaystyle\int_{-\infty}^{\infty} \frac{g(u)}{u-(ip/k)}\, du + 2\pi i g(ip/k) & Re(p) \leq 0 \qquad (A.27) \end{cases}$$

is analytic in both the lower and upper half planes $Re(p) \gtrless 0$. (A.26) and (A.27) are continuous in the limit $Re(p) \to 0$:

$$h(p) = \text{¢}\int_{-\infty}^{\infty} \frac{g(u)}{u-(ip/k)}\, du + \pi i g(ip/k) \qquad Re(p) = 0 \qquad (A.28)$$

where ¢ denotes the Cauchy principal value. Hence we have analytic continuation of h(p) as required.

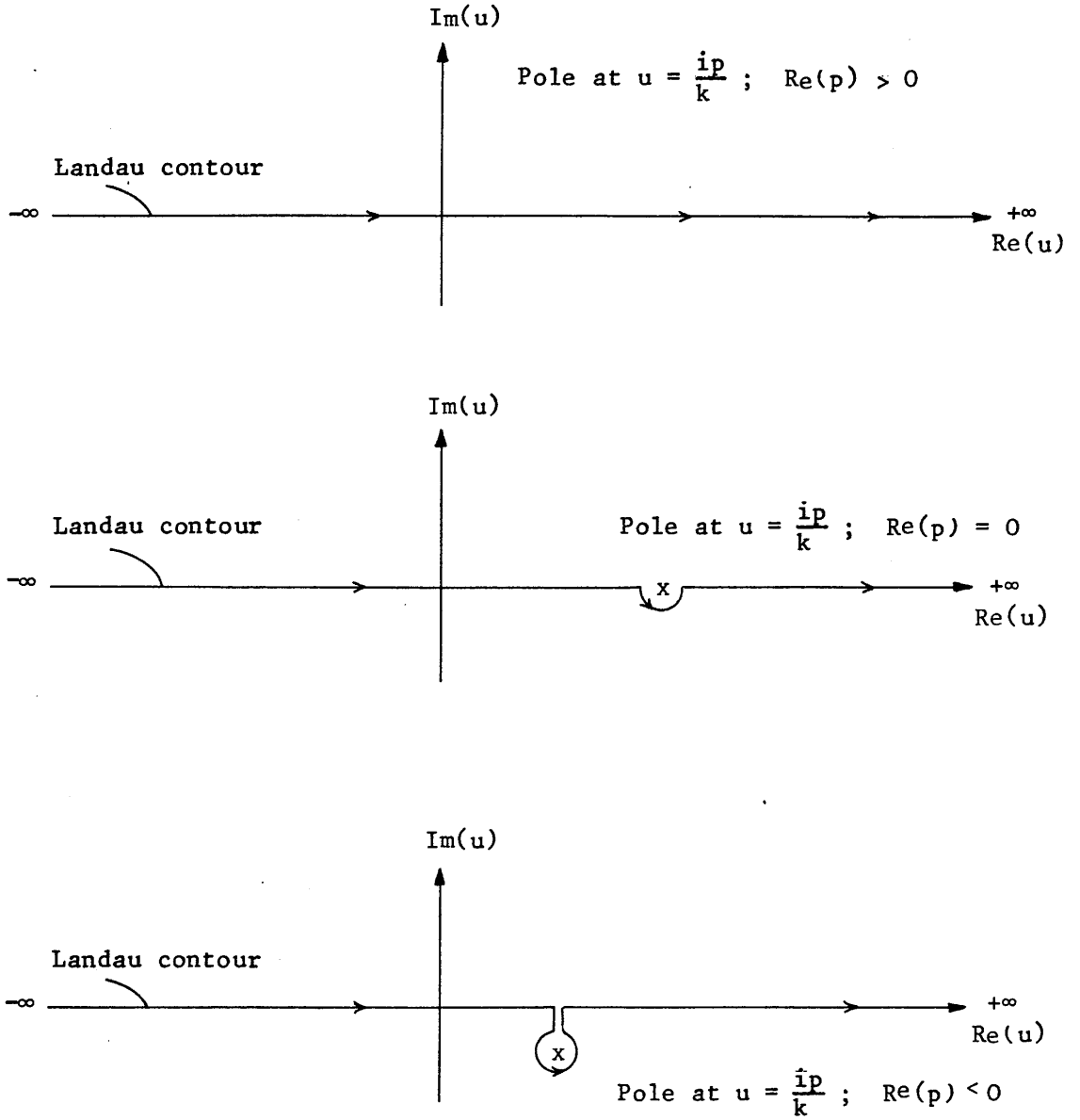

Figure A.3: Landau Contours for Different Values of Re(p).

Introducing the frequency defined by $\omega = ip$, we obtain the Fourier transform of the potential a long time after an initial perturbation in terms of the normal modes of oscillation of the plasma:

$$\phi_k(t) = \sum_j R_j e^{-i\omega_j t} \qquad (A.29)$$

Therefore, given the form of the initial disturbance, the perturbed distribution function will be found from (A.20) and (A.29). In general, ω_j is a complex quantity.

$$\omega_j = \omega_r + i\omega_i \qquad (A.30)$$

and satisfies

$$D(k,\omega_j) \equiv 1 - 4\pi \sum_\alpha \frac{q_\alpha^2}{m_\alpha k^2} \int_L \frac{\frac{\partial F_{\alpha_o}}{\partial u}}{u - (\omega_j/k)} du = 0 \qquad (A.31)$$

where L indicates integration along the relevant Landau contour (Figure A.3). Note that poles $p_j(k)$ lying to the right of the imaginary axis in Figure A.2 correspond to exponentially growing fields ($\omega_i > 0$: instability) and poles to the left correspond to damped plasma modes ($\omega_i < 0$). The solutions of the dispersion relation (A.31) give the frequency ω as a function of wave number k, or vice versa, for the oscillations resulting in the plasma after the initial perturbation from equilibrium.

The explicit form of the dispersion relation depends on the assumed form for $F_{\alpha_o}(u)$; Chapter 5 treats the case of Lorentzian profiles, which lead to algebraic equations whose roots can be found in a straightforward manner. If we take each particle species to be described by a Maxwellian,

$$F_{\alpha_o}(u) = \frac{n_{\alpha_o}}{(2\pi)^{\frac{1}{2}} v_{th_\alpha}} \exp\left[- \frac{(u - V_\alpha)^2}{2 v_{th_\alpha}^2} \right] \qquad (A.32)$$

where n_{α_o} is the unperturbed number density, V_α is the mean particle speed and $v_{th_\alpha} = T_\alpha/m_\alpha$ is the thermal speed (T_α is the temperature in energy units), then the dispersion relation (A.31) can be expressed in terms of the plasma dispersion function,

$$Z(\zeta) = \frac{1}{\pi^{\frac{1}{2}}} \int_{-\infty}^{\infty} \frac{e^{-t^2} dt}{t - \zeta} \quad , \quad \mathrm{Im}\, \zeta > 0 \qquad (A.33)$$

defined for Im $\zeta \leq 0$ by analytic continuation (see below). Specifically, (A.30) becomes

$$2k^2 = \sum_\alpha \frac{Z'(\zeta_\alpha)}{\lambda_{D\alpha}^2} \qquad (A.34)$$

where $\lambda_{D\alpha} = v_{th_\alpha}/\omega_{p\alpha}$ is the Debye length, $\omega_{p\alpha} = (4\pi n_{\alpha_o} q_\alpha^2/m_\alpha)^{\frac{1}{2}}$ is the plasma frequency and $\zeta_\alpha \equiv (\omega - k V_\alpha)/\sqrt{2} k v_{th_\alpha}$. It is easily shown that

$$Z'(\zeta) = \frac{1}{\pi^{\frac{1}{2}}} \int_{-\infty}^{\infty} \frac{e^{-t^2} dt}{(t - \zeta)^2} \qquad (A.35)$$

Integrating (A.35) by parts yields the following linear differential equation

$$Z'(\zeta) = -2 (1 + \zeta Z(\zeta)) \qquad (A.36)$$

which has solution

$$Z(\zeta) = e^{-\zeta^2} (i\pi^{\frac{1}{2}} - 2 \int_0^{\zeta} e^{t^2} dt) \qquad (A.37)$$

This can be re-expressed as

$$Z(\zeta) = 2i\, e^{-\zeta^2} \int_{-\infty}^{i\zeta} e^{-t^2} dt \qquad (A.38)$$

which is the analytic continuation of (A.33), valid for all values of ζ. We note that the plasma dispersion function can be related to the error function

$$\mathrm{erf}(\theta) = \frac{2}{\pi^{\frac{1}{2}}} \int_0^{\theta} e^{-t^2} dt \qquad (A.39)$$

in the following way

$$Z(\zeta) = i\pi^{\frac{1}{2}} e^{-\zeta^2} \left[\mathrm{erf}(i\zeta) + 1 \right] \qquad (A.40)$$

The function $Z(\zeta)$ has been tabulated by Fried and Conte (1961) and has the following asymptotic expansions

$$Z(\zeta) = i\pi^{\frac{1}{2}} e^{-\zeta^2} - 2\zeta \left[1 - \frac{2\zeta^2}{3} + \frac{4\zeta^4}{15} - \frac{8\zeta^6}{105} \cdots \right], \quad |\zeta| \ll 1 \qquad (A.41)$$

while, for $|\zeta| \gg 1$,

$$Z(\zeta) = i\pi^{\frac{1}{2}} \sigma e^{-\zeta^2} - \zeta^{-1} \left[1 + \frac{1}{2\zeta^2} + \frac{3}{4\zeta^4} + \frac{15}{8\zeta^6} + \cdots \right] \qquad (A.42)$$

with

$$\sigma = \begin{cases} 0, & \frac{\pi}{4} < \arg \zeta < \frac{3\pi}{4} \\ 1, & \frac{-\pi}{4} < \arg \zeta < \frac{\pi}{4} \ ; \ \frac{3\pi}{4} < \arg \zeta < \frac{5\pi}{4} \\ 2, & \frac{5\pi}{4} < \arg \zeta < \frac{7\pi}{4} . \end{cases}$$

Note that several authors, including Cairns (1985), have not given the correct regions of the complex ζ-plane in which the above expansion for large $|\zeta|$ holds. One consequence of such an error would be to obtain the wrong damping rates from dispersion relation (A.34).

As an example, we can find the real and imaginary parts of the frequency for weakly damped (i.e. $|\omega_i/\omega_r| \ll 1$) plasma oscillations (the Langmuir mode) with large phase velocity $\omega/k \gg v_e$ and long wavelength:

$k\lambda_{De} << 1$; we therefore use (A.42) with $\sigma = 1$

$$\omega_r \simeq \omega_{pe} \left(1 + \frac{3}{2} k^2 \lambda_{De}^2\right) \tag{A.43}$$

$$\omega_i \simeq -\left(\frac{\pi}{8}\right)^{\frac{1}{2}} \frac{\omega_{pe}}{(k\lambda_{De})^3} \exp\left[-\left(\frac{1}{2k^2\lambda_{De}^2} + \frac{3}{2}\right)\right] \tag{A.44}$$

Note the "thermal correction", $\frac{3}{2} k^2 \lambda_{De}^2$, to the real part of the frequency in (A.43).

APPENDIX B. TRANSPORT THEORY

In this appendix we consider the transport properties of an ionised hydrogen plasma comprising electrons and ions (protons). The first section treats the case of classical transport, i.e. where the electrons and ions undergo Coulomb collisions only. The second part deals briefly with anomalous transport in a weakly turbulent ($W/nT << 1$) plasma, in which particles are scattered by electrostatic waves and, as a result, the transport coefficients are modified. These can be estimated by introducing an effective collision frequency ν_{eff}.

B.1 Classical Transport

Classical transport processes in a plasma have been extensively reviewed by Braginskii (1965) and in this section we summarise those points relevant to the work of this thesis. Laing (1981) presents concisely the main results of Braginskii (1965) and a very useful "at a glance" summary is contained in the NRL Plasma Formulary (1983). The reader may be interested to note that Epperlein (1984) has recalculated Braginskii's transport coefficients and found some cross-field terms to be inaccurate for certain values of $\Omega_e \tau_e$, where Ω_e is the electron cyclotron frequency and τ_e is the mean electron-ion collision time. However, these refinements do not concern us here.

By taking the zeroth, first and second velocity moments of the Boltzmann equation (i.e. Equation (A.4)) we obtain the equations of continuity, momentum and energy respectively:

$$\frac{\partial n_\alpha}{\partial t} + \nabla.(n_\alpha \underset{\sim}{V}_\alpha) = 0 \qquad (B.1)$$

$$m_\alpha n_\alpha \frac{d_\alpha \underset{\sim}{V}_\alpha}{dt} = -\underset{\sim}{\nabla} p_\alpha - \sum_j \frac{\partial \Pi^\alpha_{ij}}{\partial x_j} + q_\alpha n_\alpha \left(\underset{\sim}{E} + \frac{\underset{\sim}{V}_\alpha \times \underset{\sim}{B}}{c}\right) + \underset{\sim}{R}_\alpha \qquad (B.2)$$

$$\frac{3}{2} n_\alpha \frac{d_\alpha T_\alpha}{dt} = - p_\alpha \underset{\sim}{\nabla}.\underset{\sim}{V}_\alpha - \sum_{i,j} \Pi^\alpha_{ij} \frac{\partial V_{\alpha i}}{\partial x_j} - \underset{\sim}{\nabla}.\underset{\sim}{h}^\alpha + Q_\alpha \qquad (B.3)$$

where α denotes electrons (e) or ions (i) and $\frac{d\alpha}{dt} \equiv \frac{\partial}{\partial t} + (\underset{\sim}{V}_\alpha.\underset{\sim}{\nabla})$. The quantity $p_\alpha = n_\alpha T_\alpha$ is the scalar pressure associated with the particles of species α . The complete pressure tensor is

$$P^\alpha_{ij} \equiv \int m_\alpha v'_{\alpha_i} v'_{\alpha_j} f_\alpha(\underset{\sim}{r},\underset{\sim}{v},t) d\underset{\sim}{v} = n_\alpha m_\alpha \langle v'_{\alpha_i} v'_{\alpha_j} \rangle = p_\alpha \delta_{ij} + \Pi^\alpha_{ij} \qquad (B.4)$$

where the particle velocity $\underset{\sim}{v}_\alpha$ is divided into two components: a mean velocity $\underset{\sim}{V}_\alpha$ (see equation (A.2)) and a random velocity $\underset{\sim}{v}'_\alpha = \underset{\sim}{v}_\alpha - \underset{\sim}{V}_\alpha$. The brackets < > indicate averaging over the particle distribution. Note the viscous heating term $- \sum_{i,j} \Pi^\alpha_{ij} \frac{\partial V_{\alpha i}}{\partial x_j}$ in Equation (B.3) which arises when the distribution function $f_\alpha(\underset{\sim}{r},\underset{\sim}{v},t)$ is anisotropic.

$\underset{\sim}{R}_\alpha$, the friction force, is the mean change in momentum due to electron-ion collisions:

$$\underset{\sim}{R}_e = \int m_e \underset{\sim}{v}'_e \left(\frac{\partial f_e}{\partial t}\right)_{coll} d\underset{\sim}{v} = - \int m_i \underset{\sim}{v}'_i \left(\frac{\partial f_i}{\partial t}\right)_{coll} d\underset{\sim}{v} = - \underset{\sim}{R}_i \qquad (B.5)$$

R comprises a part due to a relative electron-ion drift $\underset{\sim}{v}_d \equiv \underset{\sim}{V}_e - \underset{\sim}{V}_i$, $\underset{\sim}{R}_{v_d}$, and a part due to the existence of temperature gradients, $\underset{\sim}{R}_T$:

$$\underset{\sim}{R} = \underset{\sim}{R}_{v_d} + \underset{\sim}{R}_T \qquad (B.6)$$

Q_α is the heat generated in particle species α due to collisions with the other species:

$$Q_\alpha = \frac{1}{2} \int m_\alpha (v'_\alpha)^2 \left(\frac{\partial f_\alpha}{\partial t}\right)_{coll} d\underset{\sim}{v} \qquad (B.7)$$

The vector $\underset{\sim}{h}^{\alpha}$ is the flux density of heat carried by particles of type α:

$$\underset{\sim}{h}^{\alpha} = \frac{1}{2} \int m_{\alpha} (v'_{\alpha})^2 \, \underset{\sim}{V}_{\alpha} \, f_{\alpha}(\underset{\sim}{r}, \underset{\sim}{v}, t) d\underset{\sim}{v} \tag{B.8}$$

The electron heat flux $\underset{\sim}{h}^{e}$ is made up of two parts, analogously to the friction force $\underset{\sim}{R}$:

$$\underset{\sim}{h}^{e} = \underset{\sim}{h}^{e}_{v_d} + \underset{\sim}{h}^{e}_{T} \tag{B.9}$$

The total heat generated in the plasma due to collisions is

$$Q_e + Q_i = - \underset{\sim}{R} . \underset{\sim}{v}_d \tag{B.10}$$

where the heat acquired by the ions in collisions with electrons is represented by the exchange term

$$Q_i = \frac{3 m_e n_e}{m_i \tau_i} (T_e - T_i) \tag{B.11}$$

The electron and ion collision times are, respectively,

$$\tau_e = \frac{3 m_e^{\frac{1}{2}} T_e^{3/2}}{4 (2\pi)^{\frac{1}{2}} \ell n \Lambda n_e e^4} \tag{B.12}$$

$$\tau_i = \frac{3 m_i^{\frac{1}{2}} T_i^{3/2}}{4 \pi^{\frac{1}{2}} \ell n \Lambda n_i e^4} \tag{B.13}$$

(Note that $\tau \propto T^{3/2}$).

The quantity $\ell n \Lambda$ is the Coulomb logarithm and arises as a consequence of the long-range nature of the electrostatic force; the cumulative effect of many small-angle deflections is more important than the small number of large-angle deflections. The plasma parameter Λ is defined as

$$\Lambda \equiv \frac{b_{max}}{b_{min}} \tag{B.14}$$

where b_{max}, b_{min} are the maximum and minimum impact parameters, respectively, of the Coulomb interaction. Since electric fields are shielded out over a Debye length, for drift current particles we may take $b_{max} \sim \lambda_{De}$. Provided quantum effects are unimportant we take b_{min} to be the closest distance of approach assuming that the thermal kinetic energy at infinity is converted into electrostatic potential energy, i.e.

$$b_{min} \sim \frac{e^2}{\frac{1}{2} m_e v_e^2} \tag{B.15}$$

It can then be easily shown that

$$\Lambda \sim 6\pi n_e \lambda_{De}^3 \tag{B.16}$$

We can therefore see that Λ ~ number of electrons in a "Debye sphere". The Coulomb logarithm changes slowly with temperature and density, and for most plasmas lies in the range 10-30. Under solar coronal conditions, $\ell n\ \Lambda \simeq 20$; for the purposes of this thesis this approximation is adequate. From Equations (B.12) and (B.16) we can express the electron collision frequency ν_e in terms of ω_{pe} and Λ as

$$\nu_e \simeq \omega_{pe} \frac{\ell n\ \Lambda}{\Lambda} \tag{B.17}$$

Strictly speaking, τ_e (Equation (B.12)) is the electron-ion scattering time and $\tau_i \sim (m_i/m_e)^{\frac{1}{2}} \tau_e$ (Equation (B.13)) is the ion-ion scattering time. The electron-electron collision time $\tau_{ee} \sim \tau_e$ determines the timescale for the electron plasma component to relax to equilibrium and τ_i determines this process for the ion component. Energy (and momentum) exchange between ions and electrons occurs on the long timescale $\tau_{eq} \sim (m_i/m_e)\tau_e$, so that the two components can separately reach equi-

librium with each other. In summary, the collision timescales are in the ratio:

$$\tau_{ee} : \tau_e : \tau_i : \tau_{eq} = 1 : 1 : \left(\frac{m_i}{m_e}\right)^{\frac{1}{2}} : \left(\frac{m_i}{m_e}\right) \qquad (B.18)$$

We may derive the electrical conductivity of the plasma as follows. The equation of motion of an electron fluid with mean velocity $\underset{\sim}{V}_e$, under the influence of an electric field $\underset{\sim}{E}$, assuming a spatially homogeneous plasma and the ions to be infinitely massive is, from (B.2)

$$\frac{d_e \underset{\sim}{V}_e}{dt} = \frac{e}{m_e n_e} \underset{\sim}{E} - \frac{\underset{\sim}{V}_e}{n_e \tau_e} \qquad (B.19)$$

A steady state velocity is reached at which the force due to the electric field is balanced by the resistive drag of electron-ion collisions:

$$\underset{\sim}{V}_e = \frac{e \underset{\sim}{E} \tau_e}{m_e} \qquad (B.20)$$

We thus have a simple Ohm's law relating the current density $\underset{\sim}{j}$ to the $\underset{\sim}{E}$ field

$$\underset{\sim}{j} \equiv n_e e \underset{\sim}{V}_e = \frac{n_e e^2 \tau_e}{m_e} \underset{\sim}{E} \equiv \sigma \underset{\sim}{E} \qquad (B.21)$$

where the electrical conductivity is

$$\sigma = \frac{n_e e^2 \tau_e}{m_e} = \frac{\omega_{pe}^2}{4\pi \nu_e} \qquad (B.22)$$

and the resistivity $\eta = \sigma^{-1}$.

The above simple analysis is for the so-called Lorentz plasma, a hypothetical fully ionised plasma in which the electrons do not interact with each other, and the positive ions are at rest. The friction force is

$$\underset{\sim}{R}_{v_d} = - \frac{m_e n_e}{\tau_e} \underset{\sim}{v}_d \qquad (B.23)$$

(cf. Equation (B.19)). In fact, τ_e is defined (Equation (B.12)) such that the frictional force that arises when an electron Maxwellian distribution is shifted with respect to the ion function by an amount $\underset{\sim}{v}_d$ has the simple form of (B.23). In reality, if an electric field produces a mean drift $\underset{\sim}{v}_d$ along $\underset{\sim}{B}$ (or if B = 0), then the electron distribution function is a skewed Maxwellian. This occurs because the Coulomb cross-section decreases with increasing electron energy (since $\tau_e \alpha v_e^3$: see (B.12)); faster electrons are therefore shifted more than slower ones. The friction force is therefore smaller than for a simply displaced Maxwellian. Electron-electron collisions, however, tend to re-establish a Maxwellian. Since $\tau_{ee} \sim \tau_e$, these two effects are "of order unity" and, for a simple hydrogen plasma, the friction coefficient is reduced by a factor $\simeq 0.51$. In the case of large B fields (i.e. $\Omega_e \tau_e << 1$) the correction to the transverse frictional force is negligible. We therefore have

$$\underset{\sim}{R}_{v_{d//}} \simeq \frac{-0.51\, m_e n_e}{\tau e} \underset{\sim}{v}_{d//} \qquad (B.24)$$

$$\underset{\sim}{R}_{v_{d\perp}} \simeq - \frac{m_e n_e}{\tau e} \underset{\sim}{v}_{d\perp} \qquad (B.25)$$

In strong magnetic fields, then, the longitudinal electrical conductivity $\sigma_{//} \simeq 2.0\sigma_\perp$, where $\sigma_\perp$ is the transverse electrical conductivity, and

$$\sigma_{//} \simeq \frac{2.0\, n_e e^2 \tau_e}{m_e} \qquad (B.26)$$

The longitudinal resistivity is, from (B.12) and (B.26)

$$\eta_{\parallel} \simeq \left(\frac{8\pi}{9}\right)^{\frac{1}{2}} m_e^{\frac{1}{2}} e^2 \ell n \Lambda T_e^{-\frac{3}{2}} \qquad (B.27)$$

(Spitzer, 1962).

We now turn our attention to the thermal force $\underset{\sim}{R}_T$ which arises in the presence of a temperature gradient. Assume that $\underset{\sim}{\nabla} T_e$ is along the x-axis (Figure B.1) and that there is no magnetic field (or $\underset{\sim}{B} \,//\, \underset{\sim}{\nabla} T_e$).

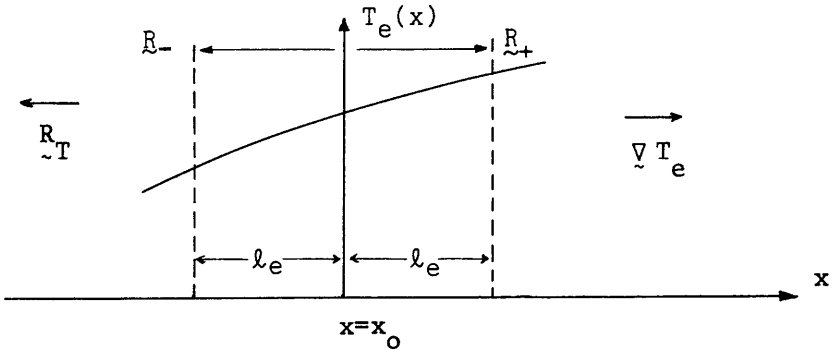

Figure B.1: Origin of the Thermal Force, $\underset{\sim}{R}_T$

Since there is a temperature gradient, the number of electrons moving in one direction per unit time is not identical to the flux in the opposite direction. As a result of electron-ion collisions, these fluxes experience frictional forces $\underset{\sim}{R}_+$ and $\underset{\sim}{R}_-$, both of order $m_e n_e v_d/\tau_e$. In the plane $x=x_o$, collisions are sustained by electrons that have traversed distances of the order of the mean free path $\ell_e \sim v_e \tau_e$. Electrons originating from the right have a temperature $\sim \ell_e \frac{\partial T_e}{\partial x}$ greater than those coming from the left. There is therefore an unbalanced force

$$R_T \sim -\frac{\ell_e}{T_e} \frac{\partial T_e}{\partial x} \frac{m_e n_e v_d}{\tau_e} \sim -\frac{m_e v_e^2}{T_e} n_e \frac{\partial T}{\partial x}$$

$$\text{i.e.} \qquad R_T \sim -n_e \frac{\partial T_e}{\partial x} \qquad (B.28)$$

A more rigorous analysis yields

$$\underset{\sim}{R}_T = - 0.71\, n_e\, \nabla_{//}\, T_e \qquad (B.29)$$

The thermal force is in the opposite direction to the temperature gradient. Having considered the friction force $\underset{\sim}{R} = \underset{\sim}{R}_{v_d} + \underset{\sim}{R}_T$, we can re-express Equation (B.10) in the following way, using (B.24) and (B.25).

$$Q_e + Q_i = - \frac{m_e n_e}{\tau_e} (0.51\, \underset{\sim}{v}_{d//} + \underset{\sim}{v}_{d\perp}).\underset{\sim}{v}_d - \underset{\sim}{R}_T.\underset{\sim}{v}_d$$

i.e.

$$Q_e + Q_i = \left(\frac{\underset{\sim}{j}_{//}}{\sigma_{//}} + \frac{\underset{\sim}{j}_{\perp}}{\sigma_{\perp}}\right) .\underset{\sim}{j} + \frac{\underset{\sim}{j}.\underset{\sim}{R}_T}{n_e} \qquad (B.30)$$

We now consider the electron heat flux $\underset{\sim}{h}^e$ which has a component $\underset{\sim}{h}^e_{v_d}$ due to a relative electron-ion drift, and a component $\underset{\sim}{h}^e_T$ due to the existence of a temperature gradient. The first component can be estimated as follows. As mentioned above, because $\tau_e \alpha\, v_e^3$, the current along B (or with no $\underset{\sim}{B}$-field present) is mainly carried by the faster electrons. In the frame in which $V_e = 0$, more fast electrons move in the direction of $\underset{\sim}{v}_d$ and more slow electrons move in the direction of $-\underset{\sim}{v}_d$. The electron fluxes are balanced in this system (since $V_e = 0$) but the energy fluxes are not: heat flows in the $\underset{\sim}{v}_d$ direction. Qualitatively, the effect is of order unity and the heat flow due to the existence of a relative electron-ion drift $\underset{\sim}{v}_d$ is $\underset{\sim}{h}^e_{v_d} \sim n_e\, T_e\, \underset{\sim}{v}_d$ or, more exactly:

$$\underset{\sim}{h}^e_{v_{d//}} = 0.71\, n_e\, T_e\, v_{d//} \qquad (B.31)$$

Before evaluating h^e_T , let us consider the process of particle diffusion as this is of importance in understanding heat transport. Suppose particles collide randomly with their neighbours, one such event leading to a displacement Δx during the time τ between two

successive collisions. The net particle flux at $x=x_o$ is

$$\Gamma = \Gamma^+ - \Gamma^- \tag{B.32}$$

where the unidirectional flux from the left to the right is

$$\Gamma^+ = \frac{1}{2} \int_{x_o-\Delta x}^{x_o} \frac{1}{\tau} \cdot n(x)dx \simeq \frac{1}{2} \left[n(x_o) - \frac{\Delta x}{2} \frac{\partial n}{\partial x} \Big|_{x=x_o} \right] \frac{\Delta x}{\tau} \tag{B.33}$$

(half of the particles between $x_o - \Delta x$, x_o suffer displacements to the right). The flux in the opposite direction is

$$\Gamma^- = \frac{1}{2} \int_{x_o+\Delta x}^{x_o} \frac{1}{\tau} \cdot n(x)dx \simeq \frac{1}{2} \left[n(x_o) + \frac{\Delta x}{2} \frac{\partial n}{\partial x} \Big|_{x=x_o} \right] \frac{\Delta x}{\tau} \tag{B.34}$$

The net flux is

$$\Gamma = - \frac{(\Delta x)^2}{2\tau} \frac{\partial n}{\partial x} \tag{B.35}$$

or, strictly, averaging over all collisions (i.e. all possible $\Delta x, \tau$):

$$\Gamma = - D \frac{\partial n}{\partial x} \tag{B.36}$$

where the diffusion coefficient is

$$D = \left\langle \frac{(\Delta x)^2}{2\tau} \right\rangle \tag{B.37}$$

Now, to find h_T^e assume that there is no relative electron-ion drift so that $v_d = 0$ and, hence, $h_{v_d}^e = 0$. The unidirectional heat flux to the right, for example, is $h^+ \sim \frac{\Delta x}{\tau_e} \cdot n_e T_e$. In the presence of an electron temperature gradient, a relative fraction $\sim \frac{\Delta x}{T_e} \cdot \frac{\partial T_e}{\partial x}$ of the unidirectional fluxes is not balanced. The net heat flux is

$$h_T^e = - \kappa^e \frac{\partial T_e}{\partial x} \tag{B.38}$$

where the electron thermal conductivity is

$$\kappa^e \sim \frac{n_e (\Delta x)^2}{\tau_e} \sim n_e D_e \qquad (B.39)$$

In other words, we may regard the transfer of heat by temperature gradients as a diffusive process. Note that in motion along $\underset{\sim}{B}$ (or with $\underset{\sim}{B} = 0$) the distance Δx between collisions is the mean free path $\ell_e \sim v_e \tau_e$. The longitudinal thermal conductivity is therefore

$$\kappa^e_{//} \sim \frac{n_e \ell_e^2}{\tau_e} \sim \frac{n_e T_e \tau_e}{m_e} \qquad (B.40)$$

For transport across a magnetic field, $\Delta x \sim r_e = v_e/\Omega_e$, the electron gyro radius. The transverse thermal conductivity is

$$\kappa^e_{\perp} \sim \frac{n_e r_e^2}{\tau_e} \sim \frac{n_e T_e}{m_e \Omega_e^2 \tau_e} \qquad (B.41)$$

More exactly, the coefficients of conductivity are:

$$\kappa^e_{//} = \frac{3.2\, n_e T_e \tau_e}{m_e} \qquad (B.42)$$

$$\kappa^e_{\perp} = \frac{4.7\, n_e T_e}{m_e \Omega_e^2 \tau_e} \qquad (B.43)$$

In addition, it can be shown that the corresponding ion coefficients, in the presence of an ion temperature gradient, are

$$\kappa^i_{//} = \frac{3.9\, n_i T_i \tau_i}{m_i} \qquad (B.44)$$

$$\kappa^i_{\perp} = \frac{2 n_i T_i}{m_i \Omega_i^2 \tau_i} \qquad (B.45)$$

From (B.42 and (B.44) we see that, if $T_e \sim T_i$, then

$$\frac{\kappa^e_{//}}{\kappa^i_{//}} \sim \frac{m_i}{m_e} \qquad (B.46)$$

i.e. heat along $\underset{\sim}{B}$ is primarily carried by the electrons. From (B.43)

and (B.45):

$$\frac{\kappa_{\perp}^{e}}{\kappa_{\perp}^{i}} \sim \frac{m_e}{m_i} \qquad (B.47)$$

i.e. transverse to $\underset{\sim}{B}$, it is the ions which transport the heat most effectively. From (B.42) and (B.43) or, similarly, from (B.44) and (B.45):

$$\frac{\kappa_{//}}{\kappa_{\perp}} \sim (\Omega\tau)^2 \qquad (5.48)$$

so that for strong fields ($\Omega\tau >> 1$), the transverse thermal coefficient may be orders of magnitude smaller than the longitudinal thermal coefficient. Contrast this with the case of the transverse and longitudinal <u>electrical</u> conductivities where, for strong fields, $\sigma_{//} \simeq 2.0\ \sigma_{\perp}$. We must bear in mind, though that σ is determined by the rate of change of momentum of the electrons and is therefore derived from the first moment of the Boltzmann equation. On the other hand, κ relates heat flow to the temperature gradient and so is obtained from the second moment of the Boltzmann equation. Physically, the difference in $\sigma_{//}$ and $\sigma_{\perp}$ comes from the reduction in friction parallel to $\underset{\sim}{B}$ due to skewing of the electron distribution friction. In the case of $\kappa_{//}$, $\kappa_{\perp}$, the orders of magnitude difference arises from the greatly different random pathlengths between collisions: mean free path ℓ_e (parallel to $\underset{\sim}{B}$) and electron gyro-radius r_e (transverse to $\underset{\sim}{B}$).

B.2 Anomalous Transport

In the previous section we reviewed the transport properties of a classical plasma in which electrons and ions undergo Coulomb collisions. There is, in fact, always a level of random ("noise") electric field

fluctuations in a plasma in thermodynamic equilibrium:

$$\frac{<(\delta E)^2>}{8\pi\, n_e\, T_e} \simeq \frac{1}{\Lambda} \qquad (B.49)$$

where $W = <(\delta E)^2> /8\pi$ is the wave energy density and δE is the electric field fluctuation (eg. Cook (1981)). If a nonthermal wave spectrum (i.e. turbulence) is produced in the plasma, then the electrons collide not only with ions but also with the self-consistent fields associated with these waves. Electron scattering by the waves represents an additional momentum loss and the resistivity can be orders of magnitude greater than classical Spitzer values. For our purposes, we regard a plasma as having a turbulent wave level when a current-driven micro-instability (i.e. one in which some critical drift velocity v_{cr} must be exceeded) is excited. The plasma then becomes unstable to the generation of electrostatic waves. As the wave amplitude grows the behaviour becomes non-linear and different plasma modes can couple and exchange energy between themselves. Saturation occurs when some physical mechanism reduces the nonlinear growth-rate to zero.

Turbulence and its complex effects on transport are of great importance in plasma physics. Standard texts include Kadomtsev (1965), Tsytovich (1970), Davidson (1972), Kaplan and Tsytovich (1973) and Alexandrov et al. (1984). Useful review articles have also been written by Hasegawa (1974) and Papadopoulos (1977). We deal here with weak turbulence, for which $W/nT \ll 1$.

Qualitatively, we may regard collisions with particles or waves as scattering by electric-field fluctuations. Stochastic fluctuations having wavelengths $\lambda < \lambda_{D_e}$ originate in the incoherent thermal motions of single particles. On the other hand, stochastic fields with $\lambda > \lambda_{D_e}$

result from the collective shielding effects of many particles. Hence, we may talk about an effective electron collision frequency ν_{eff} which is derived from the classical collision frequency as follows. From Equation (B.17)

$$\nu_{eff} \simeq \frac{\omega_{pe}}{\Lambda} \tag{B.50}$$

which, using (B.49), can be transformed into an expression which explicitly includes the wave level W:

$$\nu_{eff} \simeq \omega_{pe} \cdot \frac{W}{n_e T_e} \tag{B.51}$$

For example, if W^{IA} is the wave energy density of ion-acoustic turbulence, and W^{IC} is the wave energy density of ion-cyclotron turbulence, then they give rise to effective collision frequencies $\nu_{eff}^{IA} \simeq \omega_{pe} W^{IA}/n_e T_e$ and $\nu_{eff}^{IC} \simeq \omega_{pe} W^{IC}/n_e T_e$ respectively. Transport coefficients are then derived analogously to classical coefficients by replacing τ_e with $\tau_{eff} \equiv \nu_{eff}^{-1}$. To find $\sigma_{//}$, for instance, in a weakly turbulent plasma we replace τ_e in (B.26) by ν_{eff}^{-1} from (B.51). Similarly, we may obtain $\kappa_{//}^e$ by substituting (B.51) into (B.42).

To determine the effective ion collision frequency ν_{eff}^i we observe that, classically:

$$\frac{\nu_i}{\nu_e} = \left(\frac{m_e T_e^3}{m_i T_i^3} \right)^{\frac{1}{2}} \tag{B.52}$$

(from Equations (B.12) and (B.13)). In order that we recover the classical transport coefficients for a plasma with a random or "noise" level of fluctuations, we must have:

$$\nu_{eff}^i \equiv \nu_{eff} \left(\frac{m_e T_e^3}{m_i T_i^3} \right)^{\frac{1}{2}}$$

$$\simeq \omega_{pe} \frac{W}{n_e T_e} \left(\frac{m_e T_e^3}{m_i T_i^3} \right)^{\frac{1}{2}} \quad \text{by} \quad (B.51)$$

$$\text{i.e.} \quad \nu^i_{eff} = \omega_{pi} \frac{W}{n_e T_e} \left(\frac{T_e}{T_i} \right)^{3/2} \qquad (B.53)$$

Ion transport coefficients, for example, $\kappa^i_{//}$, $\kappa^i_{\perp}$ can then be easily derived by replacing τ_i in the classical expressions by $\nu^{i\ -1}_{eff}$.

Anomalous resistance requires a non-thermal spectrum of <u>low-frequency</u> density fluctuations which can efficiently scatter the drifting electrons. In other words, the phase velocity of the waves must satisfy $v_p \equiv \omega/k << v_e, v_d$. The reasons for this are two-fold. Firstly, resistivity cannot be a resonance phenomenon: the bulk, not just a small fraction of the electron distribution undergoes momentum loss through collisions. Secondly, if $v_p \sim v_e, v_d$, then the electrons and density fluctuations would move together with little or no momentum exchange. Therefore, precipitating electron streams which are unstable to high-frequency waves (Langmuir waves, whistler waves, etc.) will not generate anomalous plasma resistivity.

Strictly speaking, the discussion of this section is limited to plasmas which are unstable to current-driven instabilities. It is possible, though, for anomalous resistivity to arise in a plasma in which no microinstabilities have been excited. This can occur under the action of the ponderomotive force which is a non-linear low-frequency force produced by the coupling of two high-frequency waves. This force drives parametric decay instabilities which can produce and sustain low-frequency density fluctuations. An enhancement in resistivity occurs. Such effects have been observed in the ionosphere (see review by Papadopoulos (1977)) but do not concern us here.

REFERENCES

Alexandrov A.F., Bogdankevich L.S. and Rukhadze A.A.: 1984, "Principles of Plasma Electrodynamics", Springer-Verlag (New York).

Alfven H.A.: 1939, Phys. Rev. 55, 425.

Alfven H.A. and Carlquist P.: 1967, Solar Phys., 1, 220.

Antonucci E., Gabriel A.H. and Dennis B.R.: 1984, Ap.J. 287, 917.

Antonucci E., Dennis B.R., Gabriel A.H. and Simnett G.M.: 1985, Solar Phys., 96, 129.

Batchelor D.A., Crannell C.J., Wiehl H.J. and Magun A.: 1985, Ap.J. 295, 258.

Benford G.: 1976, J. Plasma Phys. 15, 431.

Benford G.: 1983, Ap.J., 269, 690.

Benford G. and Book D.L.: 1971, Adv. Plasma Phys. 4, 125.

Bennett W.H. : 1931, Phys. Rev. 37, 552.

Benz A.O.: 1977, Ap.J., 211, 270.

Benz A.O. and Smith D.F.: 1987, Solar Physics 107, 299.

Biskamp D.: 1986, Phys. Fluids, 29, 1520.

Brejzman B.N. and Ryutov D.D.: 1974, Nucl. Fusion 14, 873.

Brown J.C.: 1971, Solar Phys., 18, 489.

Brown J.C.: 1974, in "Coronal Disturbances", IAU Symp. 57 (Ed. G.A. Newkirk), Reidel (Dordrecht), p.395.

Brown J.C. and Melrose D.B. : 1977, Solar Phys. 52, 117.

Brown J.C., Melrose D.B. and Spicer D.S.: 1979, Ap.J. 228, 592.

Brown J.C. and Smith D.F.: 1980, Rep. Prog. Phys., 43, 125.

Brown J.C., Smith D.F. and Spicer D.S.: 1981, in "The Sun as a Star", (Ed. S. Jordan), NASA Sp-450, Chapter 7.

Brown J.C. and Hayward J.: 1982, Solar Phys. 41, 135.

Brown J.C. and Bingham R.: 1984, Astron. Astrophys. Lett. 131, L.11.

Cairns A.: 1985, "Plasma Physics", Blackie and Son Ltd. (Glasgow)

Chen F.F.: 1984, "Introduction to Plasma Physics and Controlled Fusion", Volume 1: Plasma Physics (Second Edition), Plenum Press (London).

Brown J.C. and Loran J.M.: 1985. Mon. Not. Roy. Ast. Soc., 212, 245.

Carlquist P.: 1969, Solar Phys. 7, 377.

Carlquist P.: 1979a, in "Wave Instabilities in Space Plasmas", Astrophysics and Space Science Book Series (Eds. P.J. Palmadesso and K. Papadopoulos), Reidel (Dordrecht), p.83.

Carlquist P.: 1979b, Solar Phys. 63, 353.

Carreras B.A., Hicks H.R., Homes J.A. and Waddell B.V.: 1980, Phys. Fluids, 23, 1811.

Carrington R.C.: 1859, Mon. Not. Roy. Astron. Soc. 20, 13.

Cook. I.: 1981, in "Plasma Physics and Nuclear Fusion Research" (Ed. R.D. Gill), Academic Press, London, Ch.12, p.293.

Cox J.D. and Bennett W.H.: 1970, Phys. Fluids 13, 182.

Craig I.J.D. and Brown J.C.: 1976, Astron. Astrophys. 49, 239.

Craig I.J.D. and Brown J.C.: 1986, "Inverse Problems in Astronomy" Adam Hilger (Bristol).

Dakin D.R., Tajima T., Benford G. and Rynn N.: 1976, J. Plasma Phys. 15, 175.

D'Angelo N. and Motley R.W.: 1962, Phys. Fluids 5, 633.

Davidson R.C.: 1972, "Methods in Nonlinear Plasma Theory", Academic Press, New York.

de Jager C.: 1986, Space Science Rev., 44, 43.

Dennis B.R.: 1985, Solar Physics, 100, 465.

Dennis B.R., Orwig L.E. and Kiplinger A.L.: 1987, "Rapid Fluctuations in Solar Flares", NASA Cp-2449.

Dreicer H.: 1959, Phys. Rev., 115, 238.

Dreicer H.: 1960, Phys. Rev., 117, 329.

Drummond W.E. and Rosenbluth M.N.: 1962, Phys. Fluids 5, 1507.

Duijveman A., Hoyng P. and Ionson J.A.: 1981, Ap.J. 245, 721.

Duijveman A., Hoyng P. and Machado M.E.: 1982, Solar Phys., 81, 137.

Dum C.T.: 1978a, Phys. Fluids 21, 945.

Dum C.T.: 1978b, Phys. Fluids 21, 956.

Dum C.T. and Dupree T.H.: 1970, Phys. Fluids 13, 2064.

Ellison D.C. and Ramaty R.: 1985, Ap.J. 298, 400.

Emslie A.G.: 1978, Ap.J. 224, 241.

Emslie A.G.: 1980, Ap.J. 235, 1055.

Emslie A.G.: 1981, Ap.J. 249, 817.

Emslie A.G.: 1985, Solar Phys. 98, 281.

Emslie A.G.: 1986, Solar Phys. 103, 103.

Emslie A.G. and Smith D.F.: 1984, Ap.J. 279, 882.

Emslie A.G. and Brown J.C.: 1985, Ap.J. 295, 648.

Emslie A.G., Phillips K.J.H. and Dennis B.R.: 1986, Solar Phys. 103, 89.

Fried B.D. and Conte S.D.: 1961, "The Plasma Dispersion Function", Academic Press (New York).

Fried B.D. and Gould R.W.: 1961, Phys. Fluids 4, 139.

Furth H.P., Killeen J. and Rosenbluth M.N.: 1963, Phys. Fluids, 6, 459.

Gold T. and Hoyle F.: 1960, Mon. Not. Roy. Astron. Soc., 120, 89.

Haber I., Huba J.D., Palmadesso P. and Papadopoulos K.: 1978, Phys. Fluids 21, 1013.

Hammer D.A. and Rostoker N.: 1970, Phys. Fluids, 13, 1831.

Hasegawa A.: 1974, Rev. Geophys. Space Phys. 12, 273.

Heyvaerts J.: 1981, "Particle Acceleration in Solar Flares" in "Solar Flare Magnetohydrodynamics" (Ed. E.R. Priest), Gordon and Breach (New York), p.429.

Heyvaerts J., Priest E.R. and Rust D.M.: 1977, Ap.J. 216, 123.

Hinata S.: 1979, Ap.J. 232, 915.

Hinata S.: 1980, Ap.J. 235, 258.

Hodgson R.: 1859, Mon. Not. Roy. Astron. Soc. 20, 15.

Holman G.D.: 1985, Ap.J. 293, 584.

Holman G.D.: 1987, in "Rapid Fluctuations in Solar Flares" (Eds. B.R. Dennis, Le Orwig and A. K. Kiplinger), NASA CP-2449, p.361.

Holman G.D., Eichler D. and Kundu M.R.: 1980, in "Radio Physics of the Sun", (Ed. M.R. Kundu and T.E. Gergely), Reidel (Dordrecht), p.457.

Hood A.W. and Priest E.R.: 1981, Solar Phys. 73, 289.

Hoyng P., Brown J.C. and Van Beek H.F.: 1976, Solar Phys. 48, 197.

Hoyng P., Knight J.W. and Spicer D.S.: 1978, Solar Phys. 58, 139.

Hudson M.K., Lysak R.L. and Mozer F.S.: 1978, Geophys. Res. Letters 5, 143.

Ionson J.A.: 1976, Physics Letters 58A, 105.

Kadomtsev B.B.: 1965 "Plasma Turbulence", Academic Press (London).

Kadomtsev B.B.: 1966 Rev. Plasma Phys. 2, 153.

Kane S.R., Anderson K.A., Evans W.D., Klebesadel R.W. and Laros J.: 1979, Ap.J. Letts., 233, L151.

Kaplan S.A. and Tsytovich V.N.: 1973, "Plasma Astrophysics", Translated and Edited by D. Ter Haar, Pergamon Press, Oxford.

Kaplan S.A., Pikelner S.B. and Tsytovich V.N.: 1974, "Plasma Physics of the Solar Atmosphere", Physics Reports, Volume 15C, Number 1.

Kindel J.M. and Kennel C.F.: 1971, J. Geophys. Res. 76, 3055.

Kiplinger A.L., Dennis B.R., Emslie A.G., Frost K.J. and Orwig L.E.: 1983, Ap.J. (Letters), 265, L99.

Knight J.W. and Sturrock P.A.: 1977, Ap.J., 218, 306.

Korchak A.A.: 1971, Solar Phys., 18, 284.

Kovrizhnykh L.M.: 1967a, JETP (USSR) 24, 1210.

Kovrizhnykh L.M.: 1967b, JETP (USSR) 25, 934.

Kundu M.R. and Holman G.D. (Eds.) 1985, "Unstable Current Systems and Plasma Instabilities in AStrophysics", Reidel (Dordrecht).

Laing E.W.: 1981, in "Plasma Physics and Nuclear Fusion Research" (Ed. R.D. Gill), Academic Press, London, Ch.8, p.155.

Landau L.: 1946, J. Phys. (USSR), 10, 25.

Lawson J.D.: 1957, J. Electron Control, 3, 587.

Lee K.F.: 1972, J. Plasma Phys. 8, 379.

Lee R. and Sudan R.N.: 1971, Phys. Fluids, 14, 1213.

Liu C.S. and Mok Y. 1977, Phys. Rev. Letters 38, 162.

Lovelace R.V. and Sudan R.N.: 1971, Phys. Rev. Letters, 27, 1256.

McClements K.G.: 1987, Astron. Astrophys., 175, 255.

McClements K.G. and Brown J.C.: 1986, Astron. Astrophys., 165, 235.

McKinnon A.L.: 1986, "Impulsive Phase of Solar Flares:Theory" in "Flares: Solar and Stellar" (Ed. P.M. Gondhalekar), RAL Conference Report 86-085.

McKinnon A.L., Brown J.C. and Hayward J.: 1985, Solar Phys., 99, 231.

MacNeice P., McWhirter R.W.P., Spicer D.S. and Burgess A.: 1984, Solar Phys., 90, 357.

Melrose D.B., and Dulk G.A.: 1982, Ap.J., 259, 844.

Michelson P. and Rasmussen J.J. (Eds.): 1982, Proc. Symp. on Plasma Double Layers, Risø June 16-18, RISØ-R.472.

Miller R.B.: 1982, "An Introduction to the Physics of Intense Charged Particle Beams", Plenum Press (New York).

Miyamoto K.: 1980, "Plasma Physics for Nuclear Fusion", MIT.

NRL Plasma Formulary: 1983, Ed. D.L. Book, Laboratory for Computational Physics, NRL, Washington, D.C.

Palmadesso P.J., Coffey T.P., Ossakow S.L. and Papadopoulos K.: 1974, Geophys. Res. Letters 1, 105.

Papadopoulos K.: 1977, Rev. Geophys. Space Phys., 15, 113.

Parail V.V. and Pogutse O.P.: 1976, Sov. J. Plasma Phys., 2, 126.

Parker E.N.: 1963, Astrophys. J. Suppl. 8, 177.

Petschek H.E.: 1964, AAS-NASA Symp. on Physics of Solar Flares (Ed. W.N. Hess), NASA (Greenbelt).

Petviashvili V.I.: 1964, Soviet Phys. - JETP, 18, 1014.

Priest E.R. (Ed.): 1981, "Solar Flare Magnetohydrodynamics", Gordon and Breach (New York).

Priest E.R.: 1984, "Solar Magnetohydrodynamics", Reidel (Dordrecht).

Priest E.R. and Forbes T. :1986, J. Geophys. Res. 91, 5579

Pritchett P.L., Ashour-Abdalla M. and Dawson J.M.: 1981, Geophys. Res. Letters 8, 611.

Raadu M.A.: 1986, Physica Scripta 33, 240.

Roberts T.G. and Bennett W.H.: 1968, Plasma Phys. 10, 381.

Rowland H.L. and Vlahos L.: 1985, Astron. Astrophys. 142, 219.

Rust D.M.: 1976, Phil. Trans. Roy. Soc. Lond. A281, 427.

Sato T. and Okuda H.: 1980, Phys. Rev. Letters 44, 740.

Sato T. and Okuda H.: 1981, J. Geophys. Rks. 86, 3357.

Schrittwieser R. and Eder G.(Eds.): 1984, Proc. Second Symp. on Plasma Double Layers and Related Topics, Institute for Theoretical Physics, University of Innsbruck.

Simnett G.A.: 1986, Solar Phys. 106, 165.

Simnett G.M. and Benz A.O.: 1986, Astron. Astrophys. submitted.

Smith D.F.: 1983, in "Unstable Current Systems and Plasma Instabilities in Astrophysics" (Eds. M.R. Kundu and G.D. Holman), Reidel (Dordrecht) p.509.

Smith D.F. and Priest E.R.: 1972, Ap.J. 176, 487.

Smith D.F. and Lilliequist C.G.: 1979, Ap.J. 232, 582.

Summers H.P. and McWhirter R.W.P.: 1979, J. Phys. B. Molec.Phys. 12, 2387.

Smith D.F. and Spicer D.S.: 1979, Solar Phys. 62, 359.

Soward A.M. and Priest E.R.: 1977, Phil. Trans. R. Soc. Lond. A 284, 369.

Spicer D.S.: 1977, Solar Phys., 53, 305.

Spicer D.S.: 1986, Solar Phys. 70, 149.

Spicer D.S.: 1983, Adv. Space Res. 2, No.11, 135.

Spicer D.S. and Brown J.C.: 1981, in "The Sun as a Star" (Ed. S. Jordan), NASA SP-450, Chapter 18.

Spicer D.S. and Sudan R.N.: 1984, Ap.J. 280, 448.

Spitzer L.: 1962, "Physics of Fully Ionised Gases", Wiley Interscience (New York).

Stringer T.E.: 1964, Plasma Phys. (J. Nucl. Energy, C) 6, 267.

Sturrock P.A.: 1966, in "Structure and Development of Solar Active Regions", IAU Symp.35 (Ed. K.D. Kipenheuer), Reidel (Dordrecht) p.3.

Sturrock P.A.: 1980, "Solar Flares. A Monograph from Skylab Solar Workshop II", Colorado Associated University Press, Boulder.

Sturrock P.A.: 1986, "Physics of the Sun, Volume II: The Solar Atmosphere", Reidel (Dordrecht).

Sudan R.N.: 1984, in "Basic Plasma Physics II" (Volume 2 of "Handbook of Plasma Physics" (Eds. A.A. Galeev and R.N. Sudan), North-Holland Physics Publishing (Amsterdam).

Svestka Z.:1976, "Solar Flares", Reidel (Dordrecht).

Sweet P.A.: 1958, "The Neutral Point Theory of Solar Flares in "Electromagnetic Phenomena in Cosmical Physics" IAU Symp.6, (Ed. B. Lehnert), Reidel (Dordrecht), p.123.

Sweet P.A.: 1969, Ann. Rev. Astron. Astrophys. 7, 149.

Tange T. and Ichimaru S.: 1974, J. Phys. Soc. Japan 36, 1437.

Thode L.E. and Sudan R.N.: 1975a, Phys. Fluids 18, 1552.

Thode L.E. and Sudan R.N.: 1975b, Phys. Fluids 18, 1564.

Thompson A.M., Brown J.C. and Kuipers J.: 1986, Astron. Astrophys. 159, 202.

Tsytovich V.N.: 1970, "Nonlinear Effects in Plasma", Translation edited by S.M. Hamberger, Plenum Press (New York).

Tsytovich V.N.: 1974, Plasma Phys. 13, 741.

Vasyliunas V.M.: 1975, Rev. Geophys. Space Phys., 13, 303.

Vlahos L. and Rowland H.L.: 1984, Astron. Astrophys. 139, 263.

Wesson J.A. and Sykes A.: 1973, Phys. Rev. Letters 31, 449.

Winglee R.M. and Dulk G.A.: 1986, Solar Physics 104, 93.